~~62-70375~~ Copy 34

[redacted]

NASA MEMO 7-18-59A

NASA MEMO 7-18-59A

Declassified by authority of NASA
Classification Change Notices No. 143
Dated ** 1-31-68

413

NASA

MEMORANDUM

~~CASE FILE~~
COPY

for SERVICE REPORT

UNITED STATES AIR FORCE

INLET PERFORMANCE CHARACTERISTICS FROM WIND-TUNNEL TESTS OF A 0.10-SCALE AIR-INDUCTION SYSTEM MODEL OF THE YF-108A AIRPLANE AT MACH NUMBERS OF 2.50, 2.76, AND 3.00 (COORD. NO. AF-AM-157)

By James R. Blackaby, E. Gene Lyman, and John A. Altermann III

Ames Research Center
Moffett Field, Calif.

[redacted]

[redacted]

[redacted]

NATIONAL AERONAUTICS AND SPACE ADMINISTRATION

WASHINGTON

Service Report prepared by the United States Air Force

July 1959

FOR NASA ACTIVITIES ONLY

[redacted]

[redacted]

NATIONAL AERONAUTICS AND SPACE ADMINISTRATION

MEMORANDUM 7-18-59A

for

UNITED STATES AIR FORCE

INLET PERFORMANCE CHARACTERISTICS FROM WIND-TUNNEL TESTS OF A 0.10-SCALE AIR-INDUCTION SYSTEM MODEL OF THE YF-108A AIRPLANE AT MACH NUMBERS OF 2.50, 2.76, AND 3.00 (COORD. NO. AF-AM-157)*

By James R. Blackaby, E. Gene Lyman, and John A. Altermann III

ABSTRACT

Inlet-performance and external-drag-coefficient characteristics are presented without analysis. Effects are shown of variations of fuselage boundary-layer diverter profile, bleed-surface porosity, bleed-exit area, and inlet ramp, and lip angle.

INDEX HEADINGS

Air Inlets, Scoops	1.4.1.4.1
Boundary Layer Control - Internal Aerodynamics	1.4.7.2
Airplanes - Specific Types	1.7.1.2

*Title, Confidential

[redacted]

[redacted]

NATIONAL AERONAUTICS AND SPACE ADMINISTRATION

MEMORANDUM 7-18-59A

for

UNITED STATES AIR FORCE

INLET PERFORMANCE CHARACTERISTICS FROM WIND-TUNNEL TESTS OF A 0.10-SCALE AIR-INDUCTION SYSTEM MODEL OF THE YF-108A AIRPLANE AT MACH NUMBERS OF 2.50, 2.76, AND 3.00 (COORD. NO. AF-AM-157)*

By James R. Blackaby, E. Gene Lyman, and John A. Altermann III

SUMMARY

Wind-tunnel tests were conducted to measure the inlet-performance characteristics and the external-drag increments associated with various configurations and operating conditions for a 0.10-scale air-induction model of the YF-108A airplane. The effects of changes of the fuselage boundary-layer diverter profile, the porosity of porous bleed surfaces in the inlet, the area of the bleed-flow exits, and the angle of the inlet ramp and lip surfaces were investigated.

The tests were conducted at free-stream Mach numbers of 2.50, 2.76, and 3.00. The corresponding Reynolds numbers were 2.8×10^6, 2.4×10^6, and 2.1×10^6 per foot, respectively. The angle-of-attack range was from 0° to 14°, and the angle of sideslip range was from -5° to $+5^\circ$.

Data from the tests are presented without analysis.

INTRODUCTION

The wind-tunnel investigation of a 0.10-scale air-induction model of the YF-108A airplane was conducted at the request of the Air Research and Development Command of the United States Air Force. The purpose of the tests was to obtain total-pressure-recovery, mass-flow-ratio, and flow-stability characteristics for various inlet configurations, and to measure drag increments associated with the various model configurations and operating conditions.

*Title, Confidential

[redacted]

[redacted]

NOTATION

A	area, sq ft
A_{ref}	maximum capture area of inlet, 0.130 sq ft
A_{th}	theoretical area of the free-stream tube captured by the inlet (a function of δ_R, δ_L, M and α), sq ft
C_D	drag coefficient, $\frac{D}{qS}$, referred to stability axes
$C_{D_{ext}}$	external-drag coefficient, $C_{D_t} - C_{D_i}$
C_{D_i}	internal-drag coefficient
C_{D_t}	total-drag coefficient (balance drag, including base pressure correction)
D	drag, lb
M	free-stream Mach number
m	mass-flow rate, ρAV, slugs/sec
m_{th}	theoretical inlet mass-flow rate, $\rho_\infty A_{th} V_\infty$, slugs/sec
p_t	total pressure, lb/sq ft
$\bar{p}_t$	average total pressure, lb/sq ft
q	free-stream dynamic pressure, lb/sq ft
S	wing area of a complete 0.10-scale model of the airplane, 18.648 sq ft
V	velocity, ft/sec
α	nominal angle of attack, deg
β	nominal angle of sideslip, deg
δ_L	reference angle of hinged cowl lip, deg ($\delta_L = 0^\circ$ corresponds to the most open setting of the lip - see fig. 3)
δ_R	reference angle of forward section of the variable ramp and throat assembly, referred to the fuselage reference line, deg (see fig. 3)

[redacted]

ξ total pressure distortion parameter at the engine-face station, $\frac{(p_{t_3})_{max} - (p_{t_3})_{min}}{\bar{p}_{t_3}}$

ρ air density, slugs/cu ft

Subscripts

1 inlet station

3 simulated engine-face station

∞ free-stream conditions

APPARATUS AND MODEL

The tests were conducted in the 8- by 7-foot test section of the Ames Unitary Plan wind tunnel.

The air-induction system model of the YF-108A airplane was furnished by North American Aviation, Incorporated. It consisted of a 0.10-scale reproduction of the forebody, the left-hand inlet, and the ducting to the face of the left-hand engine, plus a stub wing on the left side and a flow metering section of duct after the engine station. Photographs of the model installed in the wind tunnel and a drawing of the model are shown in figures 1 and 2(a).

The model was sting-mounted and included an integral strain-gage balance instrumented to measure chord force, normal force, and side force. Additional instrumentation included a 30-tube total-pressure rake and 6 static-pressure tubes at the simulated engine-face station; a calibrated flow metering nozzle; static-pressure orifices in each of four separate boundary-layer bleed plenum chambers; static-pressure orifices in the balance chamber, in the duct near the exit, and at the base around the duct exit; and a static-pressure transducer in the subsonic diffuser.

Total loads consisting of air loads on the external portion of the model ahead of section A-A in figure 2(a), and internal forces to the duct exit (station 157.75), were measured by the balance. Aft of section A-A, the model was shielded from external air loads. Inlet air flow was regulated by a motor-operated plug valve at the duct exit. Details of the engine-face rake are included in figure 2(b).

[redacted]

A schematic section drawing of the inlet is shown in figure 3. The inlet was rectangular and included a fixed, 9° initial compression ramp followed by a remotely controlled, hinged second ramp and throat assembly, and a remotely controlled hinged cowl lip which served as a third internal compression surface. Both the internal lip profile and the variable second ramp incorporated curved portions, as indicated in figure 3, to provide isentropic compression. The lip incorporated 6°, and the ramp 5°, of turning for this purpose.

The cross-sectional area variations of the duct from the lip hinge line to the total-pressure rake station are shown in figure 4 for several positions of the variable ramp and throat assembly. Forward of the lip hinge line, the area variation was a function of both lip angle and variable ramp angle.

Porous surfaces were utilized in the inlet and throat regions of the duct to bleed off the boundary layer formed on the duct walls and compression surfaces. Details of the supporting structure for the porous plates, and the size and shape of the porous-plate areas are shown in figures 5(a), 5(b), and 5(c). Details of the porous plate perforations are included in figure 6. The boundary-layer bleed flow was collected in four plenum chambers and was exhausted to the free stream through sonic exits. The porous areas and bleed exits are shown schematically in figure 6. Several porosities, or combinations of porosities, were used during the tests, and the bleed-exit areas were also varied. The porosity and bleed-exit configurations are defined in table I.

The inlet was displaced from the fuselage to provide a gutter for the fuselage boundary-layer air so that it would not be ingested into the inlet. The amount of the displacement (0.7 inch at the most forward point of the inlet, as shown in fig. 5(a)) was scaled from the actual airplane diverter height directly according to model scale, without regard to the difference between flight and wind-tunnel-test Reynolds numbers. The leading edge of the fuselage-boundary-layer diverter was located downstream from the most forward point of the inlet as shown in figure 5(a). Two boundary-layer diverter profiles were utilized during the tests; drawings of the two diverter profiles are shown in figure 7(a), and their configuration designations (convex and concave) are included in table I.

Two fuselage nose configurations were utilized in the tests. The second differed from the first only by the addition of a probe as shown in figure 7(b). Configuration designations for the two noses are included in table I.

TESTS AND PROCEDURES

Range of Test Variables

The tests were conducted at free-stream Mach numbers of 2.50, 2.76, and 3.00. The corresponding Reynolds numbers were approximately 2.8×10^6, 2.4×10^6, and 2.1×10^6 per foot, respectively. The angle-of-attack range was from 0° to 14°, and the angle-of-sideslip range was from -5° to $+5^\circ$. The angles of attack and sideslip quoted herein are all nominal angles. The nominal angles of attack differ from the true angles by a maximum of $\pm 0.1^\circ$ for a sideslip angle of 0° and by $\pm 0.3^\circ$ for a sideslip angle of $\pm 5^\circ$. The nominal angles of sideslip differ from the true angles by a maximum of $+0.3^\circ$ at nominal sideslip angles of $\pm 5^\circ$.

Test Methods

For each test Mach number, model attitude, and inlet configuration, an initial, or transient, run was made during which no data were recorded, but inlet conditions were monitored to define the supercritical, critical, and subcritical inlet-flow regimes. For the transient runs, Mach number, model attitude, and variable-ramp angle were set at the scheduled values, the flow control plug valve was opened, and the inlet area was reduced by moving the hinged lip until supersonic flow was established in the inlet. Then the lip was moved to its scheduled position and the plug valve was slowly closed while the readings of the performance-indicating instrumentation were visually monitored. For the data-recording runs, the inlet-starting process was repeated and data were then recorded for selected settings of the plug valve. In most cases, data were recorded for several plug-valve settings yielding supercritical inlet flow, and for the setting yielding critical, or maximum pressure recovery. For selected cases, additional data were recorded for the subcritical, or unstarted, inlet-flow regime.

All pressure data were measured utilizing pressure transducers. The electrical output signals of the pressure transducers were recorded by an automatic sequential digital recorder along with the output signals from the balance strain gages and the digitized tunnel-condition and model-configuration information required.

Reduction of Data

Computations of inlet-performance, total-drag coefficient, and internal-drag coefficient were accomplished utilizing automatic computing equipment.

[redacted]

[redacted]

The inlet-performance parameters computed and presented include average total-pressure ratio $\bar{p}_{t_3}/p_{t_\infty}$ at the simulated engine-face station, flow distortion parameter ξ, mass-flow ratio at the engine station m_3/m_{th}, and mass-flow ratio at the inlet m_1/m_{th}. Average total-pressure ratio was computed as the average of the local total-pressure ratios for the 30 tubes of the total-pressure rake:

$$\frac{\bar{p}_{t_3}}{p_{t_\infty}} = \frac{\sum_{1}^{30} (p_{t_3}/p_{t_\infty})_{local}}{30}$$

The flow distortion parameter at the rake station was computed by the equation

$$\xi = \frac{(p_{t_3}/p_{t_\infty})_{max} - (p_{t_3}/p_{t_\infty})_{min}}{\bar{p}_{t_3}/p_{t_\infty}}$$

Mass-flow ratio at the engine station m_3/m_{th} was computed from static pressures measured at the calibrated flow metering nozzle aft of the simulated engine station by means of standard ASME nozzle flow equations. The mass-flow presented is based on the theoretical area of the free-stream tube captured by the inlet for each individual inlet configuration, angle of attack, and test Mach number Thus, in terms of mass-flow ratio based on the fixed reference area A_{ref} of 0.130 square feet (the maximum capture area of the inlet for an angle of attack of 0° and a lip angle of 0°)

$$\frac{m_3}{m_{th}} = \left(\frac{m_3}{m_\infty}\right)\left(\frac{A_{ref}}{A_{th}}\right)$$

in which

$$m_3 = \rho_3 A_3 V_3 = \rho_\infty A_\infty V_\infty$$

$$m_\infty = \rho_\infty A_{ref} V_\infty$$

$$m_{th} = \rho_\infty A_{th} V_\infty$$

The conversion factor A_{ref}/A_{th} for each model attitude and configuration, which was based on theoretical shock-wave and flow-field patterns, was supplied by North American Aviation, Incorporated.

[redacted]

Total inlet mass-flow ratio m_1/m_{th} was computed as the sum of the engine mass-flow ratio and the four bleed mass-flow ratios:

$$\frac{m_1}{m_{th}} = \frac{m_3}{m_{th}} + \sum_{1}^{4}\left(\frac{m}{m_{th}}\right)_{bleed}$$

Mass flow through each of the four bleed exits was computed based on total pressure for the bleed-flow plenum chambers, with sonic flow assumed through the exits. Static-pressure measurements on the plenum chamber walls were taken to be equal to plenum chamber total pressures.

The measured drag data were reduced to an external-drag coefficient $C_{D_{ext}}$, defined by the equation:

$$C_{D_{ext}} = C_{D_t} - C_{D_i}$$

The total-drag coefficient C_{D_t} represents the drag indicated by the balance with an adjustment included to correct the base pressure on the model to free-stream static pressure. No such adjustment was applied to the balance chamber pressures; visual monitoring showed that balance chamber pressure was a function only of Mach number, and not of model attitude, configuration, or internal flow characteristics. The drag results are intended to show increments, not absolute values.

RESULTS

Inlet-performance characteristics and external-drag coefficients are presented without analysis in figures 8 through 34. (The chord-force gage of the balance malfunctioned during a portion of the tests; as a result, no drag data were available for certain model configurations and test conditions.) The figures are presented in five groups according to the model parameters being compared.

In the first group, figures 8 through 22, the results from a series of initial runs are plotted to show the effects of lip angle changes for selected ramp angles for each test Mach number and angle of attack for an angle of sideslip of 0°. Based on a comparison of these data, and with knowledge of previous tests of the inlet configuration by North American Aviation, Inc., the ramp and lip angle combinations tabulated in table II were selected for subsequent investigation of other configuration changes. In the first group of data, figures 21 and 22 are included to indicate the performance of the inlet with extreme settings of the ramp and lip. These represent the maximum and minimum settings which could exist as a result of a malfunction of the positioning controls in the actual airplane.

[redacted]

[redacted]

Correct values of the conversion factor A_{ref}/A_{th} were not available for the inlet with the ramp and lip in the extreme positions; the values tabulated in figures 21 and 22 were selected by North American Aviation, Inc.

In the second group of data, figures 23 and 24, the effect of the change of fuselage-boundary-layer diverter profile from convex to concave (see fig. 7(a)) is shown. Based on these data, the concave profile was used for the remainder of the tests.

In the third group of data, figures 25 and 26, the effects of changes of porosity of the boundary-layer bleed surfaces are shown, and in the fourth group of data, figures 27 through 31, the effects of changes in the bleed exit configurations are shown. The fifth group of data, figures 32 through 34, shows the effects of angles of sideslip from -5° to $+5^{\circ}$.

Ames Research Center
National Aeronautics and Space Administration
Moffett Field, Calif., May 18, 1959

[redacted]

TABLE I.- CONFIGURATION KEYS

Nose configurations (see fig. 7(b))	
Nose 1	Plain nose
Nose 2	Nose with probe

Fuselage-boundary-layer diverter configurations (see fig. 7(a))	
Diverter 1	Convex profile
Diverter 2	Concave profile

Porous surface configurations

	Porosity, percent of porous plate area				
	Inboard duct wall	Outboard duct wall	Lower duct wall	Forward ramp	Middle ramp
Porosity 1	3.5	3.5	3.5	3.5	3.5
Porosity 2	6.5	6.5	6.5	6.5	6.5
Porosity 3	1.0	1.0	1.0	1.0	1.0
Porosity 4	3.5	3.5	[1]3.5	[1]3.5	3.5
Porosity 5	3.5	3.5	6.5	6.5	3.5

Bleed exit configurations

	Bleed exit area, sq in.			
	Forward outboard	Aft outboard	Upper door	Lower
Bleed exit 1	2.093	0.450	0.908, 6° door angle	0.590
Bleed exit 2	2.093	.450	1.176, 4° door angle	.590
Bleed exit 3	0	.450	.908, 6° door angle	.590
Bleed exit 4	2.093	.450	.908, 6° door angle	.310
Bleed exit 5	2.093	.450	.882, 3° door angle	.590
Bleed exit 6	2.093	.450	1.763, 6° door angle	.590

[1]Aft 1 inch of porous plate area filled.

FIGURE LEGENDS

Figure 1.- Photographs of the model installed in the wind tunnel. (a) Upper view. (b) Lower view.

Figure 2.- Model details. (a) Model drawing.

Figure 2.- Concluded. (b) Total pressure rake.

Figure 3.- Schematic drawing of inlet geometry details.

Figure 4.- Variation of duct area aft of lip hinge line.

Figure 5.- Porous bleed system construction details. (a) Sideplates, or walls.

Figure 5.- Continued. (b) Ramp and throat assembly.

Figure 5.- Concluded. (c) Lip and cowl.

Figure 6.- Porous areas and bleed exit details.

Figure 7.- Fuselage-boundary-layer diverter and nose cone details. (a) Fuselage-boundary-layer diverters. (b) Nose cones.

Figure 8.- Effect of lip angle variation on inlet performance and external-drag coefficient; $M = 3.00$, $\alpha = 0^\circ$, $\beta = 0^\circ$. Configuration: nose 1, diverter 1, porosity 1, bleed exit 1. (a) $\delta_R = 19.0^\circ$; inlet performance.

Figure 8.- Continued. (a) Concluded. $\delta_R = 19.0^\circ$; external-drag coefficient.

Figure 8.- Continued. (b) $\delta_R = 19.5^\circ$; inlet performance.

Figure 8.- Continued. (c) $\delta_R = 20.0^\circ$; inlet performance.

Figure 8.- Concluded. (c) Concluded. $\delta_R = 20.0^\circ$; external-drag coefficient.

Figure 9.- Effect of lip angle variation on inlet performance and external-drag coefficient; $M = 3.00$, $\alpha = 2^\circ$, $\beta = 0^\circ$. Configuration: nose 1, diverter 1, porosity 1, bleed exit 1. (a) $\delta_R = 18.5^\circ$; inlet performance.

Figure 9.- Continued. (a) Concluded. $\delta_R = 18.5^\circ$; external-drag coefficient.

Figure 9.- Continued. (b) $\delta_R = 19.0^\circ$; inlet performance.

Figure 9.- Continued. (b) Concluded. $\delta_R = 19.0^\circ$; external-drag coefficient.

Figure 9.- Continued. (c) $\delta_R = 19.5^\circ$; inlet performance.

Figure 9.- Concluded. (c) Concluded. $\delta_R = 19.5^\circ$; external-drag coefficient.

[redacted]

[redacted]

Figure 10.- Effect of lip angle variation on inlet performance and external-drag coefficient; $M = 3.00$, $\alpha = 4^{\circ}$, $\beta = 0^{\circ}$. Configuration: nose 1, diverter 1, porosity 1, bleed exit 1. (a) $\delta_R = 18.0^{\circ}$; inlet performance.

Figure 10.- Continued. (a) Concluded. $\delta_R = 18.0^{\circ}$; external-drag coefficient.

Figure 10.- Continued. (b) $\delta_R = 18.5^{\circ}$; inlet performance.

Figure 10.- Continued. (b) Concluded. $\delta_R = 18.5^{\circ}$; external-drag coefficient.

Figure 10.- Continued. (c) $\delta_R = 19.0^{\circ}$; inlet performance.

Figure 10.- Concluded. (c) Concluded. $\delta_R = 19.0^{\circ}$; external-drag coefficient.

Figure 11.- Effect of lip angle variation on inlet performance and external-drag coefficient; $M = 3.00$, $\alpha = 6^{\circ}$, $\beta = 0^{\circ}$. Configuration: nose 1, diverter 1, porosity 1, bleed exit 1. (a) $\delta_R = 17.5^{\circ}$; inlet performance.

Figure 11.- Continued. (a) Concluded. $\delta_R = 17.5^{\circ}$; external-drag coefficient.

Figure 11.- Continued. (b) $\delta_R = 18.0^{\circ}$; inlet performance.

Figure 11.- Continued. (b) Concluded. $\delta_R = 18.0^{\circ}$; external-drag coefficient.

Figure 11.- Continued. (c) $\delta_R = 18.5^{\circ}$; inlet performance.

Figure 11.- Concluded. (c) Concluded. $\delta_R = 18.5^{\circ}$; external-drag coefficient.

Figure 12.- Effect of lip angle variation on inlet performance and external-drag coefficient; $M = 3.00$, $\alpha = 10^{\circ}$, $\beta = 0^{\circ}$. Configuration: nose 1, diverter 1, porosity 1, bleed exit 1. (a) $\delta_R = 18.0^{\circ}$; inlet performance.

Figure 12.- Continued. (a) Concluded. $\delta_R = 18.0^{\circ}$; external-drag coefficient.

Figure 12.- Continued. (b) $\delta_R = 20.0^{\circ}$; inlet performance.

Figure 12.- Concluded. (b) Concluded. $\delta_R = 20.0^{\circ}$; external-drag coefficient.

Figure 13.- Effect of lip and ramp angle variation on inlet performance and external-drag coefficient; $M = 3.00$, $\alpha = 14^{\circ}$, $\beta = 0^{\circ}$. Configuration: nose 1, diverter 1, porosity 1, bleed exit 1. (a) Inlet performance.

Figure 13.- Concluded. (b) External-drag coefficient.

Figure 14.- Effect of lip angle variation on inlet performance and external-drag coefficient; $M = 3.00$, $\alpha = 0^{\circ}$, $\beta = 0^{\circ}$, $\delta_R = 19.5^{\circ}$. Configuration: nose 1, diverter 2, porosity 5, bleed exit 4. (a) Inlet performance.

Figure 14.- Concluded. (b) External-drag coefficient.

[redacted]

Figure 15.- Effect of lip angle variation on inlet performance and external-drag coefficient; $M = 2.76$, $\alpha = 0^\circ$, $\beta = 0^\circ$ Configuration: nose 1, diverter 1, porosity 1, bleed exit 1. (a) $\delta_R = 17.5^\circ$; inlet performance.

Figure 15.- Continued. (a) Concluded. $\delta_R = 17.5^\circ$; external-drag coefficient.

Figure 15.- Continued. (b) $\delta_R = 18.0^\circ$; inlet performance.

Figure 15.- Continued. (b) Concluded. $\delta_R = 18.0^\circ$; external-drag coefficient.

Figure 15.- Continued. (c) $\delta_R = 18.5^\circ$; inlet performance.

Figure 15.- Concluded. (c) Concluded. $\delta_R = 18.5^\circ$; external-drag coefficient.

Figure 16.- Effect of lip angle variation on inlet performance and external-drag coefficient; $M = 2.76$, $\alpha = 2^\circ$, $\beta = 0^\circ$. Configuration: nose 1, diverter 1, porosity 1, bleed exit 1. (a) $\delta_R = 17.5^\circ$; inlet performance.

Figure 16.- Continued. (a) Concluded. $\delta_R = 17.5^\circ$; external-drag coefficient.

Figure 16.- Continued. (b) $\delta_R = 18.0^\circ$; inlet performance.

Figure 16.- Continued. (b) Concluded. $\delta_R = 18.0^\circ$; external-drag coefficient.

Figure 16.- Continued. (c) $\delta_R = 18.5^\circ$; inlet performance.

Figure 16.- Concluded. (c) Concluded. $\delta_R = 18.5^\circ$; external-drag coefficient.

Figure 17.- Effect of lip angle variation on inlet performance and external-drag coefficient; $M = 2.76$, $\alpha = 4^\circ$, $\beta = 0^\circ$. Configuration: nose 1, diverter 1, porosity 1, bleed exit 1. (a) $\delta_R = 17.0^\circ$; inlet performance.

Figure 17.- Continued. (a) Concluded. $\delta_R = 17.0^\circ$; external-drag coefficient.

Figure 17.- Continued. (b) $\delta_R = 17.5^\circ$; inlet performance.

Figure 17.- Continued. (b) Concluded. $\delta_R = 17.5^\circ$; external-drag coefficient.

Figure 17.- Continued. (c) $\delta_R = 18.0^\circ$; inlet performance.

Figure 17.- Concluded. (c) Concluded. $\delta_R = 18.0^\circ$; external-drag coefficient.

Figure 18.- Effect of lip angle variation on inlet performance and external-drag coefficient; $M = 2.76$, $\alpha = 6^\circ$, $\beta = 0^\circ$. Configuration: nose 1, diverter 1, porosity 1, bleed exit 1. (a) $\delta_R = 17.0^\circ$; inlet performance.

Figure 18.- Continued. (a) Concluded. $\delta_R = 17.0^\circ$; external-drag coefficient.

Figure 18.- Continued. (b) $\delta_R = 17.5^\circ$; inlet performance.

[redacted]

Figure 18.- Continued. (b) Concluded. $\delta_R = 17.5^\circ$; external-drag coefficient.

Figure 18.- Continued. (c) $\delta_R = 18.0^\circ$; inlet performance.

Figure 18.- Concluded. (c) Concluded. $\delta_R = 18.0^\circ$; external-drag coefficient.

Figure 19.- Effect of lip angle variation on inlet performance and external-drag coefficient; $M = 2.76$, $\alpha = 10^\circ$, $\beta = 0^\circ$. Configuration: nose 1, diverter 1, porosity 1, bleed exit 1. (a) $\delta_R = 17.0^\circ$; inlet performance.

Figure 19.- Continued. (a) Concluded. $\delta_R = 17.0^\circ$; external-drag coefficient.

Figure 19.- Continued. (b) $\delta_R = 18.5^\circ$; inlet performance.

Figure 19.- Concluded. (b) Concluded. $\delta_R = 18.5^\circ$; external-drag coefficient.

Figure 20.- Effect of lip angle variation on inlet performance and external-drag coefficient; $M = 2.50$, $\alpha = 0^\circ$, $\beta = 0^\circ$. Configuration: nose 1, diverter 1, porosity 1, bleed exit 1. (a) $\delta_R = 17.5^\circ$; inlet performance.

Figure 20.- Continued. (a) Concluded. $\delta_R = 17.5^\circ$; external-drag coefficient.

Figure 20.- Continued. (b) $\delta_R = 18.0^\circ$; inlet performance.

Figure 20.- Concluded. (b) Concluded. $\delta_R = 18.0^\circ$; external-drag coefficient.

Figure 21.- Inlet performance and external-drag coefficient for extreme lip and ramp angle combinations; $M = 3.00$, $\alpha = 2^\circ$, $\beta = 0^\circ$. Configuration: nose 2, diverter 2, porosity 5, bleed exit 6. (a) Inlet performance.

Figure 21.- Concluded. (b) External-drag coefficient.

Figure 22.- Inlet performance and external-drag coefficient for extreme lip and ramp angle combinations; $M = 2.76$, $\alpha = 2^\circ$, $\beta = 0^\circ$. Configuration: nose 2, diverter 2, porosity 5, bleed exit 6. (a) Inlet performance.

Figure 22.- Concluded. (b) External-drag coefficient.

Figure 23.- Effect of fuselage-boundary-layer diverter profile on inlet performance and external-drag coefficient; $M = 3.00$, $\beta = 0^\circ$. Configuration: nose 1, porosity 1, bleed exit 1. (a) $\alpha = 0^\circ$, $\delta_R = 19.5^\circ$, $\delta_L = 0.5^\circ$, $A_{ref}/A_{th} = 1.0432$; inlet performance.

Figure 23.- Continued. (b) $\alpha = 2^\circ$, $\delta_R = 19.5^\circ$, $\delta_L = 4.0^\circ$, $A_{ref}/A_{th} = 1.0930$; inlet performance.

Figure 23.- Continued. (b) Concluded. External-drag coefficient.

Figure 23.- Continued. (c) $\alpha = 4^\circ$, $\delta_R = 18.5^\circ$, $\delta_L = 1.0^\circ$, $A_{ref}/A_{th} = 0.9325$; inlet performance.

Figure 23.- Continued. (c) Concluded. External-drag coefficient.

Figure 23.- Continued. (d) $\alpha = 6^{\circ}$, $\delta_R = 18.0^{\circ}$, $\delta_L = 1.5^{\circ}$, $A_{ref}/A_{th} = 0.8968$; inlet performance.

Figure 23.- Continued. (d) Concluded. External-drag coefficient.

Figure 23.- Continued. (e) $\alpha = 10^{\circ}$, $\delta_R = 20.0^{\circ}$, $\delta_L = 4.0^{\circ}$, $A_{ref}/A_{th} = 0.9792$; inlet performance.

Figure 23.- Concluded. (e) Concluded. External-drag coefficient.

Figure 24.- Effect of fuselage-boundary-layer diverter profile on inlet performance and external-drag coefficient; $M = 2.76$, $\beta = 0^{\circ}$. Configuration: nose 1, porosity 1, bleed exit 1. (a) $\alpha = 0^{\circ}$, $\delta_R = 18.5^{\circ}$, $\delta_L = 0.5^{\circ}$, $A_{ref}/A_{th} = 1.0968$; inlet performance.

Figure 24.- Continued. (a) Concluded. External-drag coefficient.

Figure 24.- Continued. (b) $\alpha = 2^{\circ}$, $\delta_R = 18.5^{\circ}$, $\delta_L = 1.5^{\circ}$, $A_{ref}/A_{th} = 1.0706$; inlet performance.

Figure 24.- Continued. (b) Concluded. External-drag coefficient.

Figure 24.- Continued. (c) $\alpha = 4^{\circ}$, $\delta_R = 18.0^{\circ}$, $\delta_L = 3.5^{\circ}$, $A_{ref}/A_{th} = 1.0703$; inlet performance.

Figure 24.- Continued. (c) Concluded. External-drag coefficient.

Figure 24.- Continued. (d) $\alpha = 6^{\circ}$, $\delta_R = 17.5^{\circ}$, $\delta_L = 4.0^{\circ}$, $A_{ref}/A_{th} = 1.0313$; inlet performance.

Figure 24.- Continued. (d) Concluded. External-drag coefficient.

Figure 24.- Concluded. (e) $\alpha = 10^{\circ}$, $\delta_R = 17.0^{\circ}$, $\delta_L = 7.5^{\circ}$, $A_{ref}/A_{th} = 1.0624$; inlet performance.

Figure 25.- Effect of variation of bleed-surface porosity on inlet performance and external-drag coefficient; $M = 3.00$, $\beta = 0^{\circ}$. Configuration: nose 1, diverter 2, bleed exit 1. (a) $\alpha = 0^{\circ}$, $\delta_R = 19.5^{\circ}$, $\delta_L = 0.5^{\circ}$, $A_{ref}/A_{th} = 1.0432$; inlet performance.

Figure 25.- Continued. (a) Continued. Inlet performance.

Figure 25.- Continued. (a) Concluded. External-drag coefficient.

Figure 25.- Continued. (b) $\alpha = 2^{\circ}$, $\delta_R = 19.5^{\circ}$, $\delta_L = 4.0^{\circ}$, $A_{ref}/A_{th} = 1.0930$; inlet performance.

Figure 25.- Continued. (b) Continued. Inlet performance.

[redacted]

Figure 25.- Continued. (b) Concluded. External-drag coefficient.

Figure 25.- Continued inlet performance. (c) $\alpha = 4^{\circ}$, $\delta_R = 18.5^{\circ}$, $\delta_L = 1.0^{\circ}$, $A_{ref}/A_{th} = 0.9325$;

Figure 25.- Continued. (c) Continued. Inlet performance.

Figure 25.- Continued. (c) Concluded. External-drag coefficient.

Figure 25.- Continued inlet performance. (d) $\alpha = 6^{\circ}$, $\delta_R = 18.0^{\circ}$, $\delta_L = 1.5^{\circ}$, $A_{ref}/A_{th} = 0.8968$;

Figure 25.- Continued. (d) Continued. Inlet performance.

Figure 25.- Continued. (d) Concluded. External-drag coefficient.

Figure 25.- Concluded. inlet performance. (e) $\alpha = 10^{\circ}$, $\delta_R = 20.0^{\circ}$, $\delta_L = 4.0^{\circ}$, $A_{ref}/A_{th} = 0.9792$;

Figure 26.- Effect of variation of bleed surface porosity on inlet performance and external-drag coefficient; $M = 2.76$, $\beta = 0^{\circ}$. Configuration: nose 1, diverter 2, bleed exit 1. (a) $\alpha = 0^{\circ}$, $\delta_R = 18.5^{\circ}$, $\delta_L = 0.5^{\circ}$, $A_{ref}/A_{th} = 1.0968$; inlet performance.

Figure 26.- Continued. (a) Continued. Inlet performance.

Figure 26.- Continued. (a) Concluded. External-drag coefficient.

Figure 26.- Continued. inlet performance. (b) $\alpha = 2^{\circ}$, $\delta_R = 18.5^{\circ}$, $\delta_L = 1.5^{\circ}$, $A_{ref}/A_{th} = 1.0706$;

Figure 26.- Continued. (b) Continued. Inlet performance.

Figure 26.- Continued. (b) Concluded. External-drag coefficient.

Figure 26.- Continued. inlet performance. (c) $\alpha = 4^{\circ}$, $\delta_R = 18.0^{\circ}$, $\delta_L = 3.5^{\circ}$, $A_{ref}/A_{th} = 1.0703$;

Figure 26.- Continued. (c) Continued. Inlet performance.

Figure 26.- Continued. (c) Concluded. External-drag coefficient.

Figure 26.- Continued. inlet performance. (d) $\alpha = 6^{\circ}$, $\delta_R = 17.5^{\circ}$, $\delta_L = 4.0^{\circ}$, $A_{ref}/A_{th} = 1.0313$;

Figure 26.- Continued. (d) Concluded. Inlet performance.

Figure 26.- Concluded. inlet performance. (e) $\alpha = 10^{\circ}$, $\delta_R = 17.0^{\circ}$, $\delta_L = 7.5^{\circ}$, $A_{ref}/A_{th} = 1.0624$;

[redacted]

Figure 27.- Effect of variation of bleed-exit configuration on inlet performance; M = 3.00, $\beta = 0^\circ$. Configuration: nose 1, diverter 2, porosity 4. (a) $\alpha = 0^\circ$, $\delta_R = 19.5^\circ$, $\delta_L = 0.5^\circ$, $A_{ref}/A_{th} = 1.0432$.

Figure 27.- Continued. (b) $\alpha = 2^\circ$, $\delta_R = 19.5^\circ$, $\delta_L = 4.0^\circ$, $A_{ref}/A_{th} = 1.0930$.

Figure 27.- Continued. (c) $\alpha = 4^\circ$, $\delta_R = 18.5^\circ$, $\delta_L = 1.0^\circ$, $A_{ref}/A_{th} = 0.9325$.

Figure 27.- Concluded. (d) $\alpha = 6^\circ$, $\delta_R = 18.0^\circ$, $\delta_L = 1.5^\circ$, $A_{ref}/A_{th} = 0.8968$.

Figure 28.- Effect of variation of bleed-exit configuration on inlet performance; M = 2.76, $\beta = 0^\circ$. Configuration: nose 1, diverter 2, porosity 4. (a) $\alpha = 0^\circ$, $\delta_R = 18.5^\circ$, $\delta_L = 0.5^\circ$, $A_{ref}/A_{th} = 1.0968$.

Figure 28.- Continued. (b) $\alpha = 2^\circ$, $\delta_R = 18.5^\circ$, $\delta_L = 1.5^\circ$, $A_{ref}/A_{th} = 1.0706$.

Figure 28.- Continued. (c) $\alpha = 4^\circ$, $\delta_R = 18.0^\circ$, $\delta_L = 3.5^\circ$, $A_{ref}/A_{th} = 1.0703$.

Figure 28.- Concluded. (d) $\alpha = 6^\circ$, $\delta_R = 17.5^\circ$, $\delta_L = 4.0^\circ$, $A_{ref}/A_{th} = 1.0313$.

Figure 29.- Effect of variation of bleed-exit configuration on inlet performance; M = 2.50, $\beta = 0^\circ$. Configuration: nose 1, diverter 2, porosity 4. (a) $\alpha = 0^\circ$, $\delta_R = 18.0^\circ$, $\delta_L = 3.0^\circ$, $A_{ref}/A_{th} = 1.2483$.

Figure 29.- Continued. (b) $\alpha = 2^\circ$, $\delta_R = 18.0^\circ$, $\delta_L = 4.5^\circ$, $A_{ref}/A_{th} = 1.2448$.

Figure 29.- Continued. (c) $\alpha = 4^\circ$, $\delta_R = 17.5^\circ$, $\delta_L = 5.0^\circ$, $A_{ref}/A_{th} = 1.1977$.

Figure 29.- Concluded. (d) $\alpha = 6^\circ$, $\delta_R = 17.5^\circ$, $\delta_L = 6.0^\circ$, $A_{ref}/A_{th} = 1.1939$.

Figure 30.- Effect of variation of bleed-exit configuration on inlet performance and external-drag coefficient; M = 3.00, $\beta = 0^\circ$. Configuration: nose 1, diverter 2, porosity 5. (a) $\alpha = 0^\circ$, $\delta_R = 19.5^\circ$, $\delta_L = 0.5^\circ$, $A_{ref}/A_{th} = 1.0432$; inlet performance.

Figure 30.- Continued. (a) Continued. Inlet performance.

Figure 30.- Continued. (a) Continued. External-drag coefficient.

Figure 30.- Concluded. (a) Concluded. External-drag coefficient.

Figure 30.- Continued. (b) $\alpha = 2^\circ$, $\delta_R = 19.5^\circ$, $\delta_L = 4.0^\circ$, $A_{ref}/A_{th} = 1.0930$; inlet performance.

Figure 30.- Continued. (b) Continued. Inlet performance.

Figure 30.- Continued. (b) Continued. External-drag coefficient.

Figure 30.- Continued. (b) Concluded. External-drag coefficient.

[redacted]

Figure 30.- Continued. (c) $\alpha = 4^{\circ}$, $\delta_R = 18.5^{\circ}$, $\delta_L = 1.0^{\circ}$, $A_{ref}/A_{th} = 0.9325$; inlet performance.

Figure 30.- Continued. (c) Continued. Inlet performance.

Figure 30.- Continued. (c) Continued. External-drag coefficient.

Figure 30.- Continued. (c) Concluded. External-drag coefficient.

Figure 30.- Continued. (d) $\alpha = 6^{\circ}$, $\delta_R = 18.0^{\circ}$, $\delta_L = 1.5^{\circ}$, $A_{ref}/A_{th} = 0.8968$; inlet performance.

Figure 30.- Continued. (d) Continued. Inlet performance.

Figure 30.- Continued. (d) Continued. External-drag coefficient.

Figure 30.- Concluded. (d) Concluded. External-drag coefficient.

Figure 31.- Effect of variation of bleed-exit configuration on inlet performance and external-drag coefficient; $M = 2.76$, $\beta = 0^{\circ}$. Configuration: nose 1, diverter 2, porosity 5. (a) $\alpha = 0^{\circ}$, $\delta_R = 18.5^{\circ}$, $\delta_L = 0.5^{\circ}$, $A_{ref}/A_{th} = 1.0968$; inlet performance.

Figure 31.- Continued. (a) Continued. Inlet performance.

Figure 31.- Continued. (a) Continued. External-drag coefficient.

Figure 31.- Continued. (a) Concluded. External-drag coefficient.

Figure 31.- Continued. (b) $\alpha = 2^{\circ}$, $\delta_R = 18.5^{\circ}$, $\delta_L = 1.5^{\circ}$, $A_{ref}/A_{th} = 1.0706$; inlet performance.

Figure 31.- Continued. (b) Continued. Inlet performance.

Figure 31.- Continued. (b) Continued. External-drag coefficient.

Figure 31.- Continued. (b) Concluded. External-drag coefficient.

Figure 31.- Continued. (c) $\alpha = 4^{\circ}$, $\delta_R = 18.0^{\circ}$, $\delta_L = 3.5^{\circ}$, $A_{ref}/A_{th} = 1.0703$; inlet performance.

Figure 31.- Continued. (c) Continued. Inlet performance.

Figure 31.- Continued. (c) Continued. External-drag coefficient.

Figure 31.- Concluded. (c) Concluded. External-drag coefficient.

Figure 32.- Effect of variation of angle of sideslip on inlet performance; $M = 3.00$. Configuration: nose 1, diverter 2, porosity 1, bleed exit 1. (a) $\alpha = 2^{\circ}$, $\delta_R = 19.5^{\circ}$, $\delta_L = 4.0^{\circ}$, $A_{ref}/A_{th} = 1.0930$.

[redacted]

Figure 32.- Continued. (a) Concluded

Figure 32.- Continued. (b) $\alpha = 6^\circ$, $\delta_R = 18.0^\circ$, $\delta_L = 1.5^\circ$, $A_{ref}/A_{th} = 0.8968$.

Figure 32.- Continued. (b) Concluded.

Figure 32.- Continued. (c) $\alpha = 10^\circ$, $\delta_R = 20.0^\circ$, $\delta_L = 4.0^\circ$, $A_{ref}/A_{th} = 0.9792$.

Figure 32.- Concluded. (c) Concluded

Figure 33.- Effect of variation of angle of sideslip on inlet performance; M = 2.76. Configuration: nose 1, diverter 2, porosity 1, bleed exit 1. (a) $\alpha = 2^\circ$, $\delta_R = 18.5^\circ$, $\delta_L = 1.5^\circ$, $A_{ref}/A_{th} = 1.0706$.

Figure 33.- Continued. (a) Concluded.

Figure 33.- Continued. (b) $\alpha = 6^\circ$, $\delta_R = 17.5^\circ$, $\delta_L = 4.0^\circ$, $A_{ref}/A_{th} = 1.0313$.

Figure 33.- Continued. (b) Concluded

Figure 33.- Continued. (c) $\alpha = 10^\circ$, $\delta_R = 17.0^\circ$, $\delta_L = 7.5^\circ$, $A_{ref}/A_{th} = 1.0624$.

Figure 33.- Concluded. (c) Concluded.

Figure 34.- Effect of variation of angle of sideslip on inlet performance and external-drag coefficient; M = 3.00, $\alpha = 2^\circ$, $\delta_R = 19.5^\circ$, $\delta_L = 4.0^\circ$, $A_{ref}/A_{th} = 1.0930$. Configuration: nose 2, diverter 2, porosity 5, bleed exit 6. (a) Inlet performance.

Figure 34.- Continued. (b) External-drag coefficient.

Figure 34.- Continued (c) Inlet performance.

Figure 34.- Concluded. (d) External-drag coefficient.

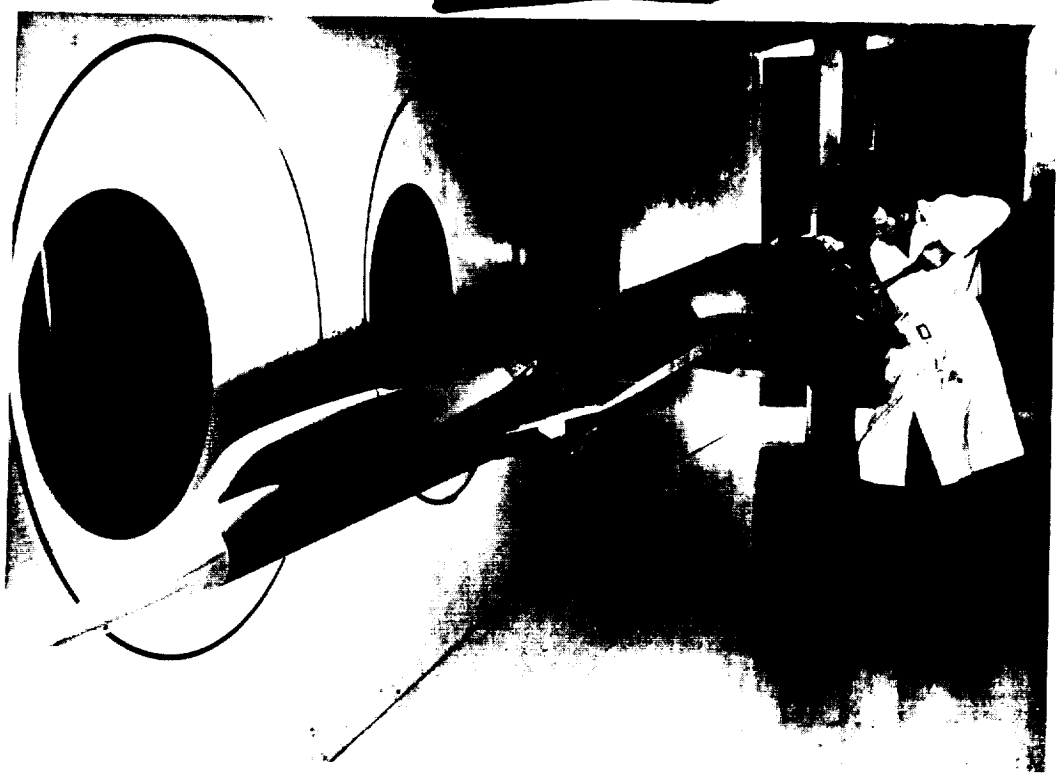

A-24570

(a) Upper view.

A-24572

(b) Lower view.

Figure 1.- Photographs of the model installed in the wind tunnel.

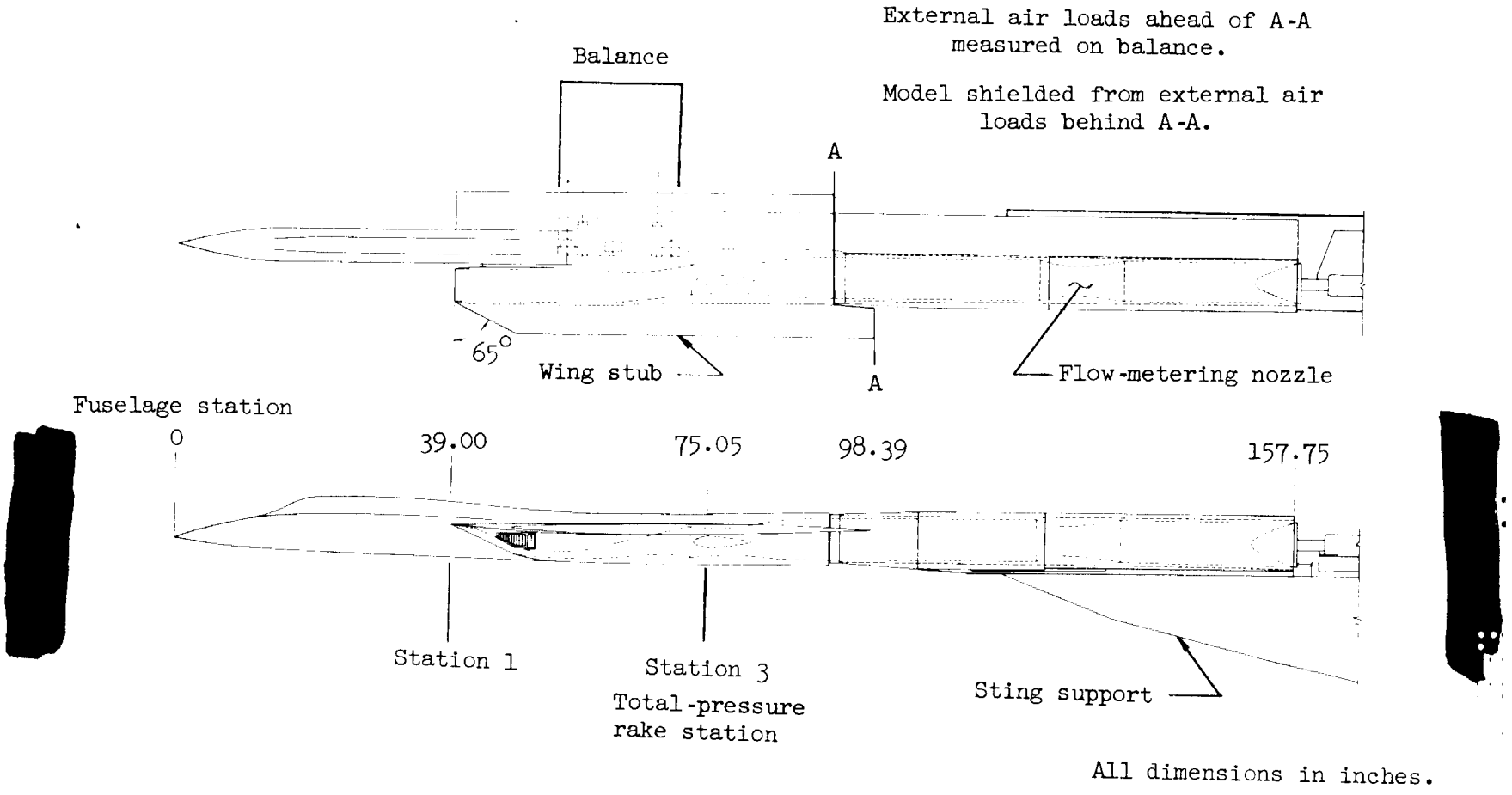

(a) Model drawing.

Figure 2.- Model details.

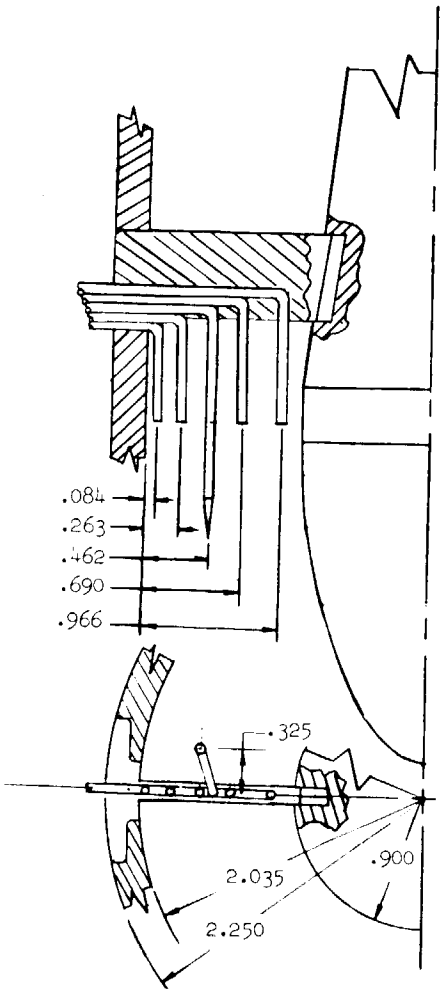

Typical rake installation
All dimensions in inches.

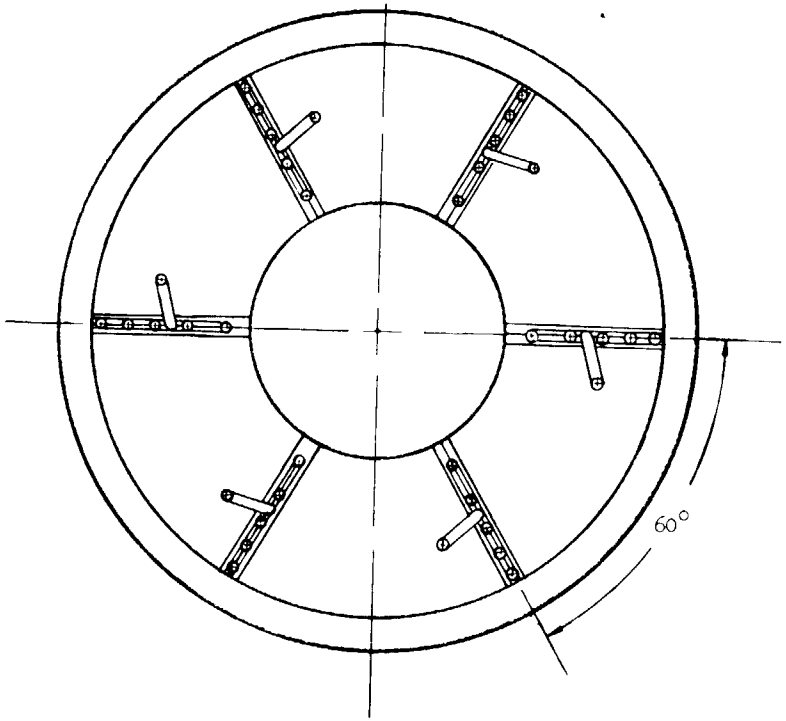

Downstream view of total pressure rake

(b) Total-pressure rake.

Figure 2.- Concluded.

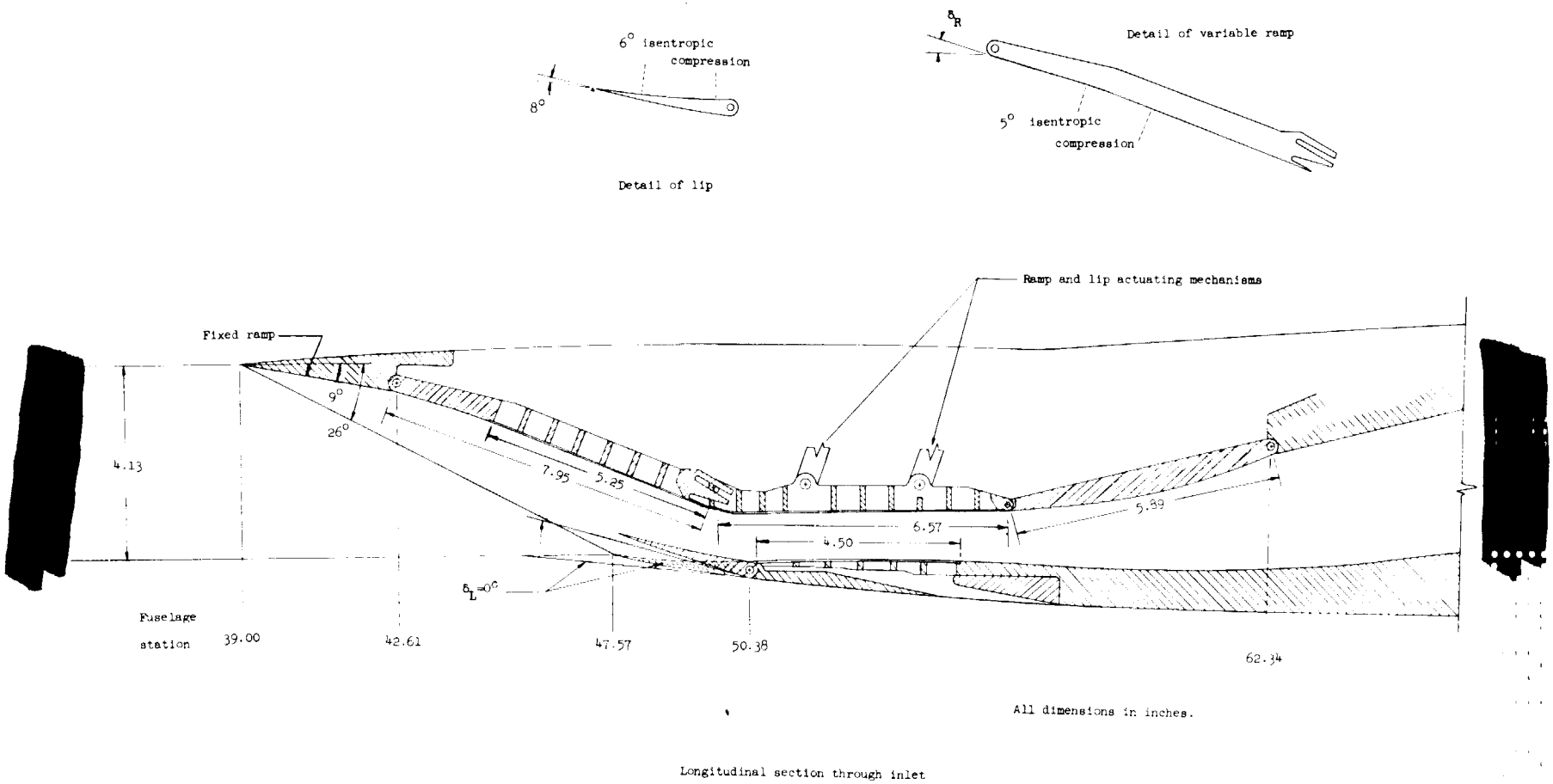

Figure 3.- Schematic drawing of inlet geometry details.

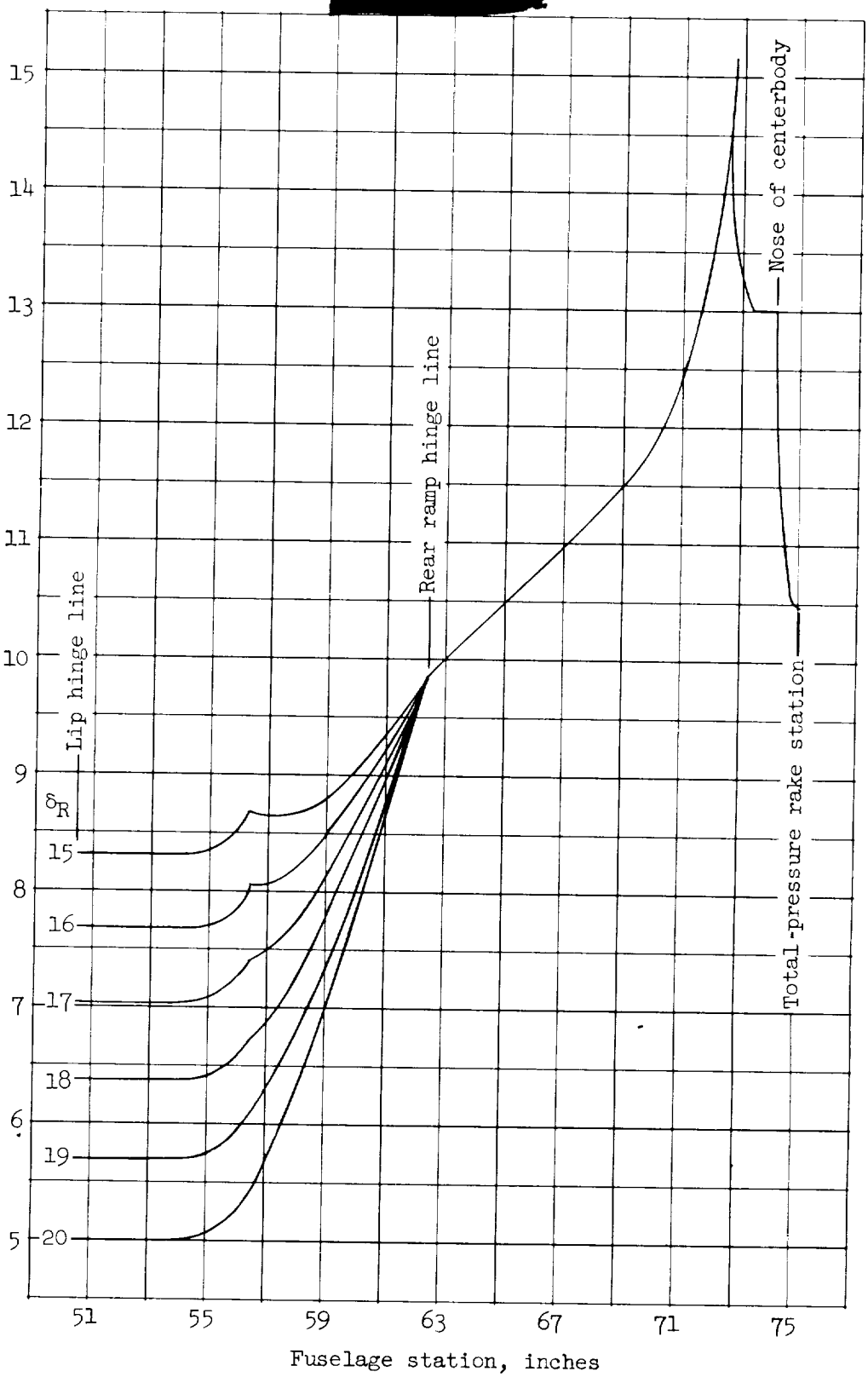

Figure 4.- Variation of duct area aft of lip hinge line.

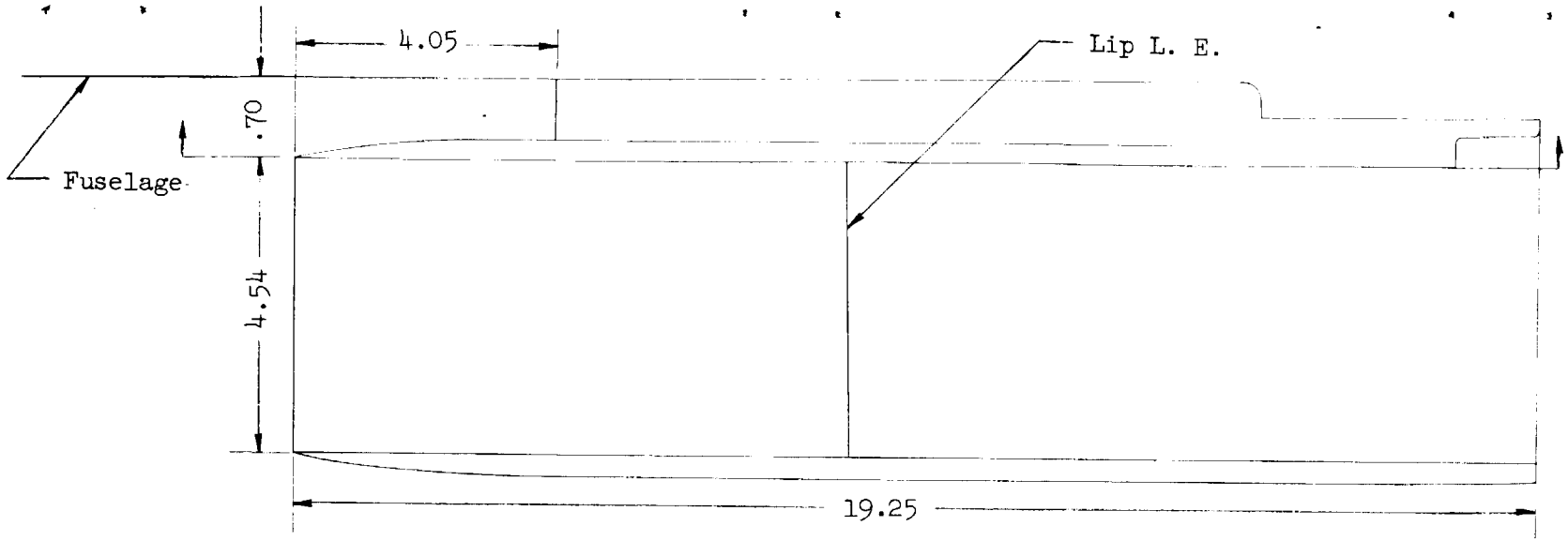

Top view of inlet with upper surface, ramps, removed

All dimensions in inches.

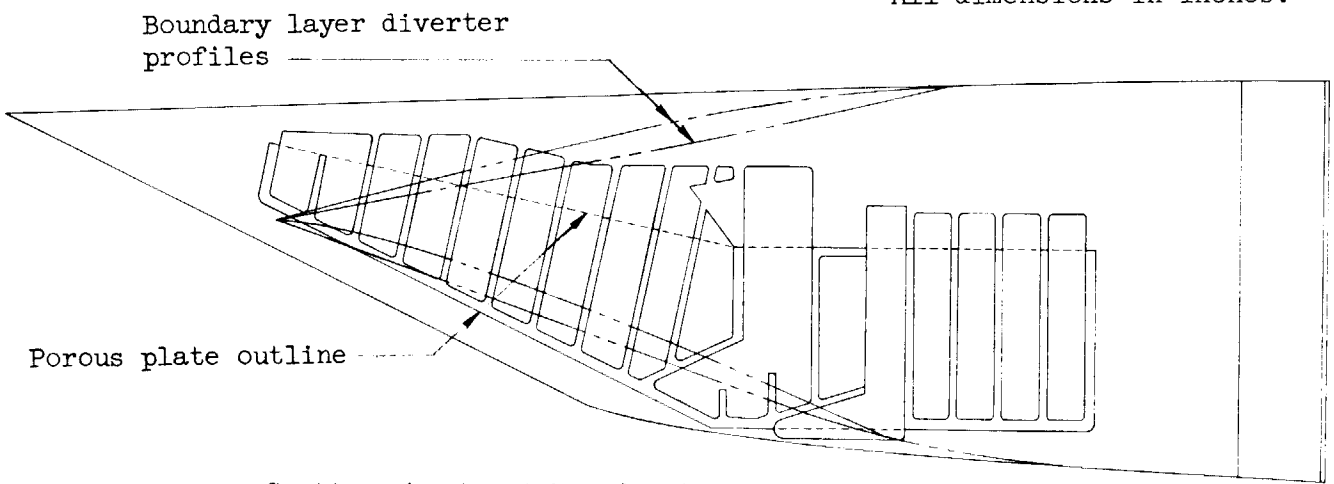

Section showing inboard wall only

(Outboard wall identical)

(a) Sideplates, or walls.

Figure 5.- Porous bleed system construction details.

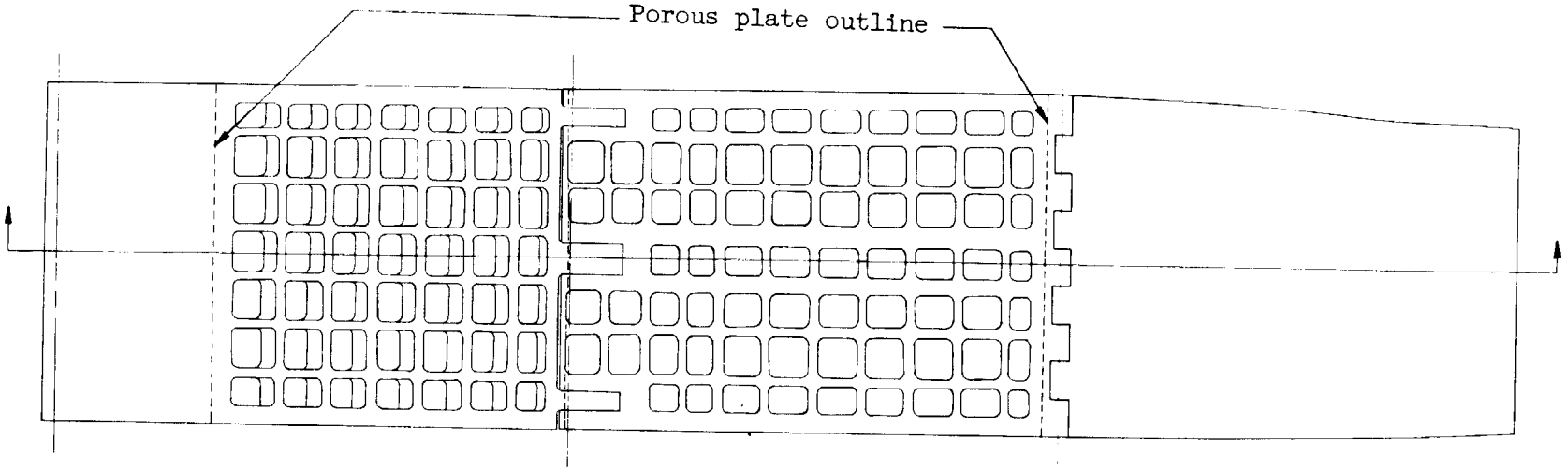

View showing variable ramp and throat assembly only, from the top (or back) side

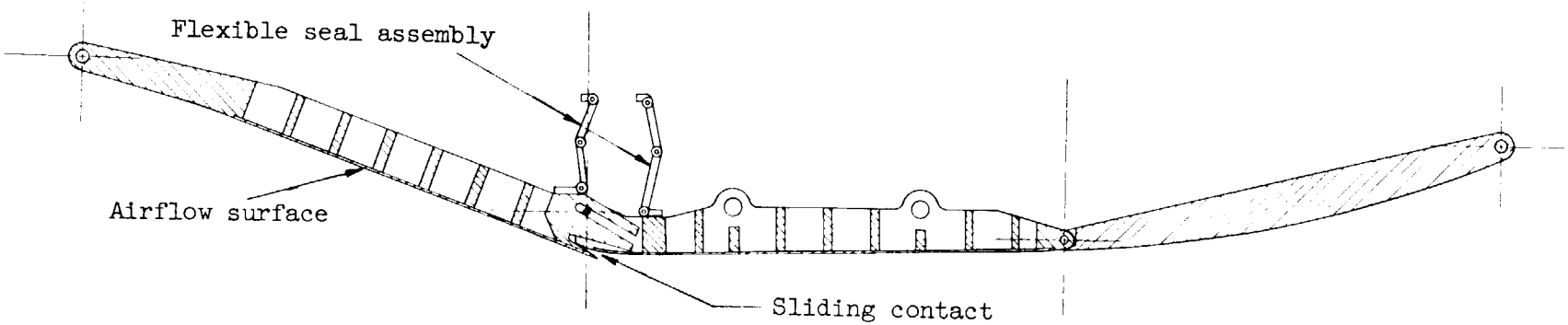

Section view showing location of flexible seal assembly

(b) Ramp and throat assembly.

Figure 5.- Continued.

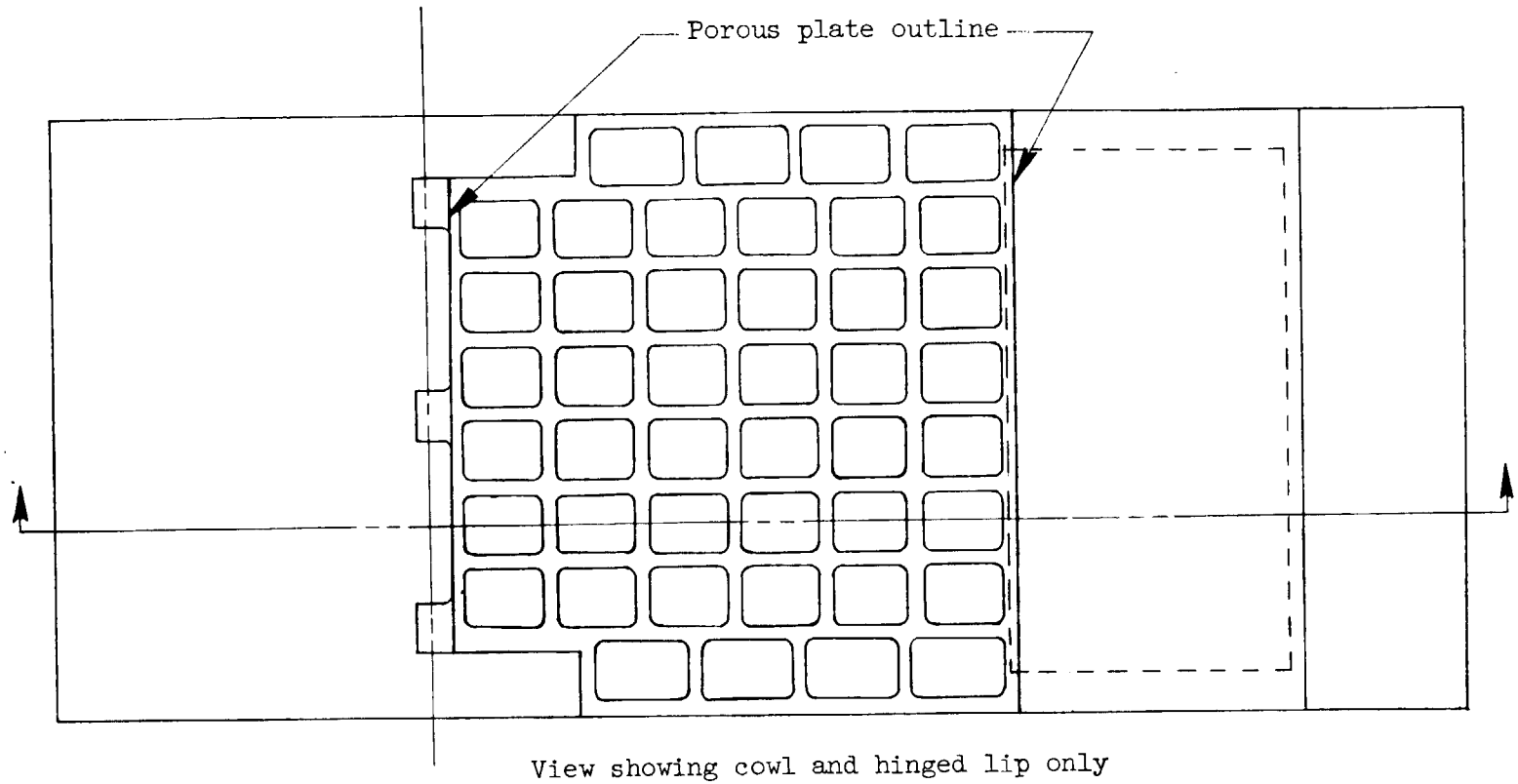

View showing cowl and hinged lip only
(Porous plate removed)

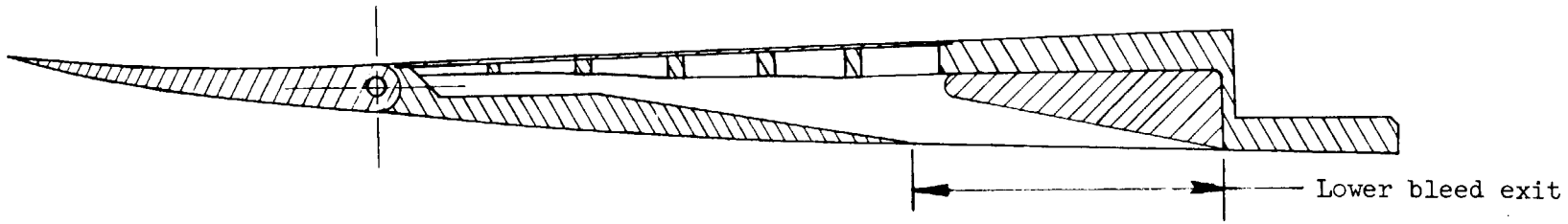

Section view showing lower bleed exit location

(c) Lip and cowl.

Figure 5.- Concluded.

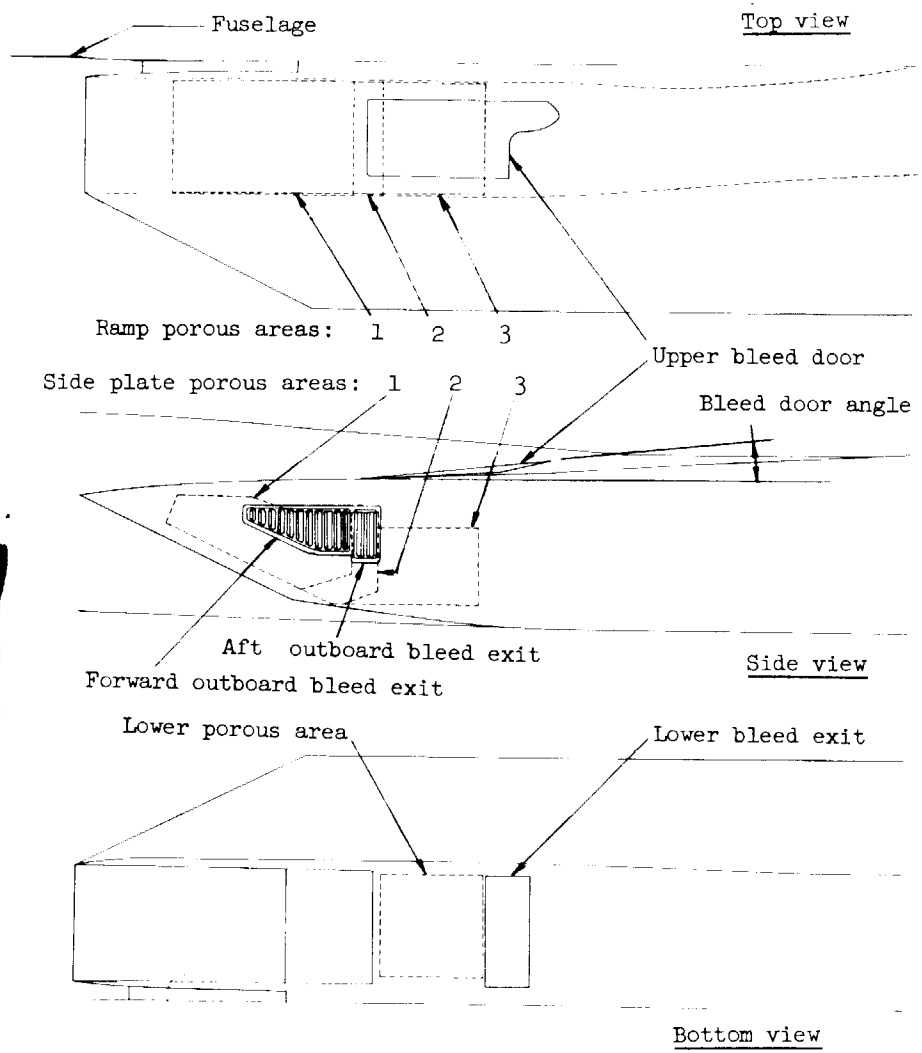

Porous area	Associated bleed exit
Ramp No. 1 Outboard sideplate No. 1 Inboard sideplate No. 1	Forward outboard
Ramp No. 2 Outboard sideplate No. 2 Inboard sideplate No. 2	Aft. outboard
Ramp No. 3 Outboard sideplate No. 3 Inboard sideplate No. 3	Upper door
Lower	Lower

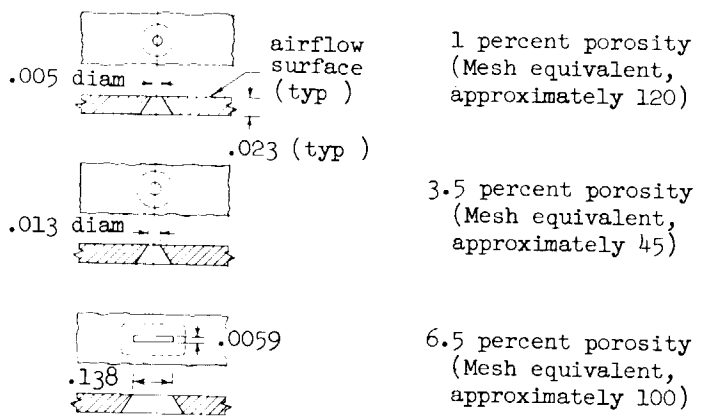

Details of porous plate perforations

Figure 6.- Porous areas and bleed exit details.

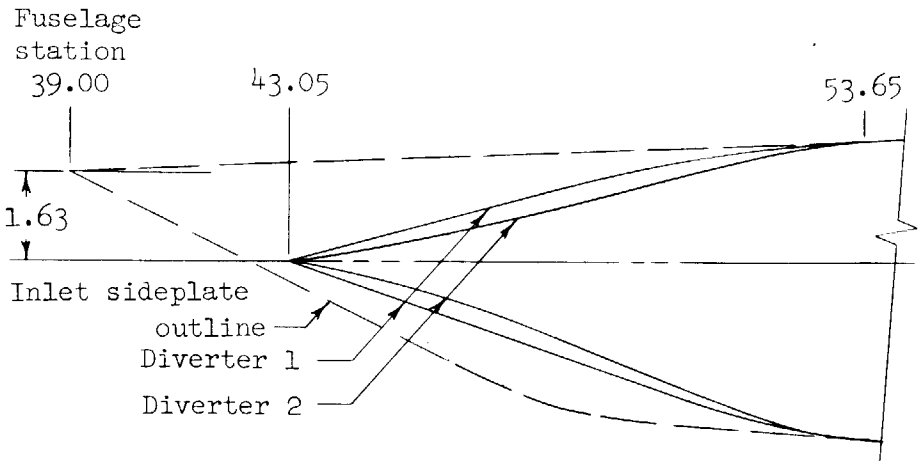

Diverter ordinates

Fuselage station	upper	lower	
43.05	0	0	Diverter 1 (Convex)
48.20	1.38*	-	
50.45	1.87	-2.55*	
52.05	2.08	-3.00	
53.65	2.19	-3.24	
* Profile straight to these points			
43.05	0	0	Diverter 2 (Concave)
46.00	.53	-.67	
48.00	.97	-1.38	
50.00	1.47	-2.13	
52.00	2.00	-2.91	
53.65	2.19	-3.24	

(a) Fuselage-boundary-layer diverters.

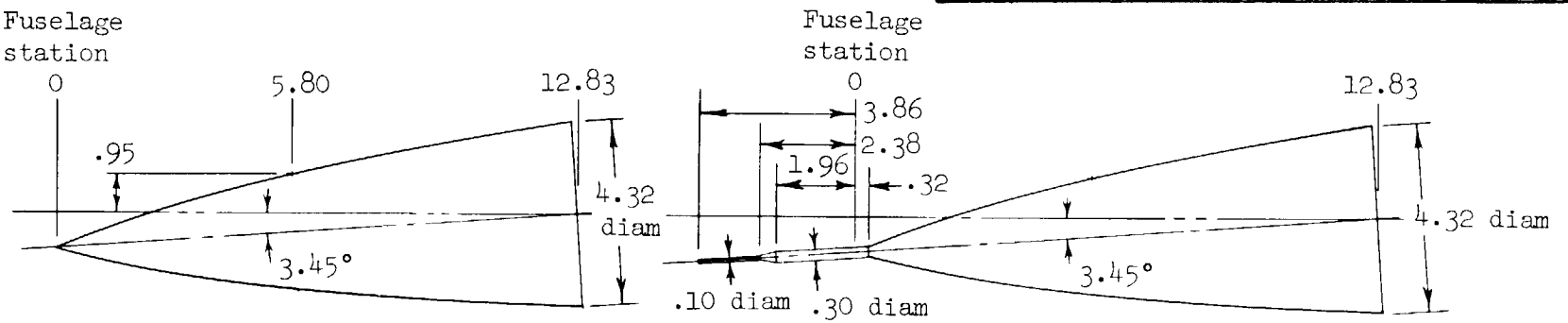

Nose 1

Nose 2

All dimensions in inches.

(b) Nose cones.

Figure 7.- Fuselage-boundary-layer diverter and nose cone details.

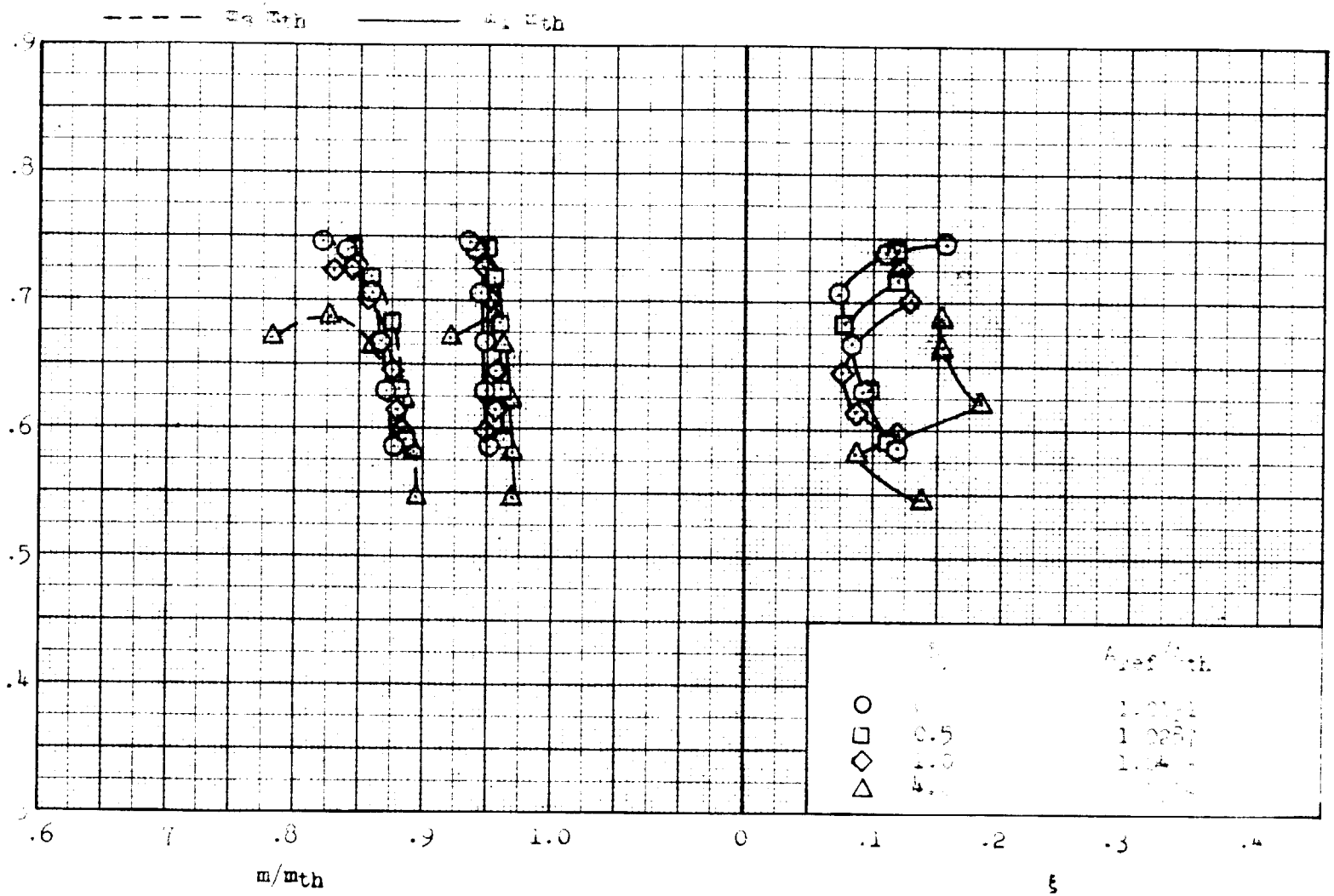

(a) $\delta_R = 19.0°$; inlet performance.

Figure 8.- Effect of lip angle variation on inlet performance and external-drag coefficient; M = 3.00, $\alpha = 0°$, $\beta = 0°$. Configuration: nose 1, diverter 1, porosity 1, bleed exit 1.

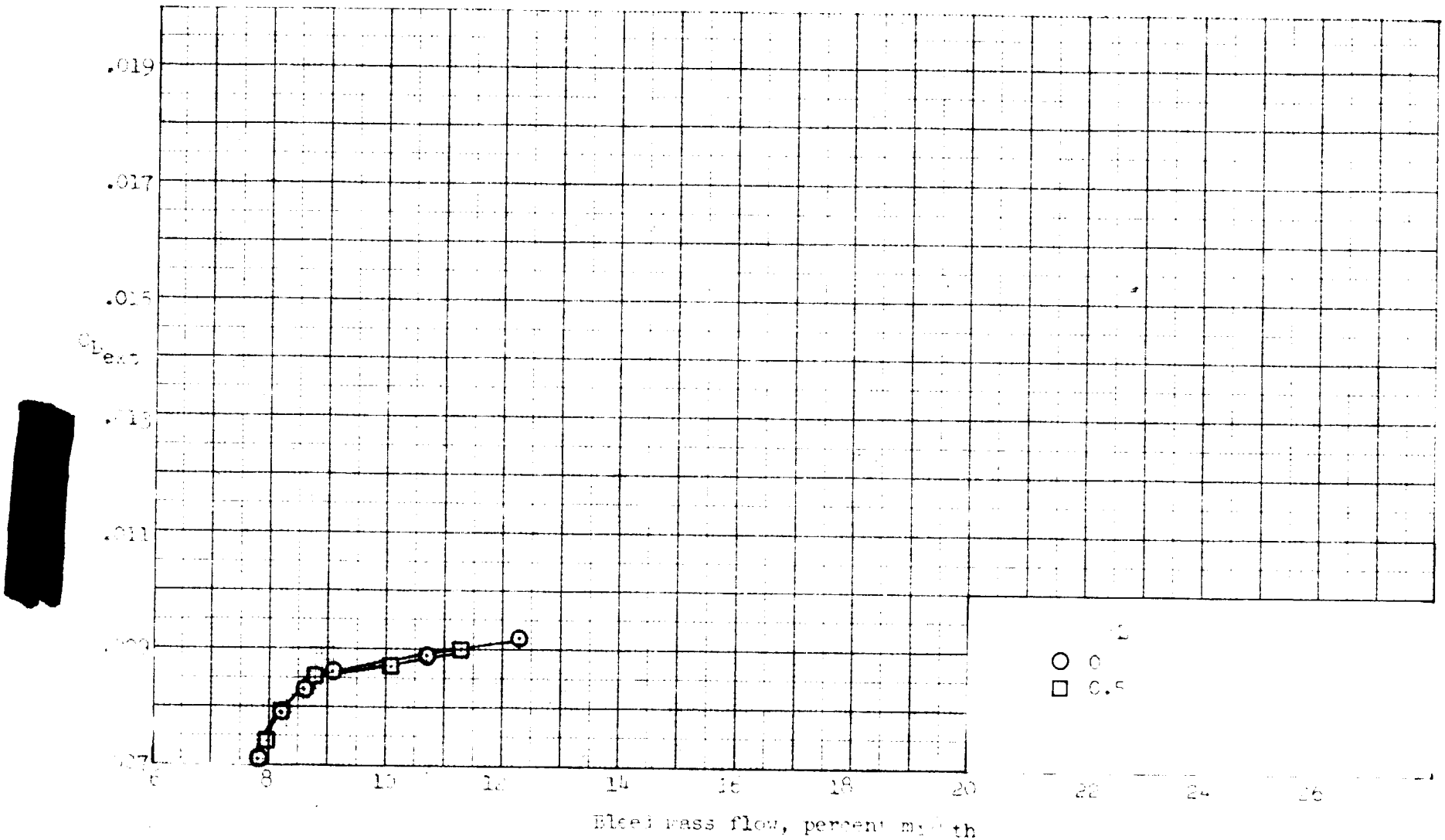

(a) [illegible] = 19.0°; external-drag coefficient.

Figure 8.- Continued.

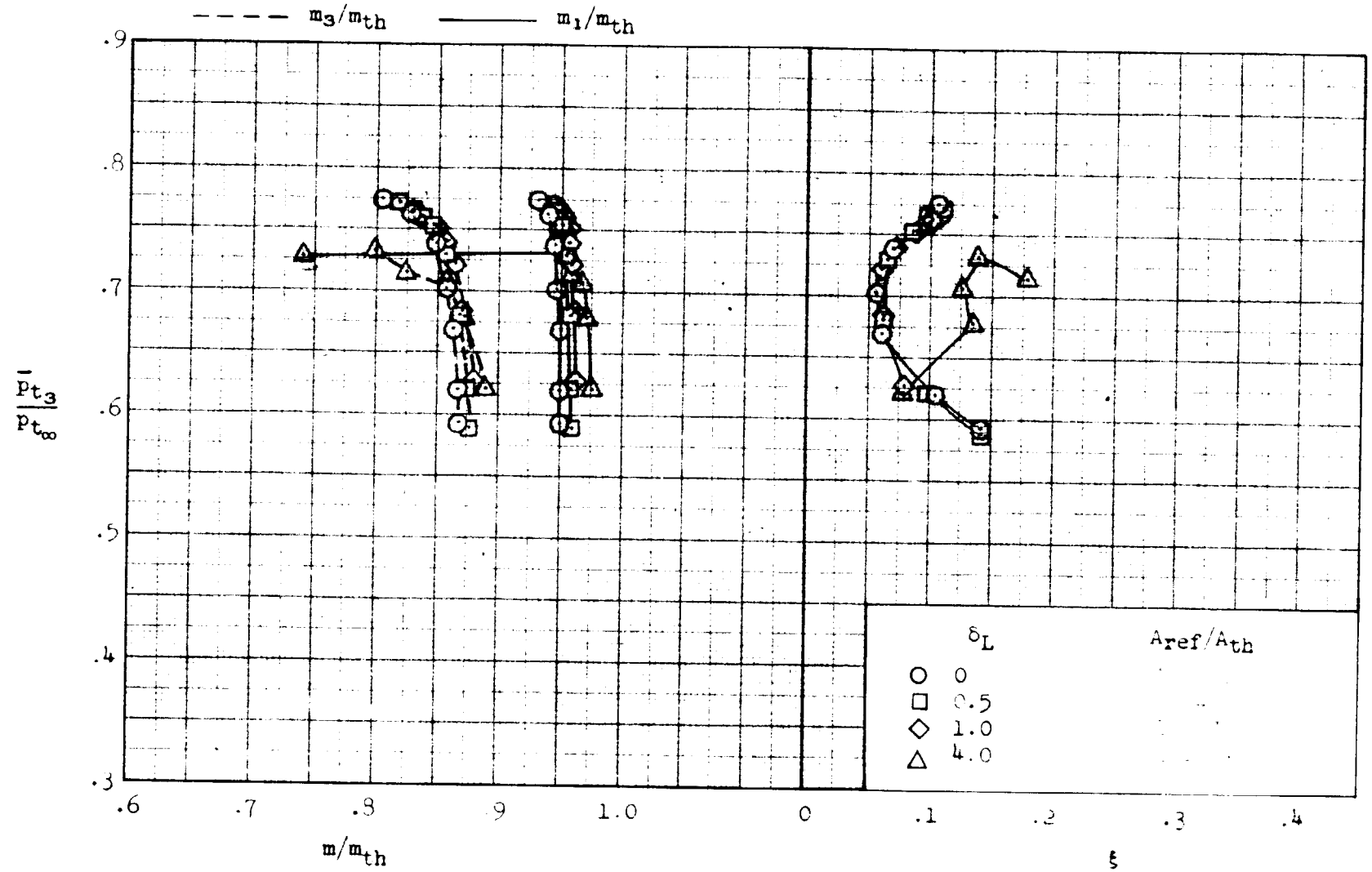

(b) δ_R = 19.6°; inlet performance.

Figure 8.- Continued.

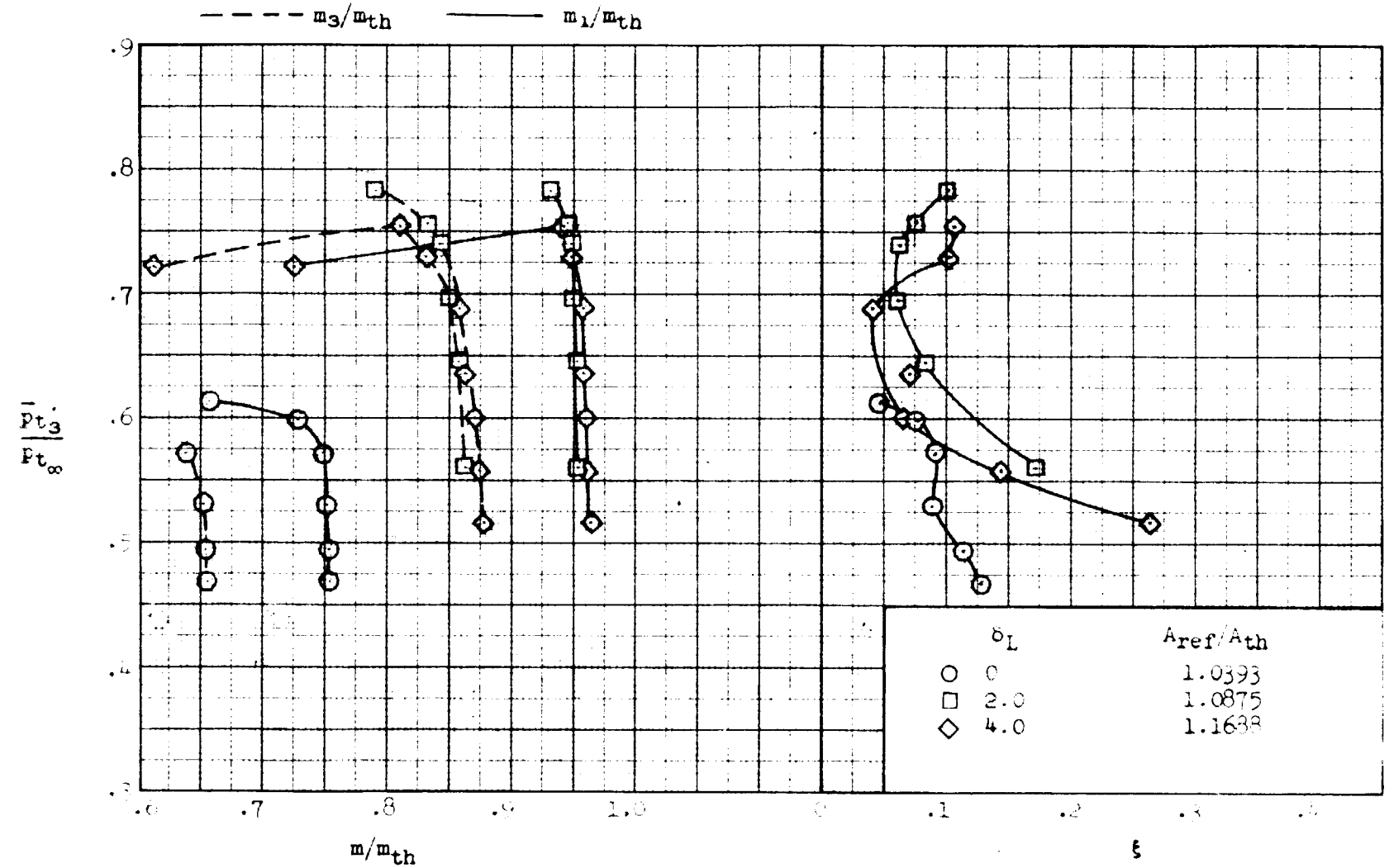

(c) δ_R = 20.0°; inlet performance.

Figure 8.- Continued.

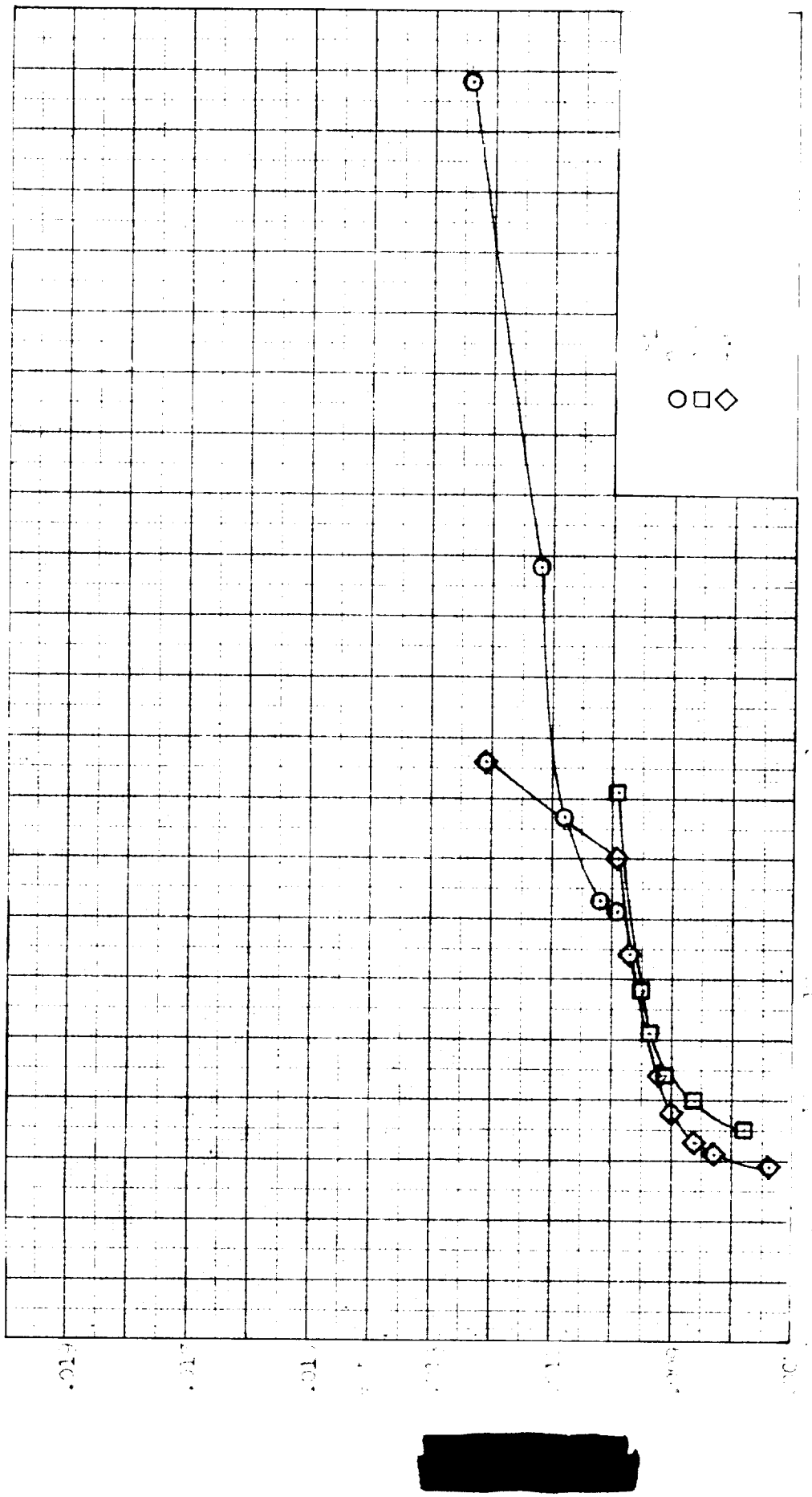

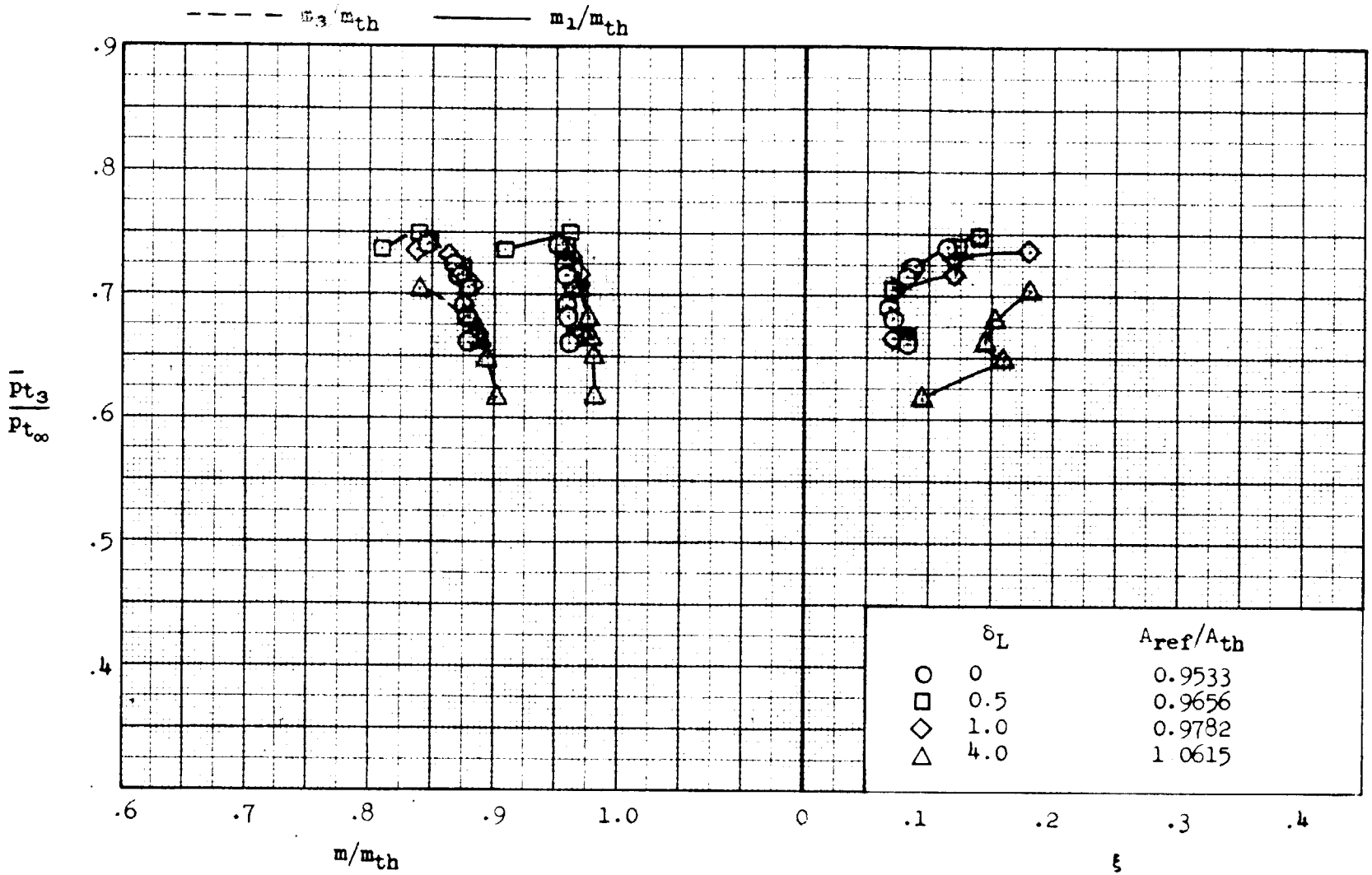

(a) δ_R = 18.5°; inlet performance.

Figure 9.- Effect of lip angle variation on inlet performance and external-drag coefficient; M = 3.00, α = 2°, β = 0°. Configuration: nose 1, diverter 1, porosity 1, bleed exit 1.

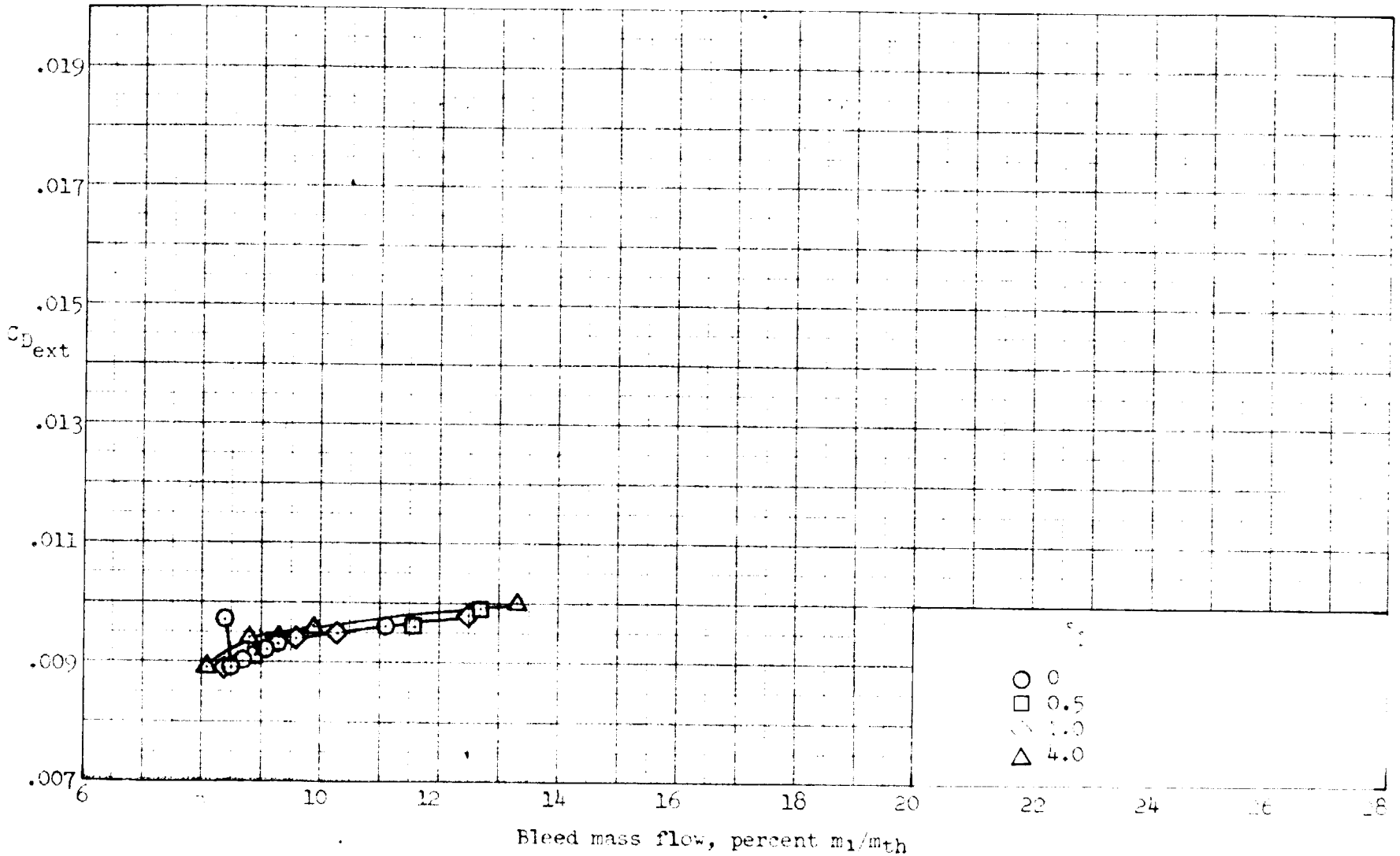

(a) Concluded. α = 18.5°; external-drag coefficient.

Figure 9.- Continued.

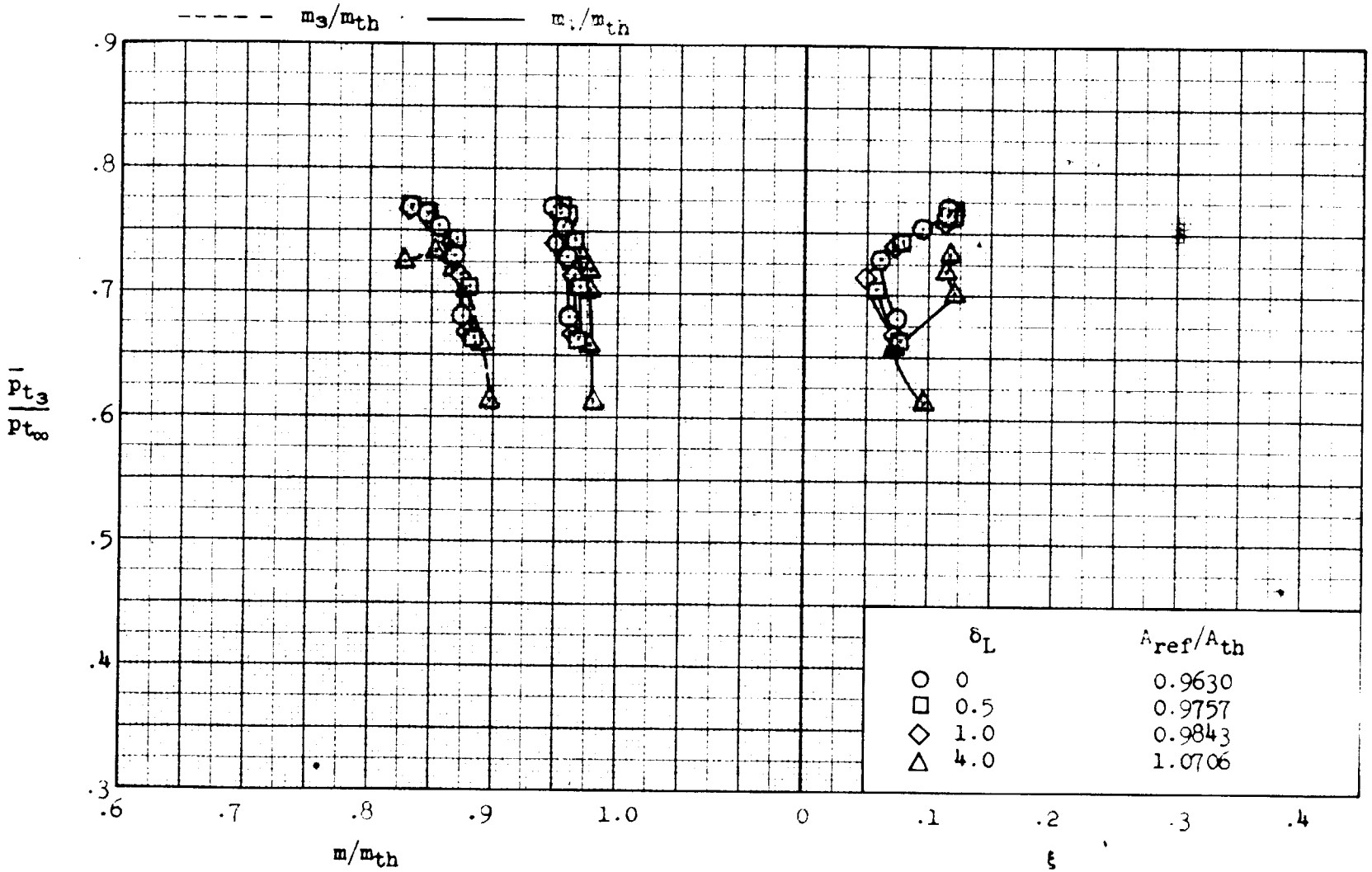

(b) δ_R = 19.0°; inlet performance.

Figure 9.- Continued.

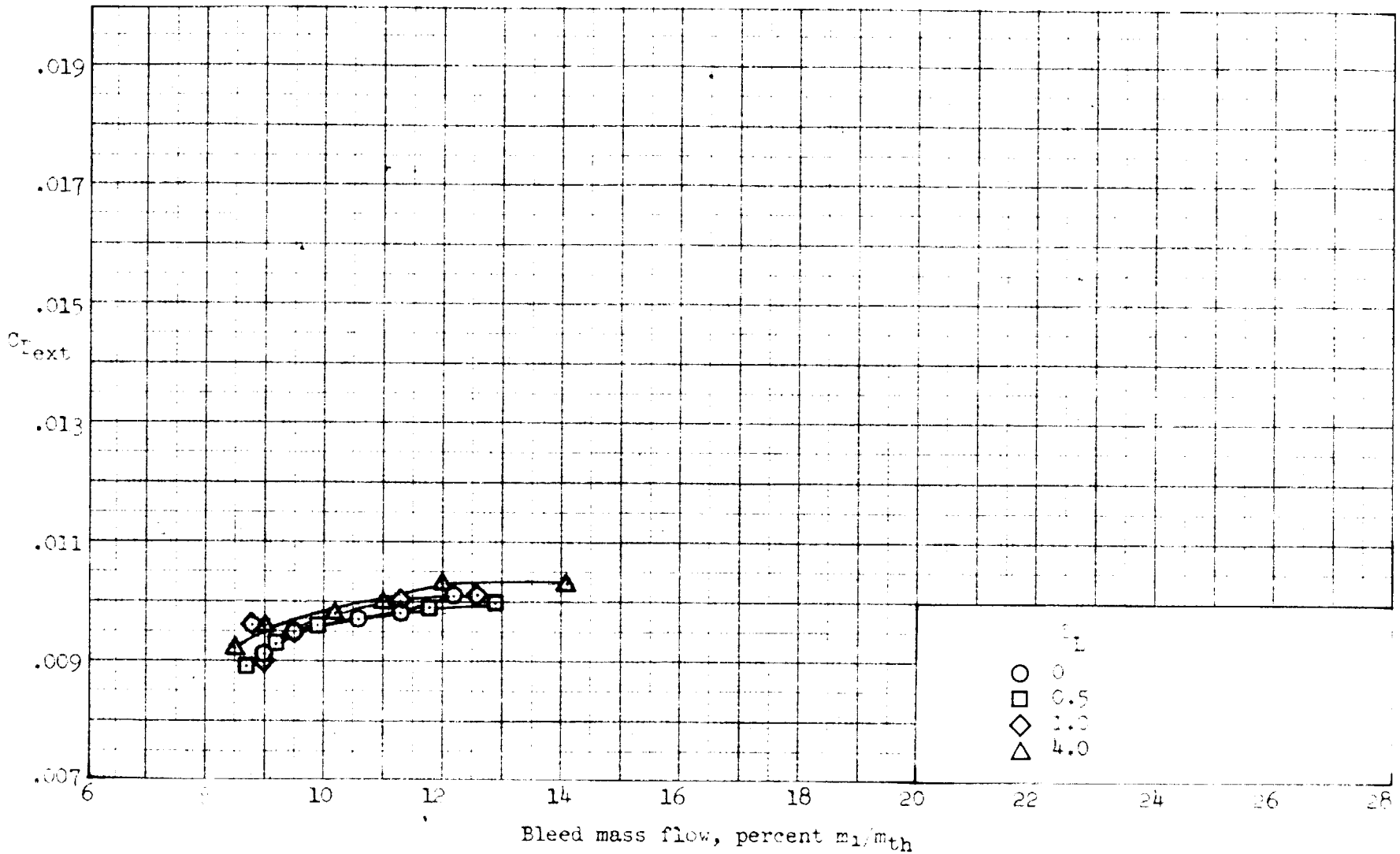

(b) Concluded. i_L = 19.0°; external-drag coefficient.

Figure 9.- Continued.

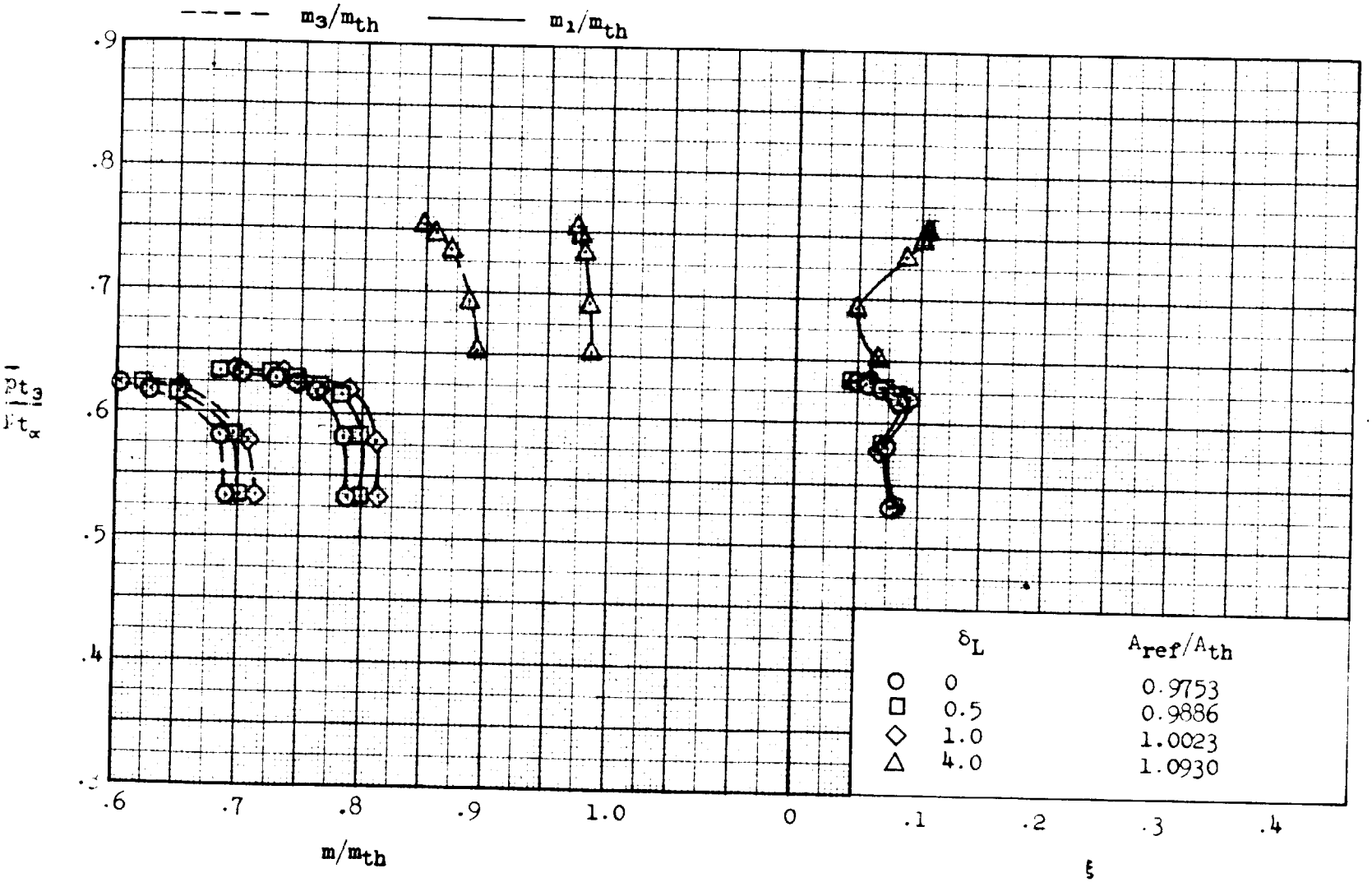

(c) δ_R = 19.5°; inlet performance

Figure 9.- Continued.

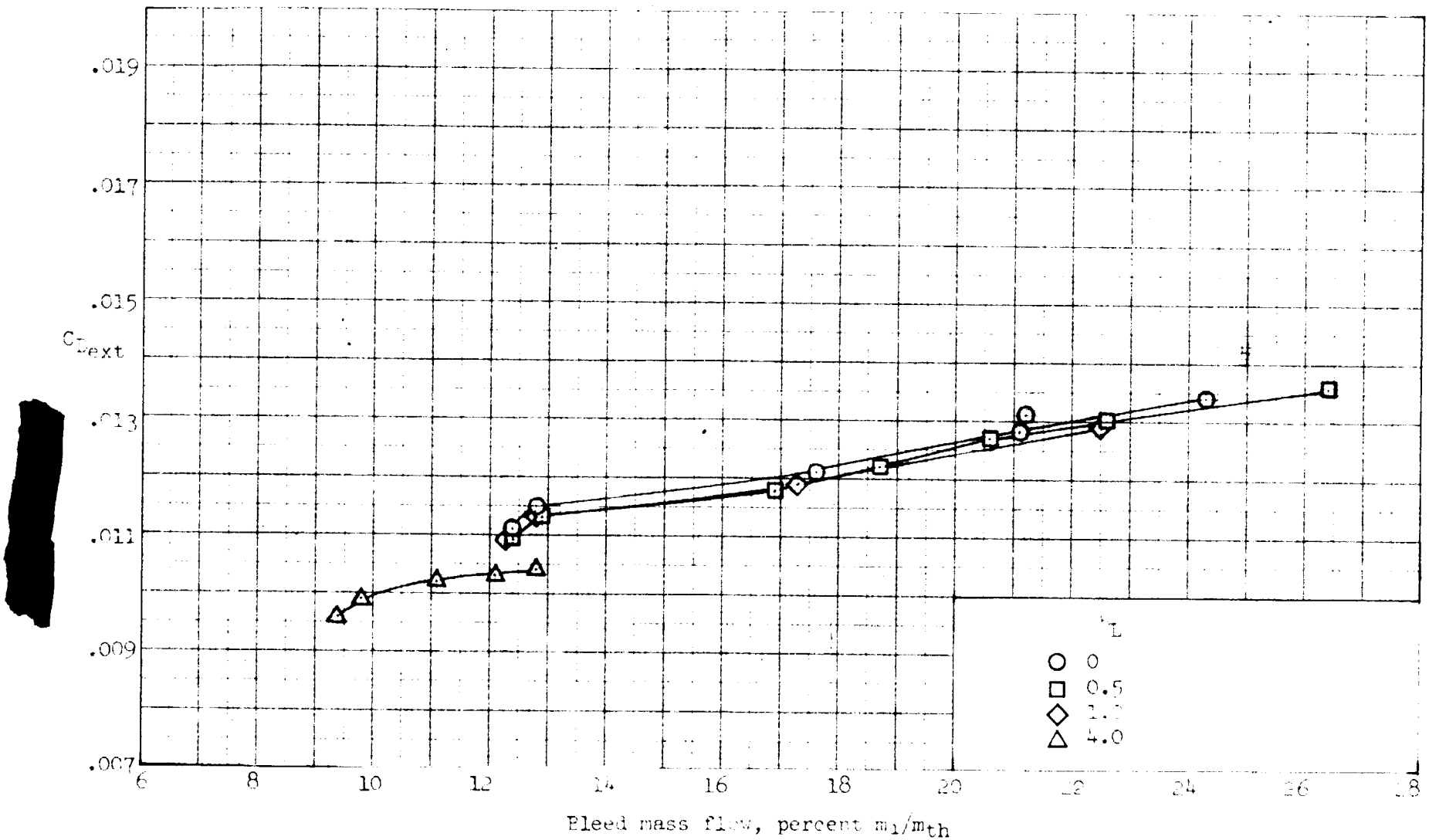

Figure 9.- Concluded.

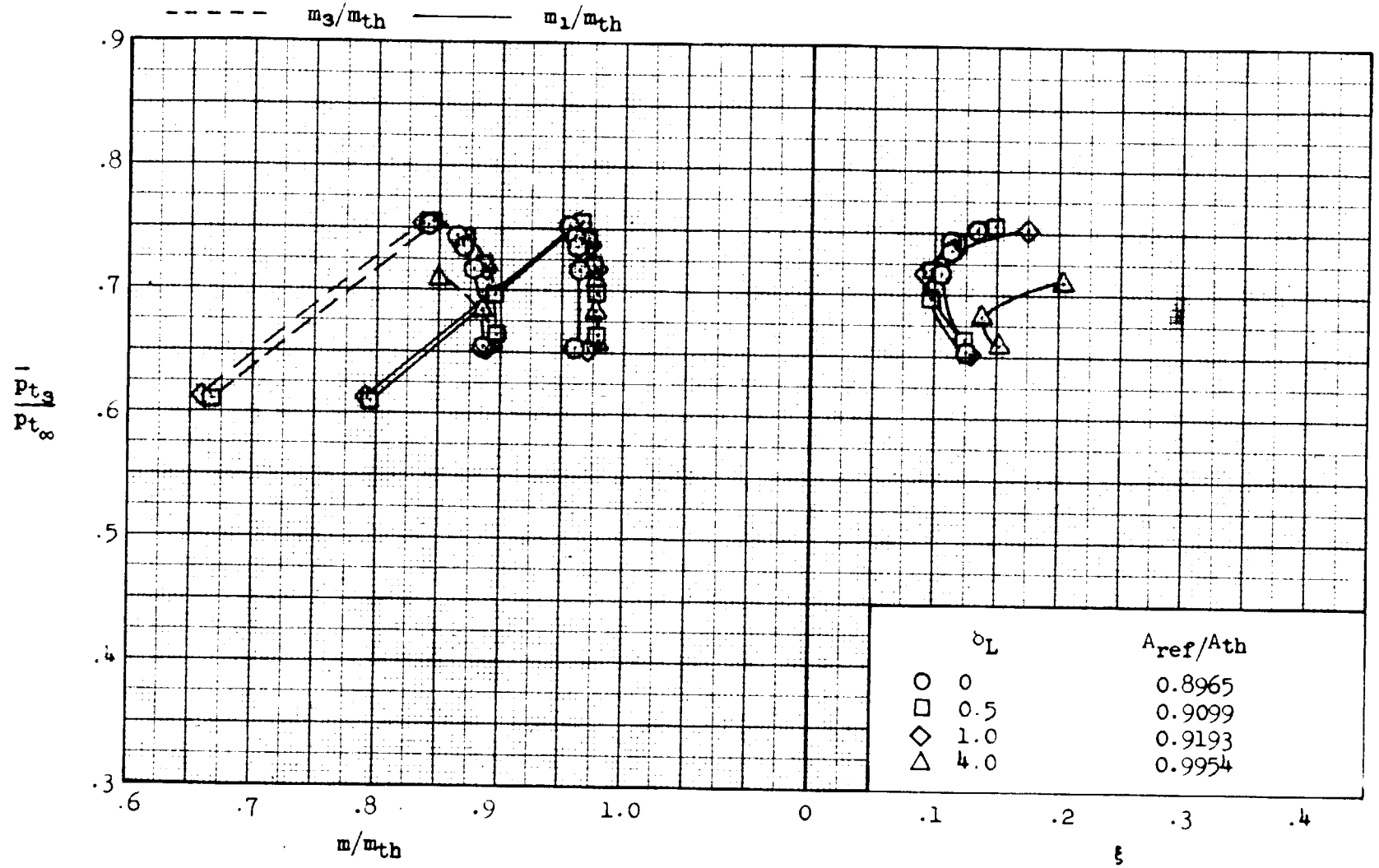

(a) δ_R = 18.0°: inlet performance.

Figure 10.- Effect of lip angle variation on inlet performance and external-drag coefficient; M = 3.0, α = 4°, β = 0°. Configuration: nose 1, diverter 1, porosity 1, bleed exit 1.

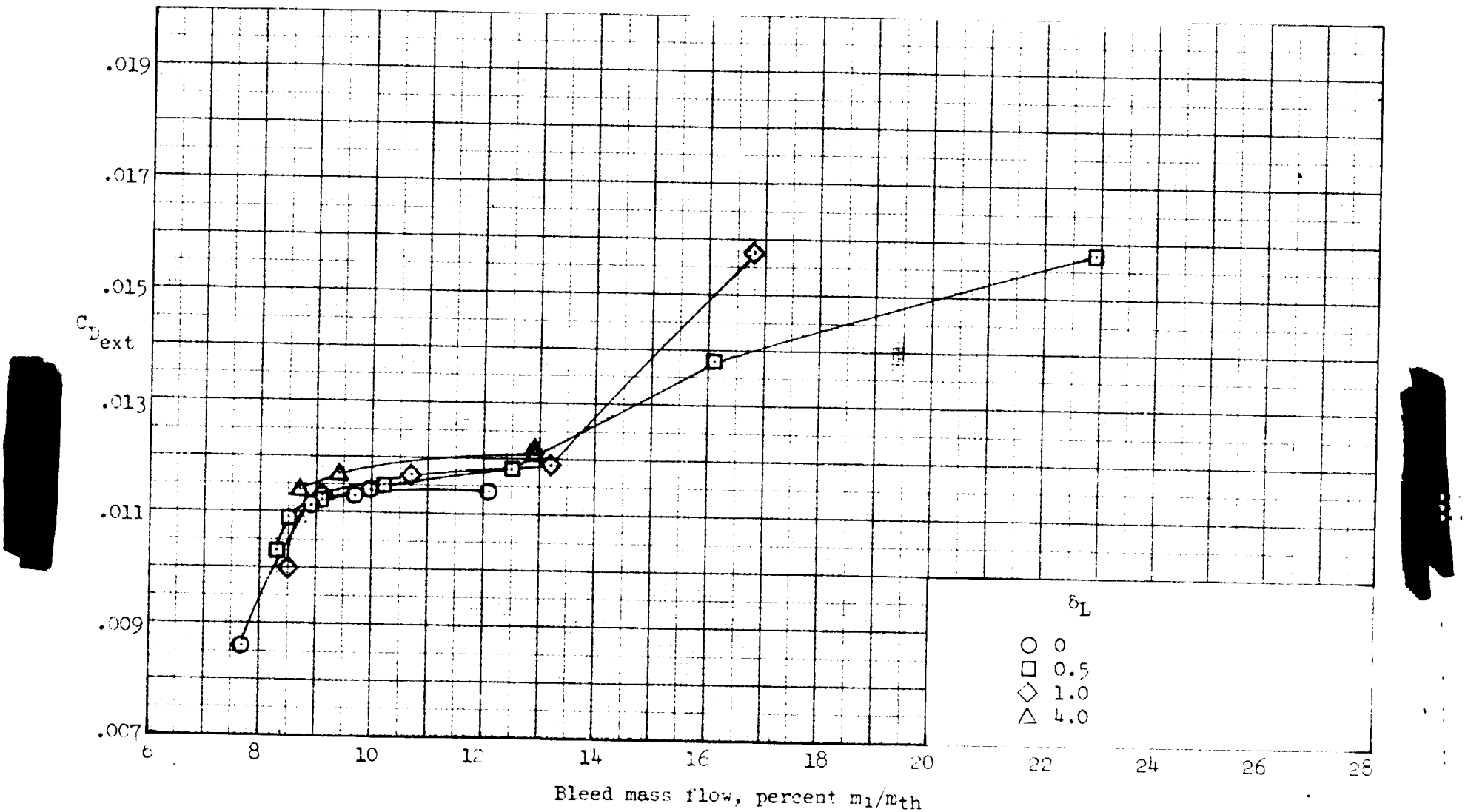

(a) Concluded. δ_R = 18.0°; external-drag coefficient.

Figure 10.- Continued.

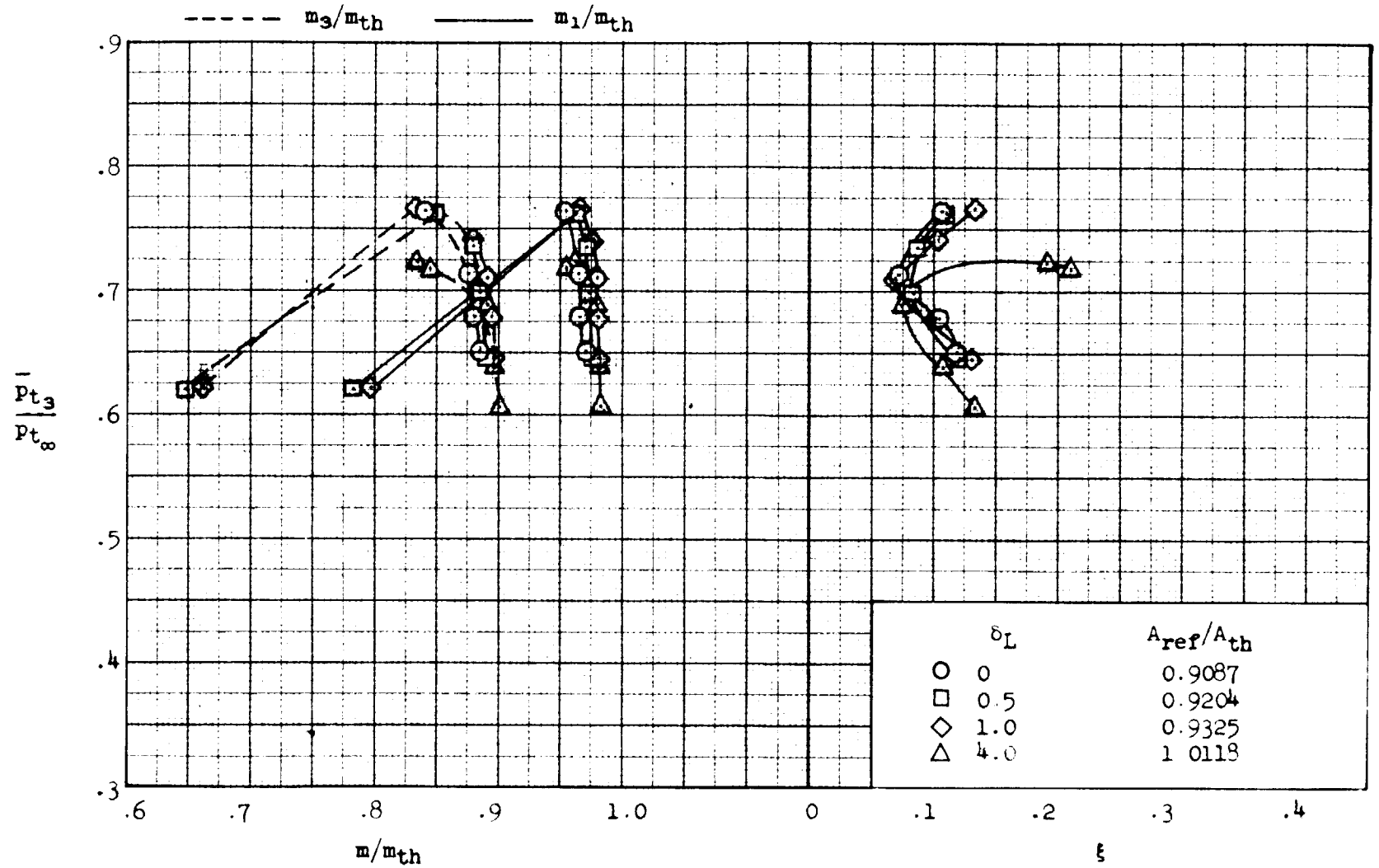

(b) δ_R = 18.5°; inlet performance.

Figure 10.- Continued.

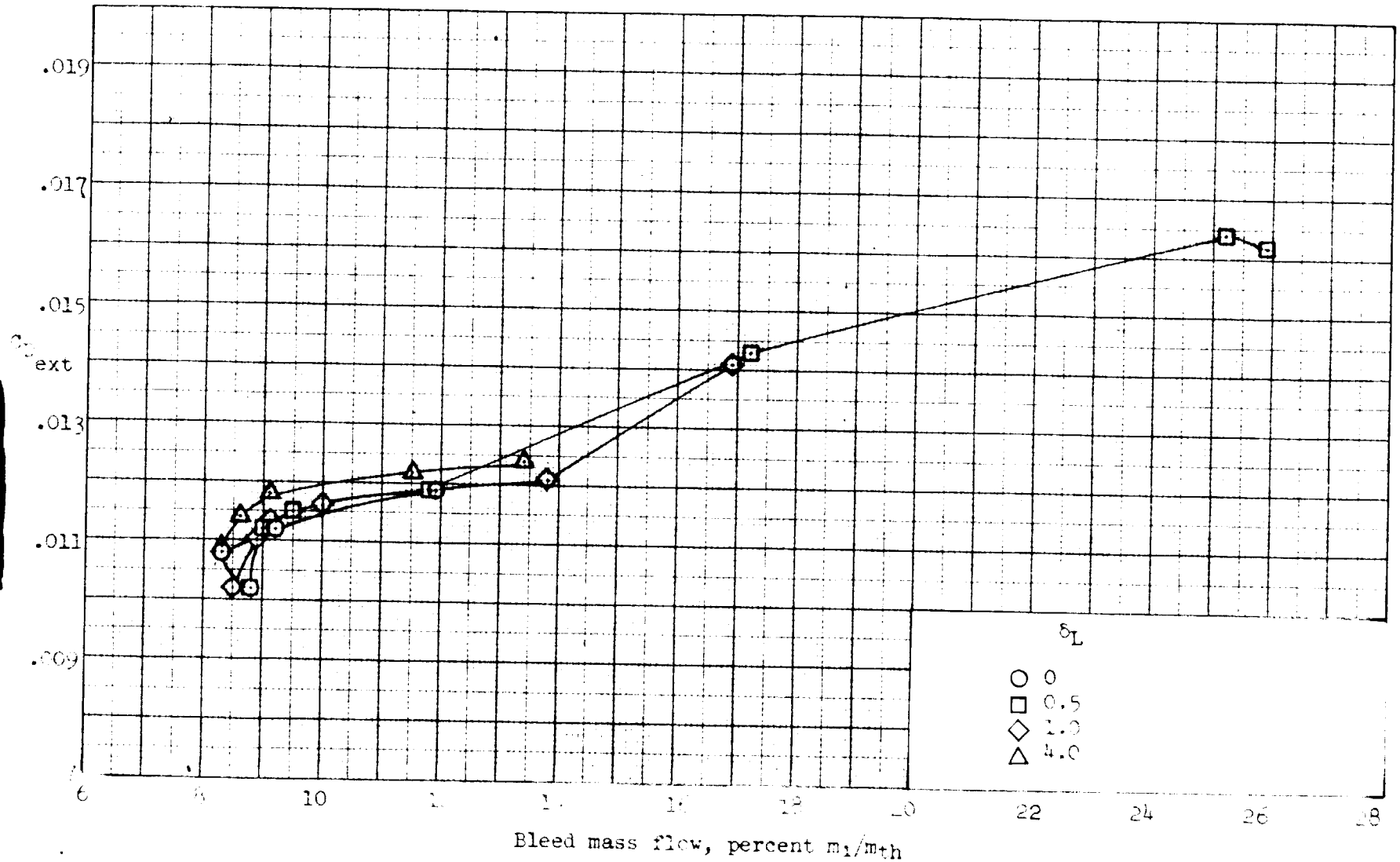

(b) Concluded. δ_R = 18.5°; external-drag coefficient.

Figure 10.- Continued.

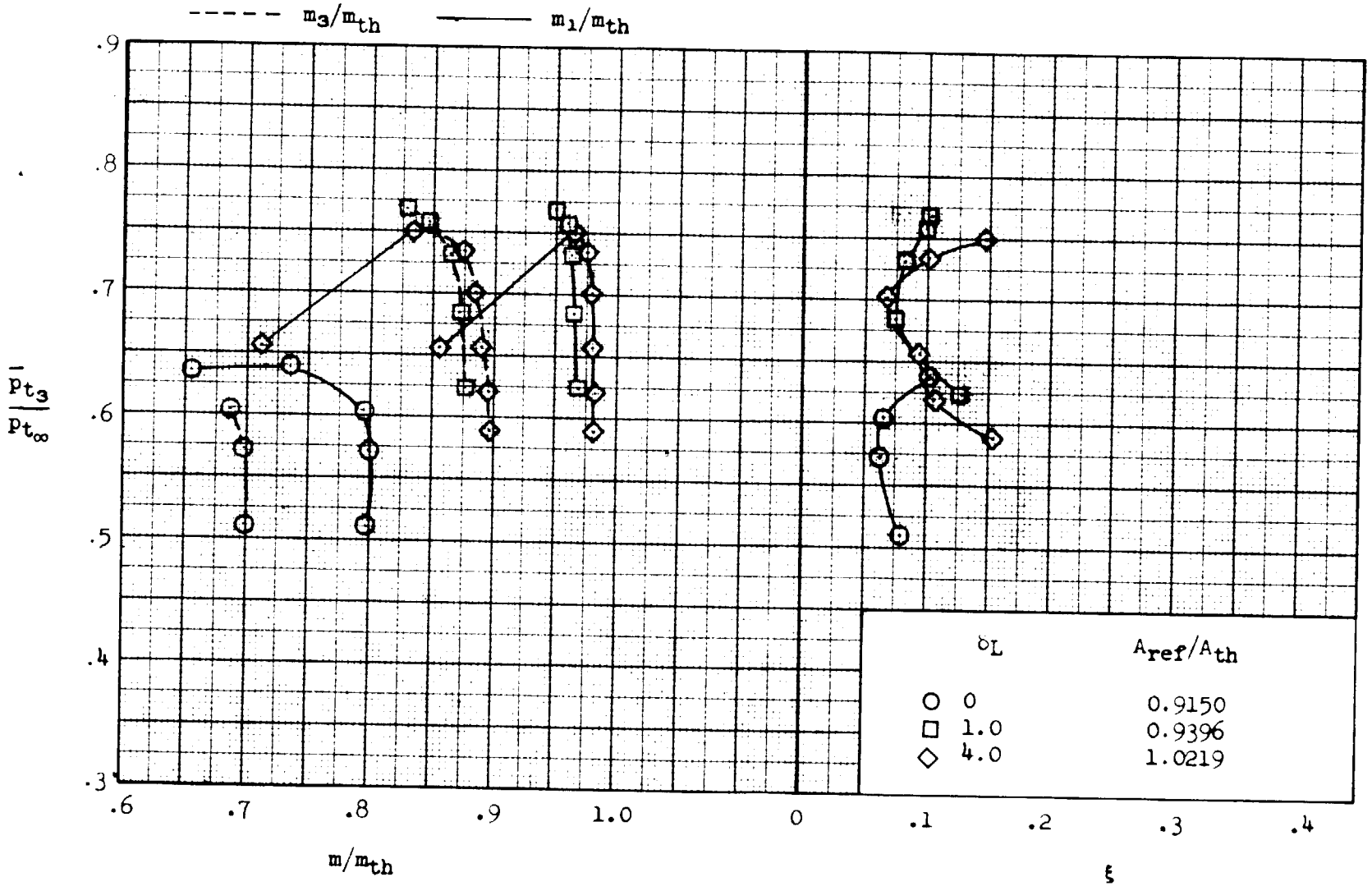

(c) δ_R = 19.0°; inlet performance.

Figure 10.- Continued.

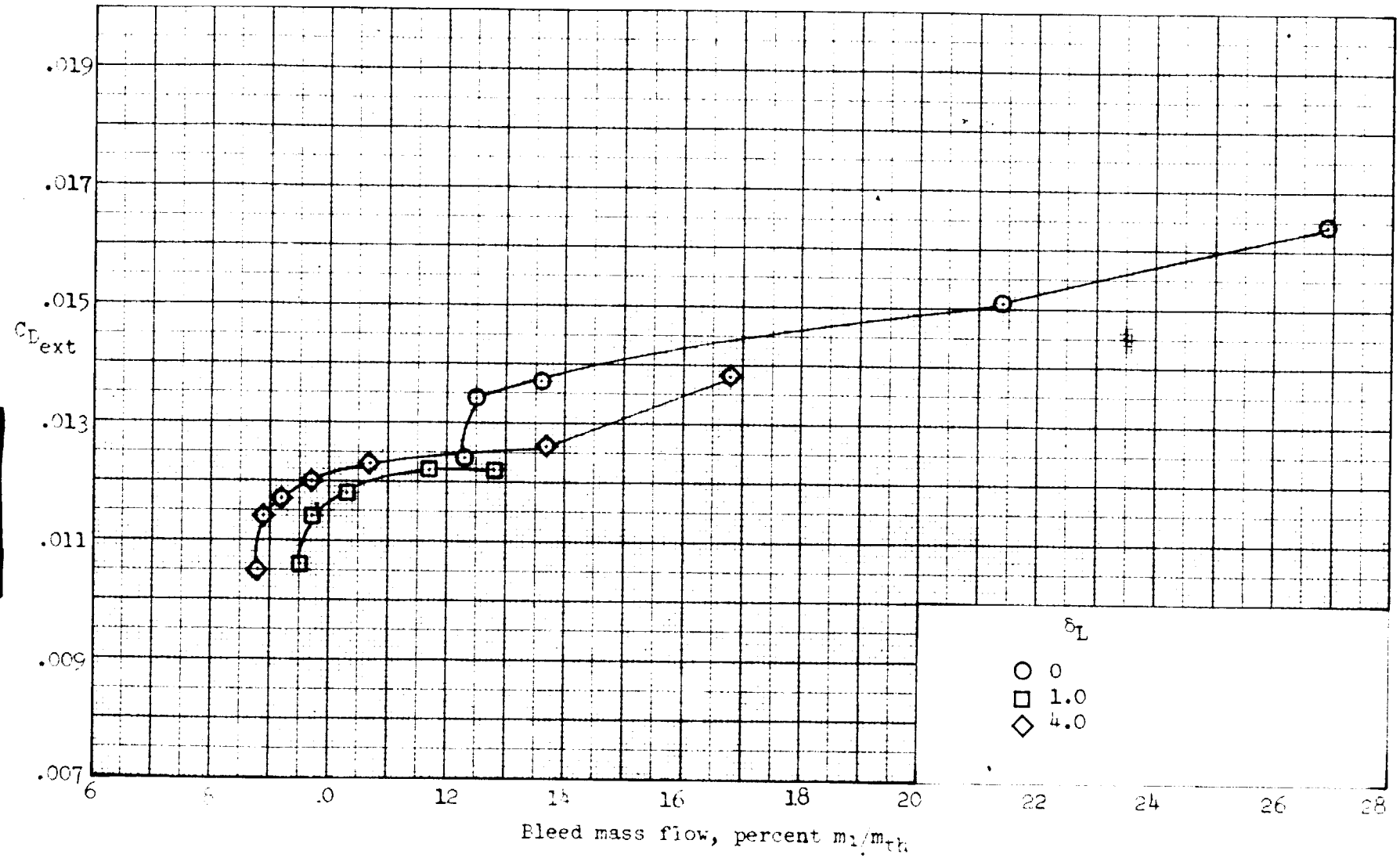

(c) Concluded. δ_R = 19.0°; external-drag coefficient.

Figure 10.- Concluded.

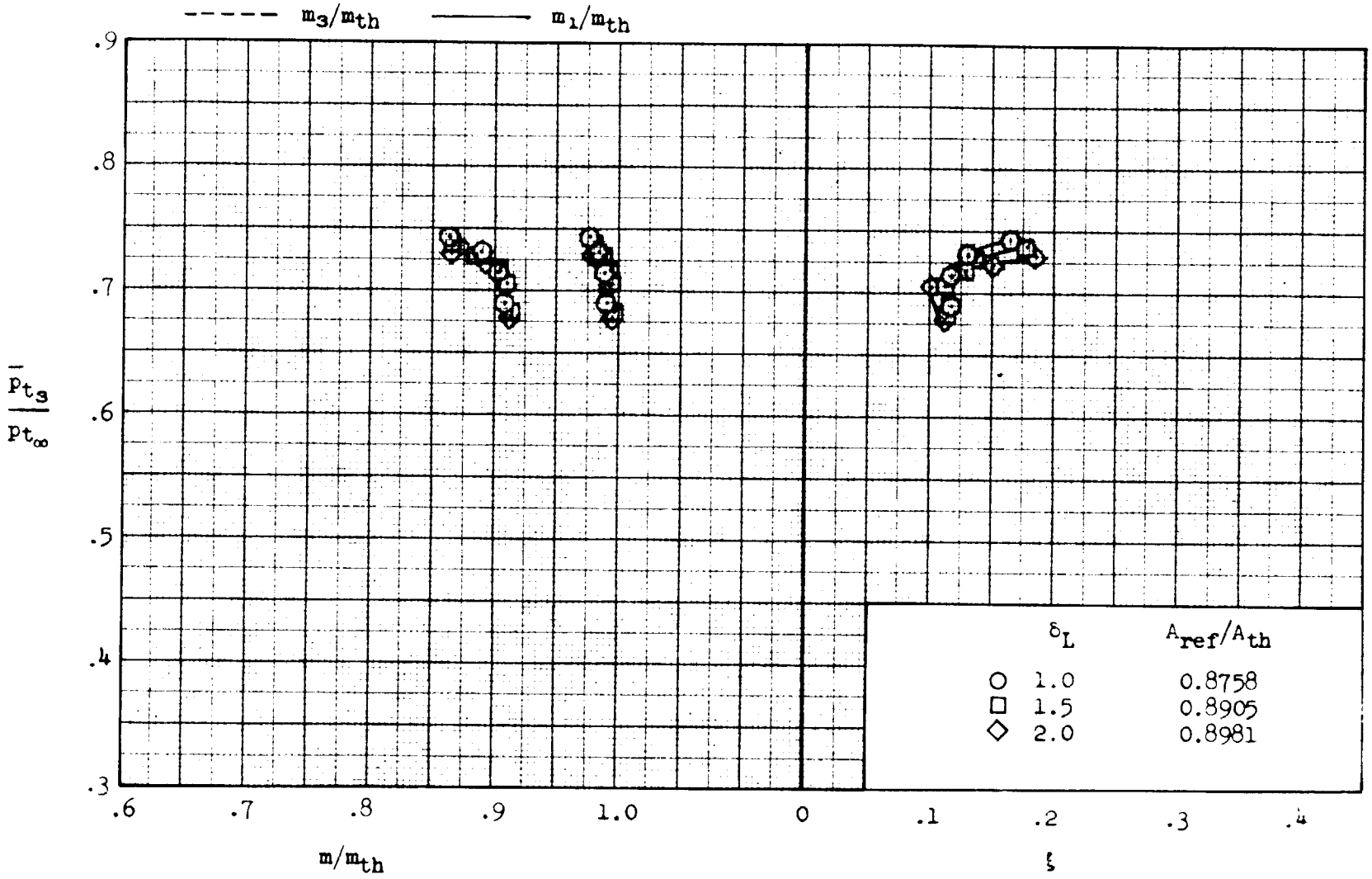

(a) $\delta_R = 17.5°$; inlet performance.

Figure 11.- Effect of lip angle variation on inlet performance and external-drag coefficient; M = 3.00, $\alpha = 6°$, $\beta = 0°$. Configuration: nose 1, diverter 1, porosity 1, bleed exit 1.

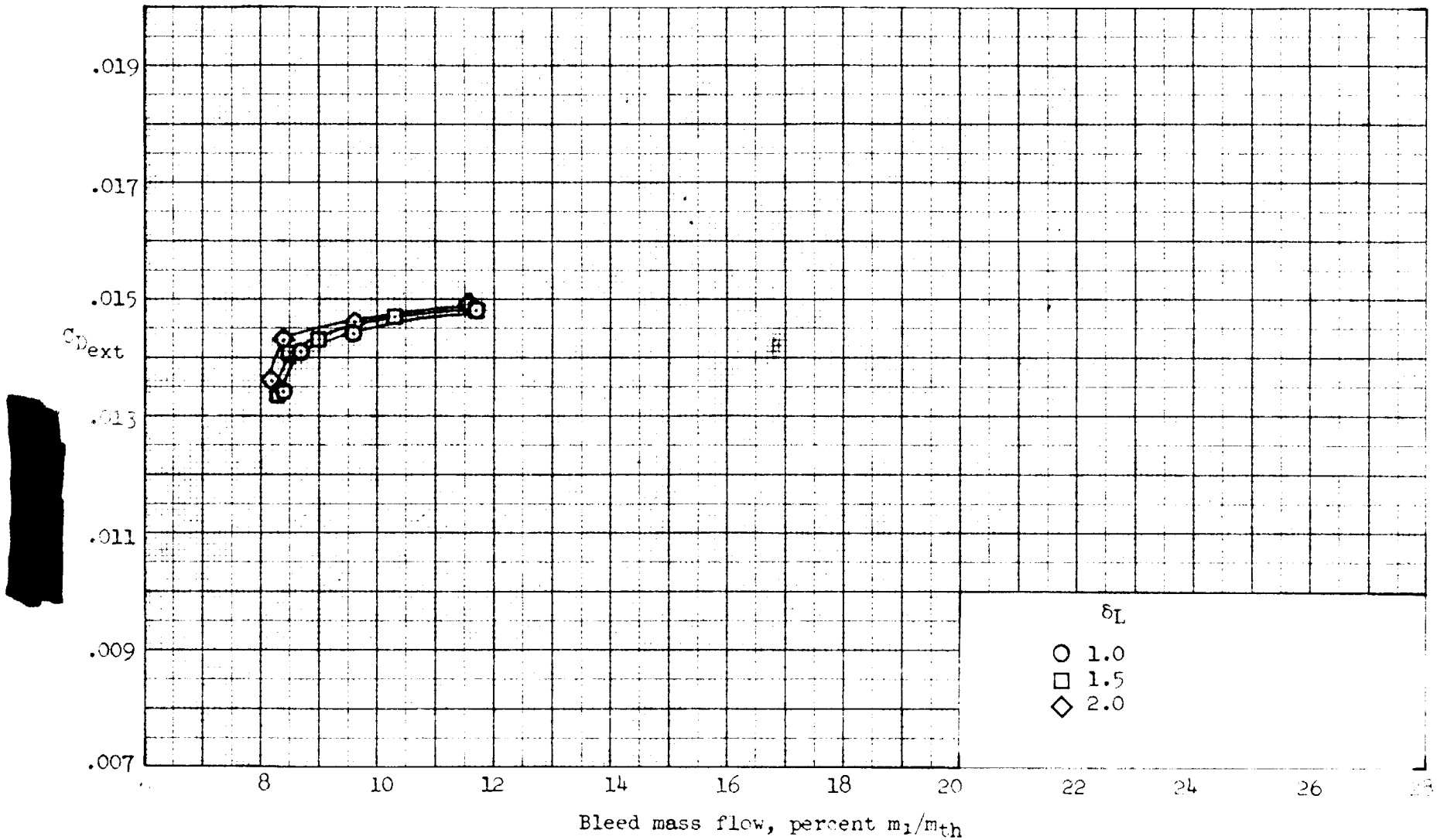

(a) Concluded. δ_R = 17.5°; external-drag coefficient.

Figure 11.- Continued.

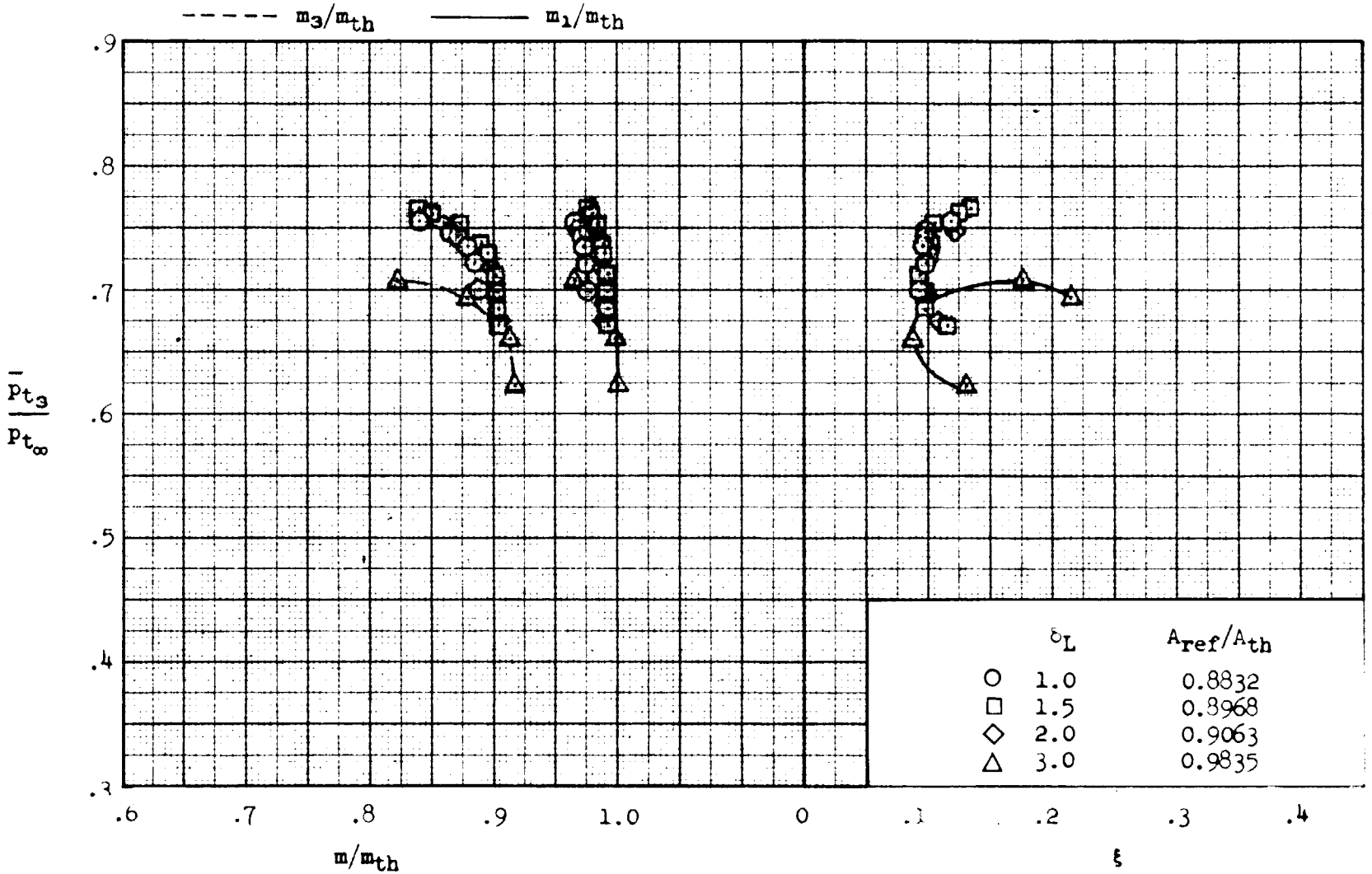

(b) δ_R = 18.0°; inlet performance.

Figure 11.- Continued.

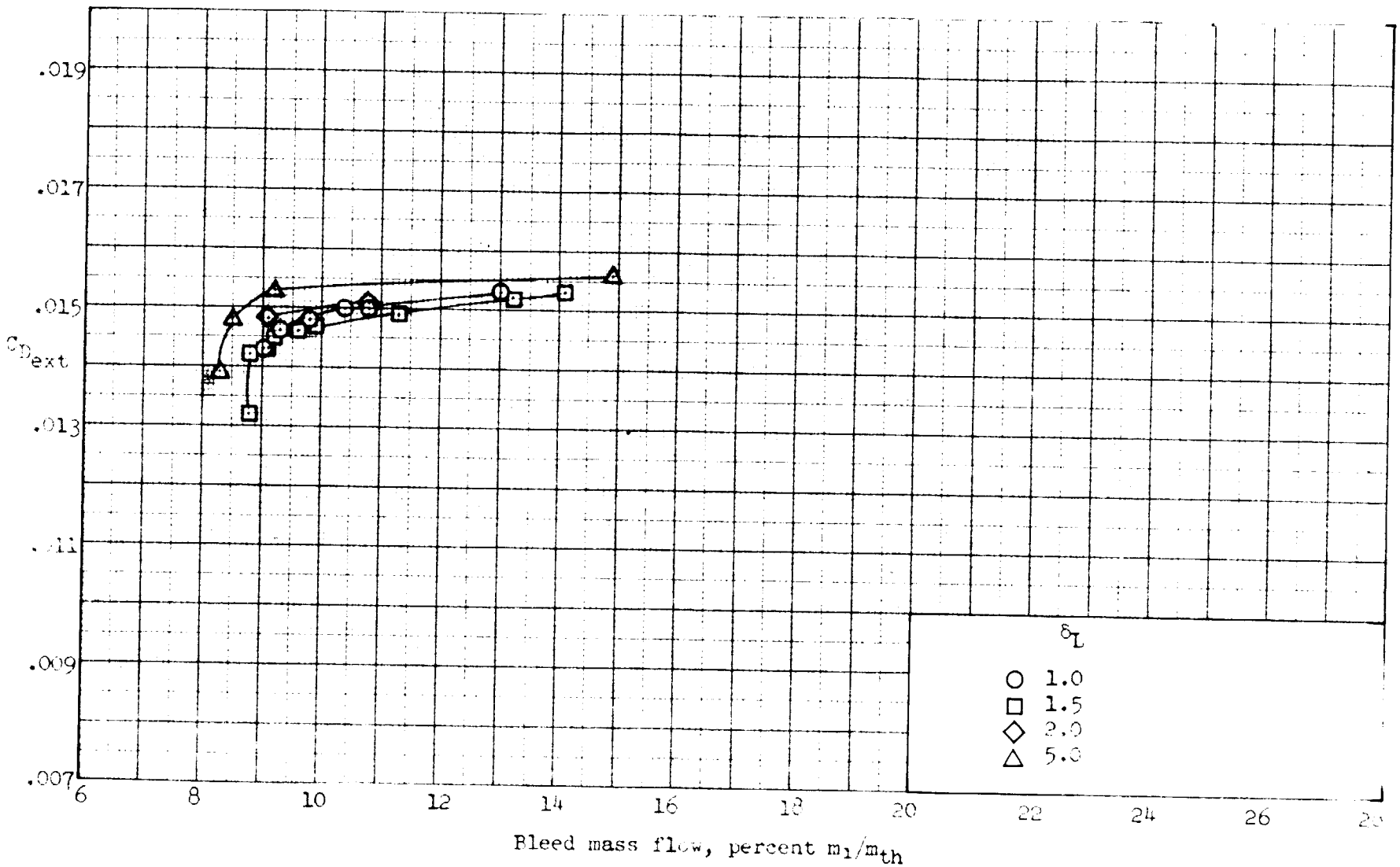

(b) Concluded. δ_R = 18.0°; external-drag coefficient.

Figure 11.- Continued.

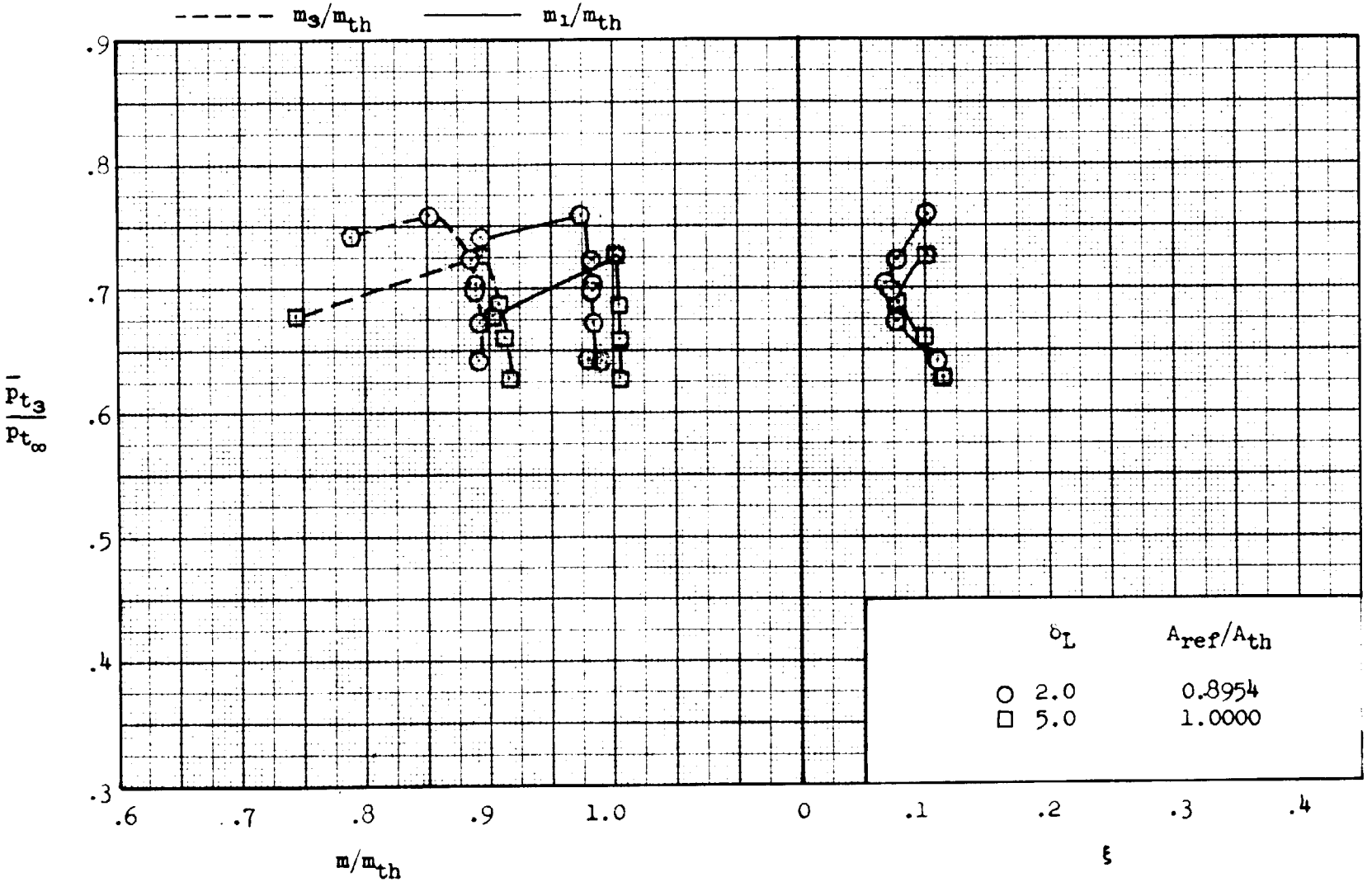

(c) δ_R = 18.5°; inlet performance.

Figure 11.- Continued.

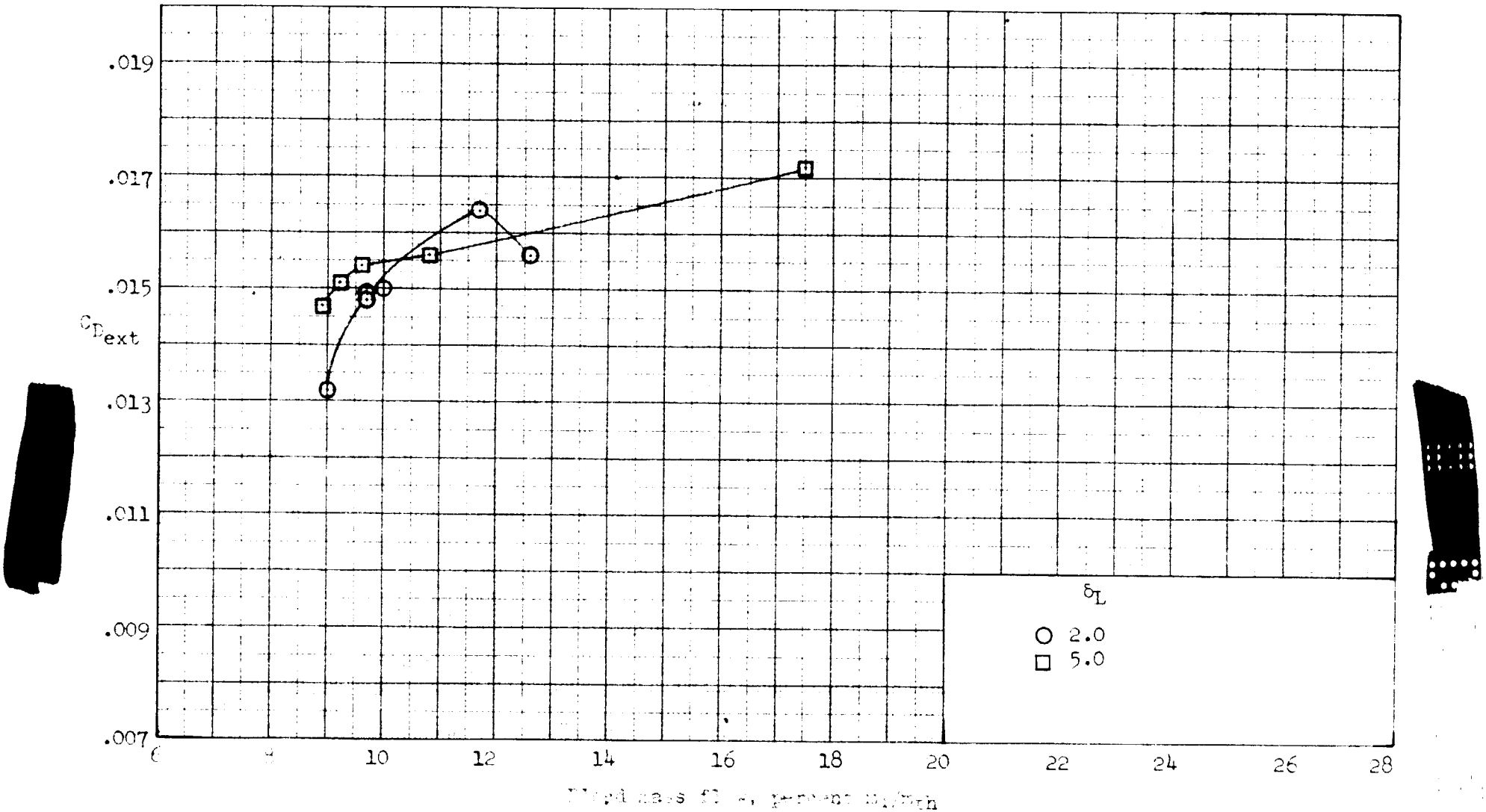

(c) Concluded. δ_R = 18.5°; external drag coefficient.

Figure 11.- Concluded.

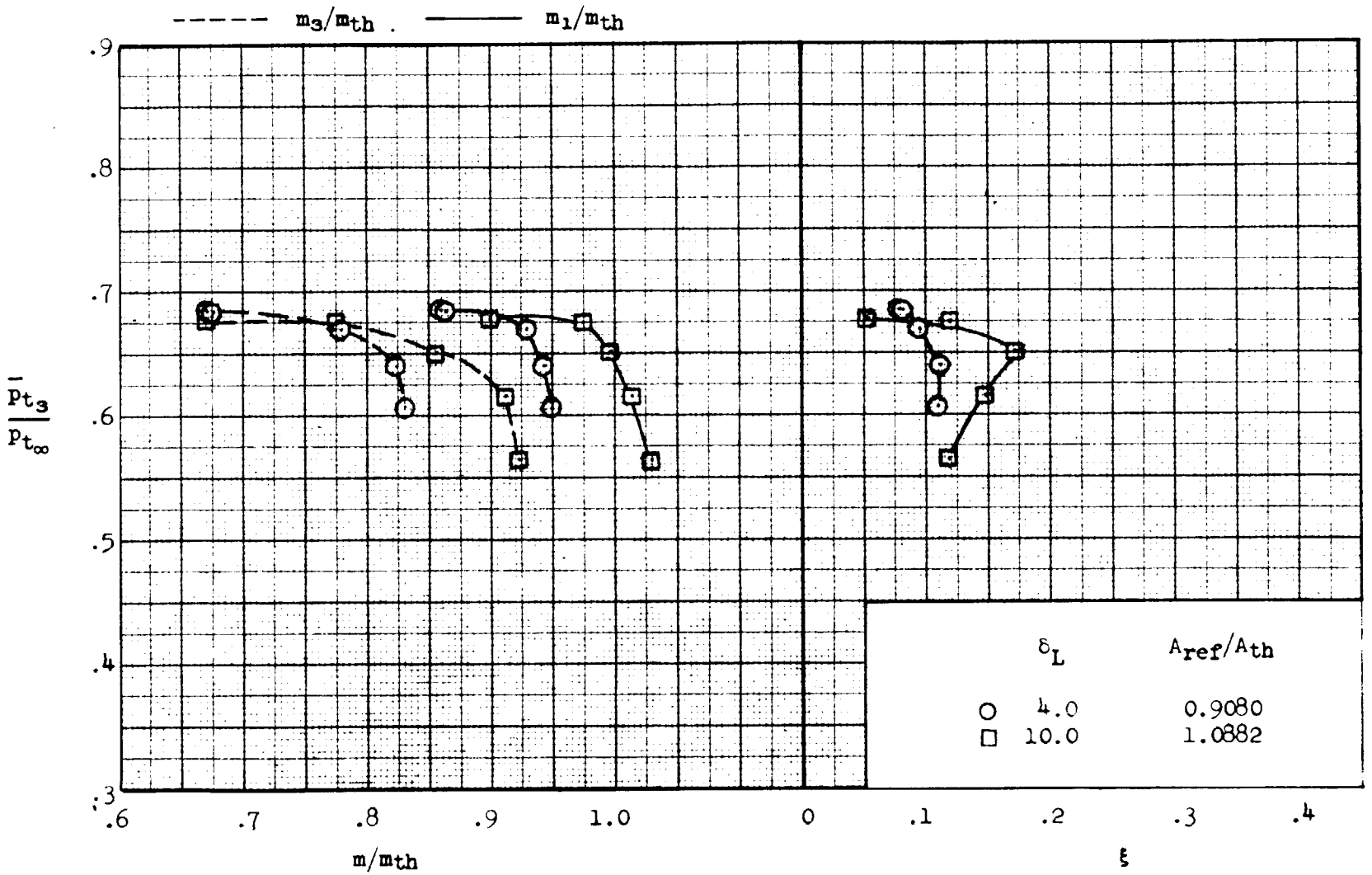

(a) δ_R = 18.0°; inlet performance.

Figure 12.- Effect of lip angle variation on inlet performance and external-drag coefficient; M = 3.00, α = 10°, β = 0°. Configuration: nose 1, diverter 1, porosity 1, bleed exit 1.

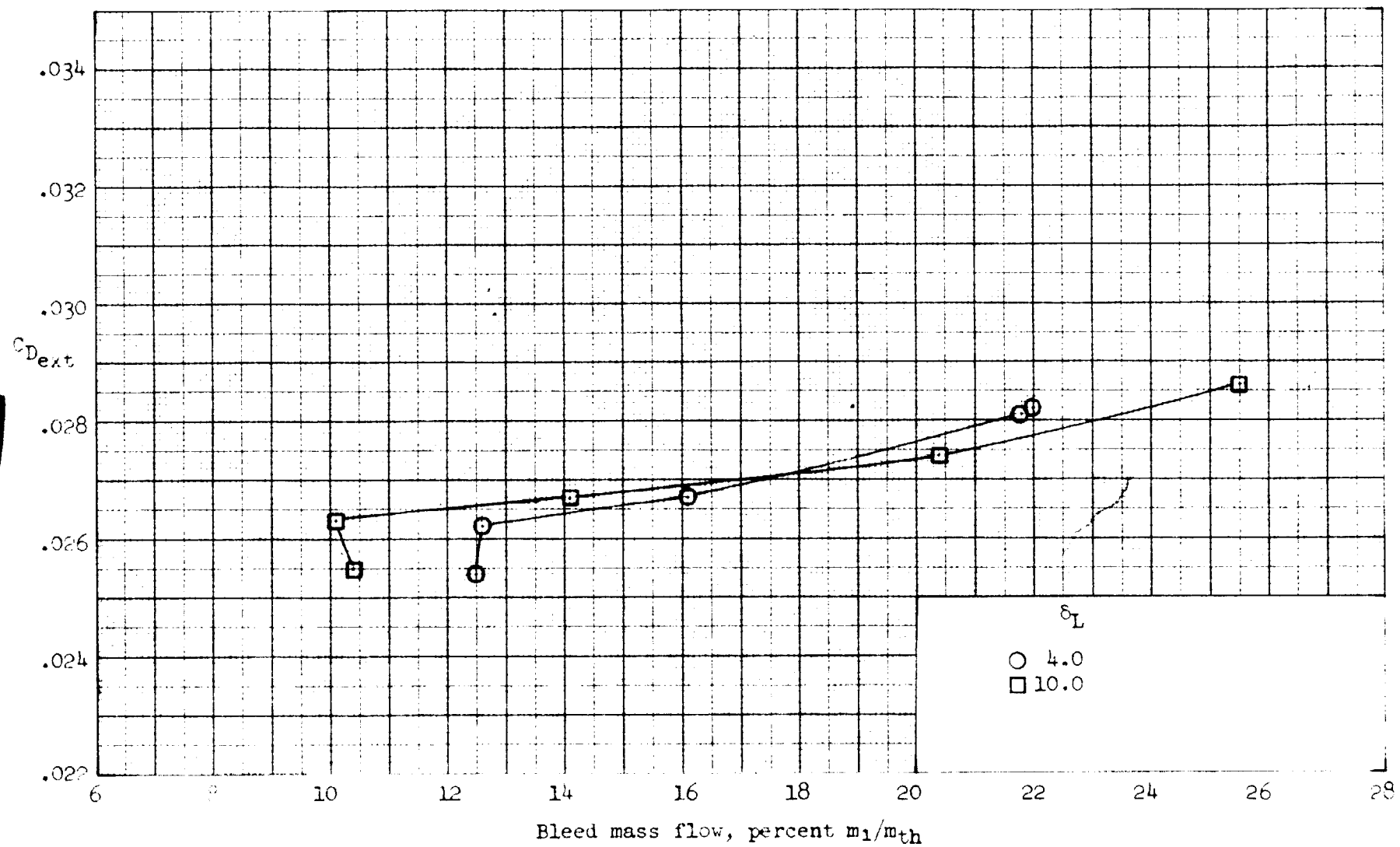

(a) Concluded. δ_R = 18.0°; external-drag coefficient.

Figure 12.- Continued.

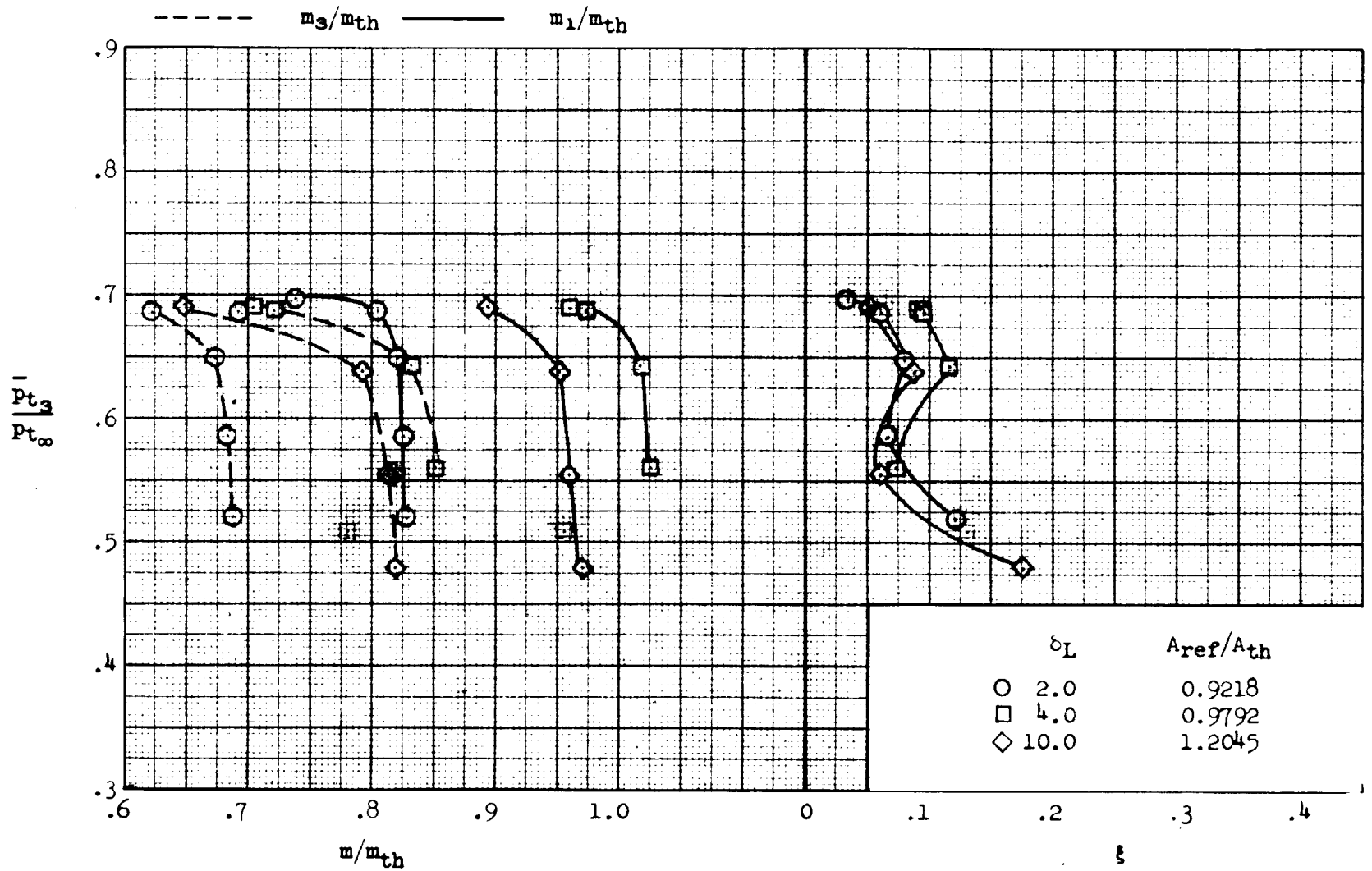

(b) δ_R = 20.0°; inlet performance.

Figure 12.- Continued.

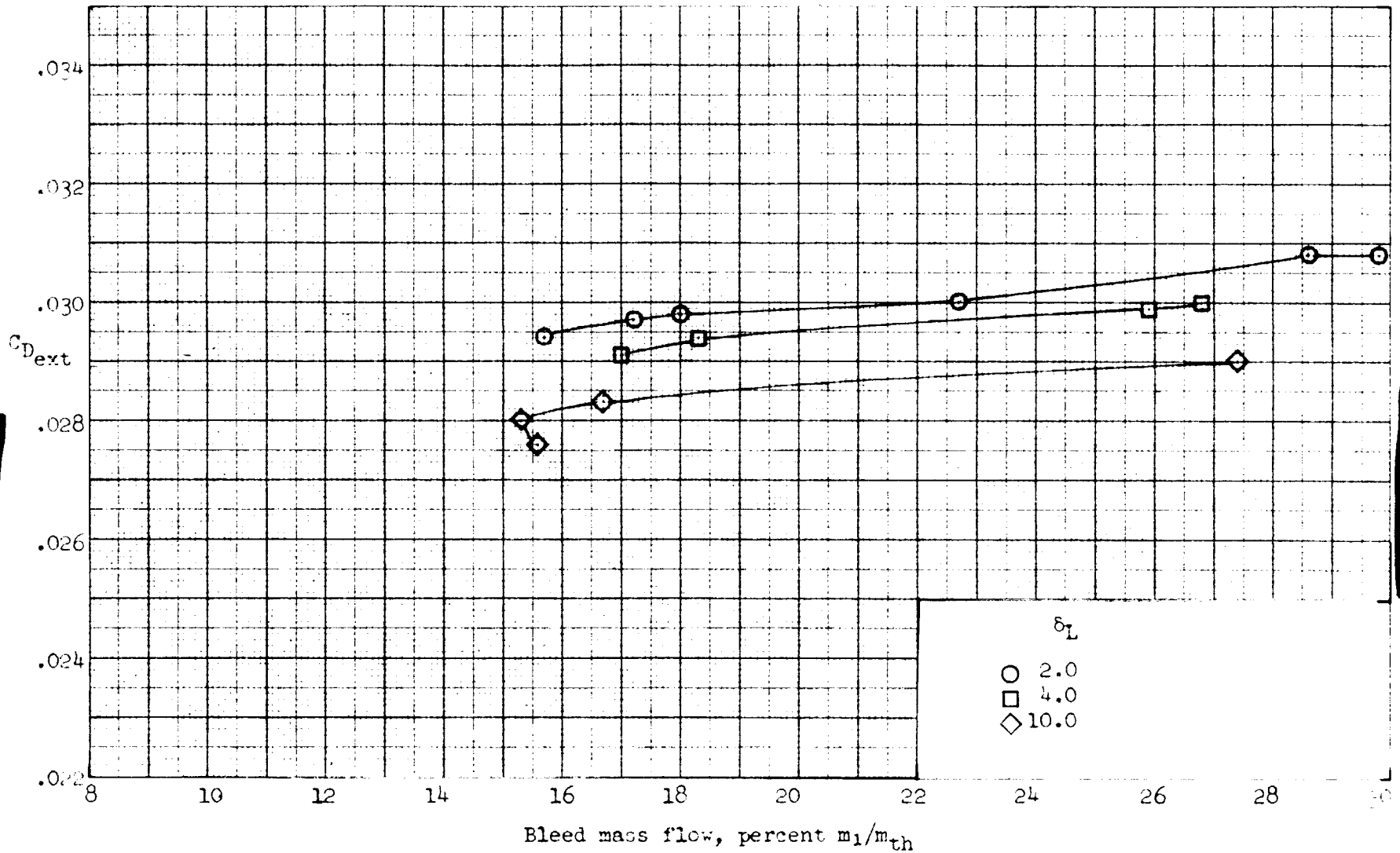

(b) Concluded. δ_R = 20.0°; external-drag coefficient.

Figure 12.- Concluded.

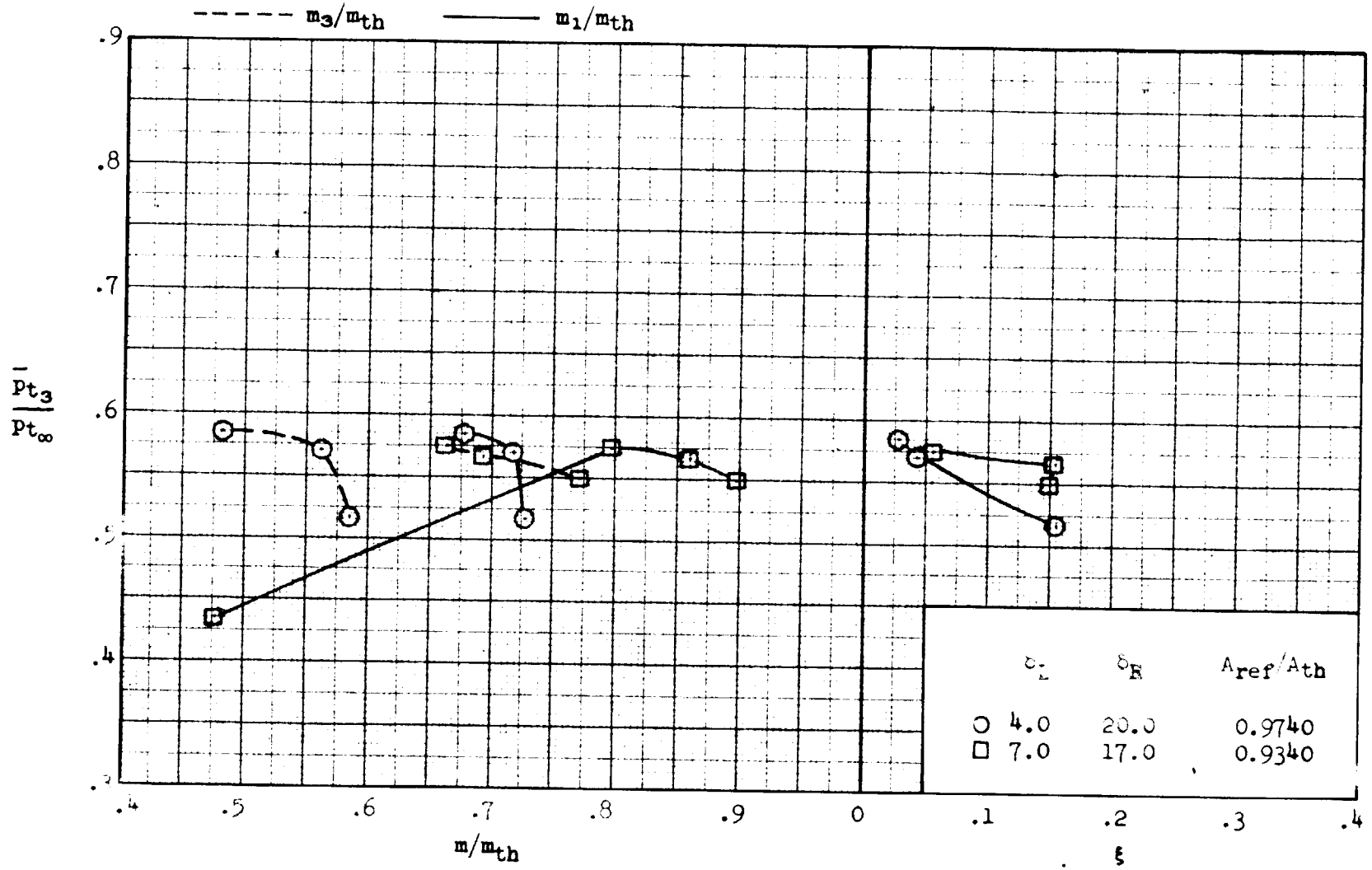

(a) Inlet performance.

Figure 13.- Effect of lip and ramp angle variation on inlet performance and external-drag coefficient; M = 3.00, α = 14°, β = 0°. Configuration: nose 1, diverter 1, porosity 1, bleed exit 1.

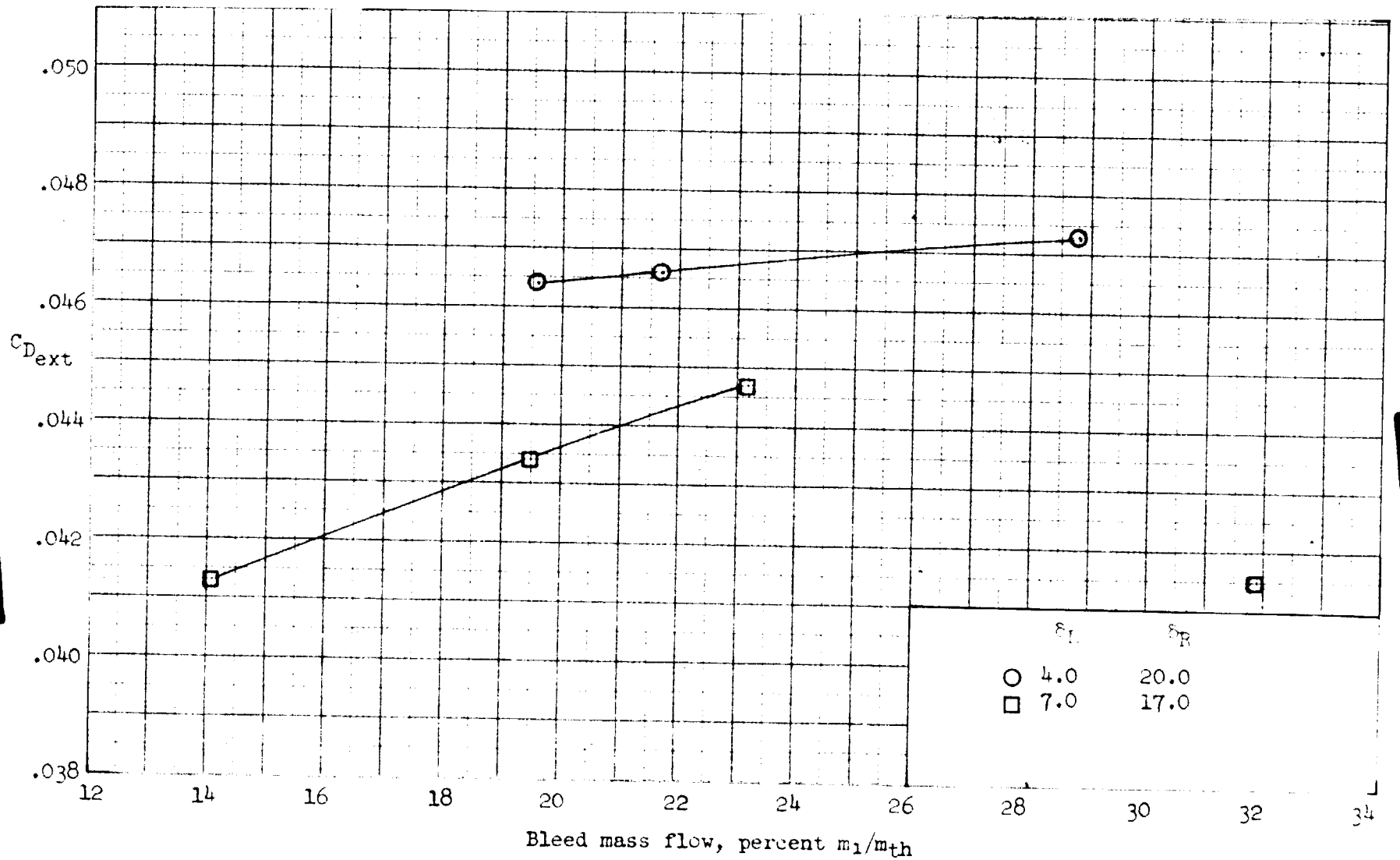

b. External-drag coefficient.

Figure 13.- Concluded.

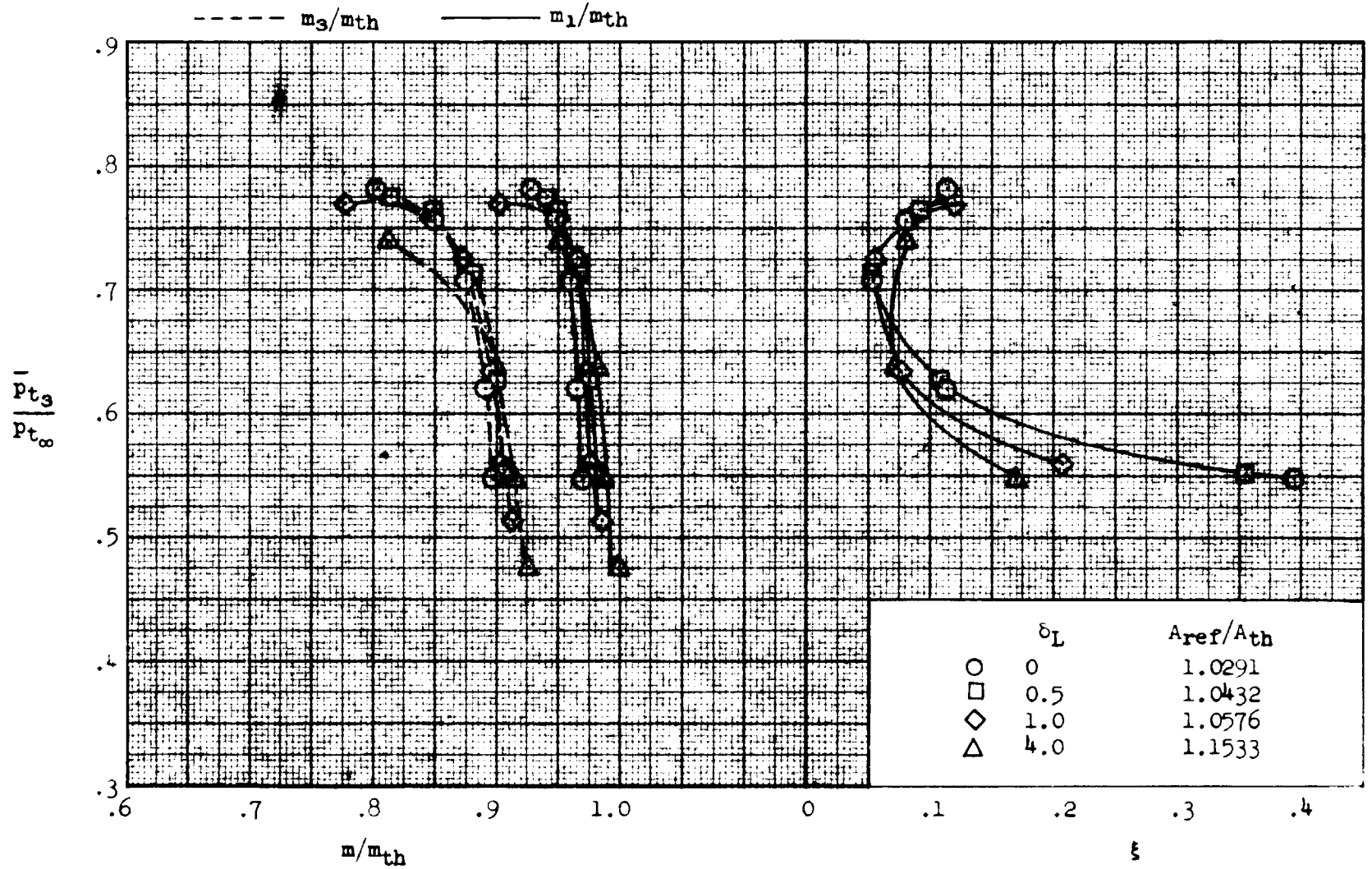

(a) Inlet performance.

Figure [illegible] Effect of lip [illegible] variation on inlet performance and [illegible] $\beta = 0°$, [illegible] configuration: [illegible] 1, diverter [illegible]

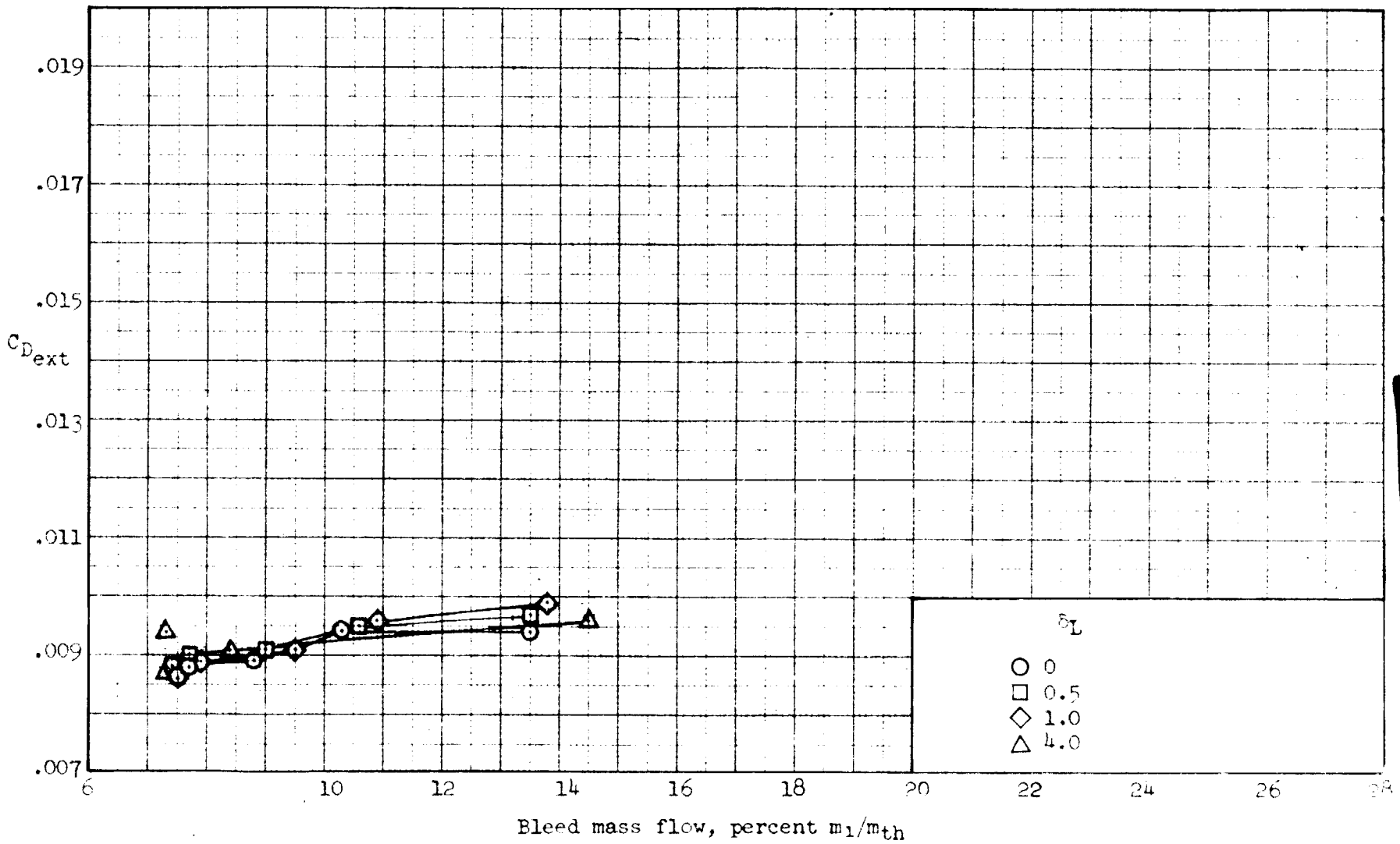

(b) External-drag coefficient.

Figure 14.- Concluded.

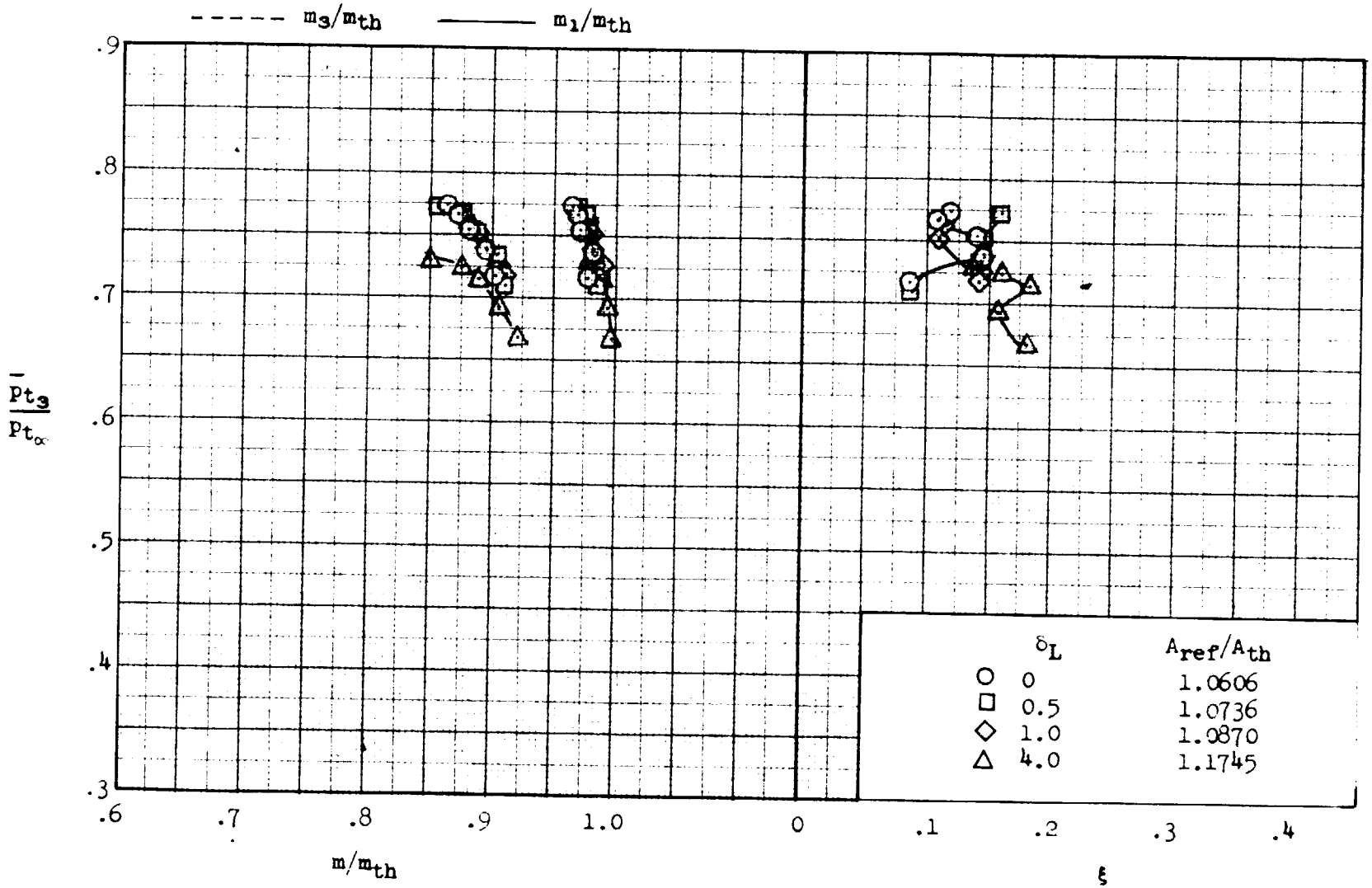

(a) $\delta_R = 17.5°$: Inlet performance.

Figure 15.- Effect of lip angle variation on inlet performance and external-drag coefficient; M = 2.70, $\alpha = 0°$, $\beta = 0°$. Configuration: nose 1, diverter 1, porosity 1, bleed exit 1.

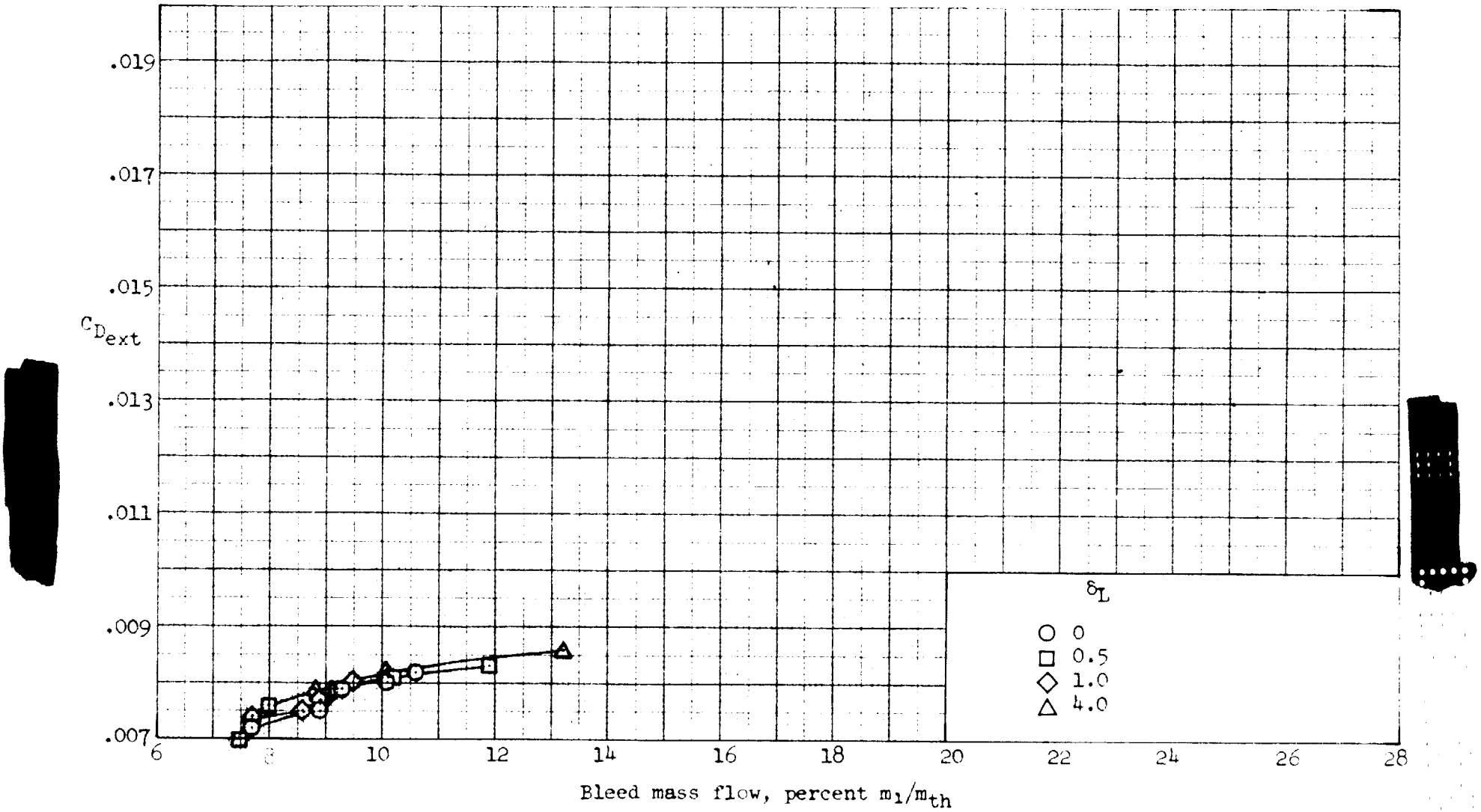

(a) Concluded. δ_R = 17.5°; external-drag coefficient.

Figure 15.- Continued.

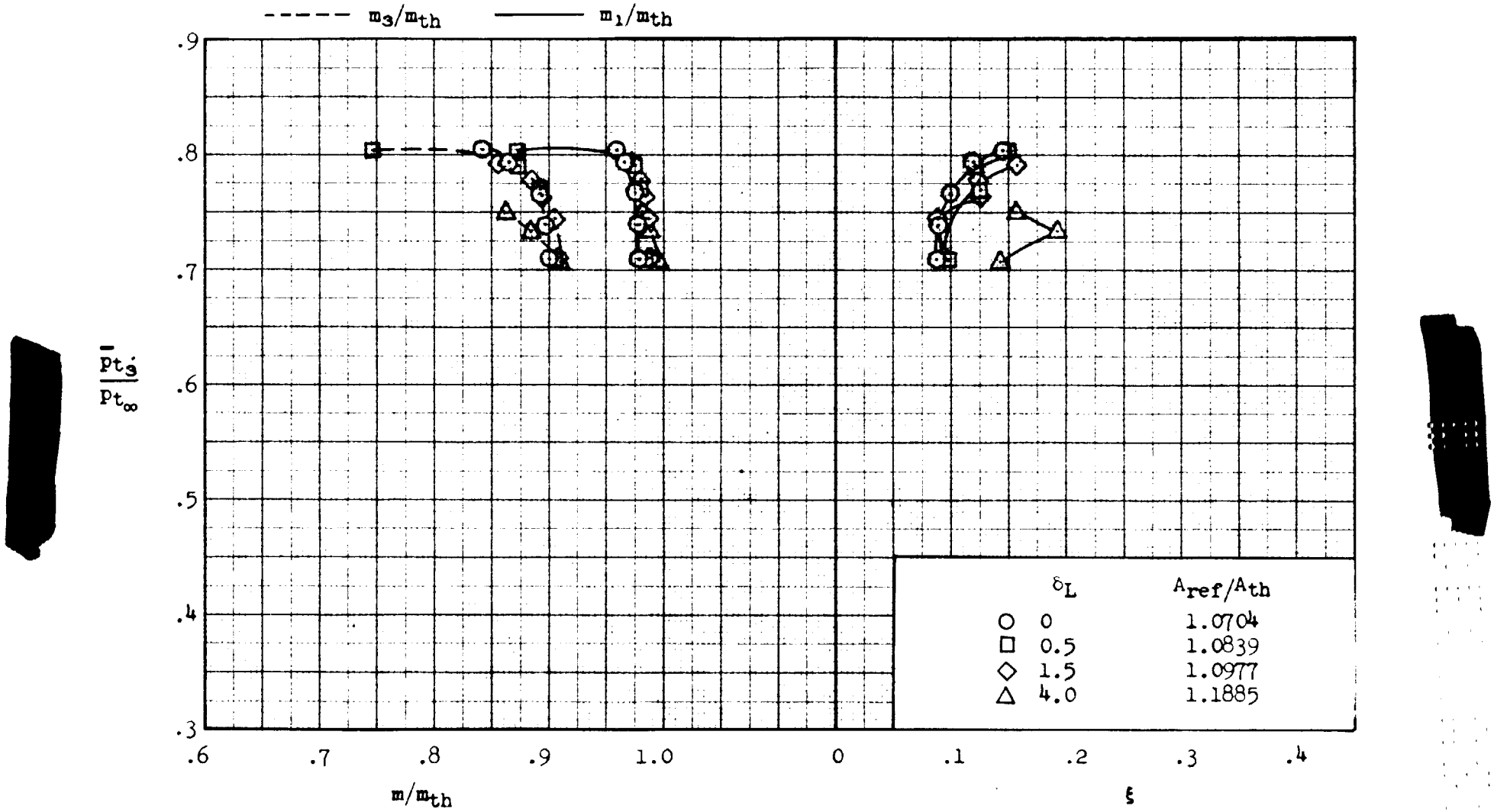

(b) δ_R = 18.0°; inlet performance.

Figure 15.- Continued.

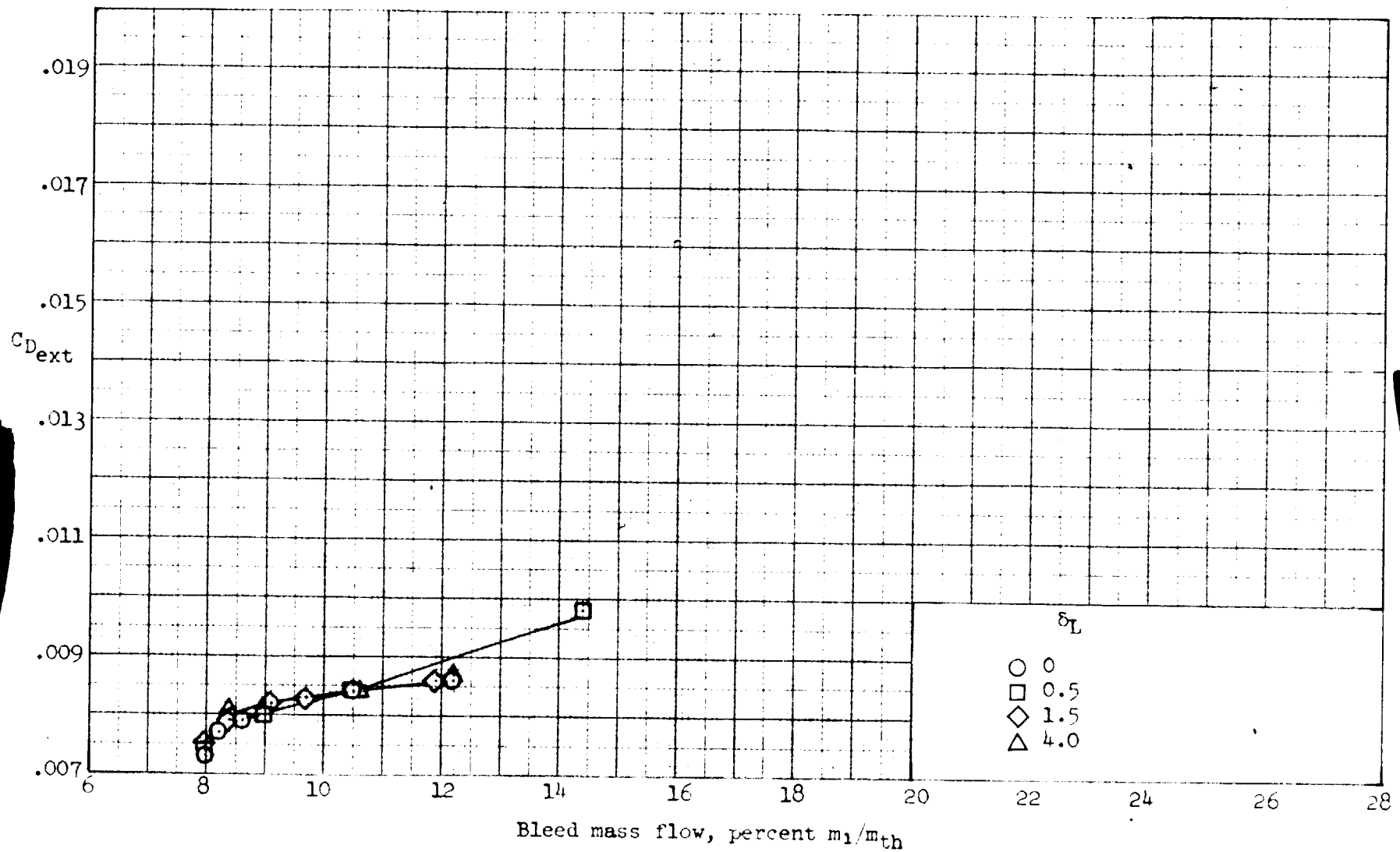

(b) Concluded. δ_R = 18.0°; external-drag coefficient.

Figure 15.- Continued.

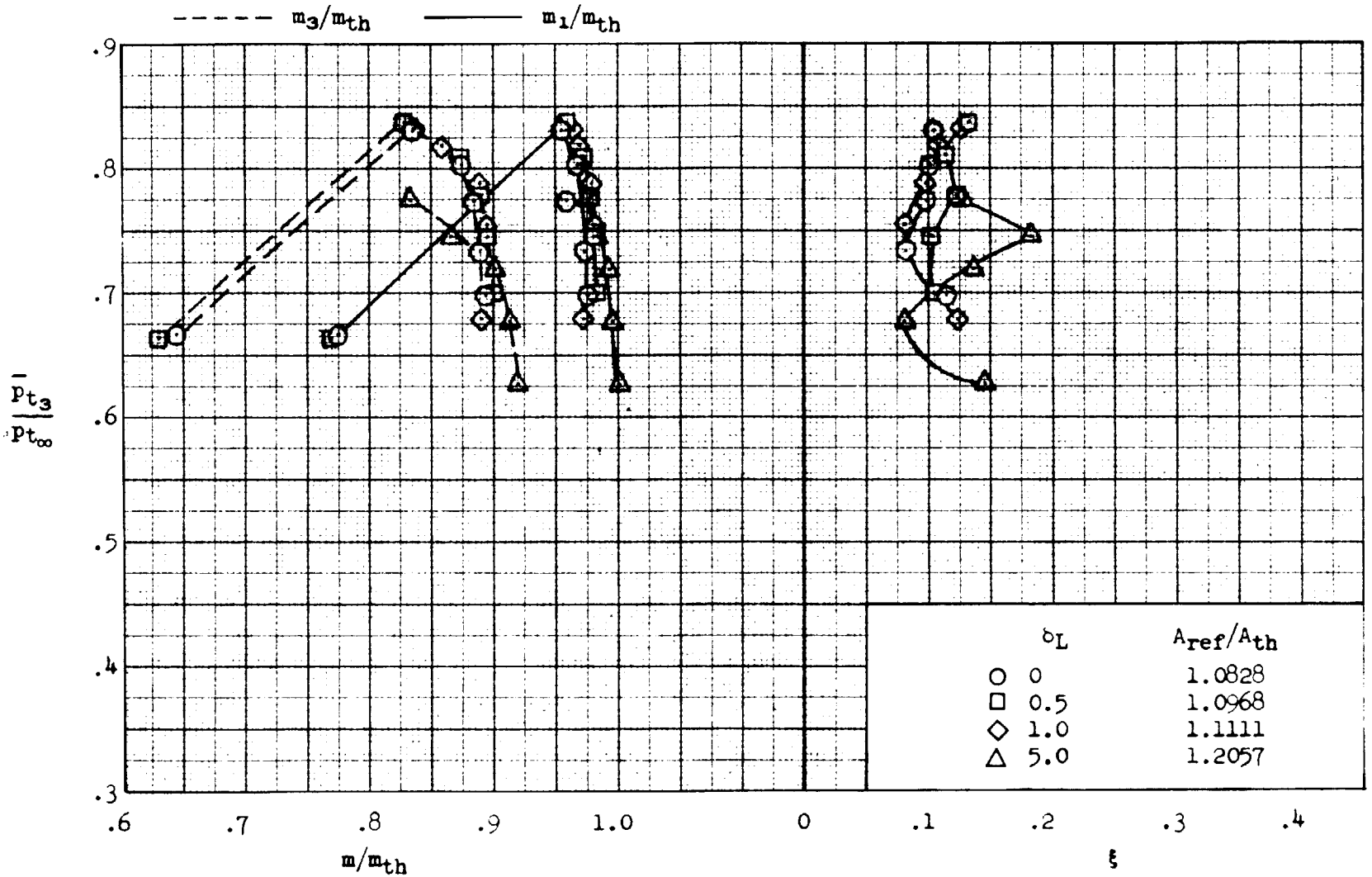

(c) δ_R = 18.5°; inlet performance.

Figure 15.- Continued.

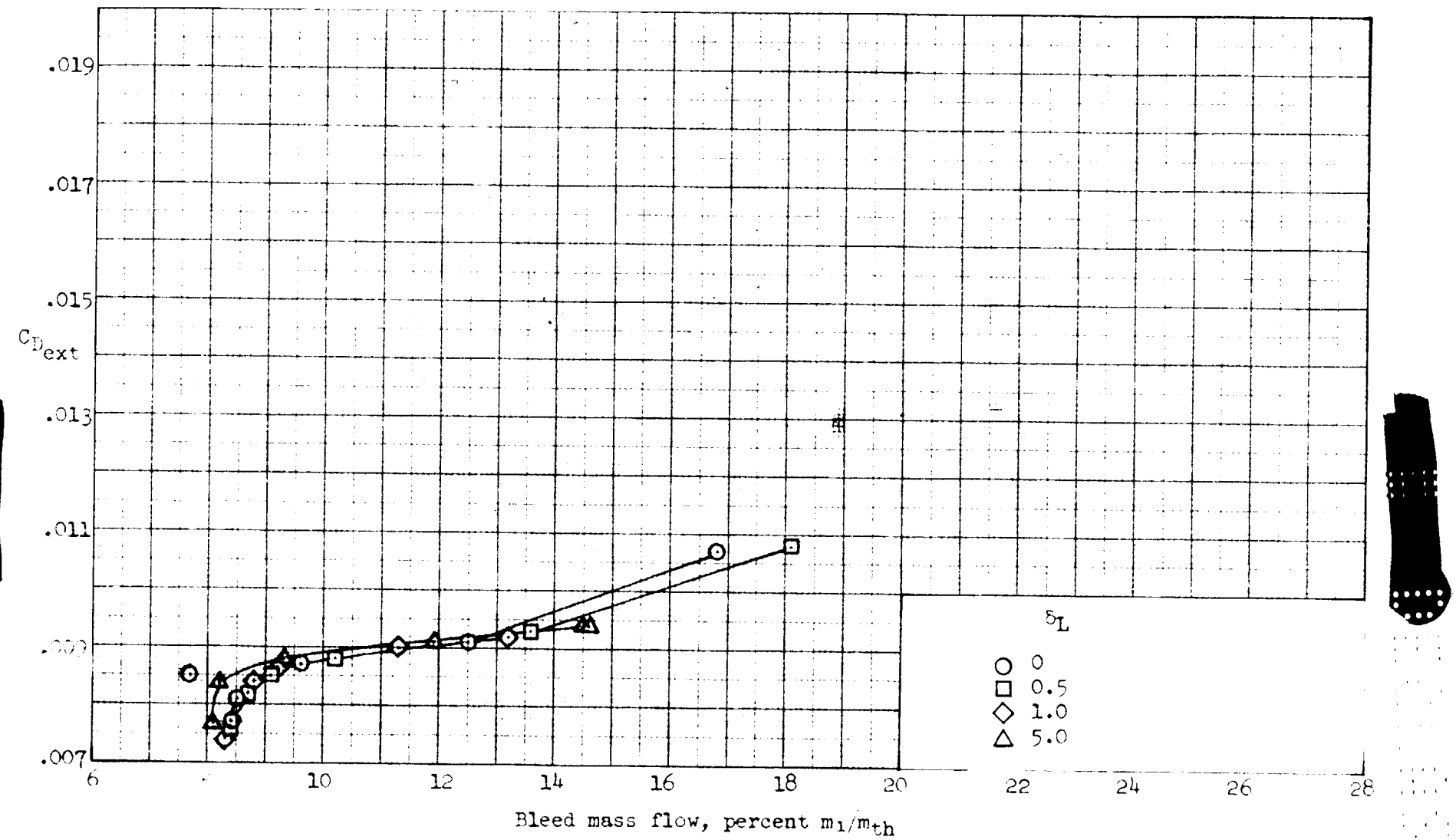

(c) Concluded. δ_R = 18.5°; external-drag coefficient.

Figure 15.- Concluded.

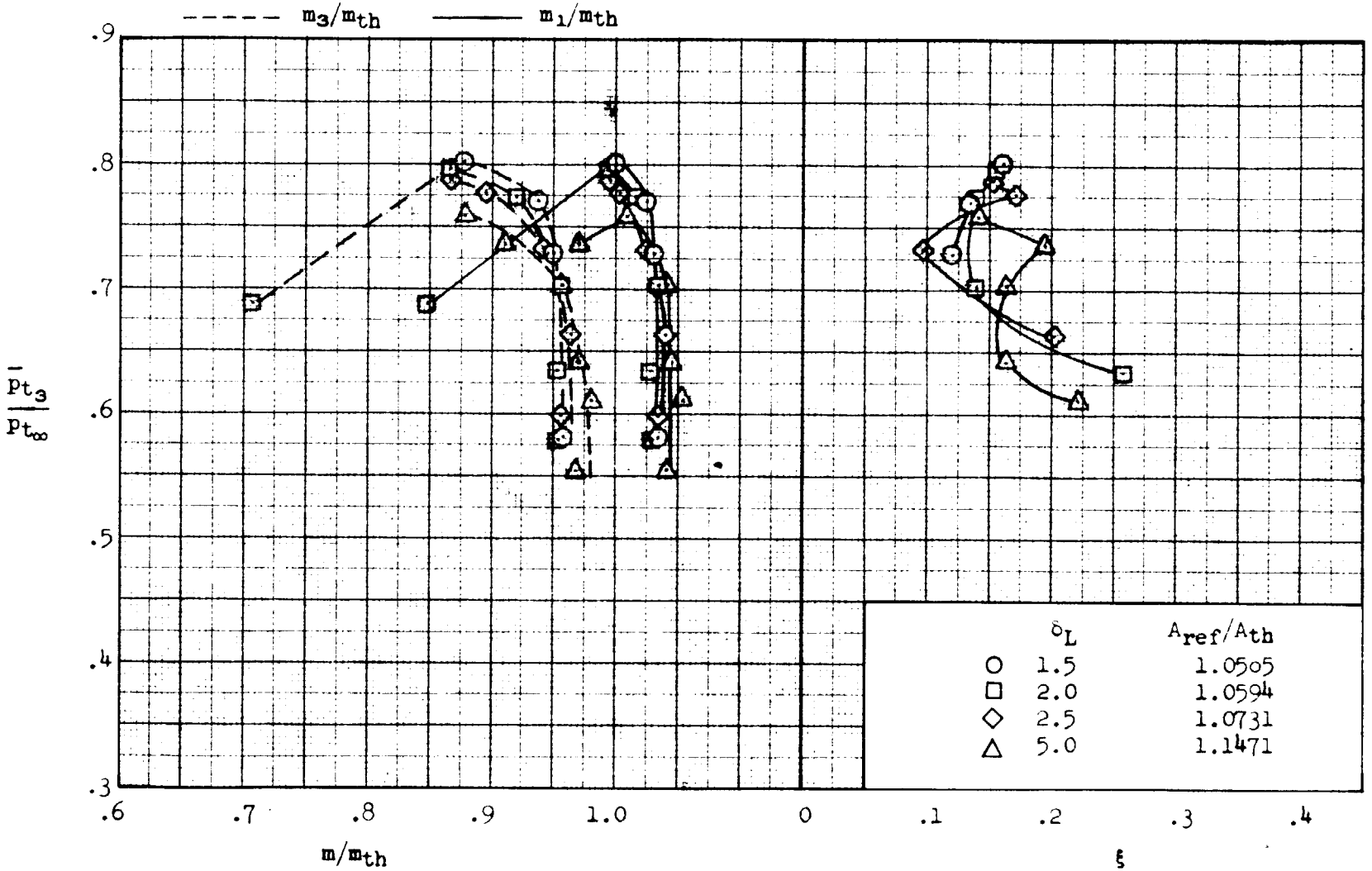

(a) δ_R = 17.5°; inlet performance

Figure 16.- Effect of lip angle variation on inlet performance and external-drag coefficient; M = 2.75, α = 2°, β = 0°. Configuration: nose 1, diverter 1, porosity 1, bleed exit 1.

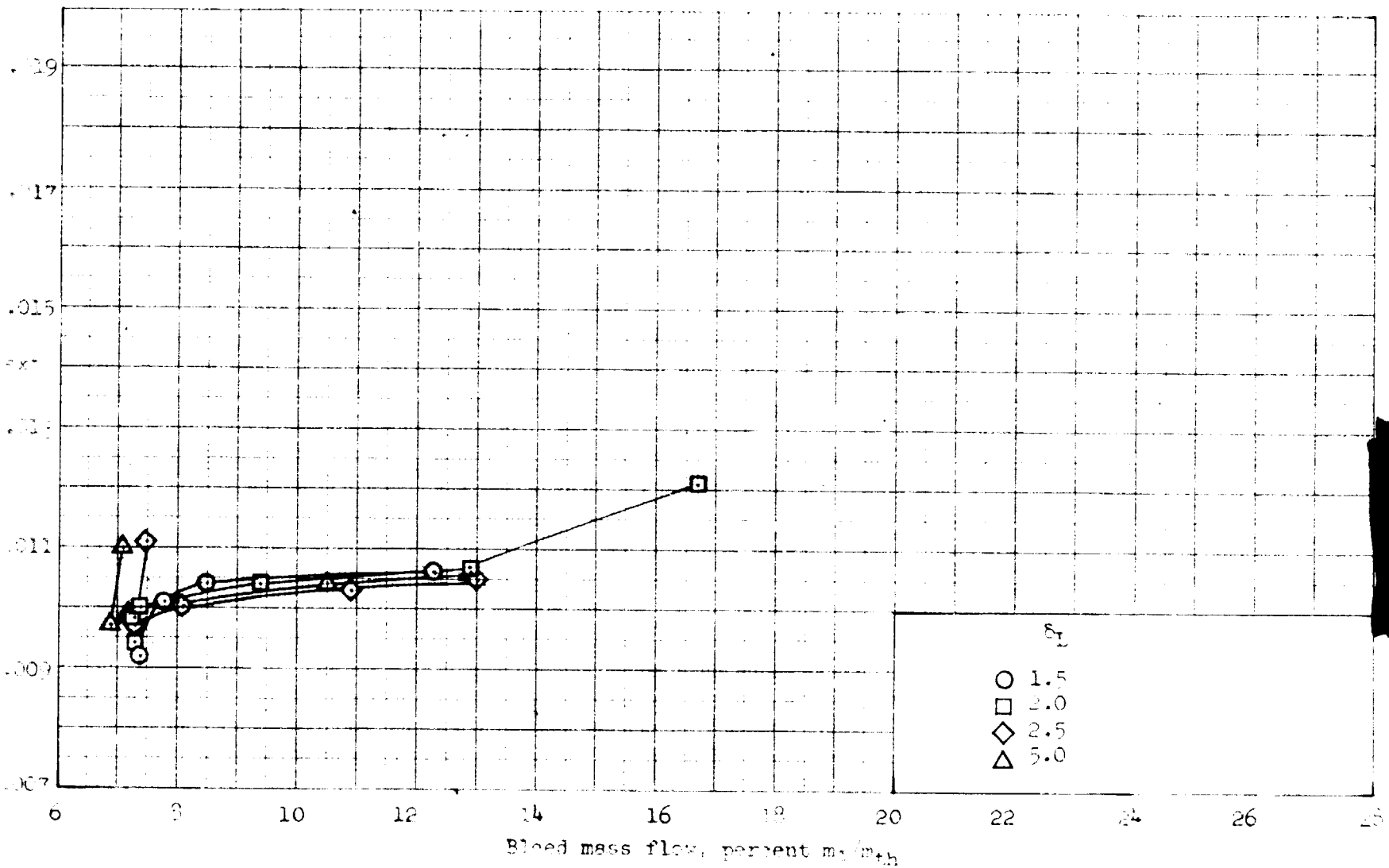

Figure 16.- Continued.

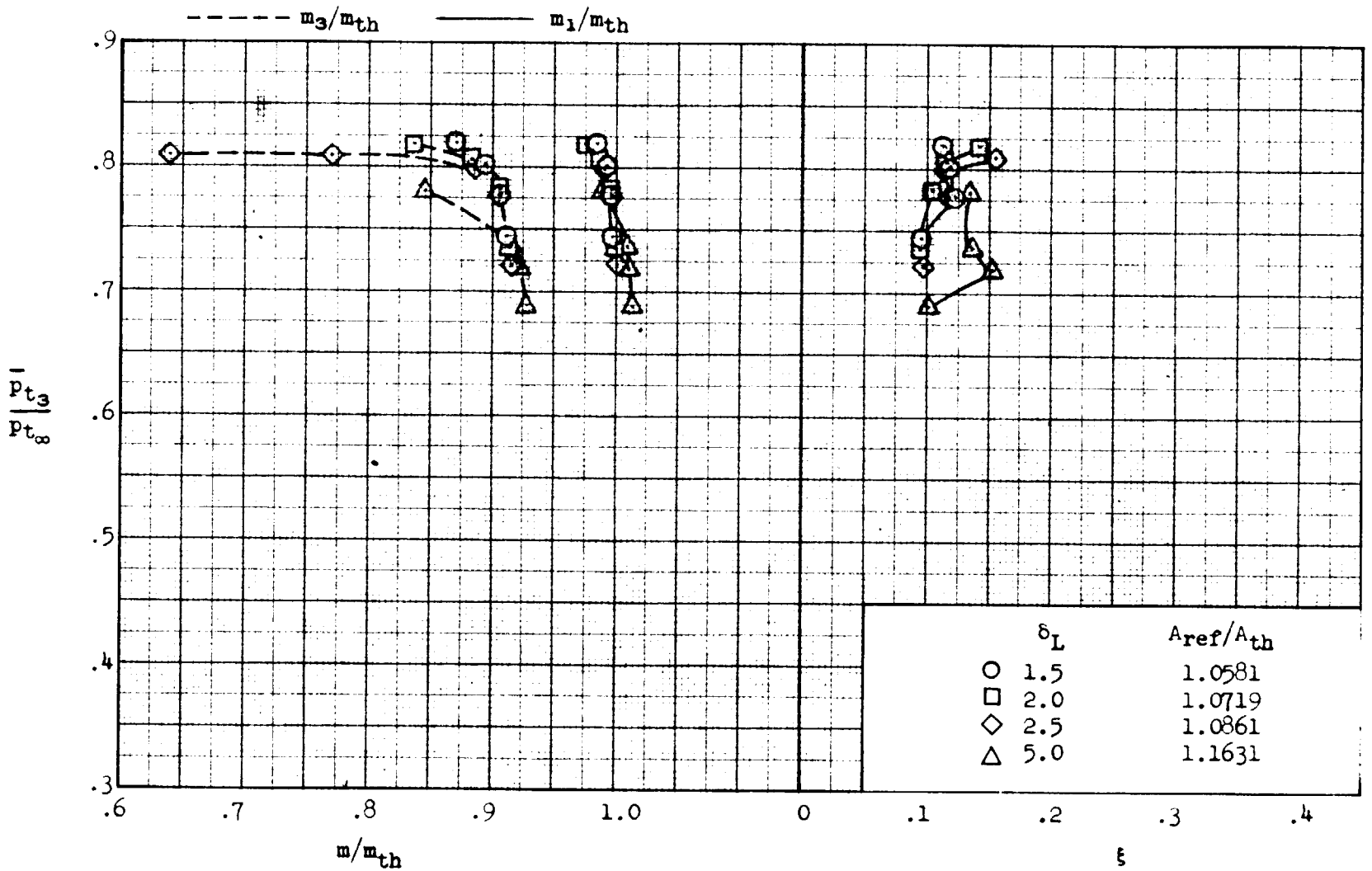

(b) δ_R = 18.0°; inlet performance.

Figure 16.- Continued.

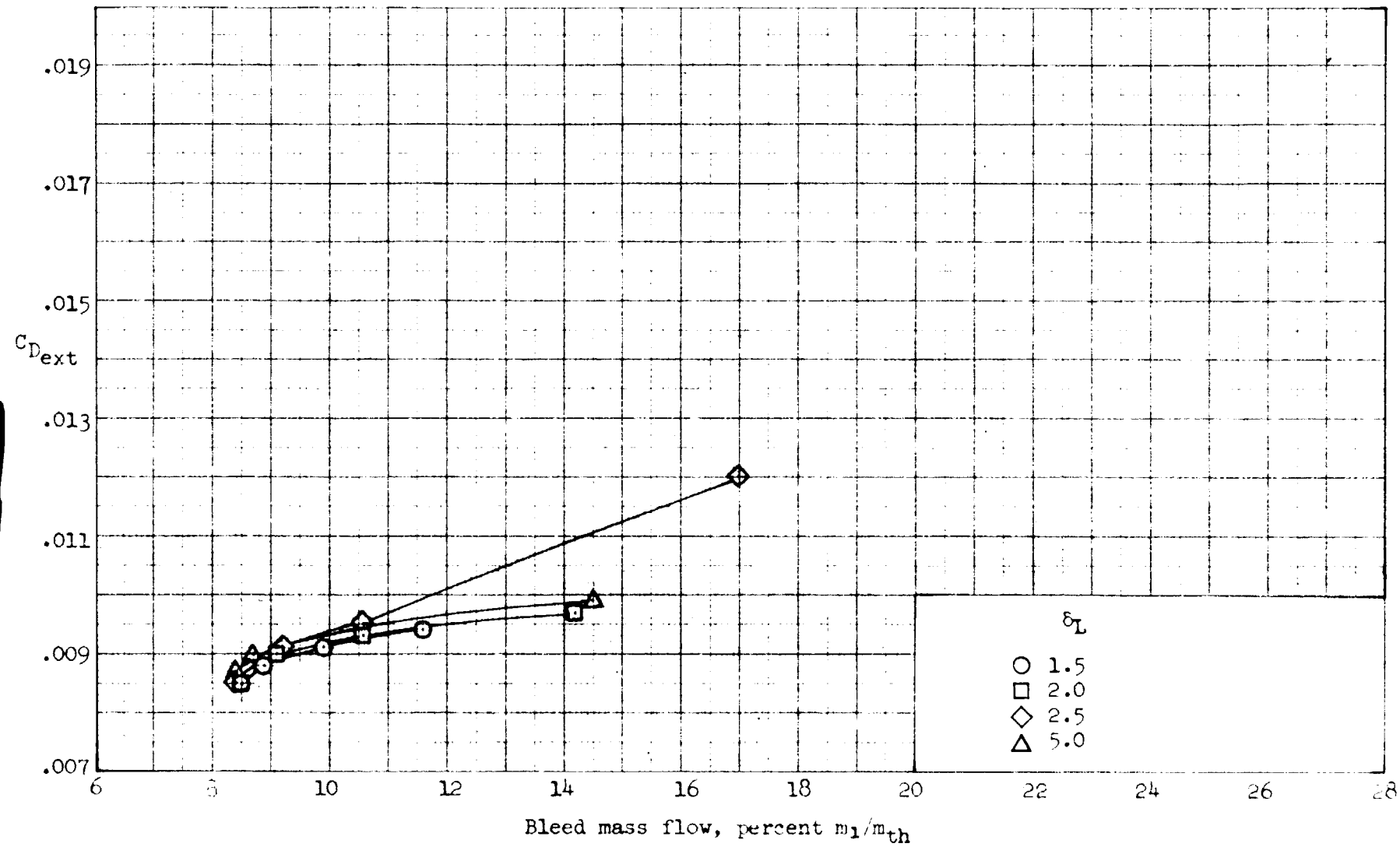

Figure 16.- Continued.

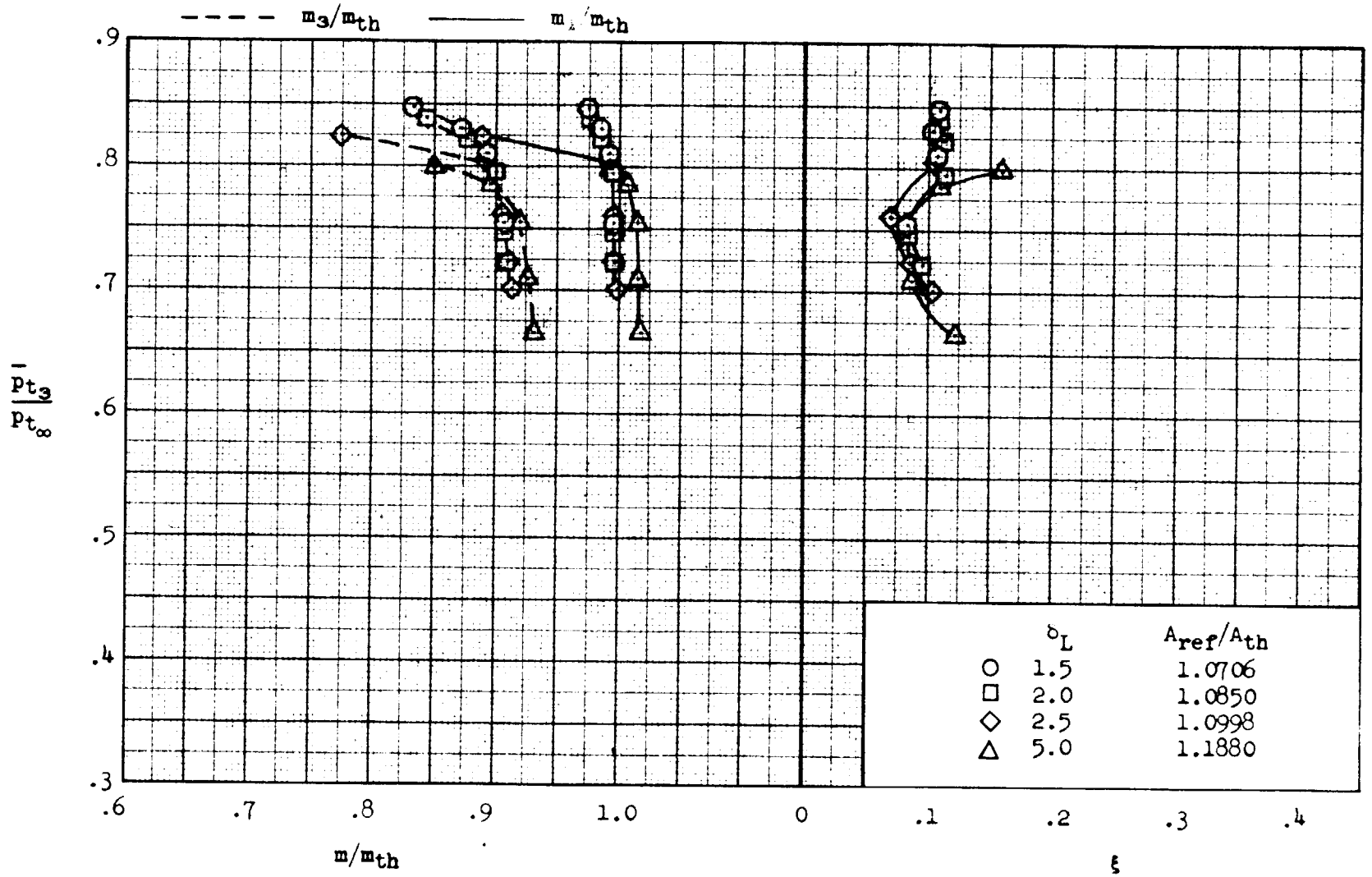

(c) δ_R = 18.5°; inlet performance.

Figure 16.- Continued.

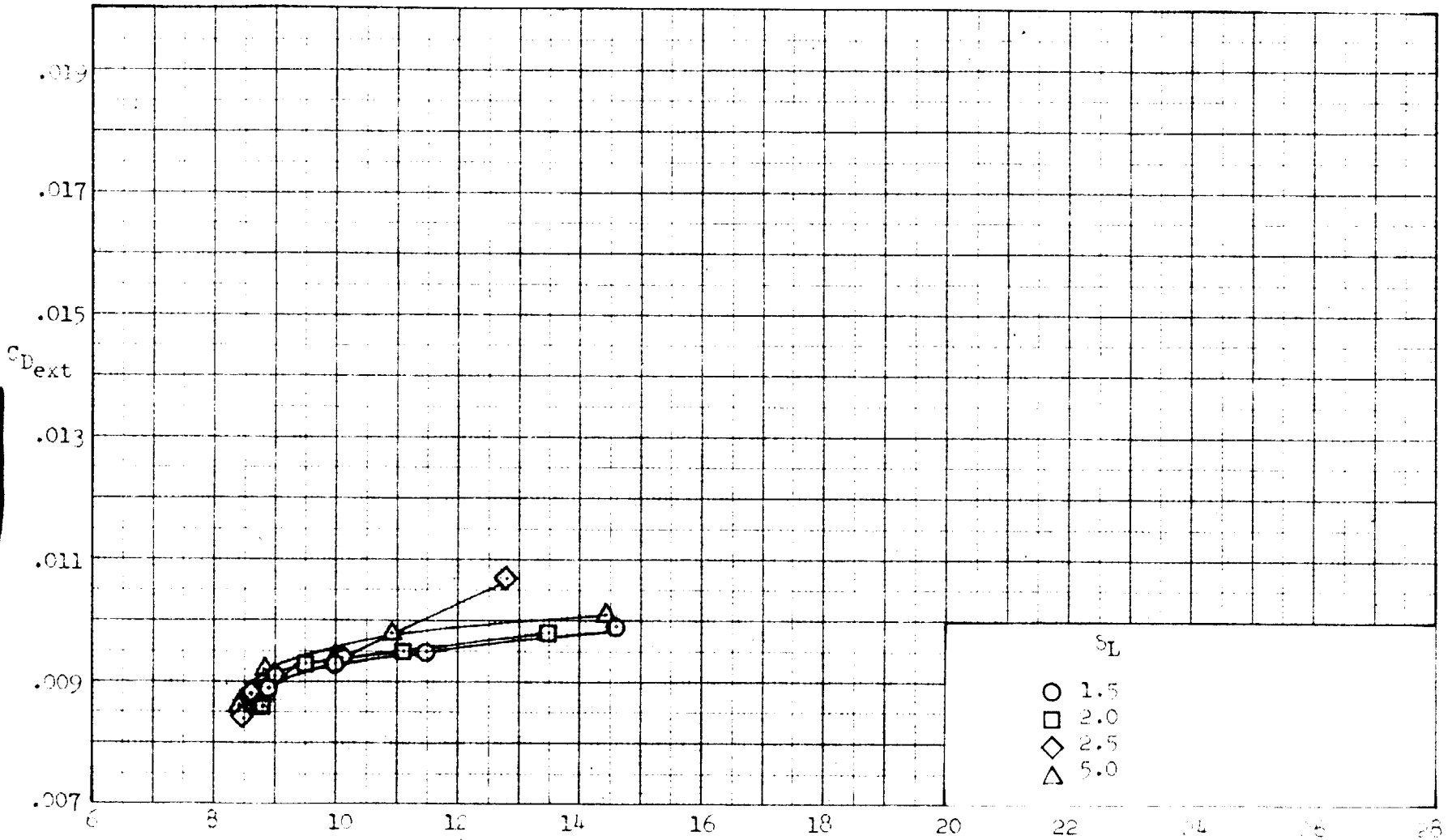

Figure 16.- Concluded.

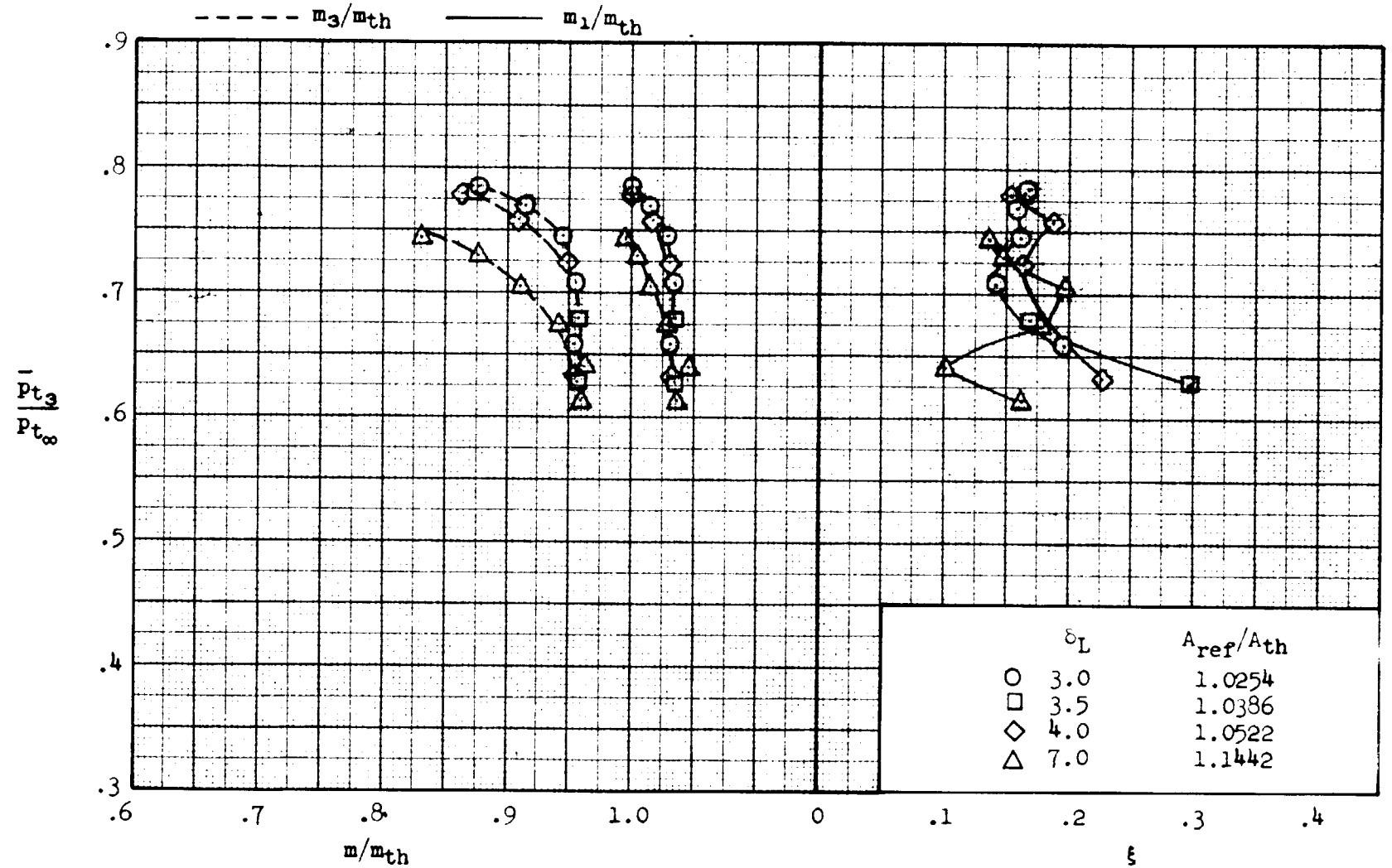

(a) δ_R = 17.0°; inlet performance.

Figure 17.- Effect of lip angle variation on inlet performance and external-drag coefficient: M = 1.70, α = 4°, β = 0°. Configuration: nose 1, diverter 1, porosity 1, bleed exit 1.

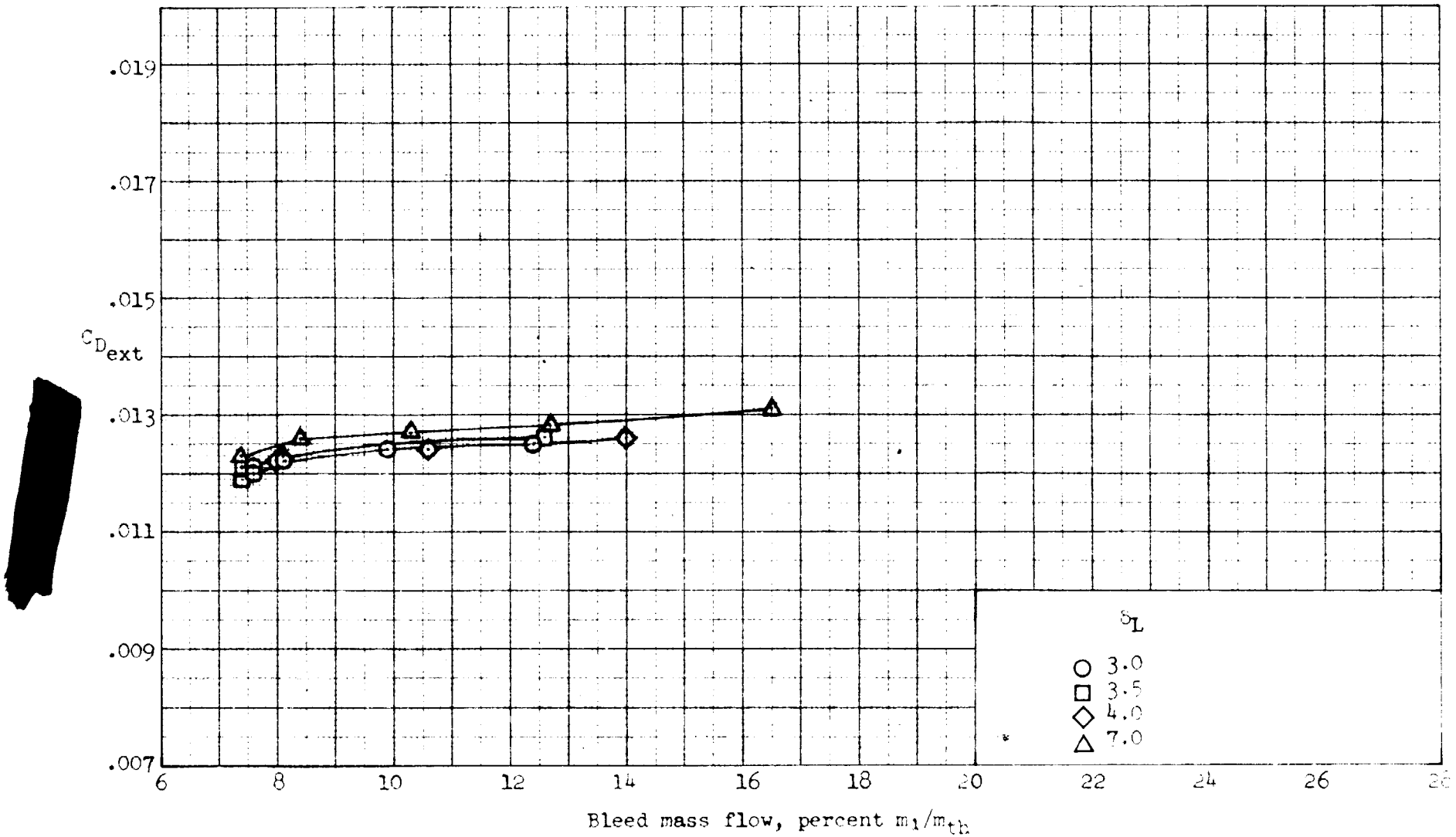

(a) Concluded. δ_R = 17.0°; external drag coefficient.

Figure 17.- Continued.

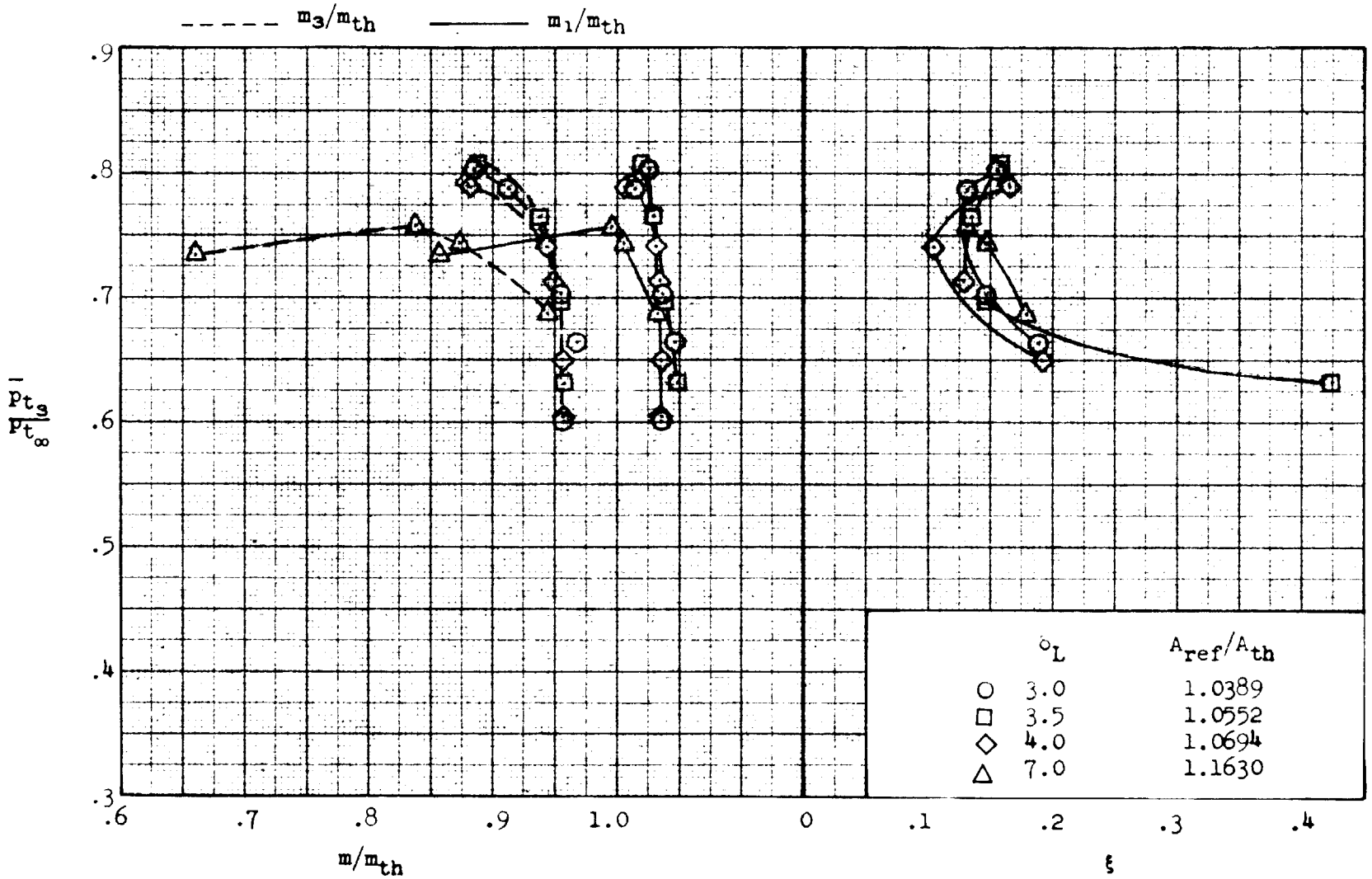

(b) δ_R = 17.5°; inlet performance.

Figure 17.- Continued.

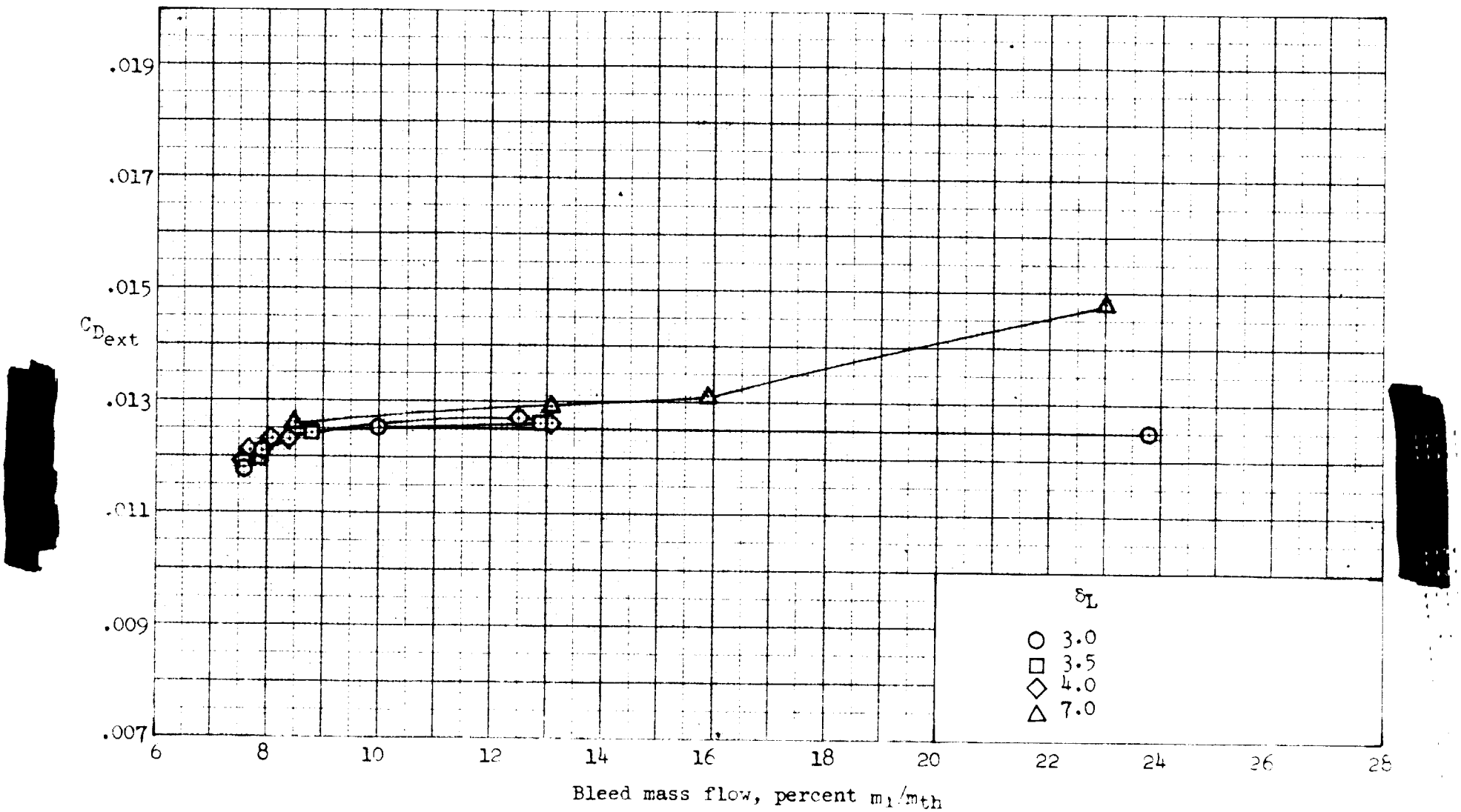

(b) Concluded. δ_R = 17.5°; external-drag coefficient.

Figure 17.- Continued.

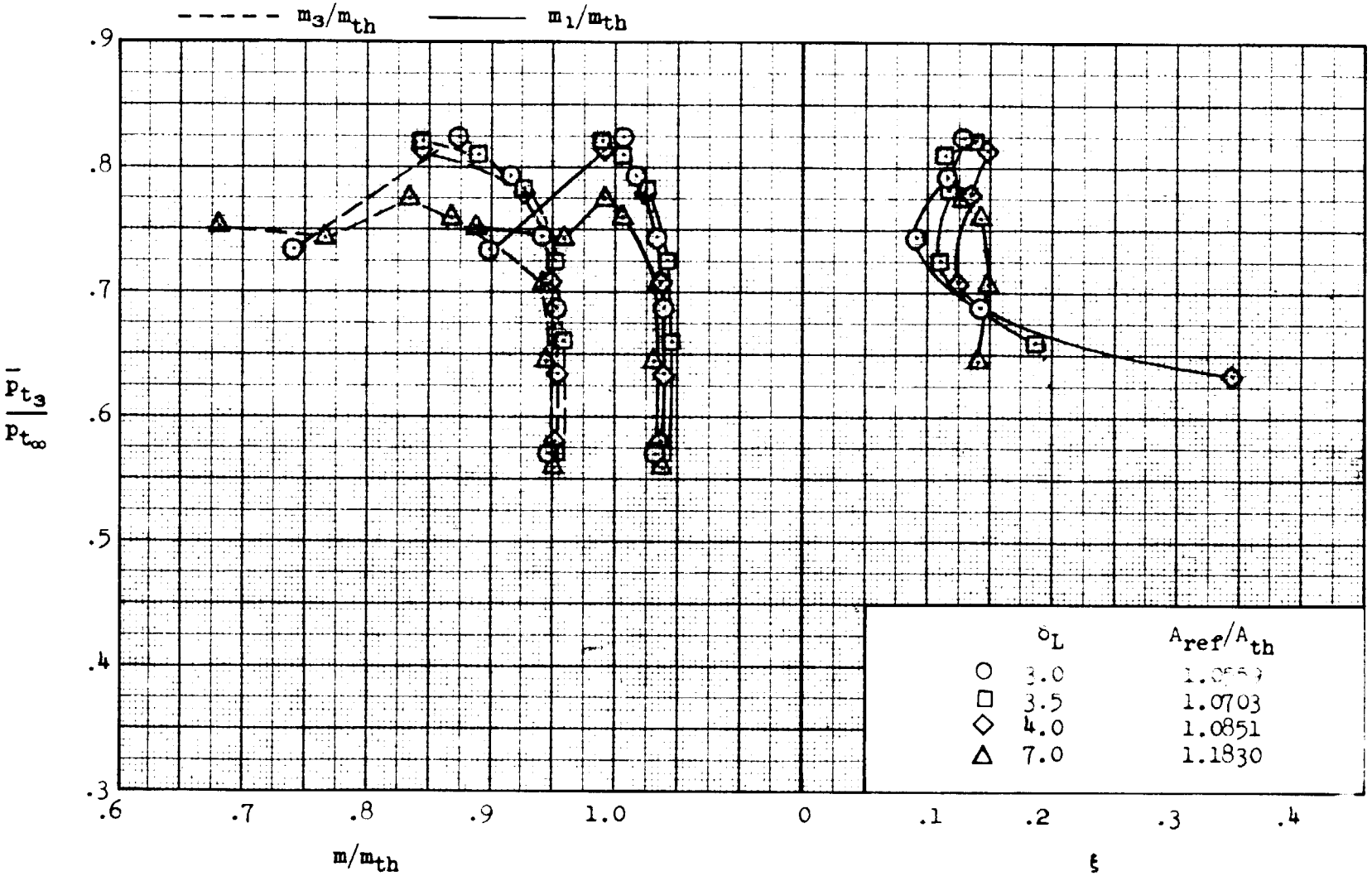

(c) δ_R = 18.0°; inlet performance.

Figure 17.- Continued.

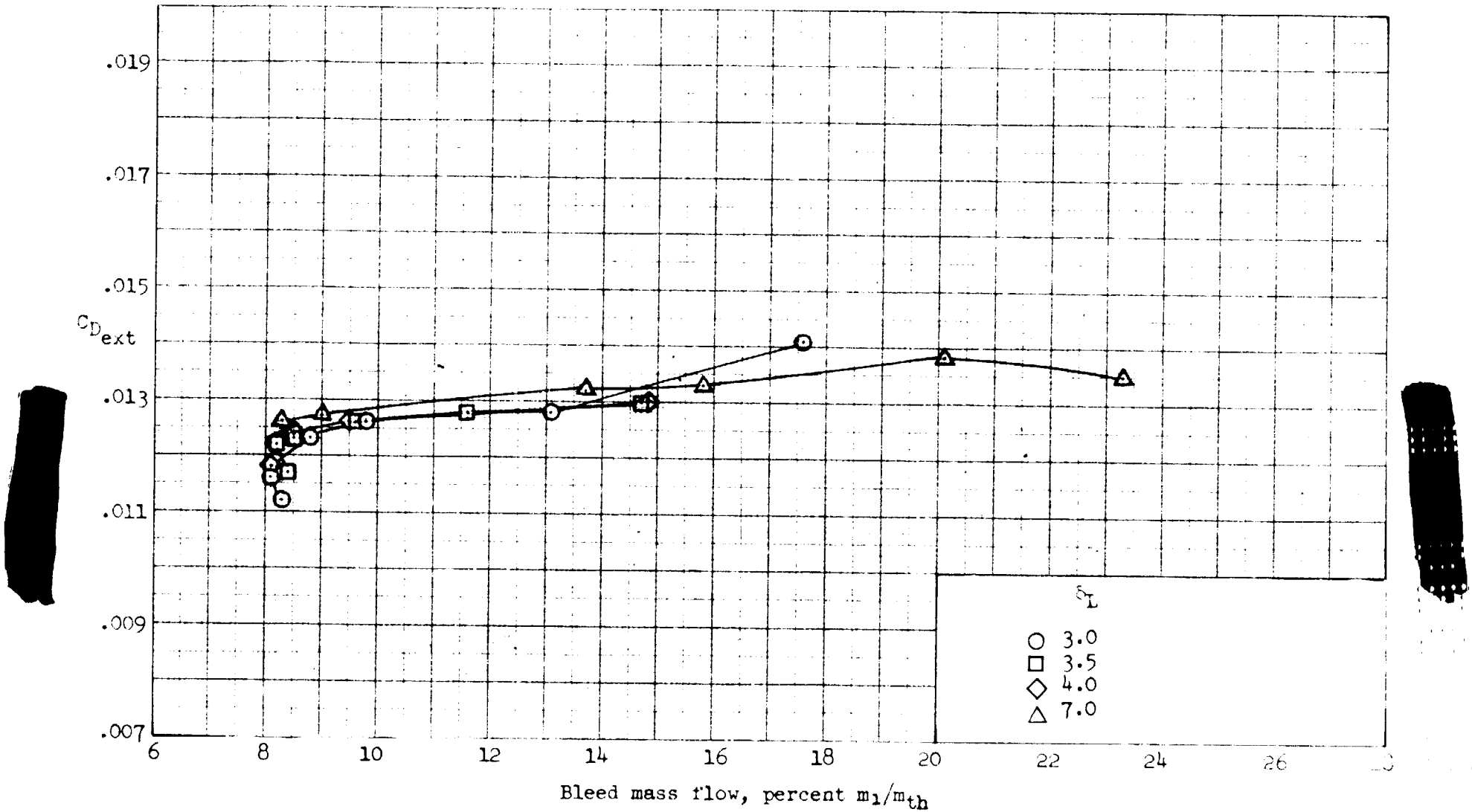

(c) Concluded. δ_R = 18.0°; external-drag coefficent.

Figure 17.- Concluded.

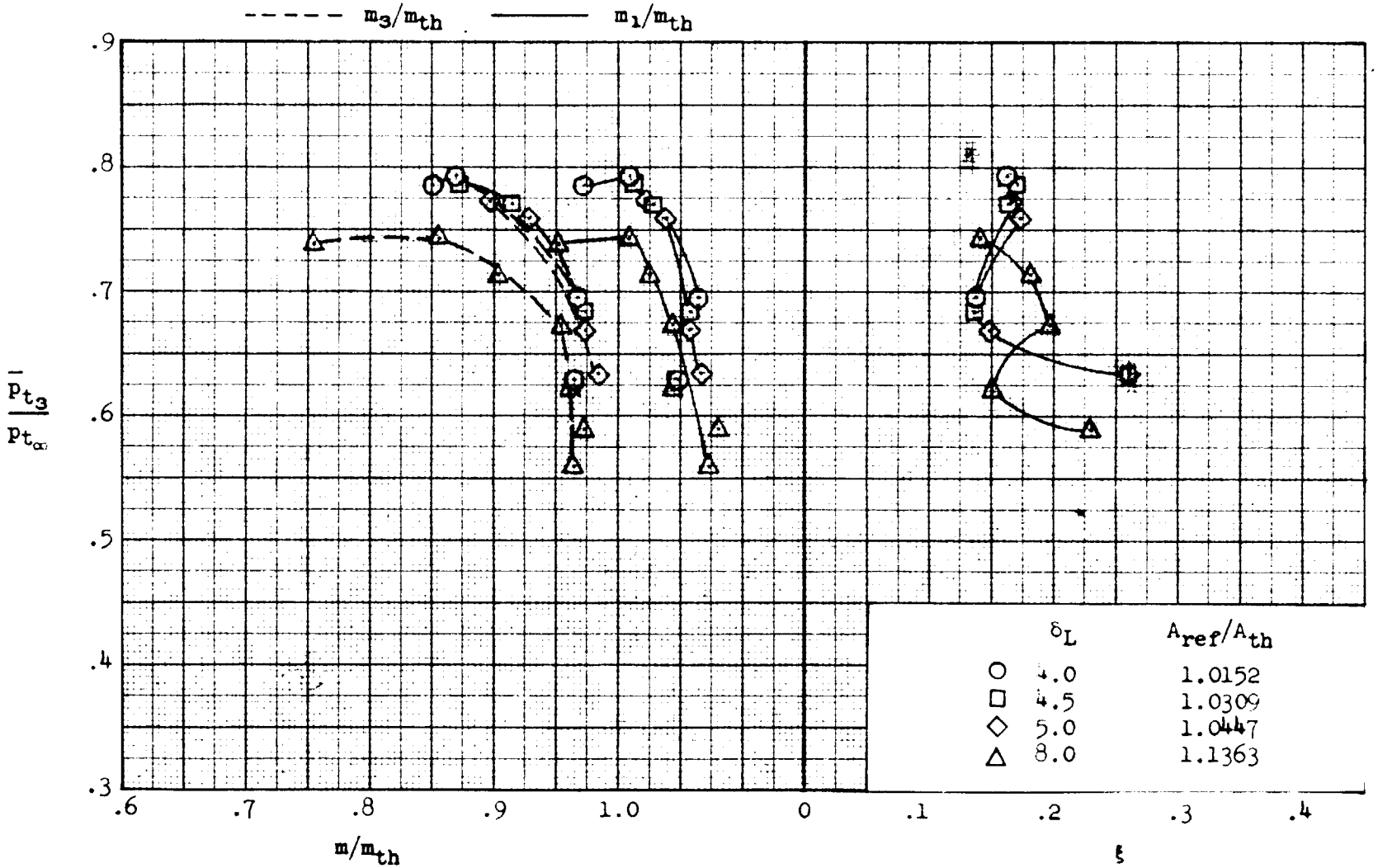

(a) δ_R = 17.0°; inlet performance.

Figure 18.- Effect of lip angle variation on inlet performance and external-drag coefficient; M = 2.7, = 0°, β = 0°. Configuration: nose 1, diverter 1, porosity 1, bleed exit 1.

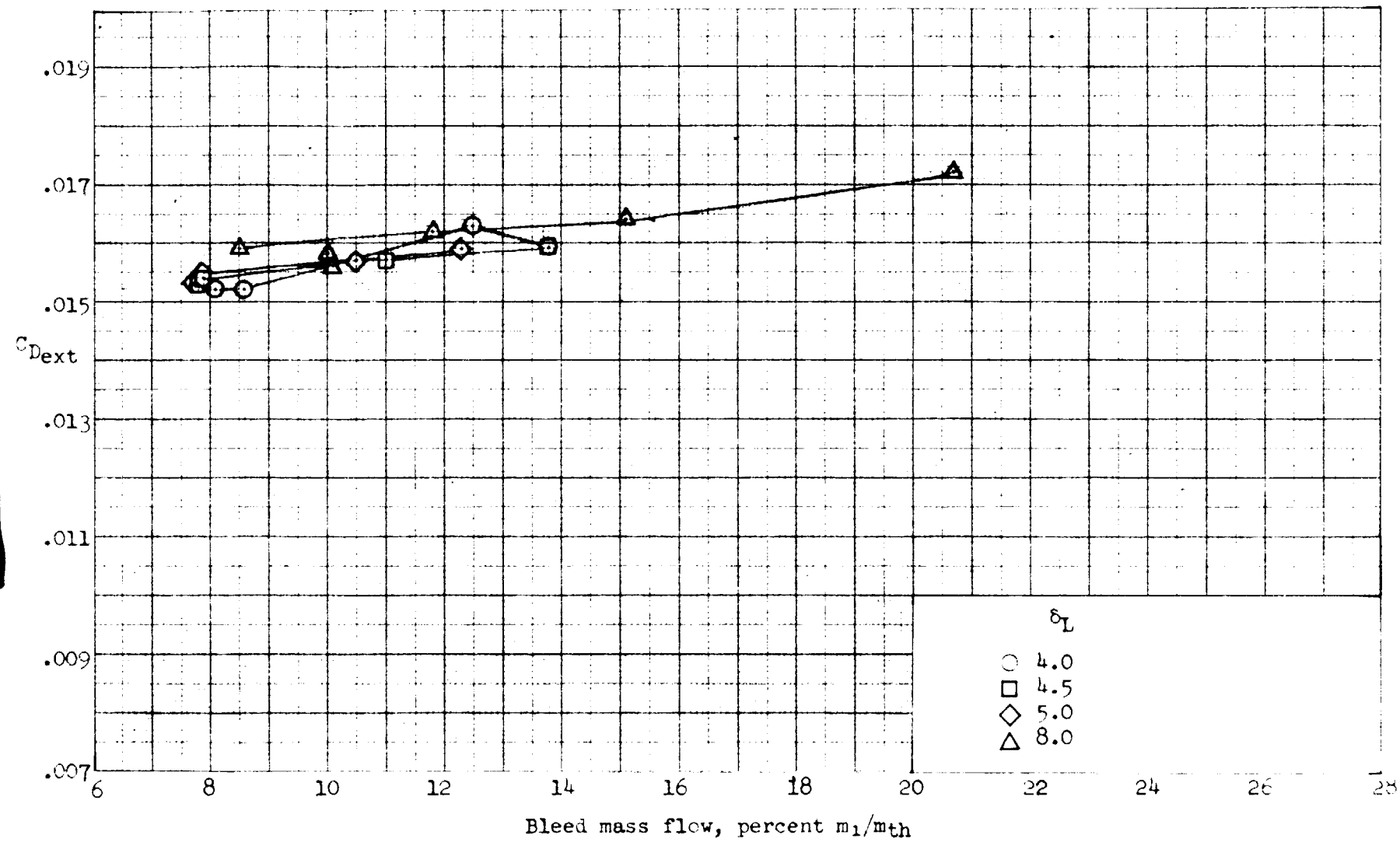

(a) Concluded. δ_R = 17.0°; external-drag coefficient.

Figure 18.- Continued.

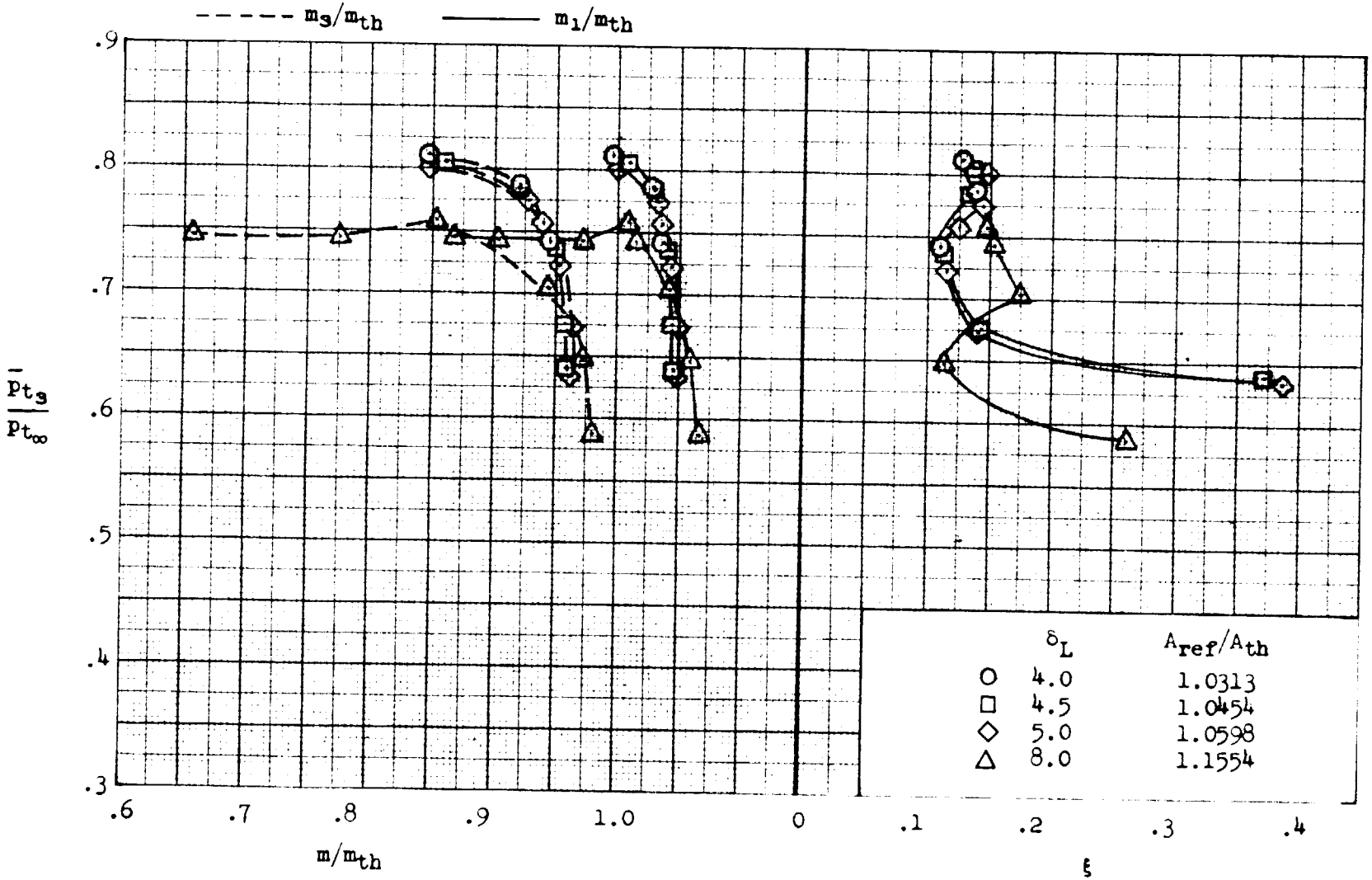

(b) δ_R = 17.5°; inlet performance.

Figure 18.- Continued.

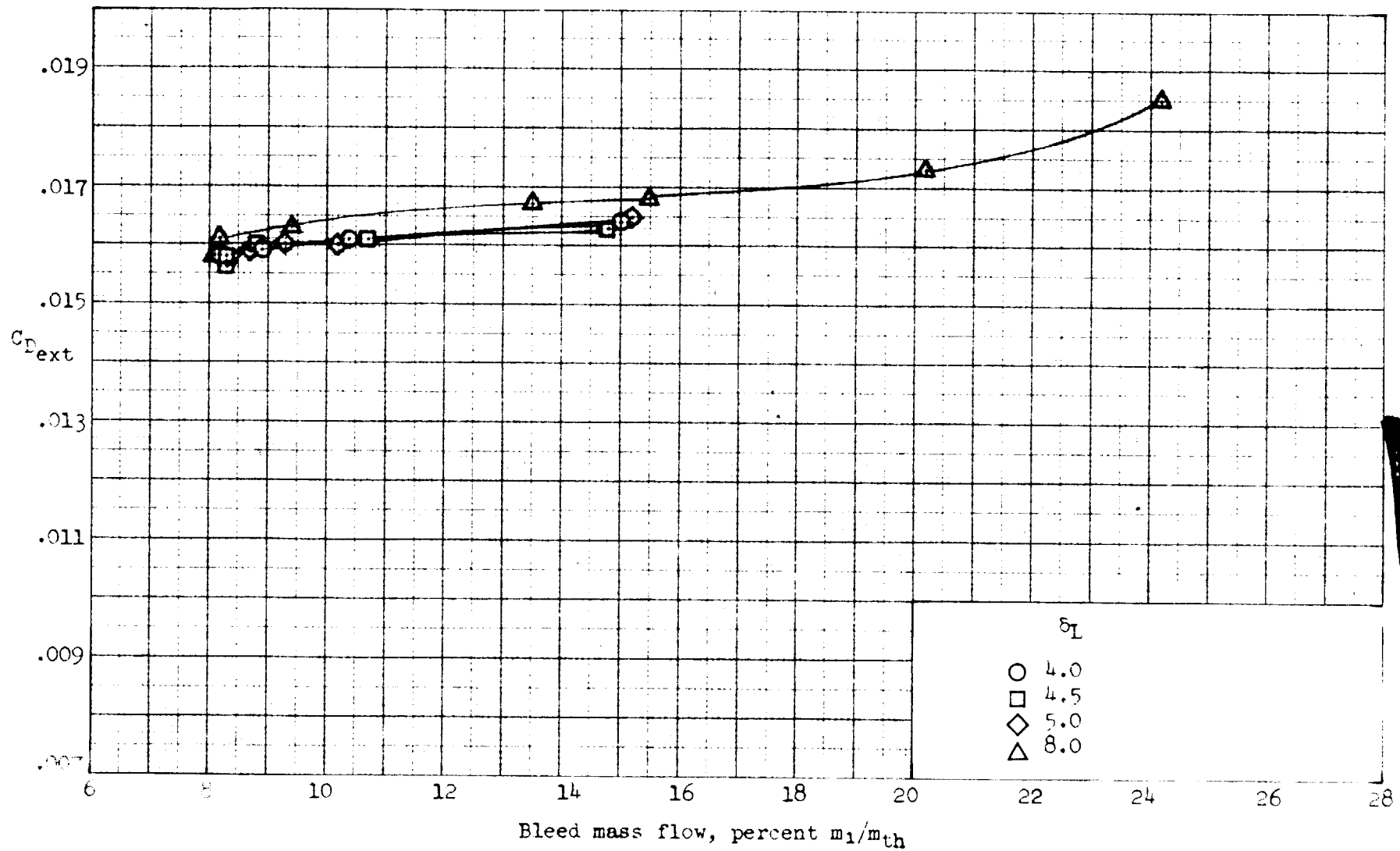

(b) Concluded. δ_R = 17.0°; external-drag coefficient.

Figure 18.- Continued.

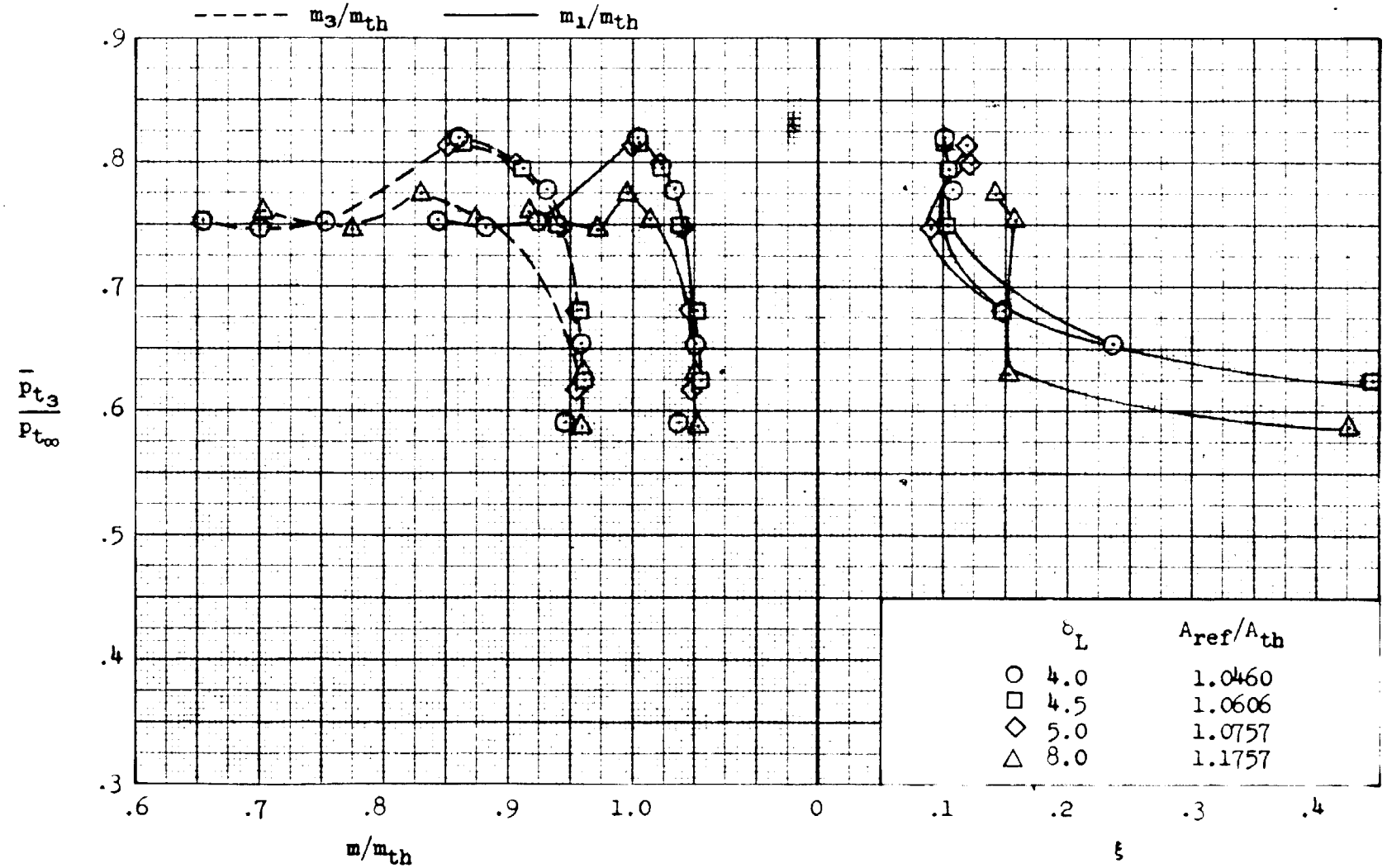

(c) δ_R = 18.0°; inlet performance.

Figure 18.- Continued.

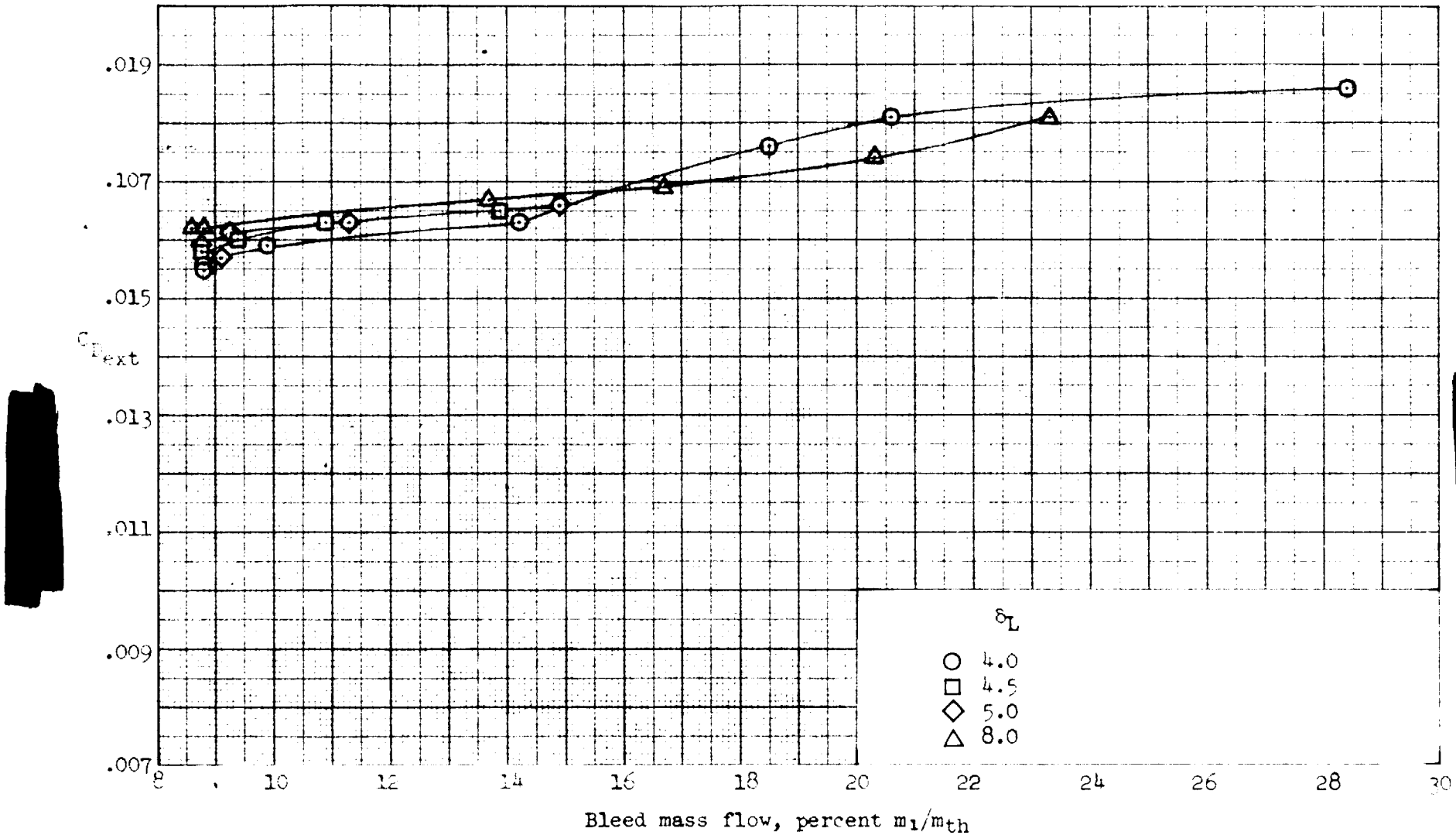

(c) Concluded. δ_R = 18.0°; external-drag coefficient.

Figure 18.- Concluded.

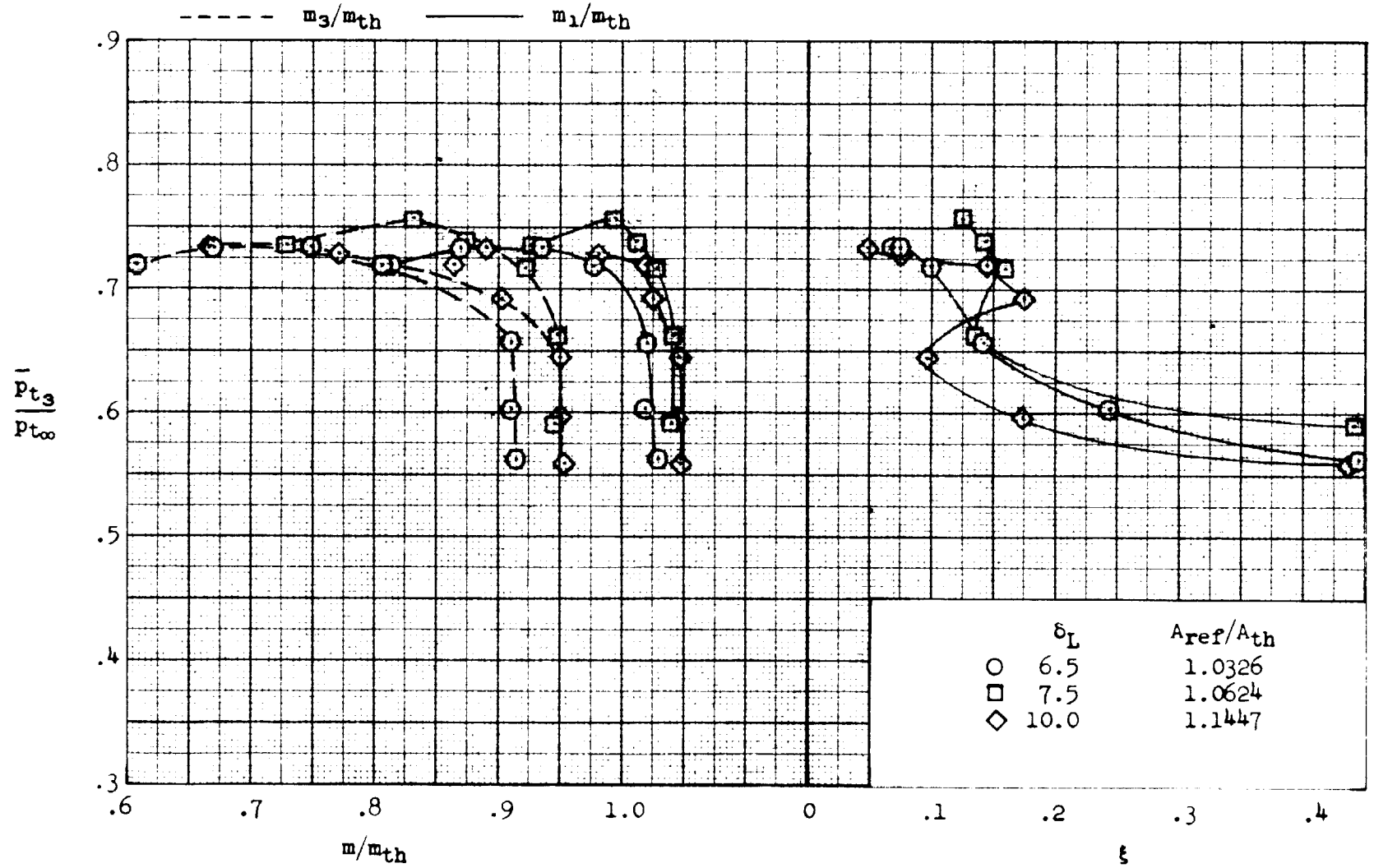

(a) δ_R = 17.0°; inlet performance.

Figure 19.- Effect of lip angle variation on inlet performance and external-drag coefficient: M = 2.76, α = 10°, β = 0°. Configuration: nose 1, diverter 1, porosity 1, bleed exit 1.

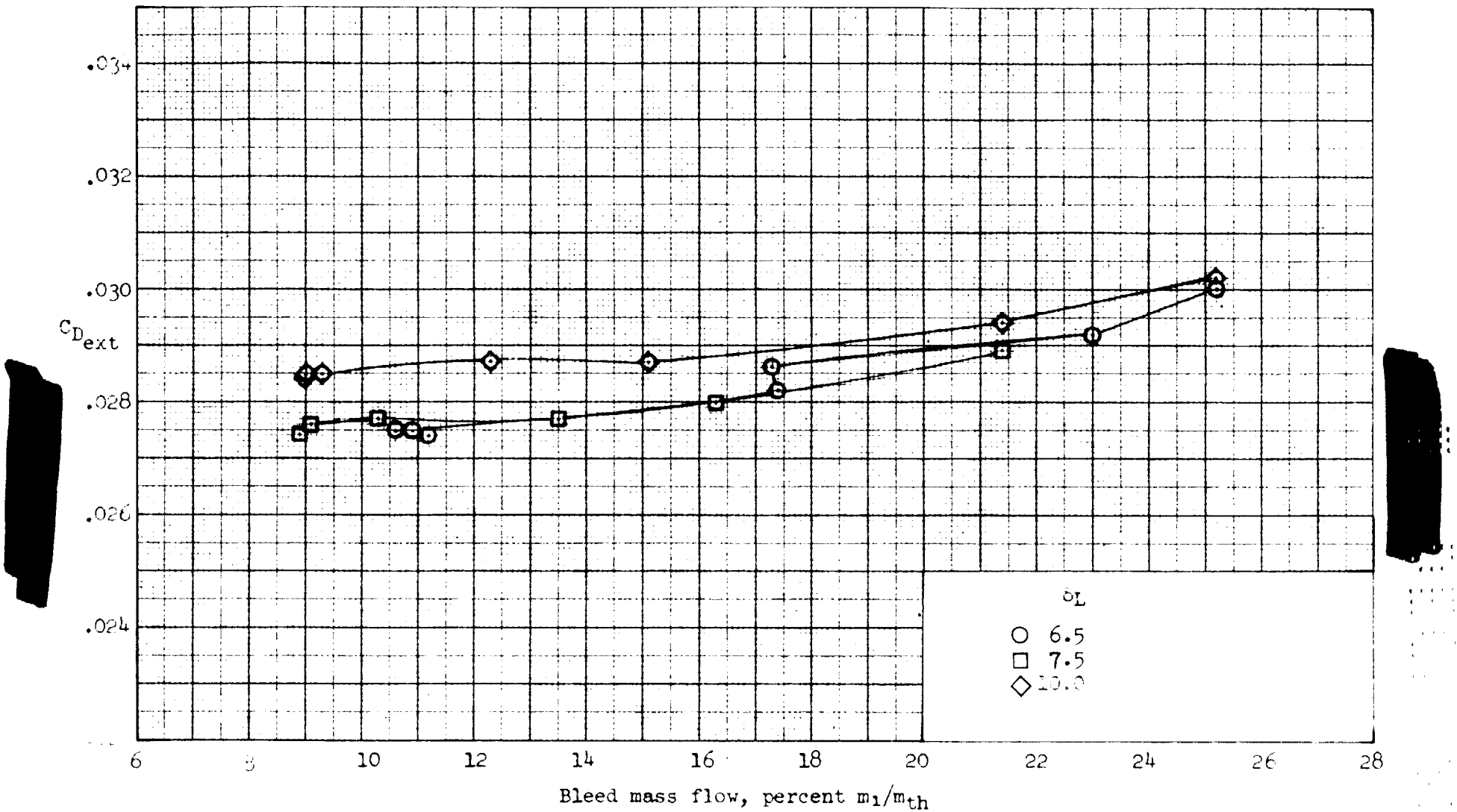

(a) Concluded. δ_R = 17.0°; external-drag coefficient.

Figure 19.- Continued.

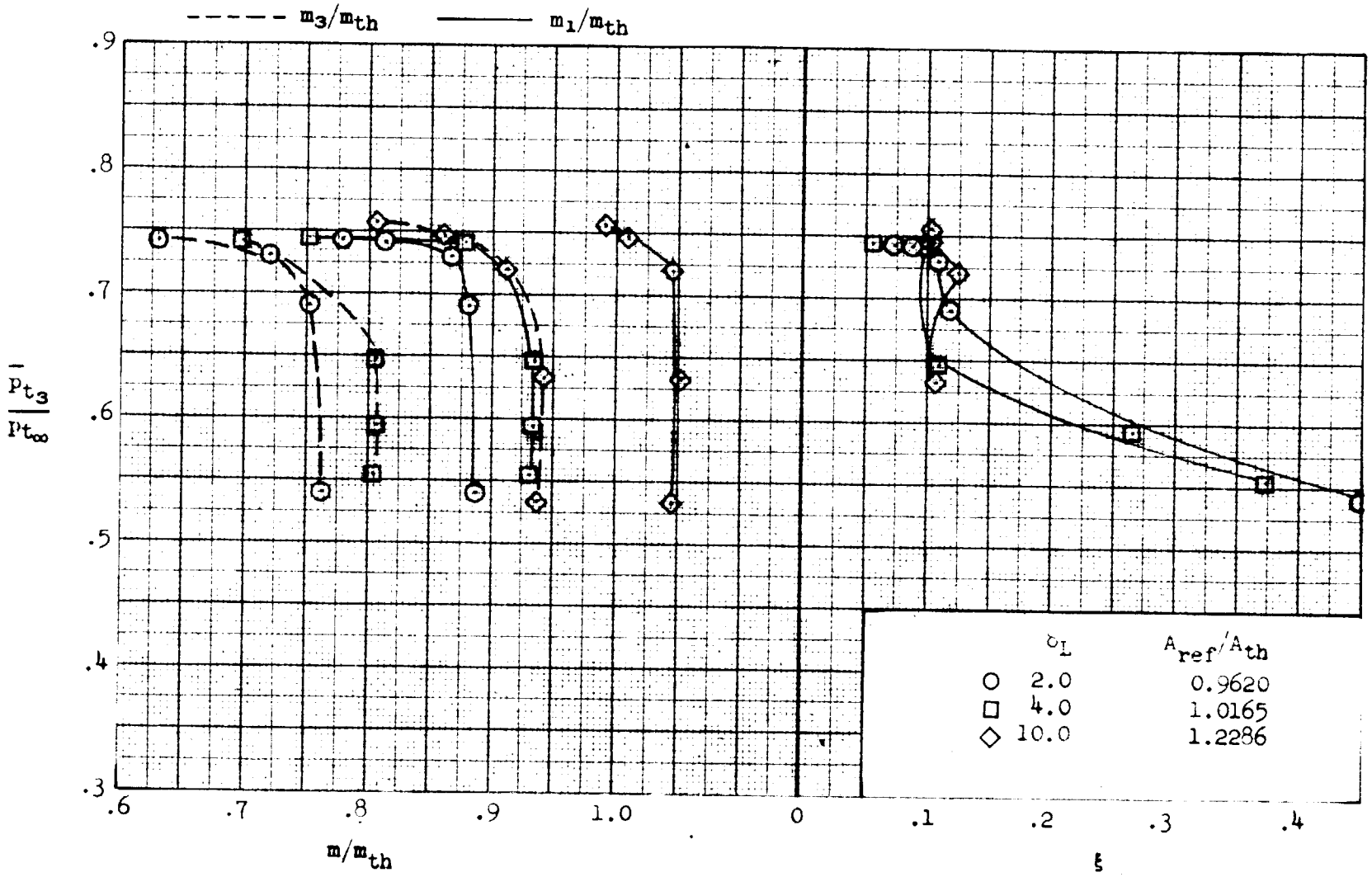

(b) δ_p = 18.5°; inlet performance.

Figure 19.- Continued.

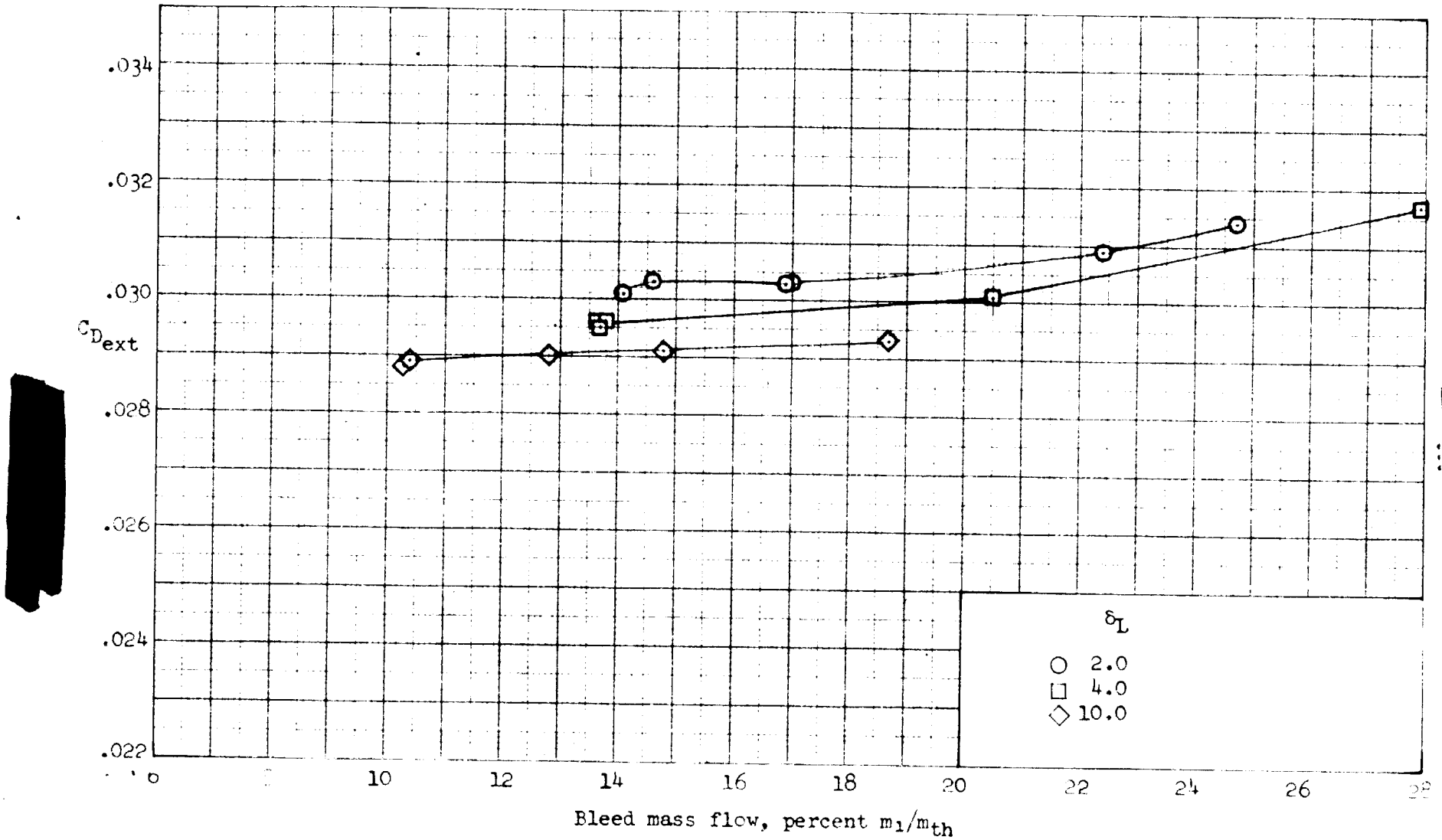

(b) Concluded. δ_R = 18.5°; external-drag coefficient.

Figure 19.- Concluded.

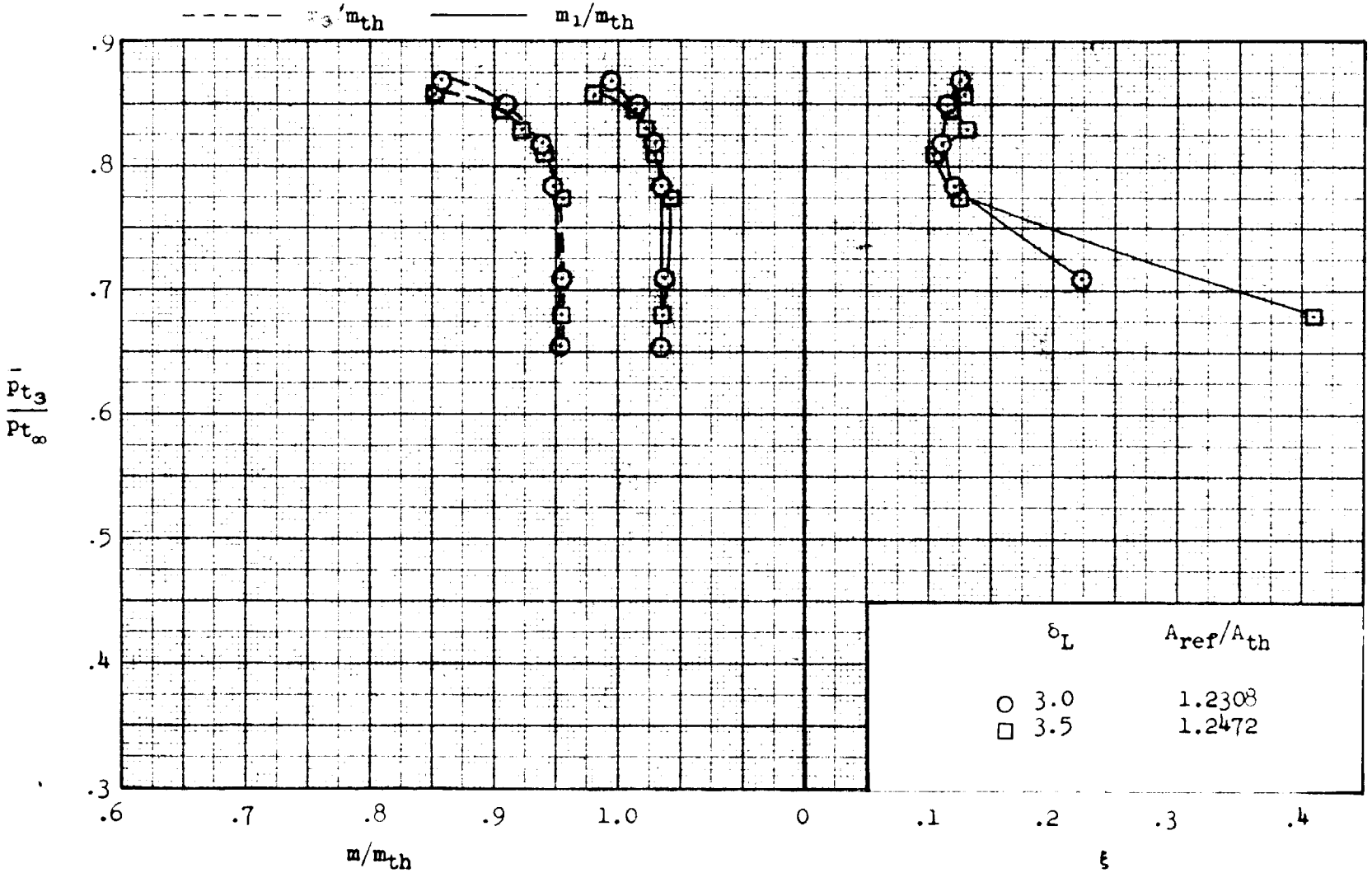

(a) δ_R = 17.5°; inlet performance.

Figure 20.- Effect of lip angle variation on inlet performance and external-drag coefficient: M = 1.50, α = 0°, β = 0°. Configuration: nose 1, diverter 1, porosity 1, bleed exit 1.

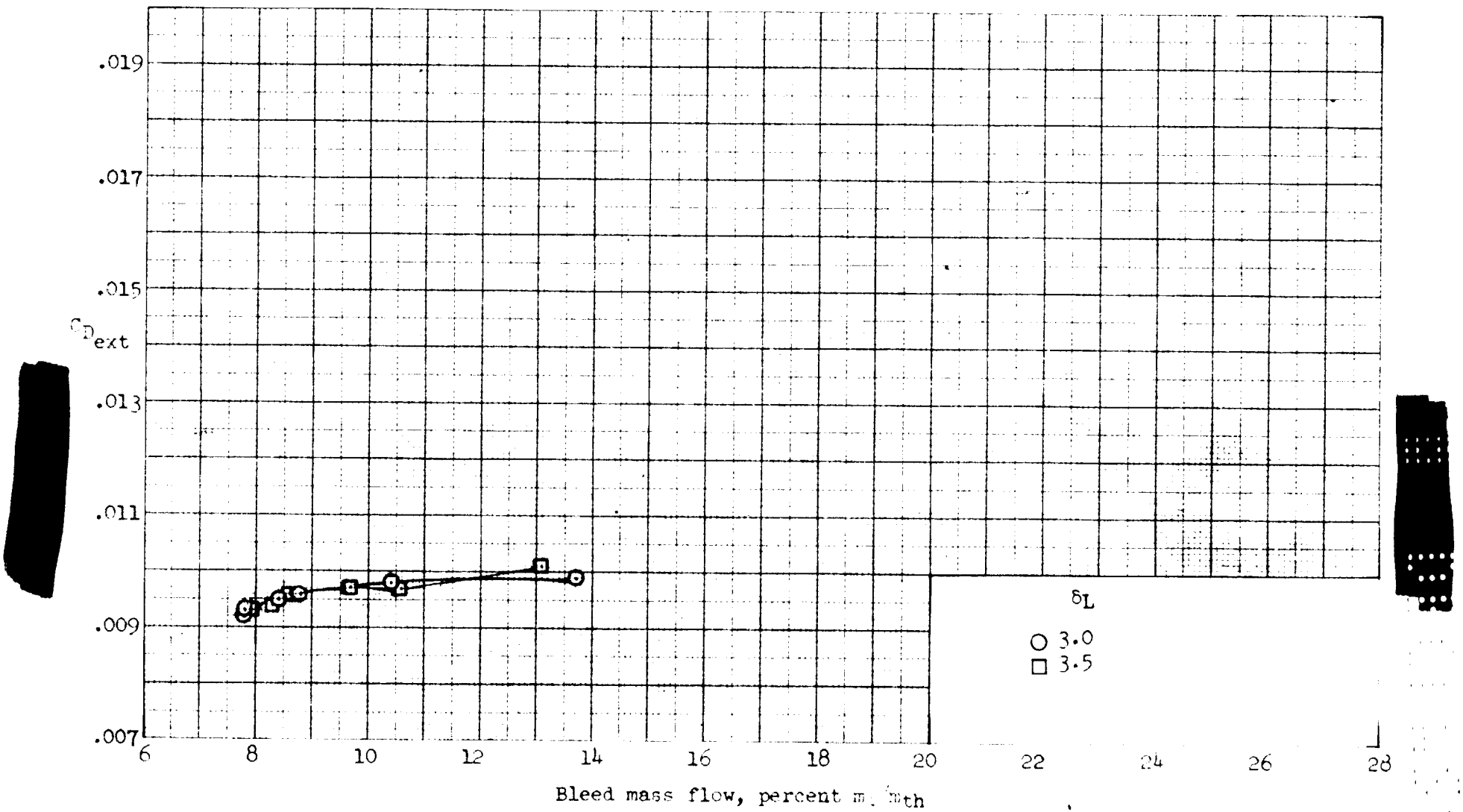

(a) Concluded. δ_F = 17.5°; external-drag coefficient.

Figure 20.- Continued.

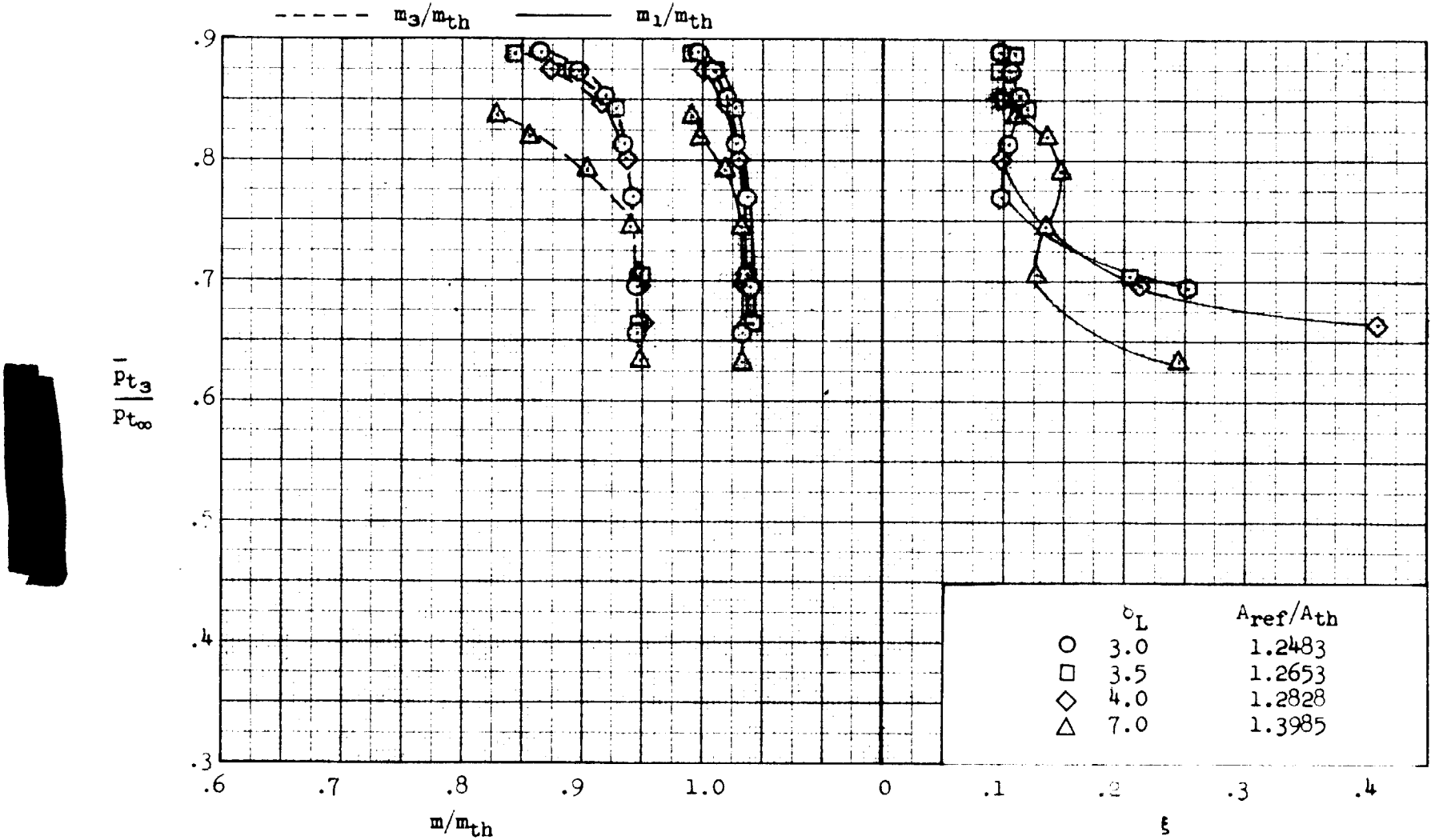

(b) δ_R = 18.0°; inlet performance.

Figure 20.- Continued.

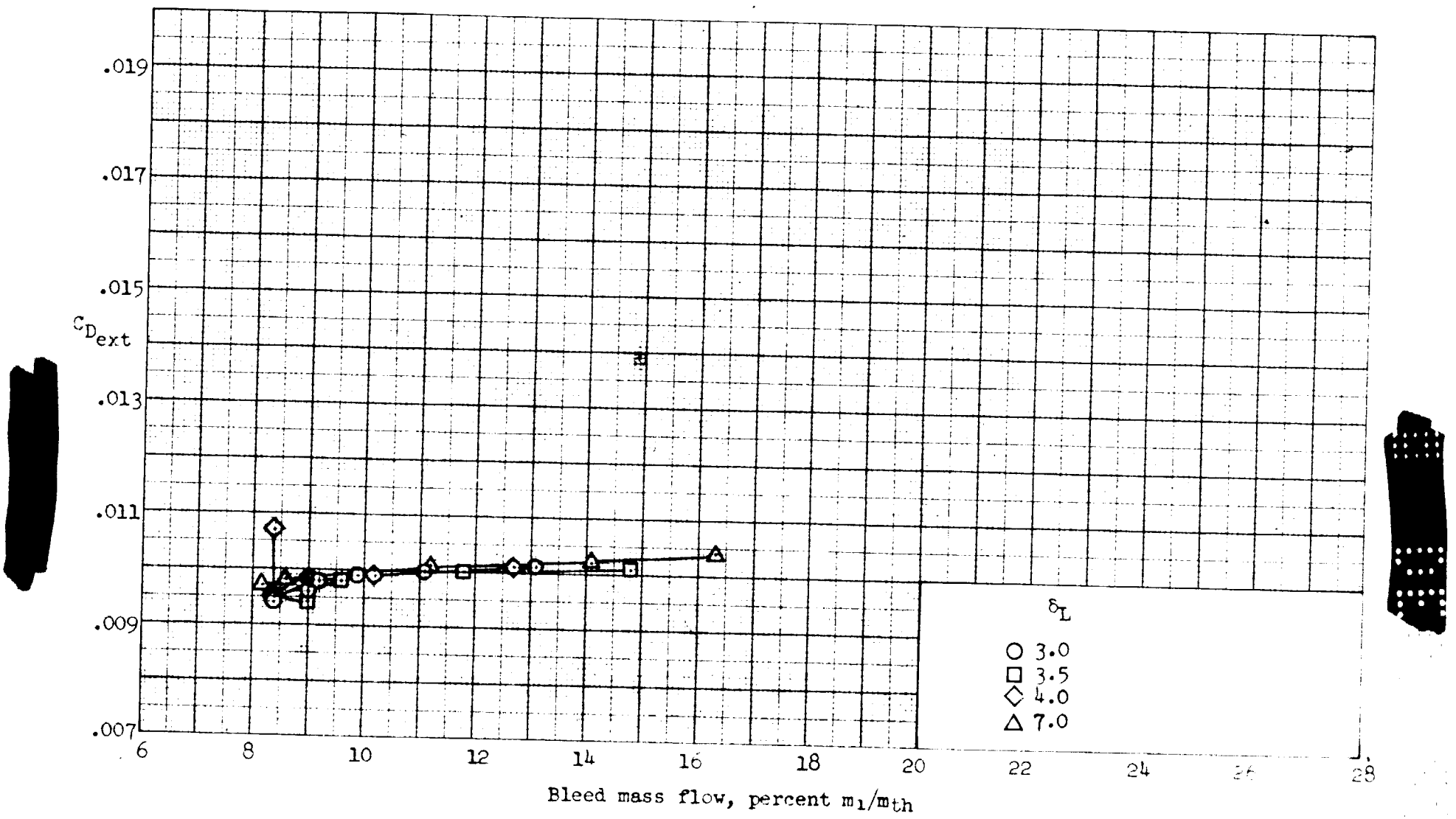

(b) Concluded. δ_R = 18.0°; external-drag coefficient.

Figure 20.- Concluded.

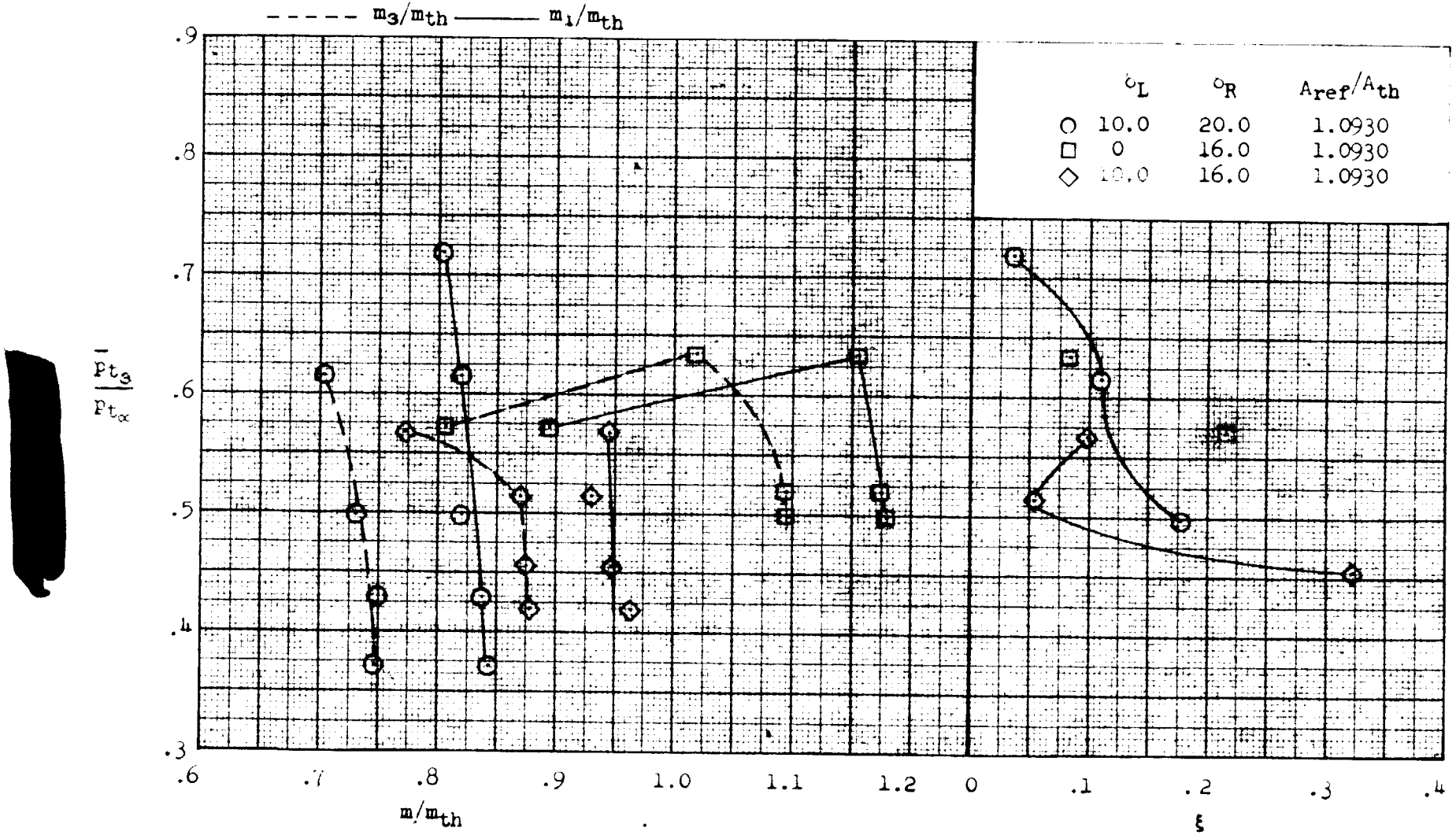

(a) Inlet performance.

Figure 1.- Inlet performance and external-drag coefficient for external lip and ramp angle combinations. M = 3.00, [illegible]°, β = [illegible]°. Baffle [illegible], diverter [illegible], bleed [illegible].

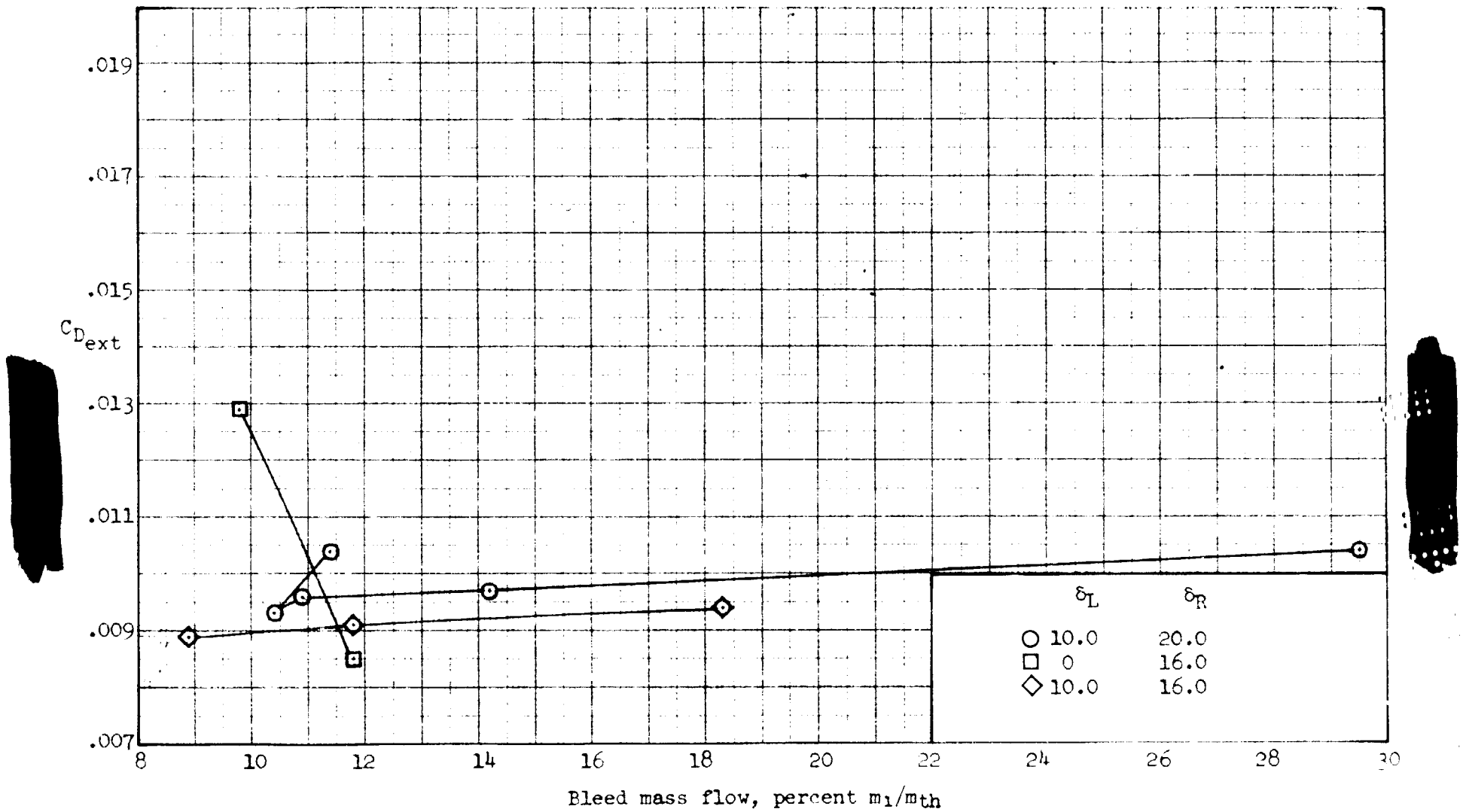

(b) External-drag coefficient.

Figure 21.- Concluded.

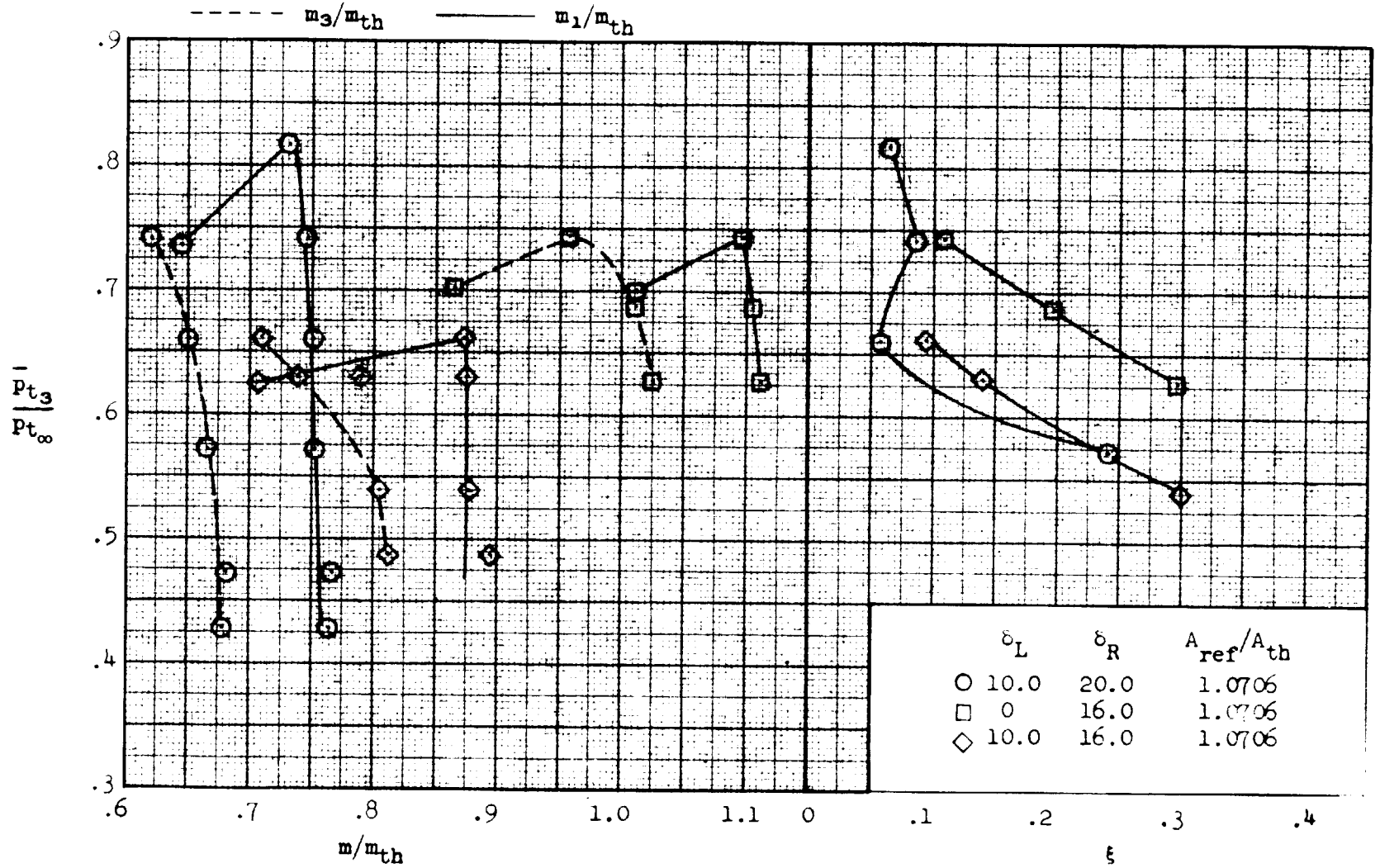

(a) Inlet performance.

Figure 22.- Inlet performance and external-drag coefficient for extreme lip and ramp angle combinations: M = 2.76, α = 2°, β = 0°. Configuration: nose 2, diverter 2, porosity 5, bleed exit 1.

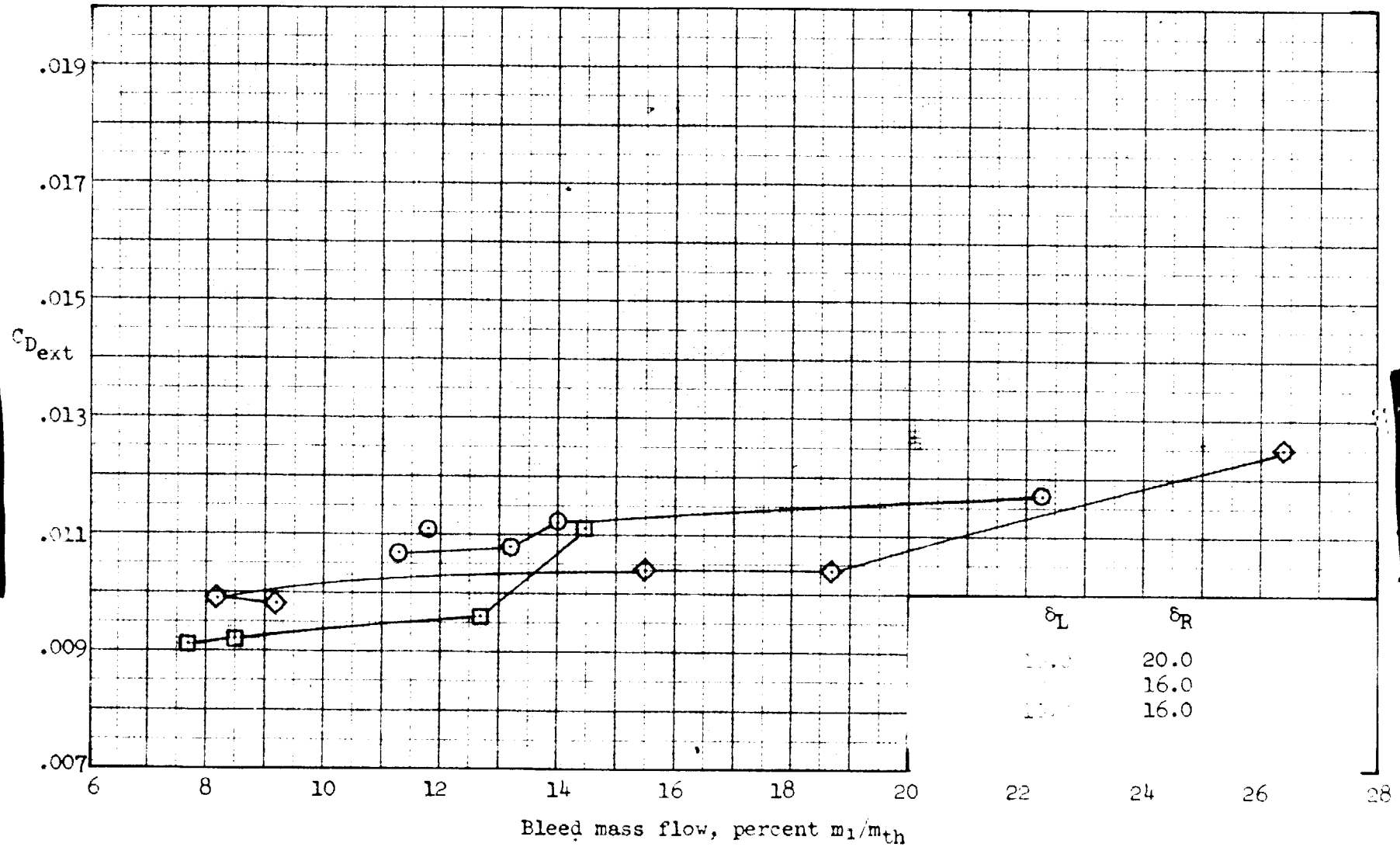

(b) External-drag coefficient.

Figure 22.- Concluded.

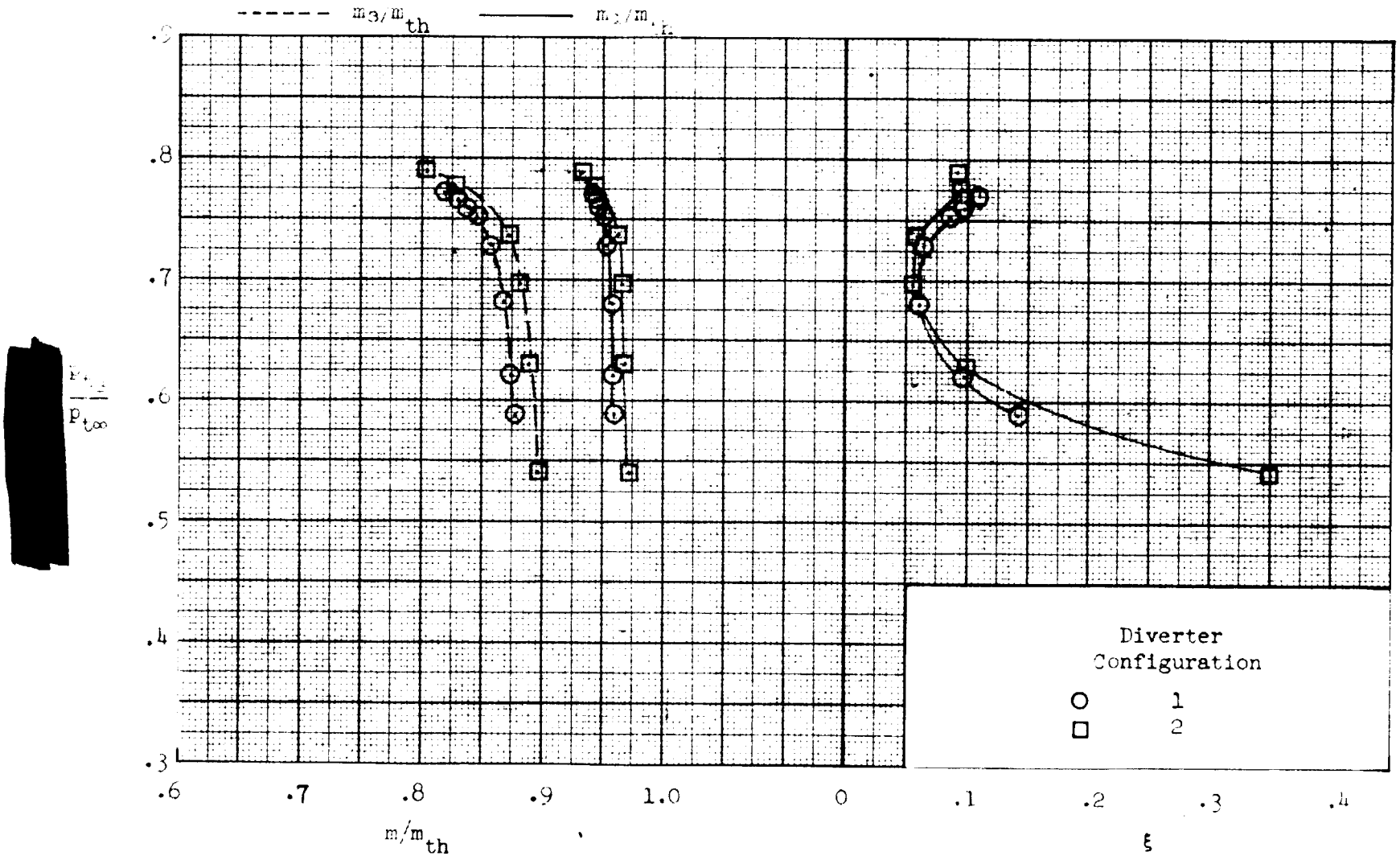

(a) $\alpha = 0°$, $\delta_R = 19.5°$, $\delta_L = 0°$, $A_{r_1}/A_{th} = 1.0$; inlet performance.

Figure 23.- Effect of fuselage-boundary-layer diverter profile on inlet performance and external-drag coefficient; M = 3.00, $\beta = 0°$. [illegible], porosity 1, bleed exit 1.

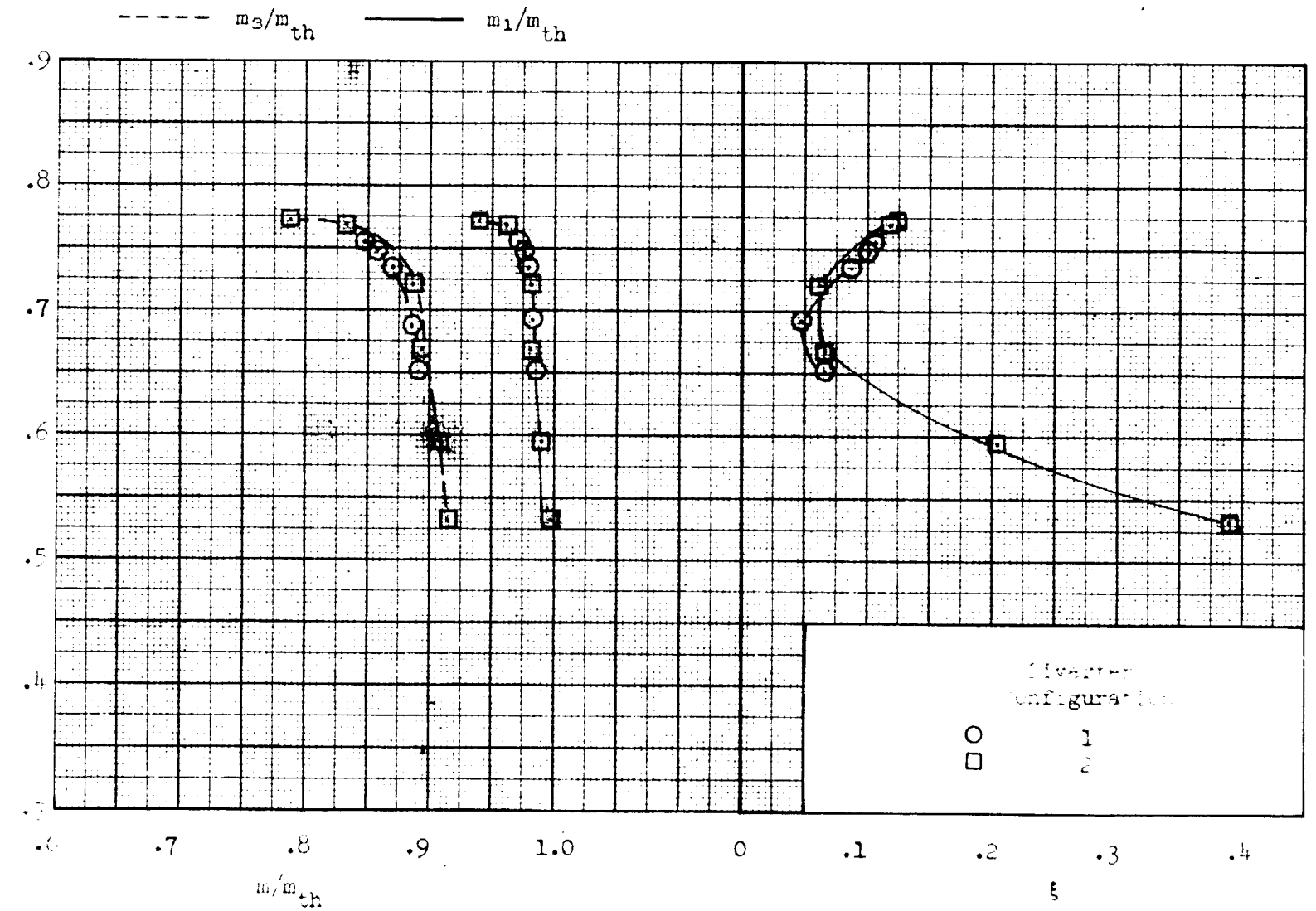

(b) $\alpha = 2°$, $\delta_R = 10.5°$, [illegible] inlet performance.

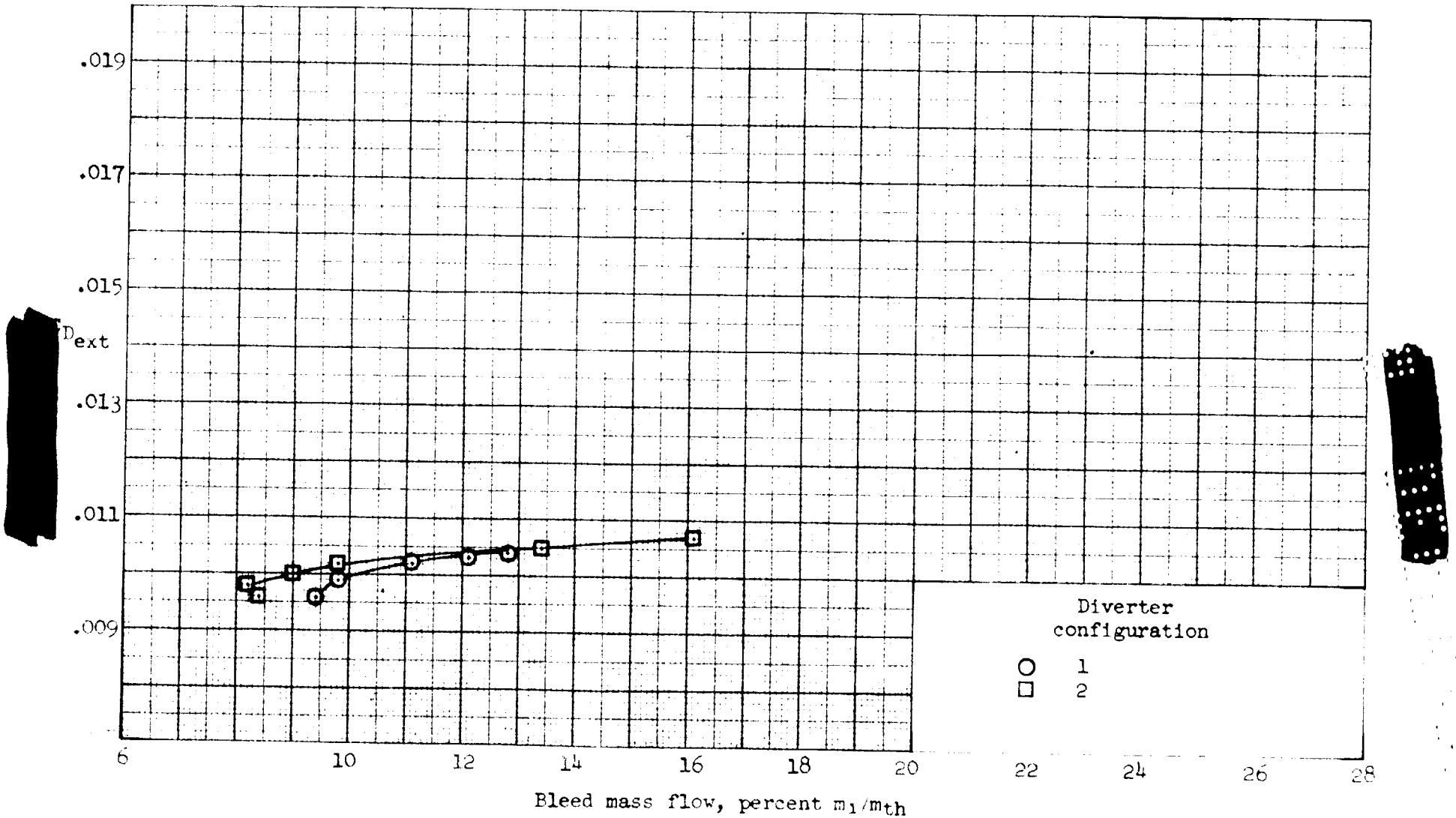

(b) Concluded. External-drag coefficient

Figure 23.- Continued.

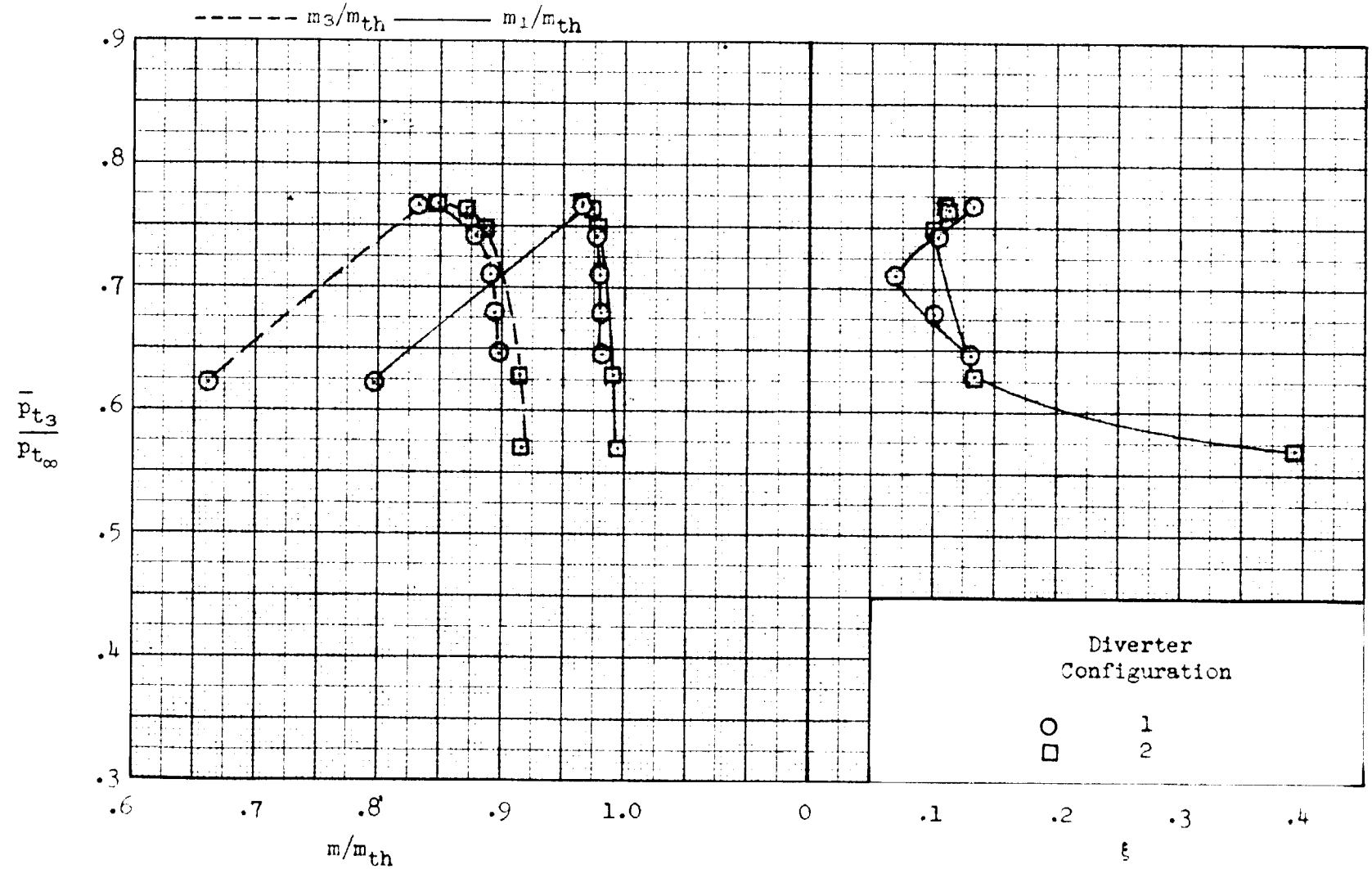

(c) α = 4°, δ_R = 18.5°, δ_L = 1.0°, A_{ref}/A_{th} = 0.9325; inlet performance.

Figure 23.- Continued.

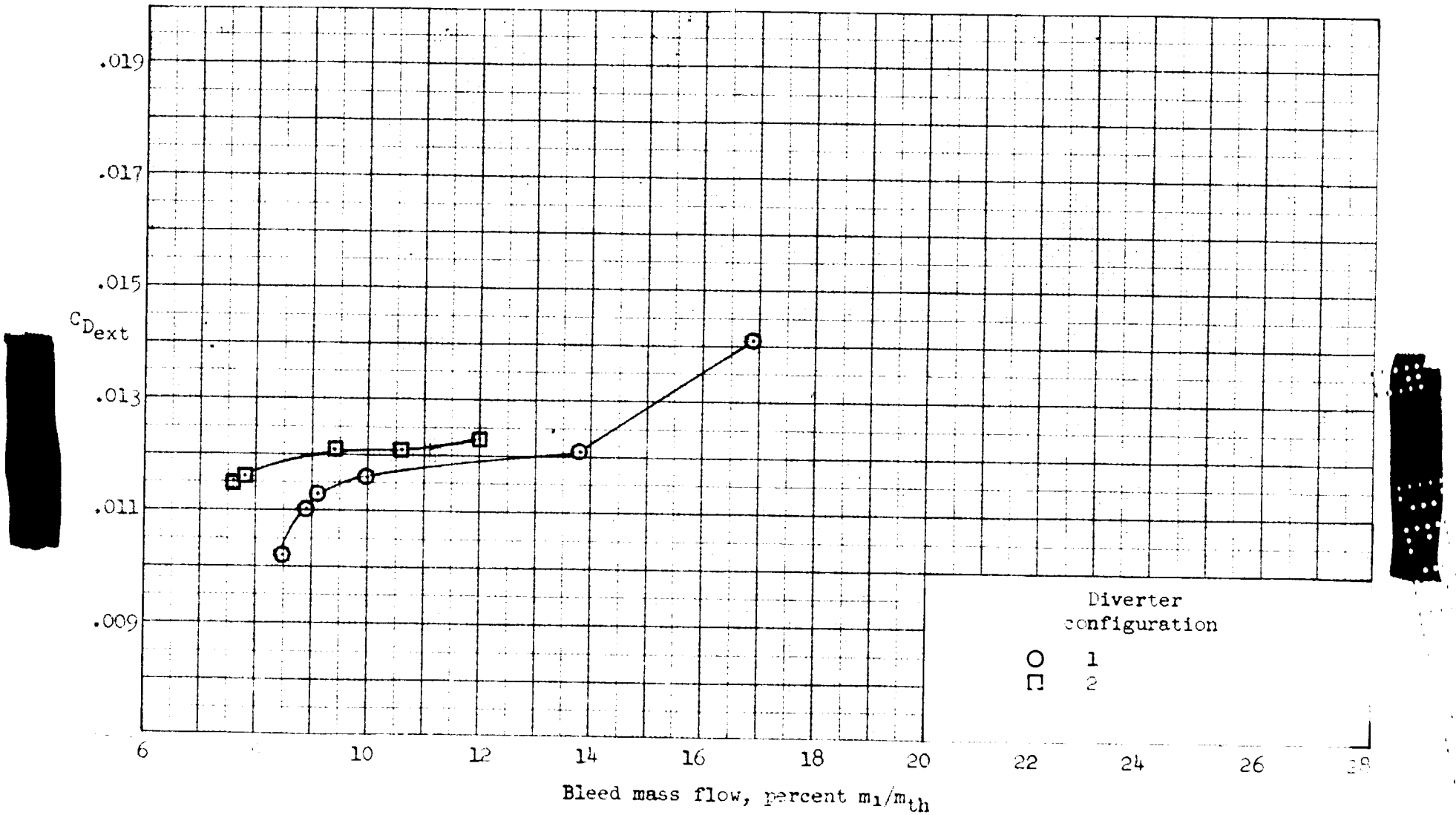

(c) Concluded. External-drag coefficient.

Figure 23.- Continued.

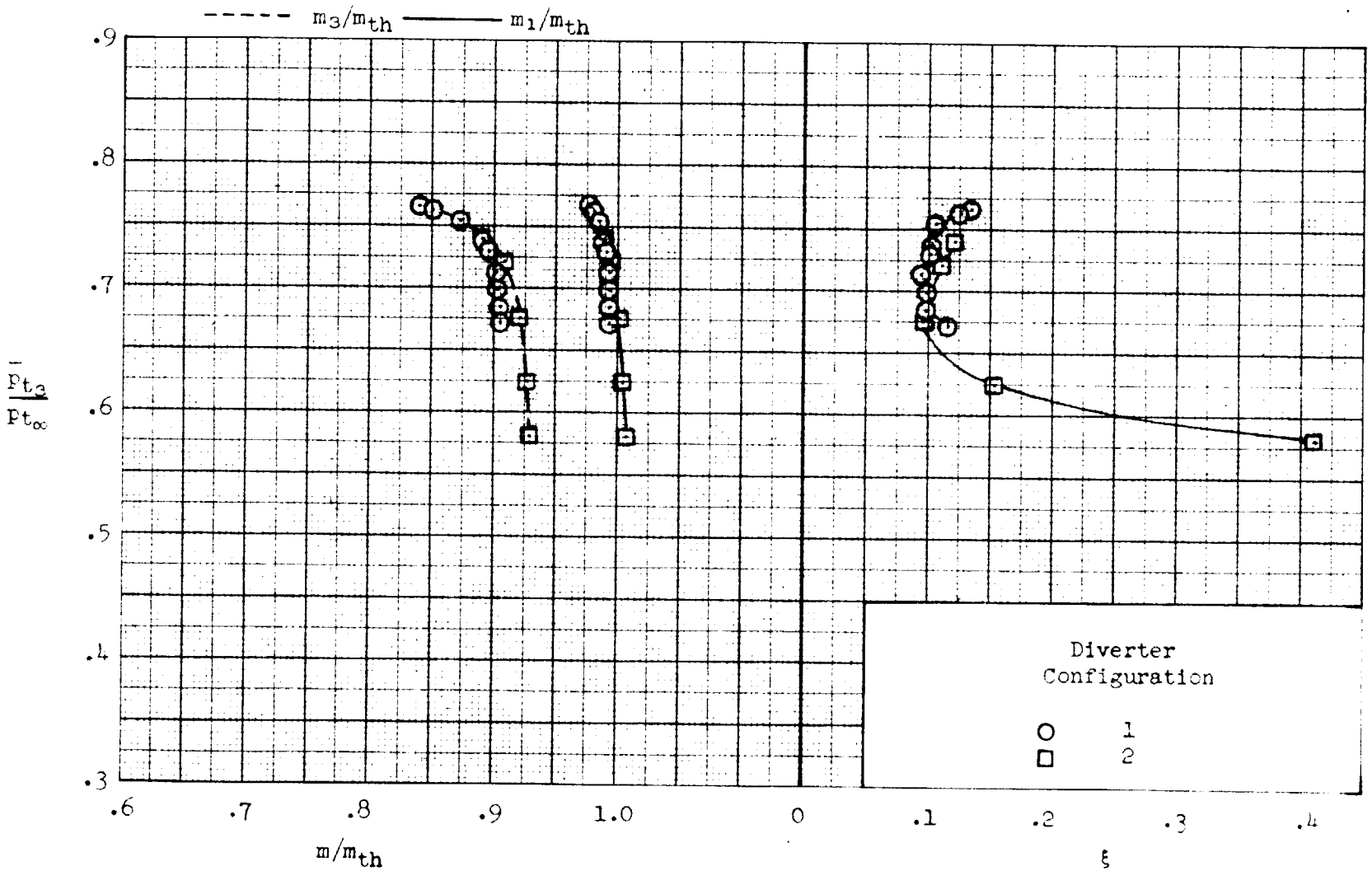

(d) $\alpha = 6°$, $\delta_R = 18.0°$, $\delta_L = 1.5°$, $A_{ref}/A_{th} = 0.8968$; inlet performance.

Figure 23.- Continued.

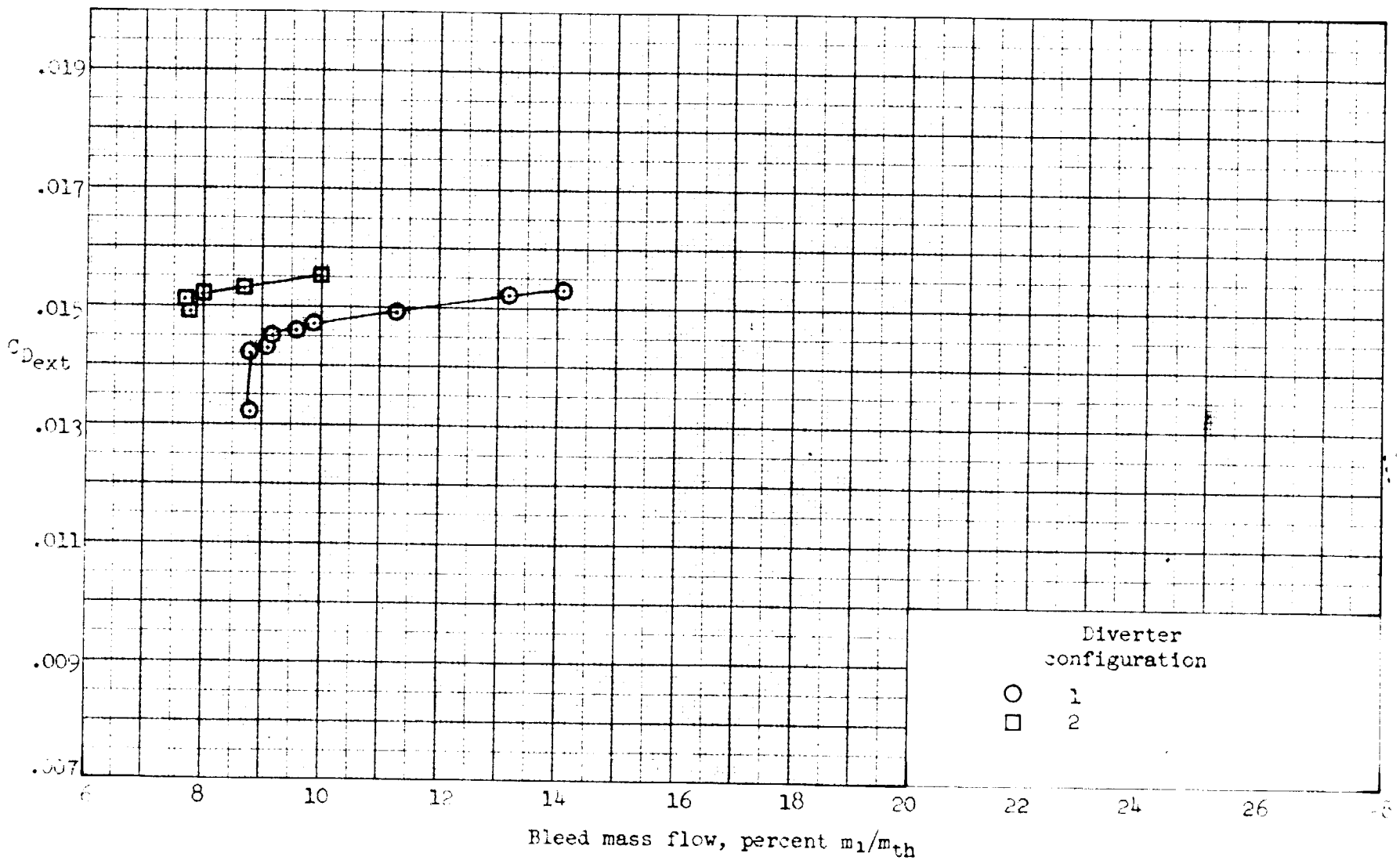

(d) Concluded. External-drag coefficient.

Figure 23.- Continued.

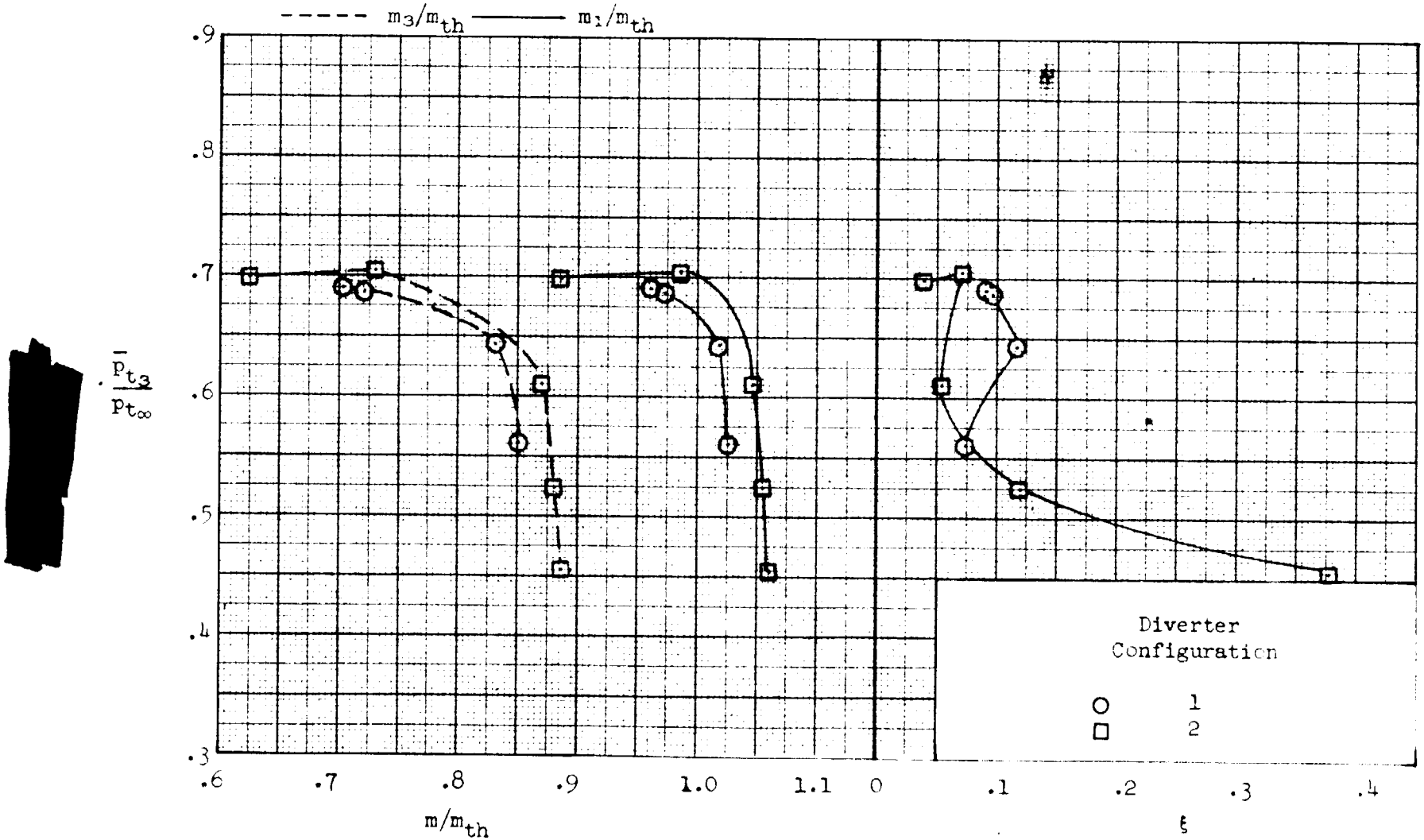

(e) $\alpha = 10°$, $\delta_R = 20.0°$, $\delta_L = 4.0°$, $A_{ref}/A_{th} = 0.9792$; inlet performance.

Figure 23.- Continued.

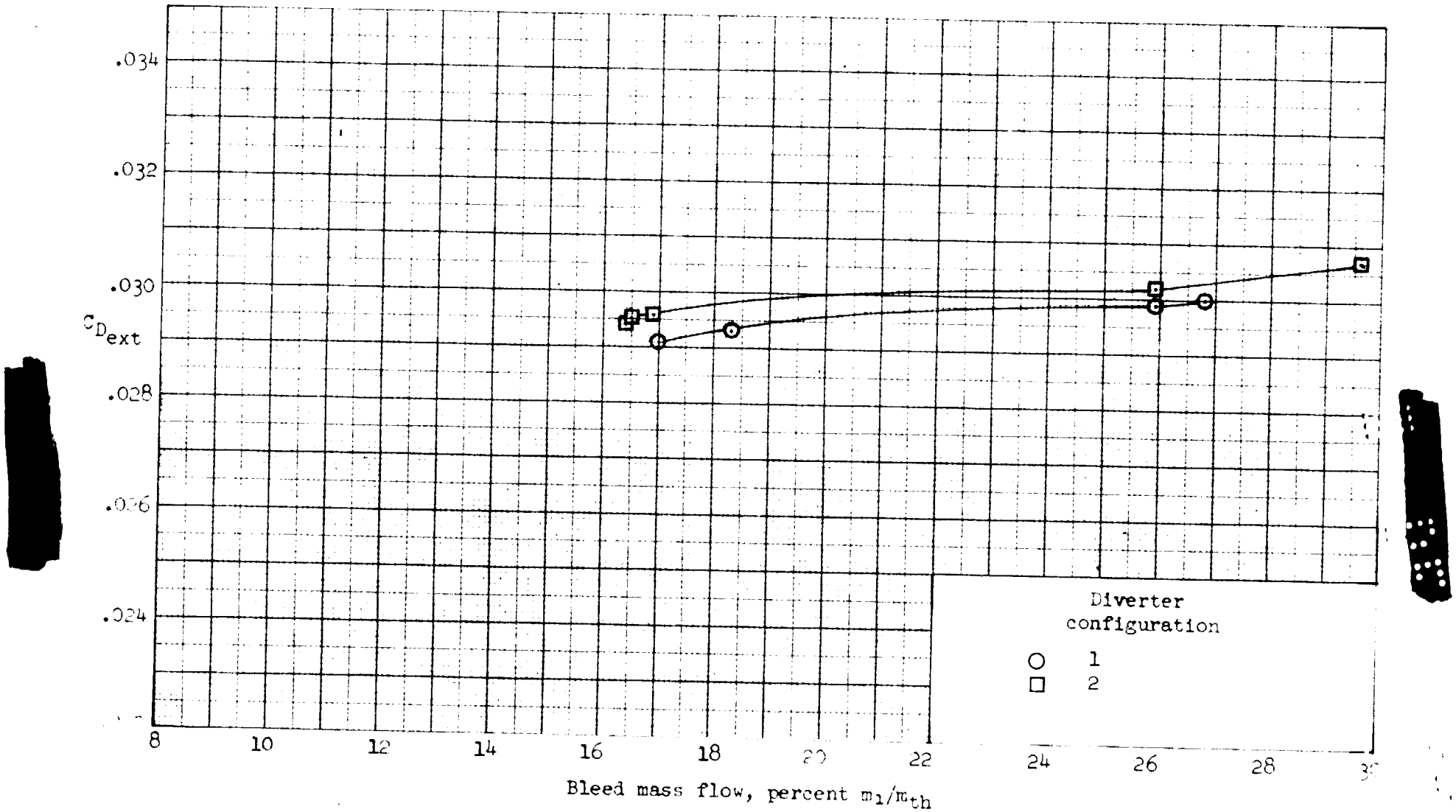

(e) Concluded. External-drag coefficient.

Figure 23.- Concluded.

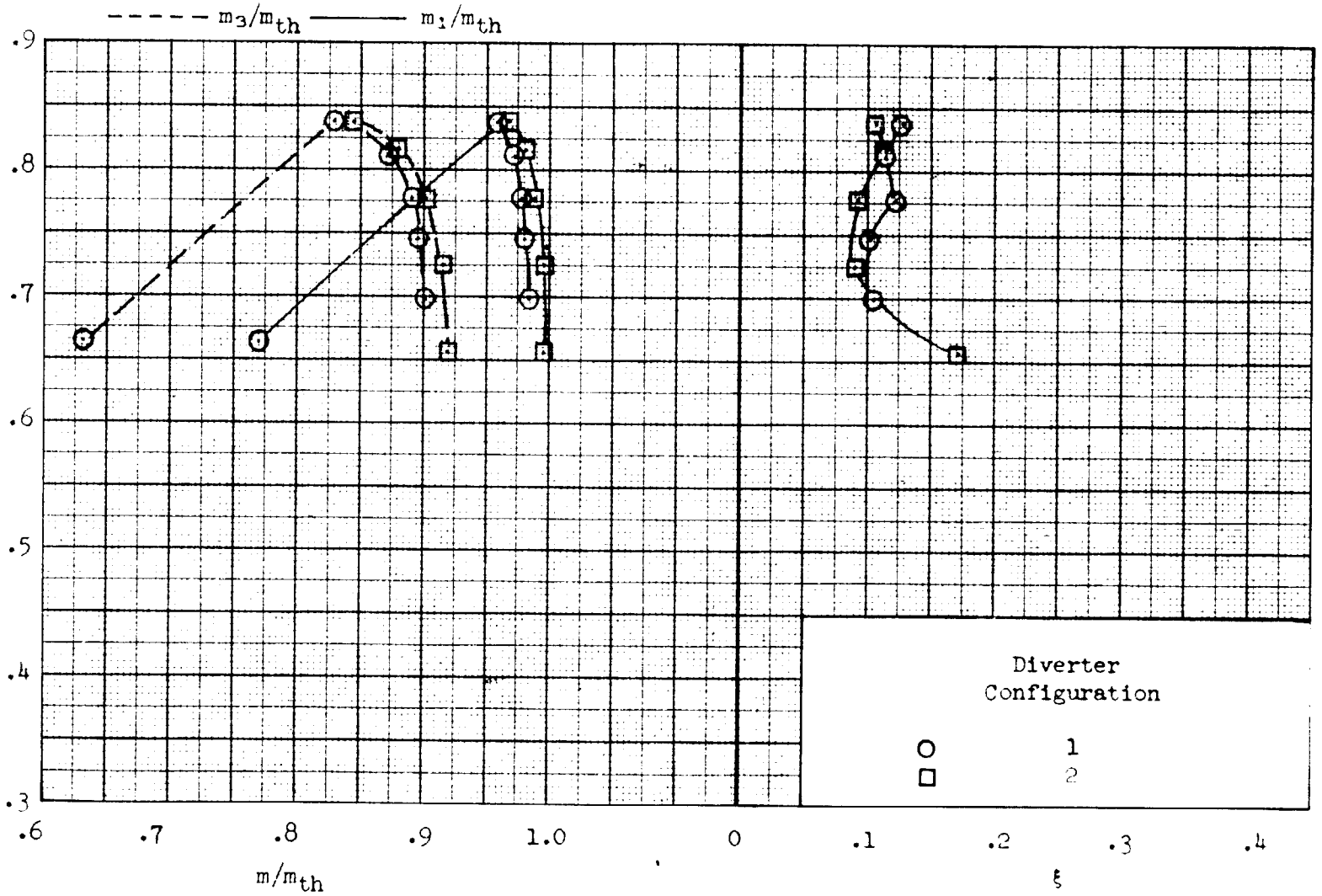

(a) $\alpha = 0°$, $\delta_R = 18.5°$, $\delta_L = 0.5°$, $A_{ref}/A_{th} = 1.0968$; inlet performance.

Figure 24.- Effect of fuselage-boundary-layer diverter profile on inlet performance and external-drag coefficient; M = 2.76, $\beta = 0°$. Configuration: nose 1, porosity 1, bleed exit 1.

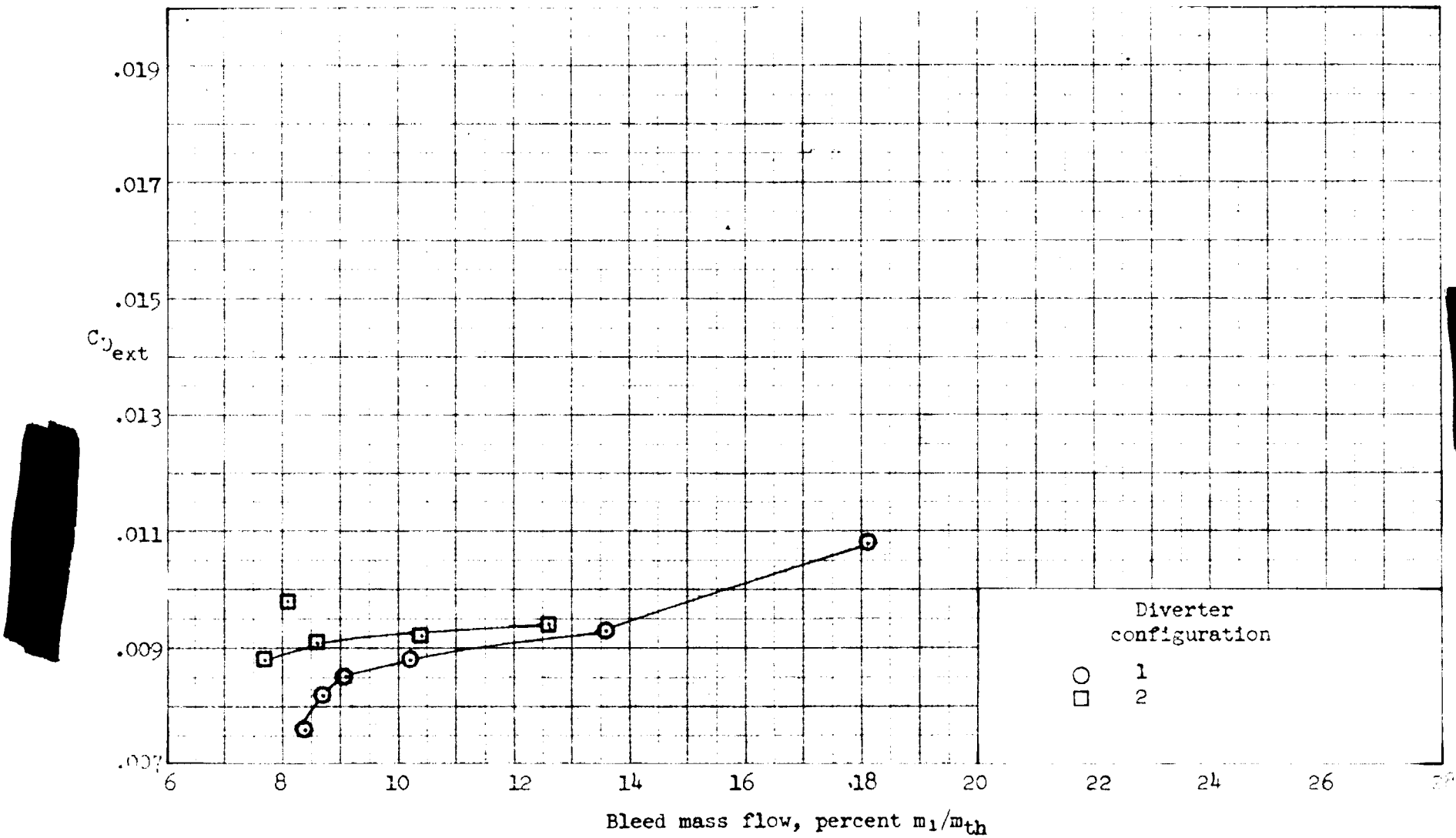

a. Concluded. External-drag coefficient.

Figure 24.- Continued.

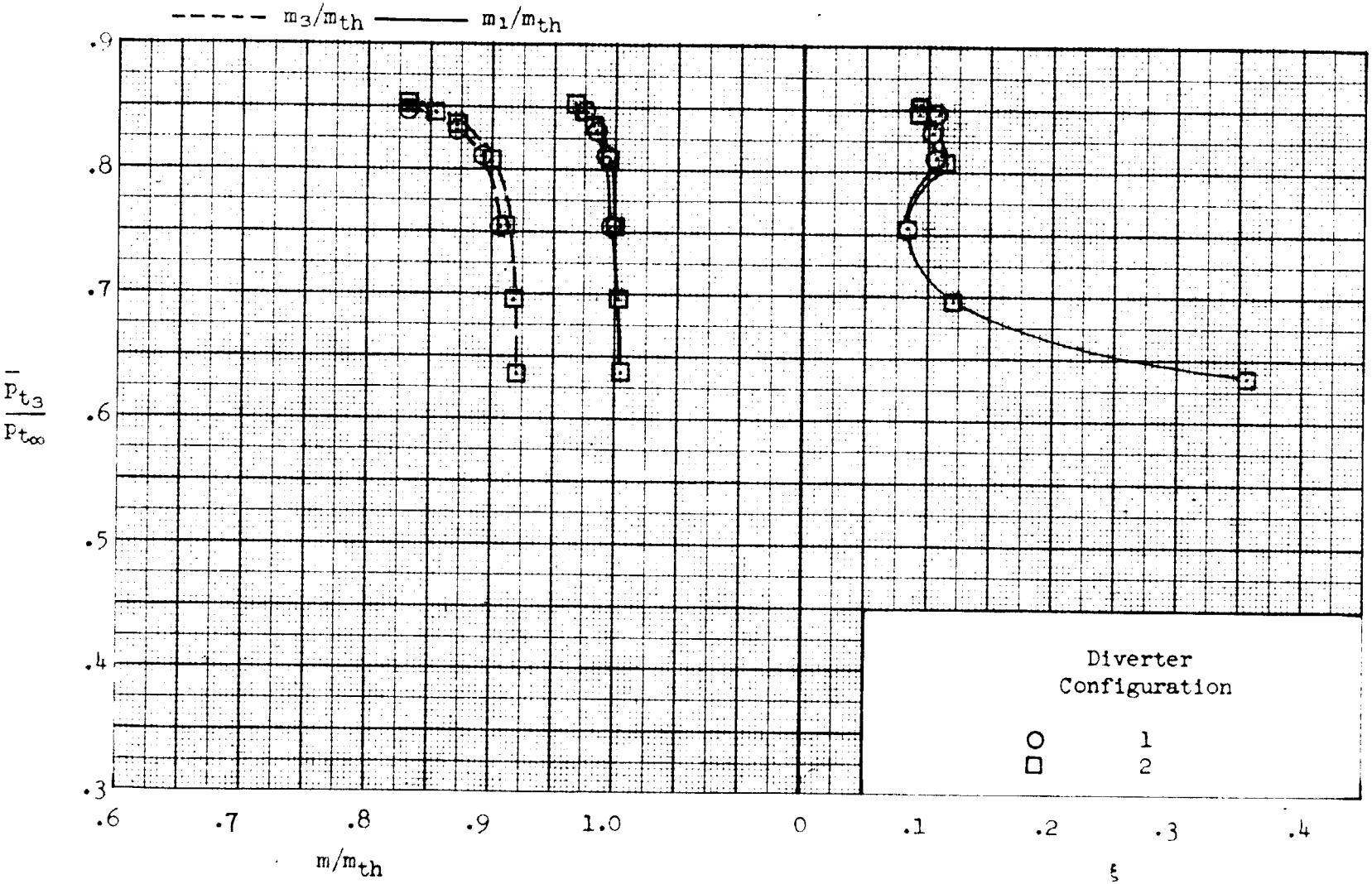

(b) α = 2°, δ_R = 18.5°, δ_L = 1.5°, A_{ref}/A_{th} =1.0706; inlet performance.

Figure 24. Continued.

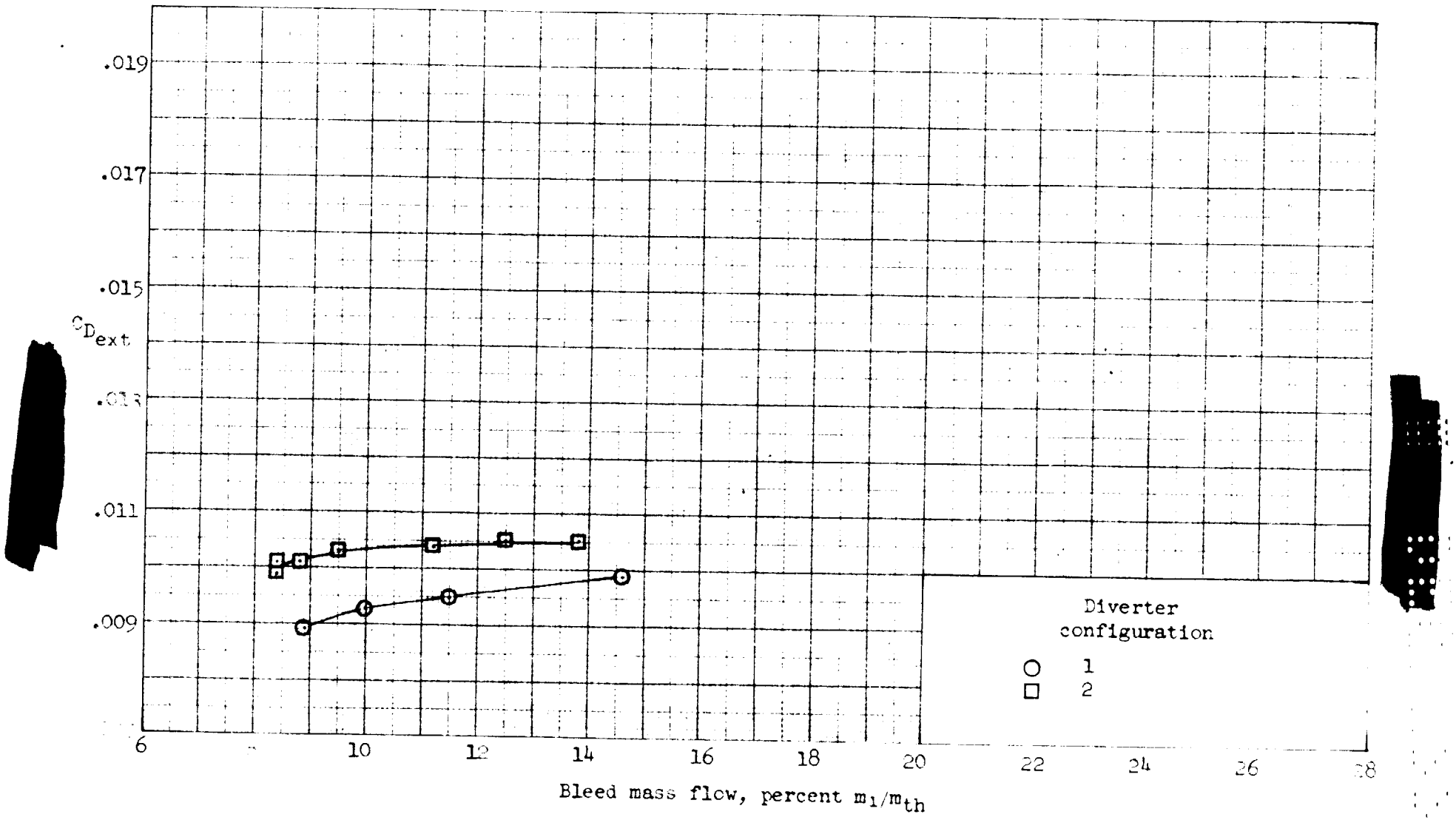

(b) Concluded. External-drag coefficient.

Figure 24.- Continued.

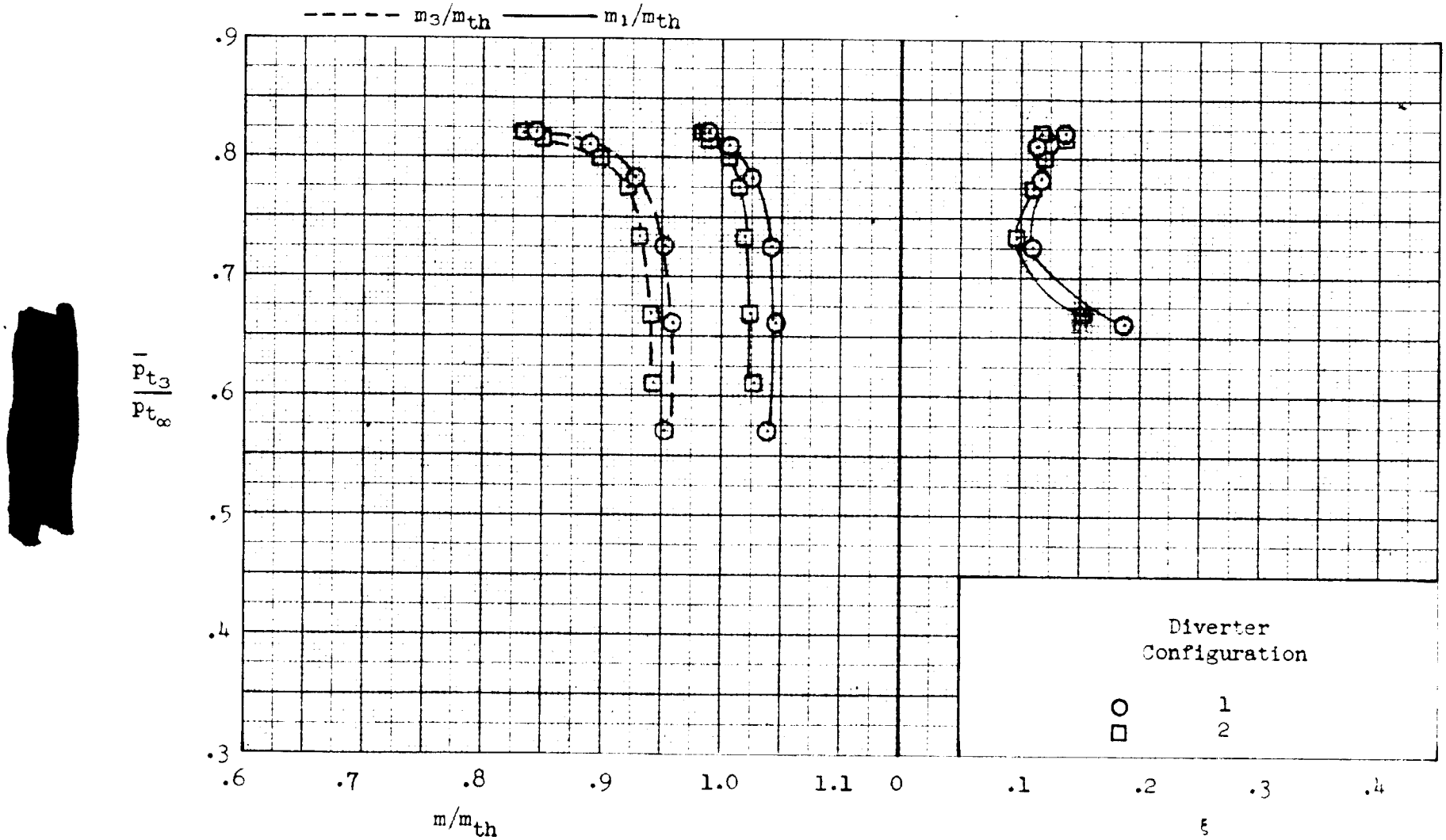

(c) $\alpha = 4°$, $\delta_R = 18.0°$, $\delta_L = 3.5°$, $A_{ref}/A_{th} = 1.0703$; inlet performance.

Figure 24.- Continued.

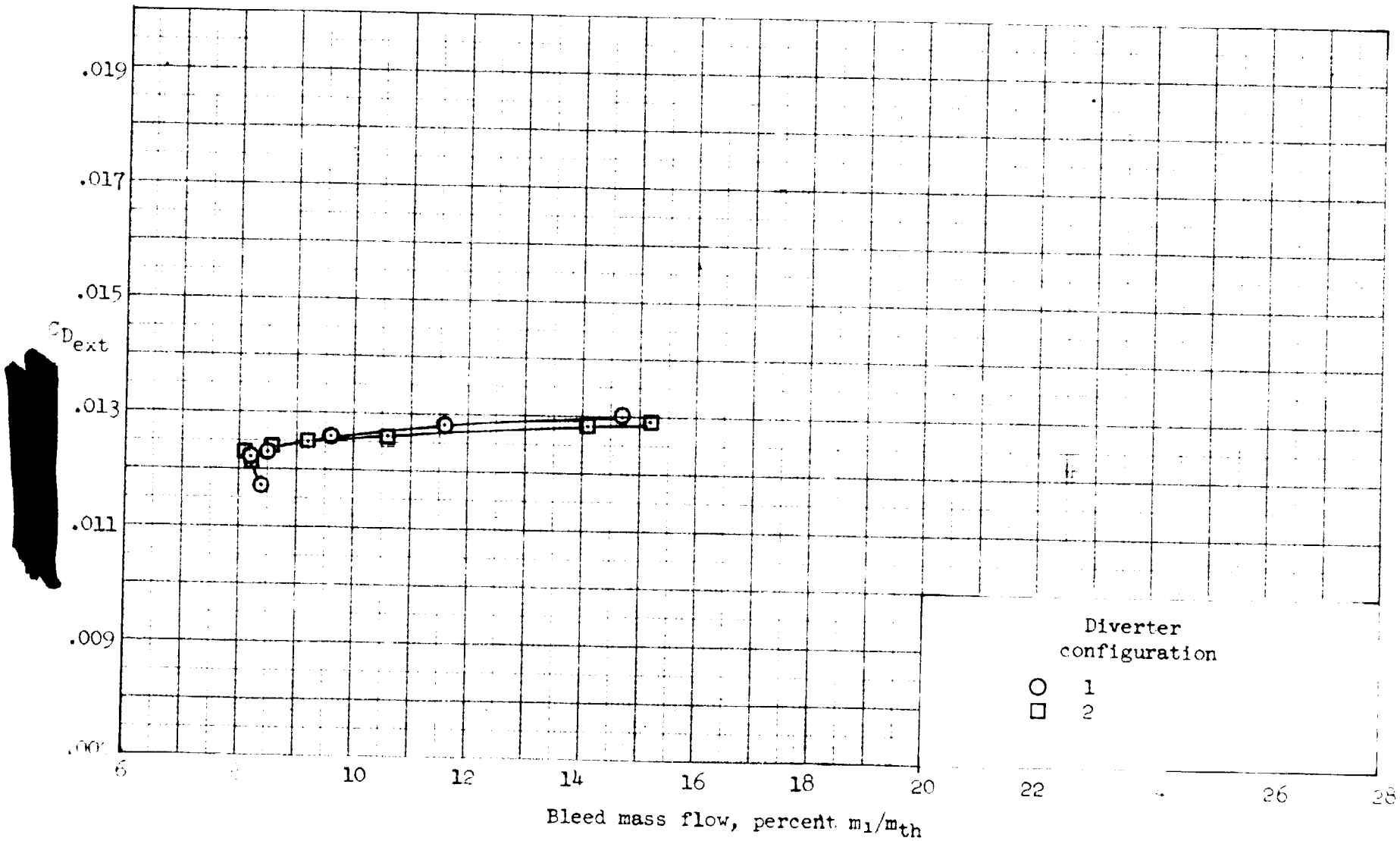

(c) Concluded. External-drag coefficient.

Figure 24.- Continued.

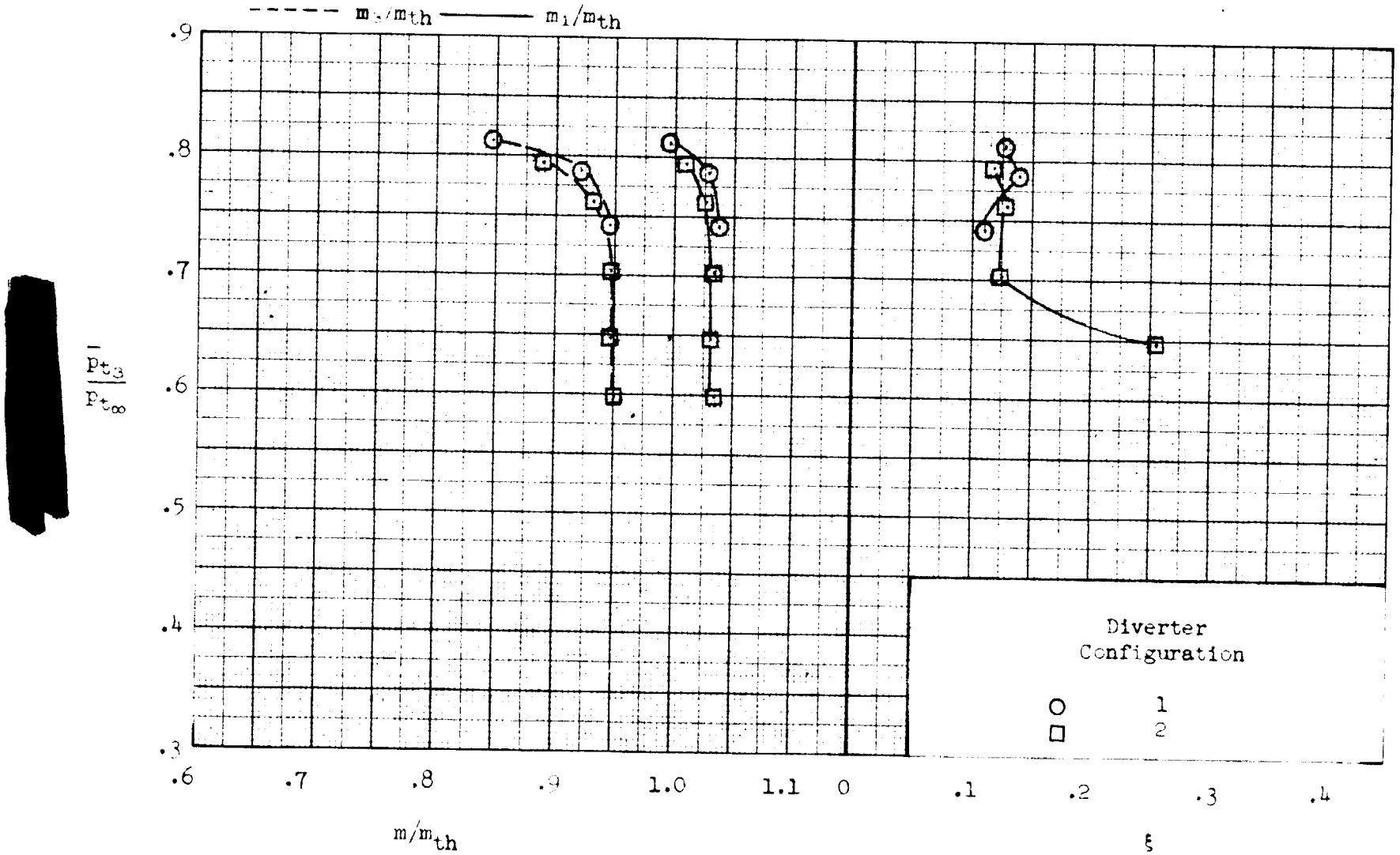

(d) $\alpha = 6°$, $\delta_R = 17.5°$, $\delta_L = 4.0°$, $A_{ref}/A_{th} = 1.0313$; inlet performance.

Figure 24.- Continued.

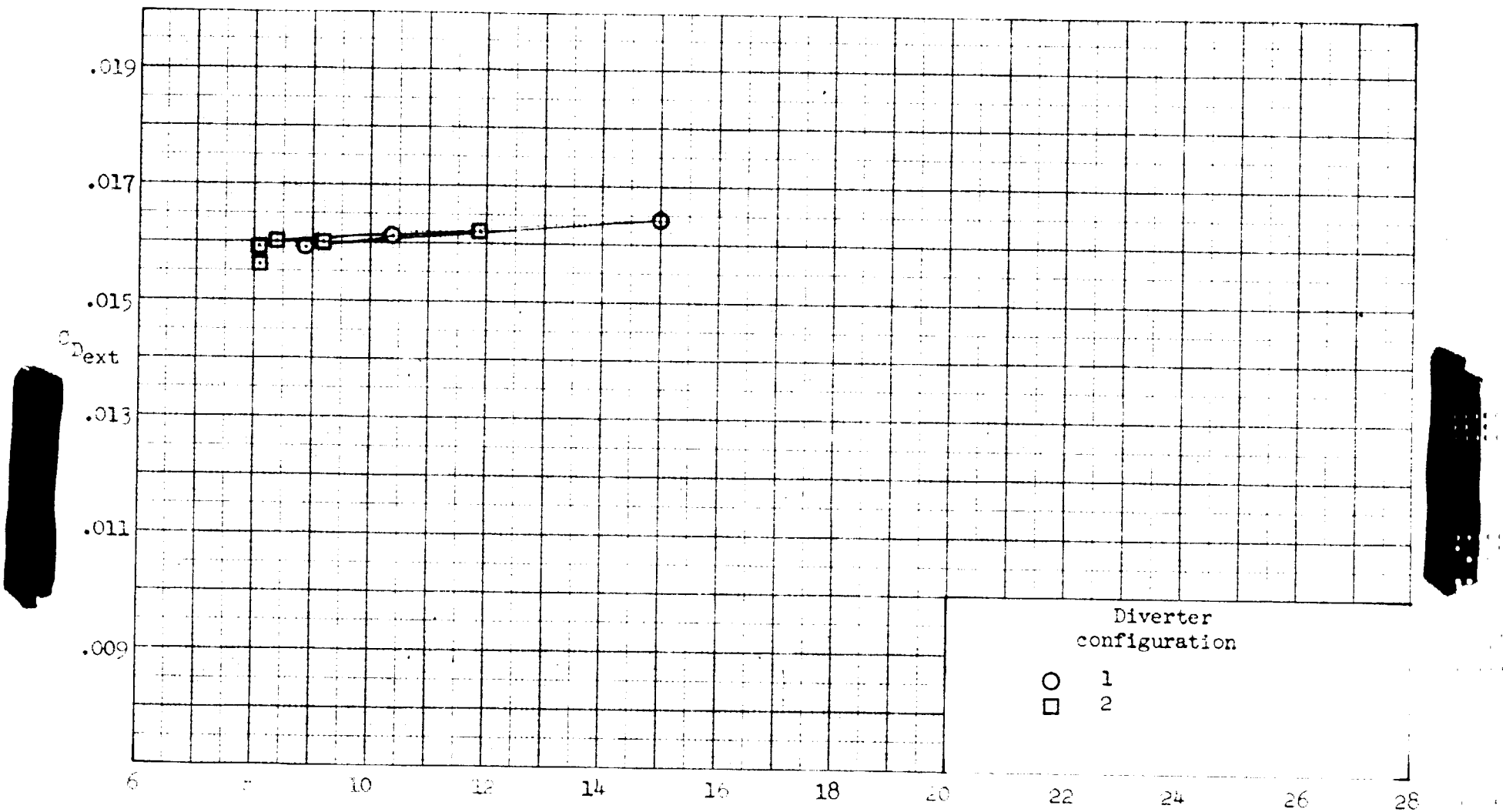

(d) Concluded. External drag coefficient.

Figure [illegible]

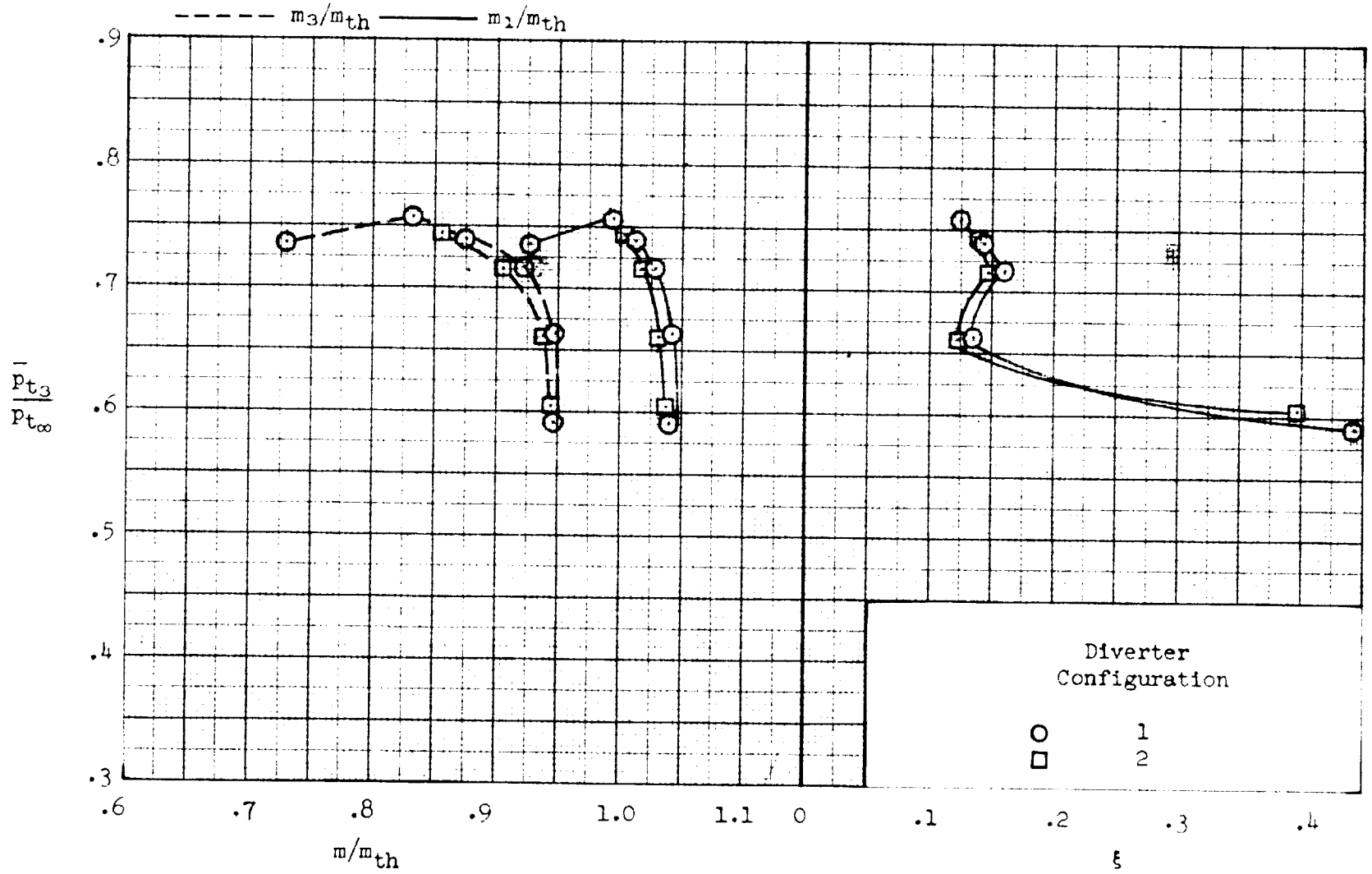

(e) $\alpha = 10°$, $\delta_R = 17.0°$, $\delta_L = 7.5°$, $A_{ref}/A_{th} = 1.0624$; inlet performance.

Figure 24.- Concluded.

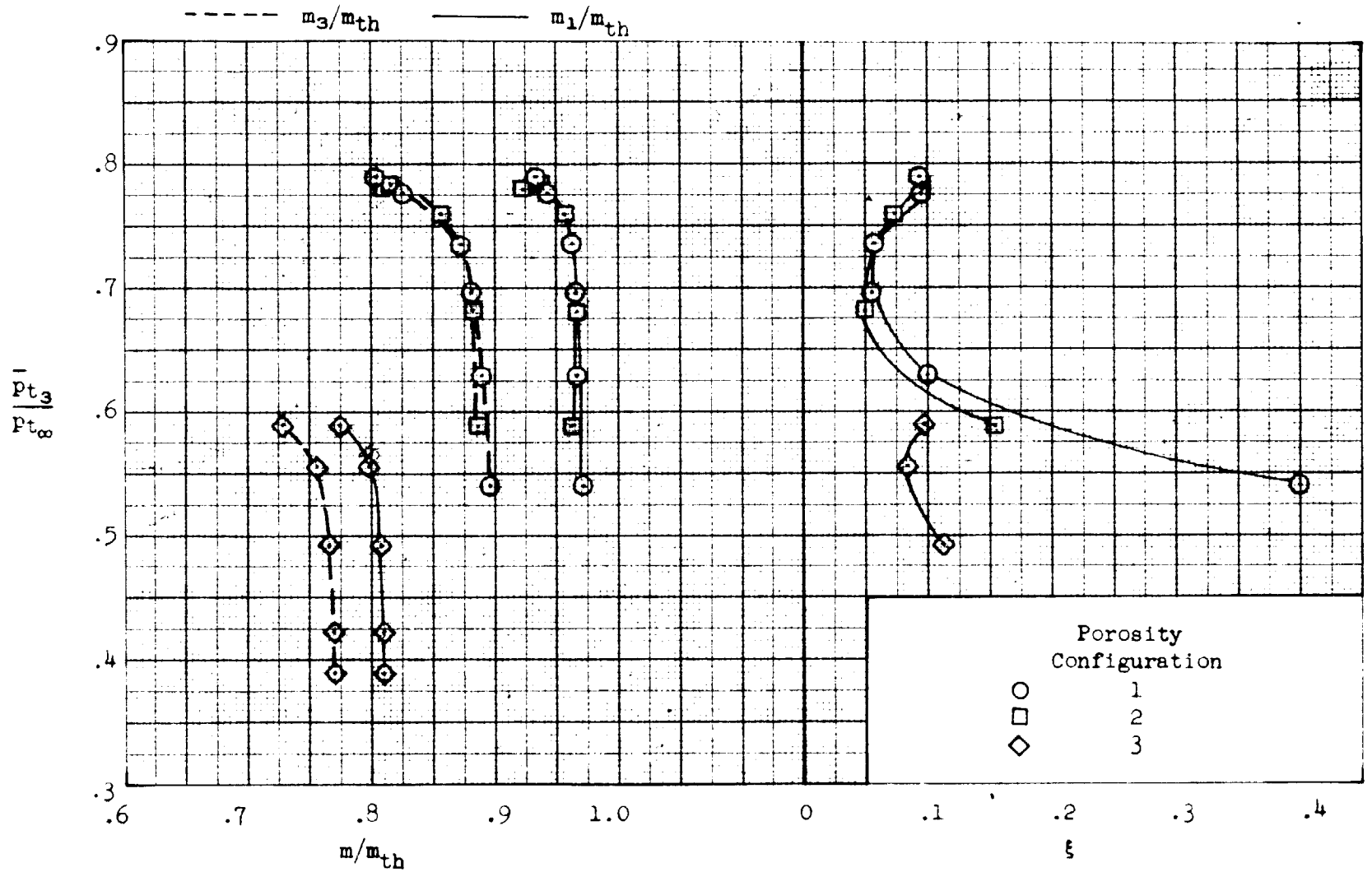

(a) $\alpha = 0°$, $\delta_R = 19.5°$, $\delta_L = 0.5°$, $A_{ref}/A_{th} = 1.0432$; inlet performance.

Figure 25.- Effect of variation of bleed-surface porosity on inlet performance and external-drag coefficient; $M = 3.00$, $\beta = 0°$. Configuration: nose 1, diverter 3, bleed exit 1.

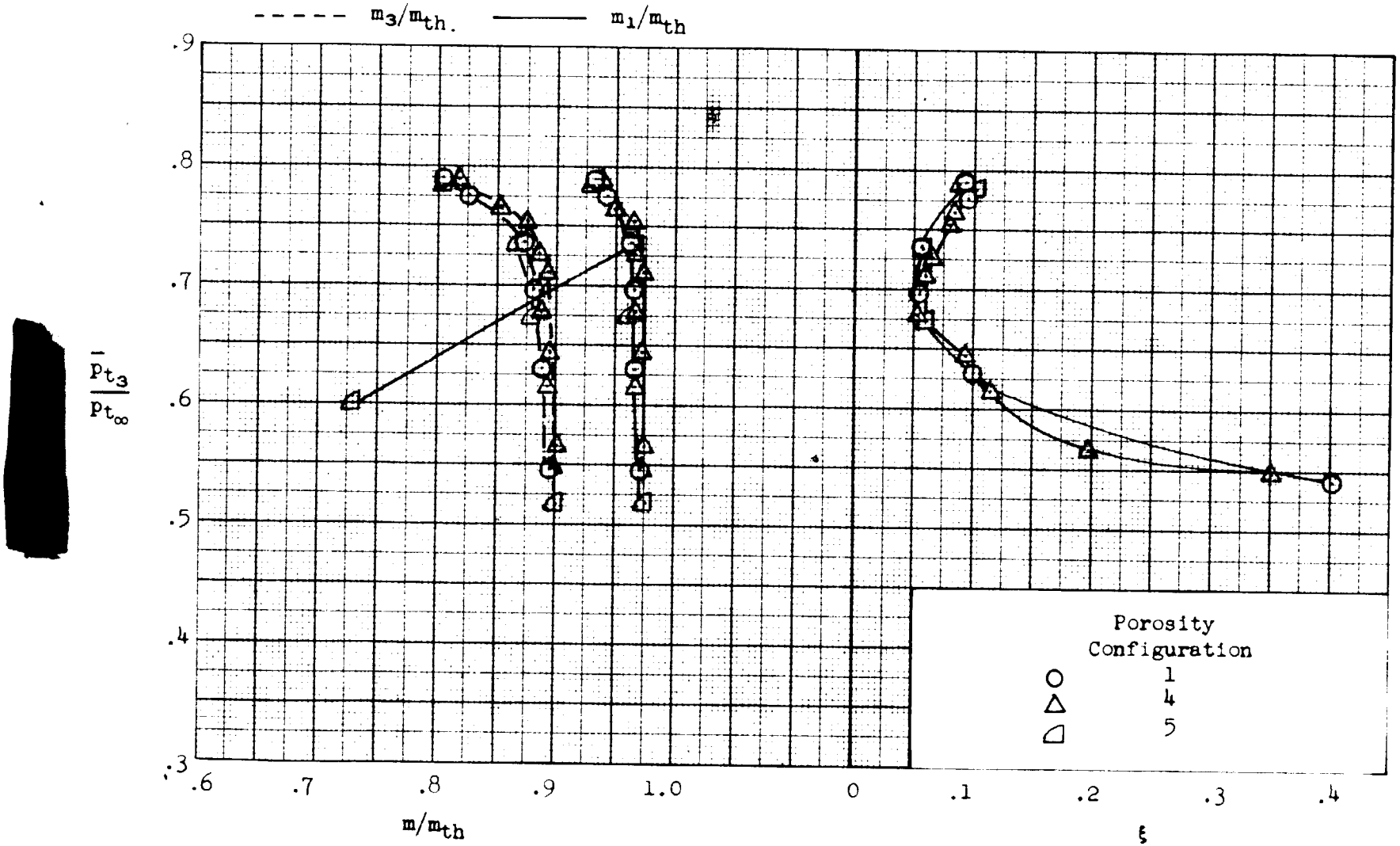

(a) Continued. Inlet performance.

Figure 25.- Continued.

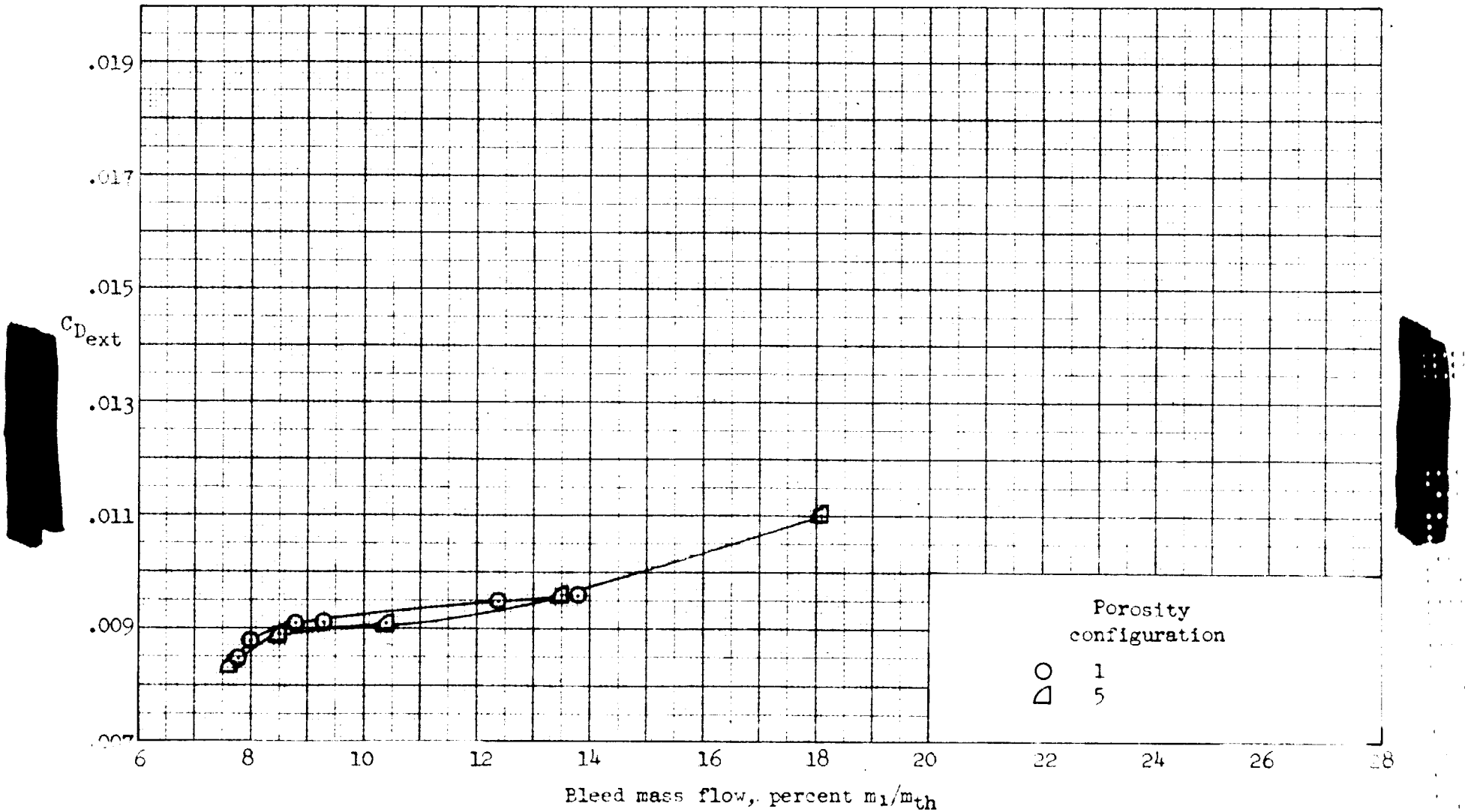

(a) Concluded. External-drag coefficient.

Figure 25.- Continued.

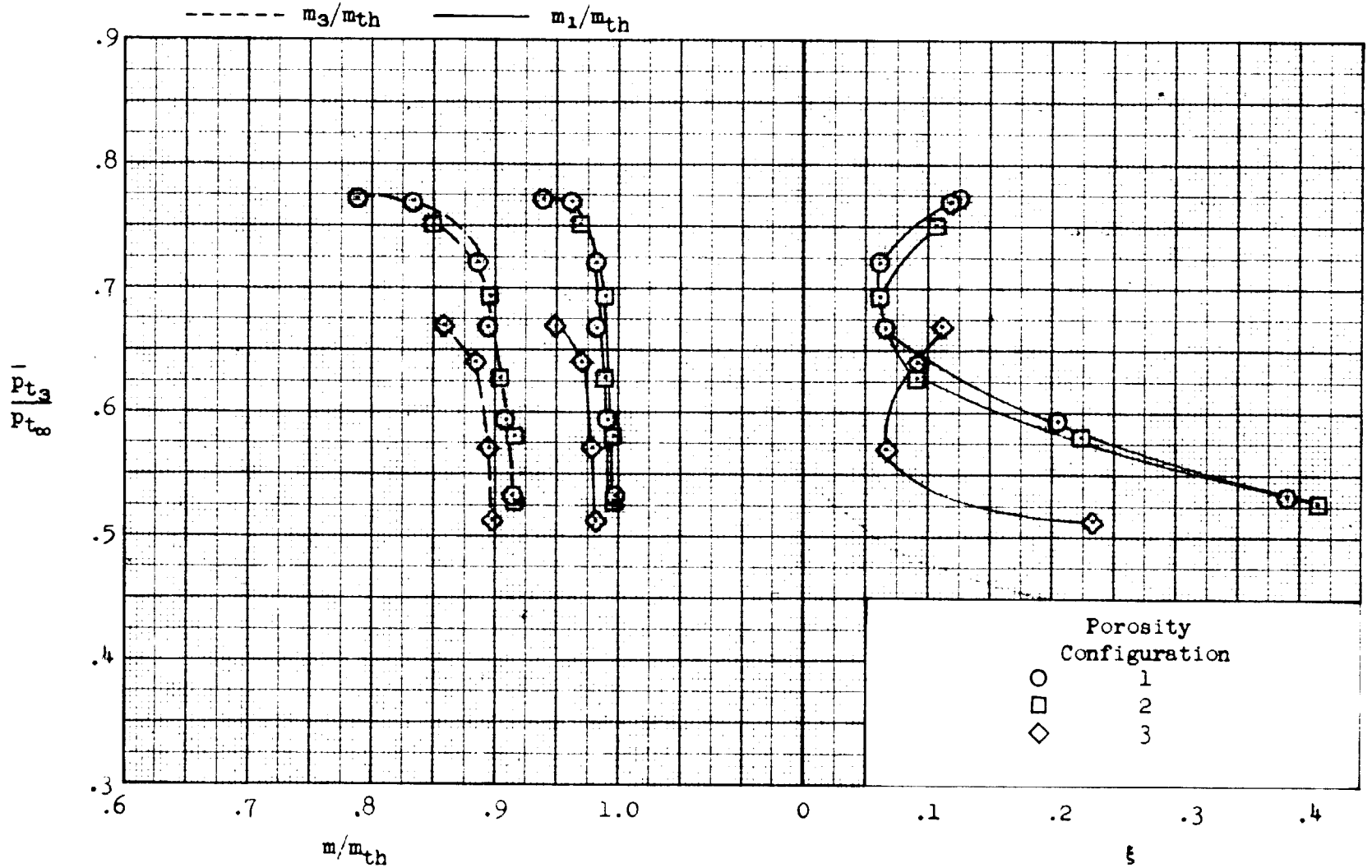

(b) $\alpha = 2°$, $\delta_R = 19.5°$, $\delta_L = 4.0°$, $A_{ref}/A_{th} = 1.0930$; inlet performance.

Figure 25.- Continued.

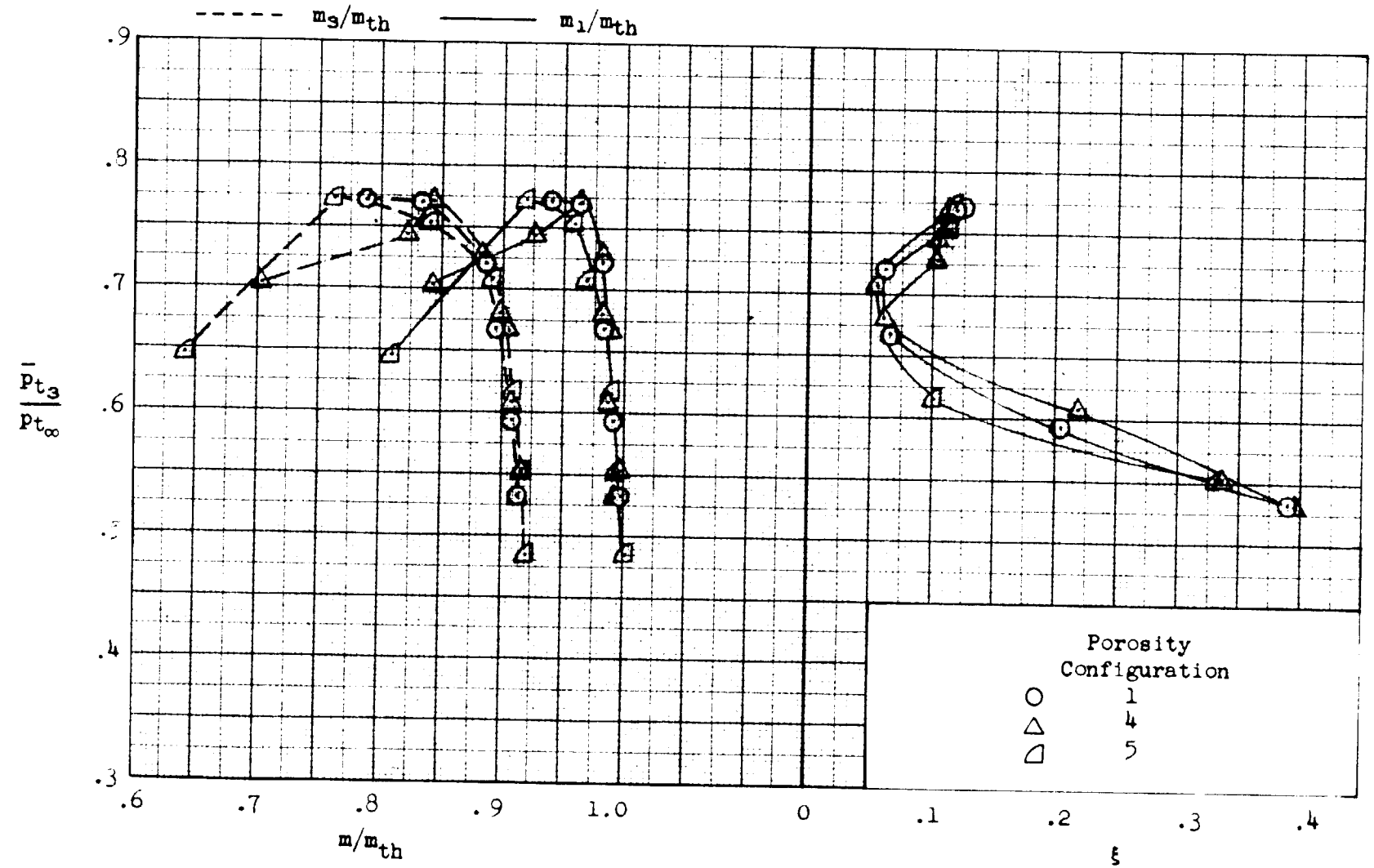

(b) Continued. Inlet performance.

Figure 25.- Continued.

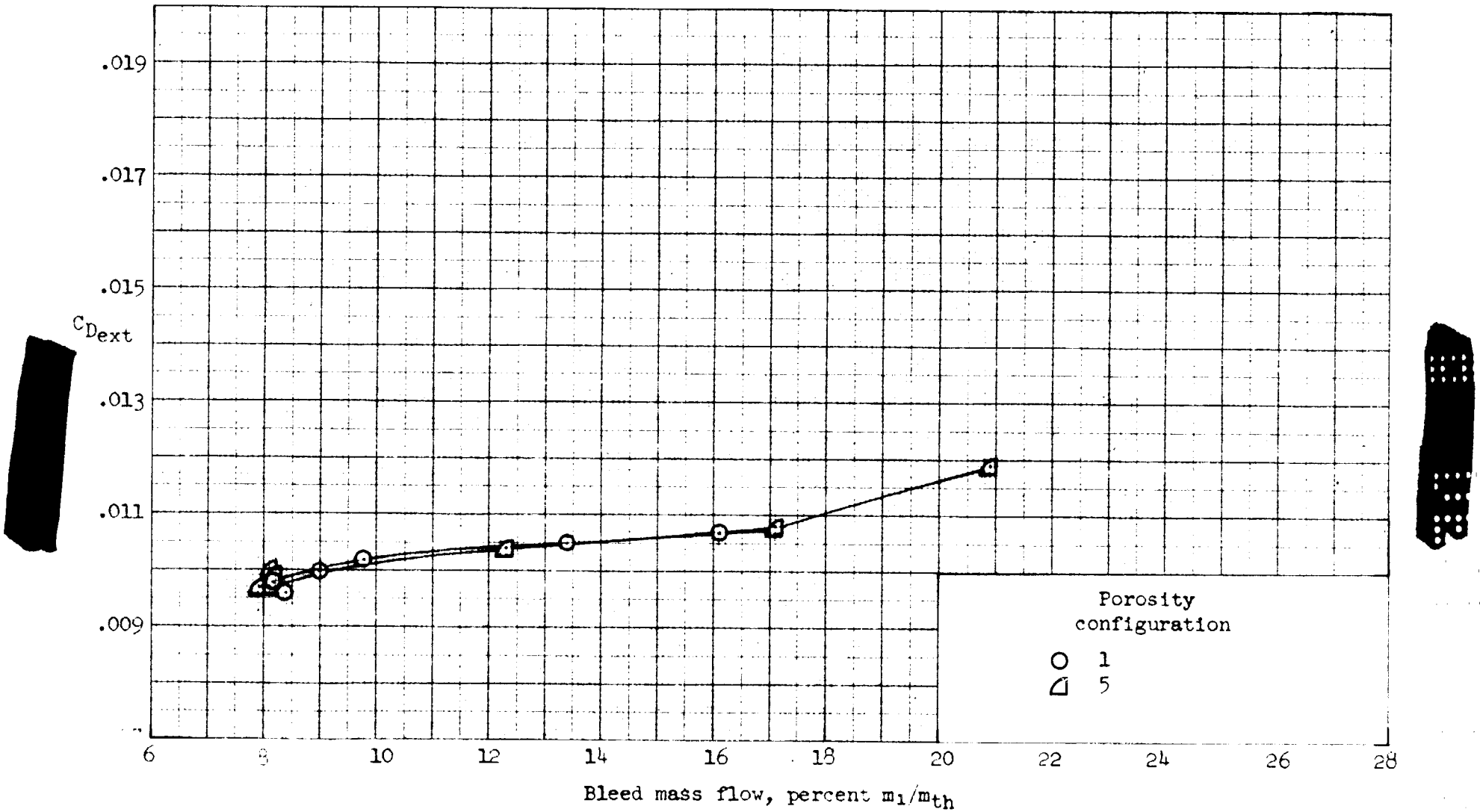

(b) Concluded. External-drag coefficient.

Figure 25.- Continued.

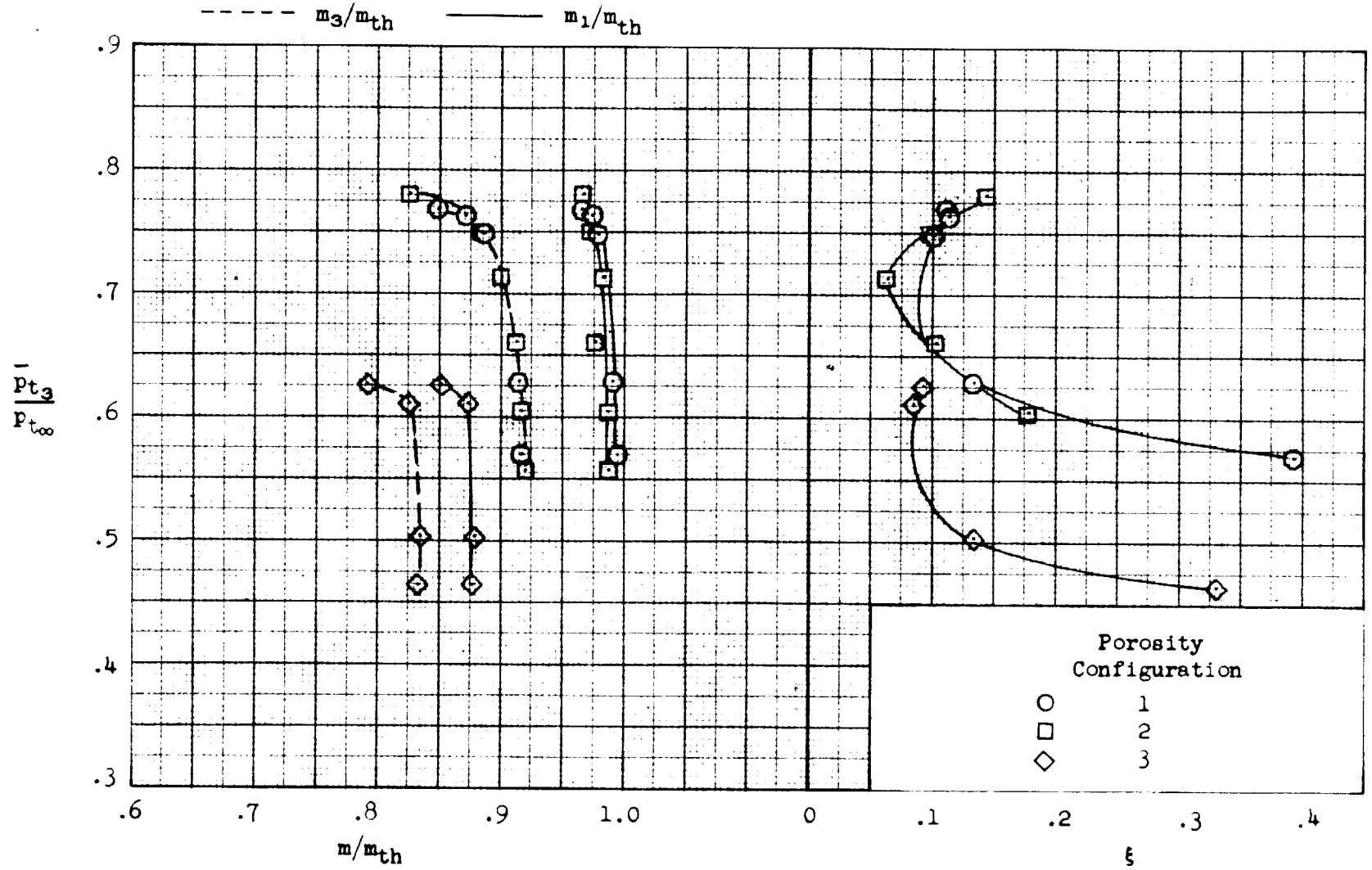

(c) $\alpha = 4°$, $\delta_R = 18.5°$, $\delta_L = 1.0°$, $A_{ref}/A_{th} = 0.9325$; inlet performance.

Figure 25.- Continued.

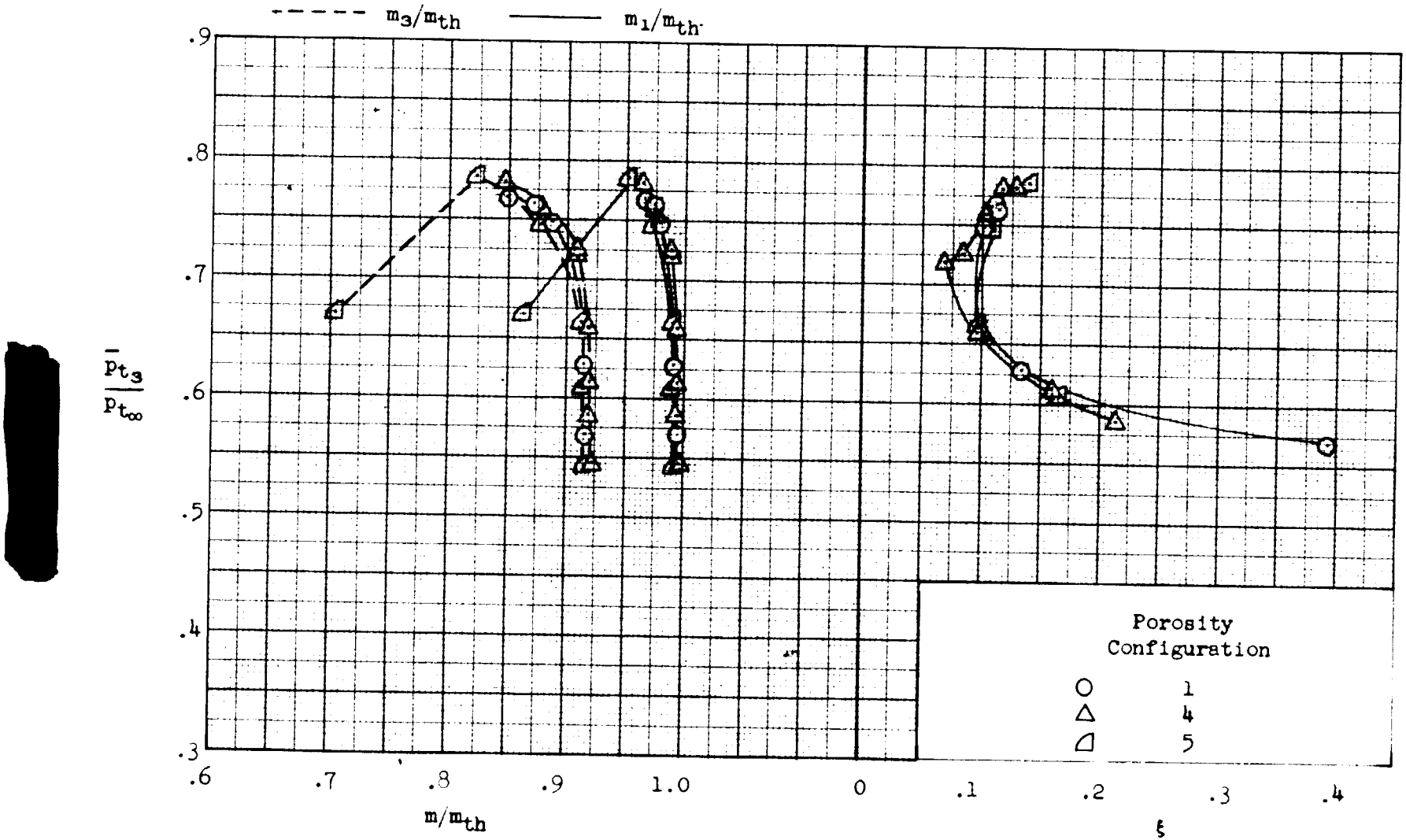

(c) Continued. Inlet performance.

Figure 25.- Continued.

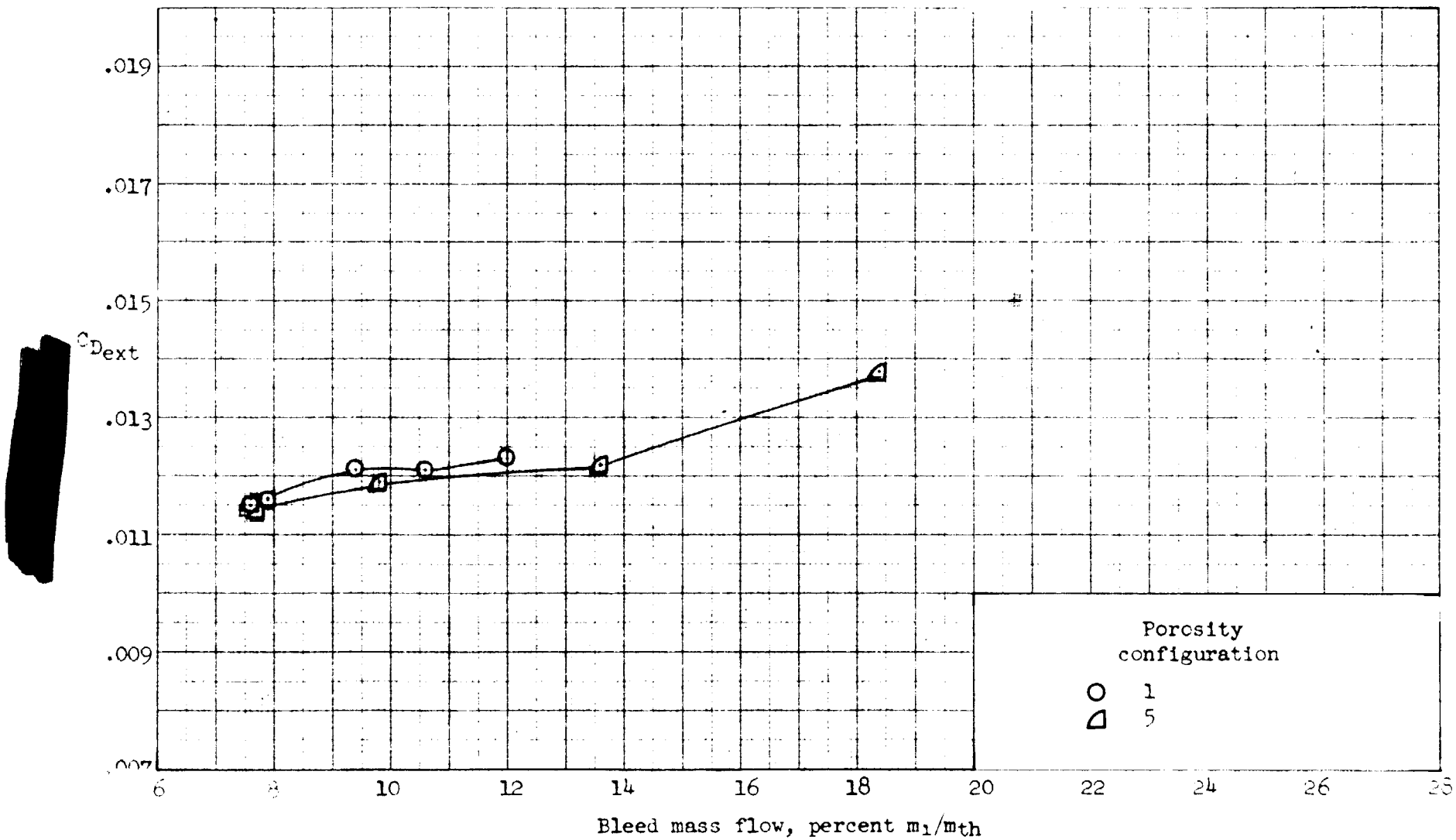

(c) Concluded. External-drag coefficient.

Figure 25.- Continued.

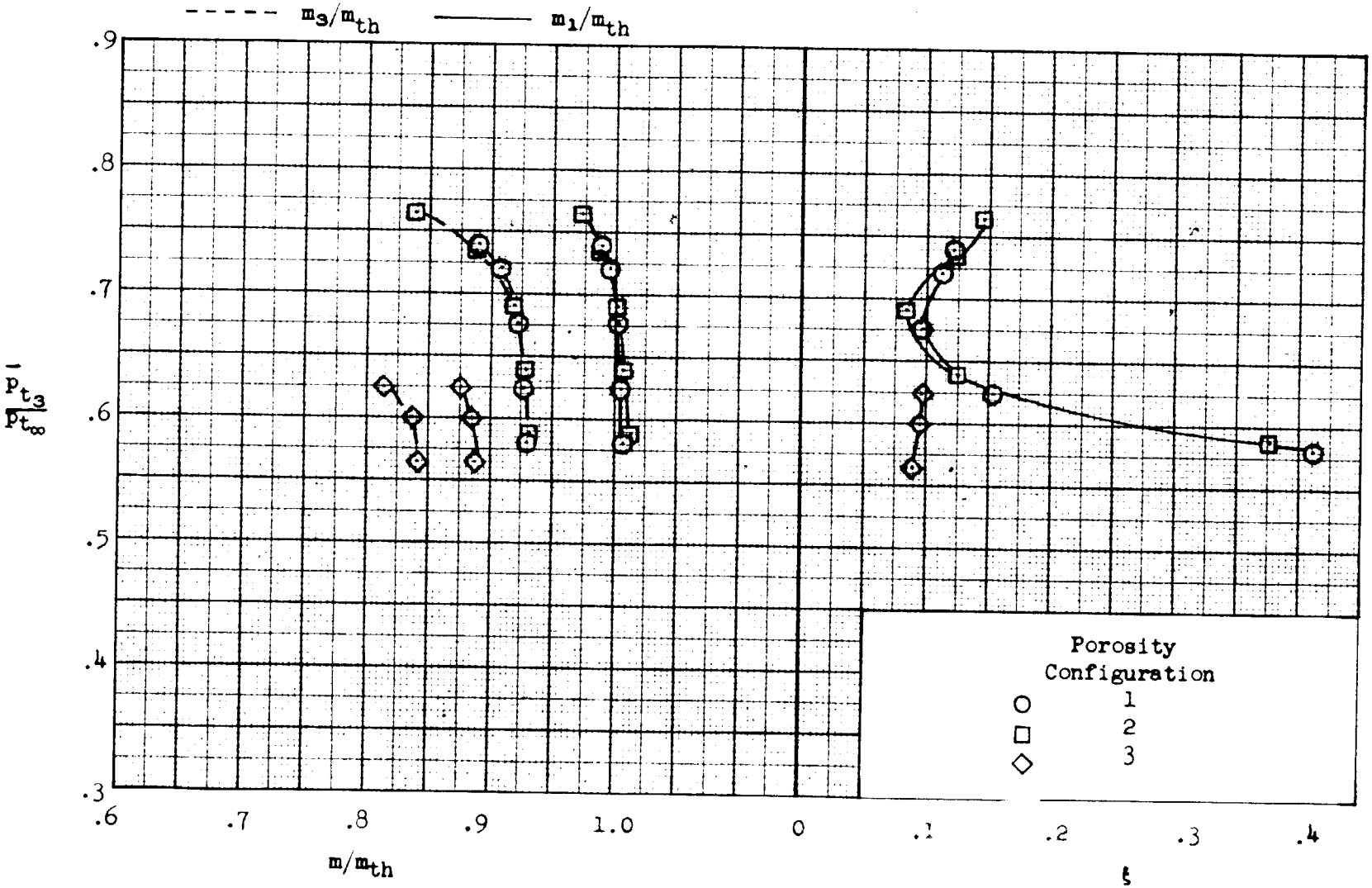

(d) $\alpha = 6°$, $\delta_R = 18.0°$, $\delta_L = 1.5°$, $A_{ref}/A_{th} = 0.8968$; inlet performance.

Figure 25.- Continued.

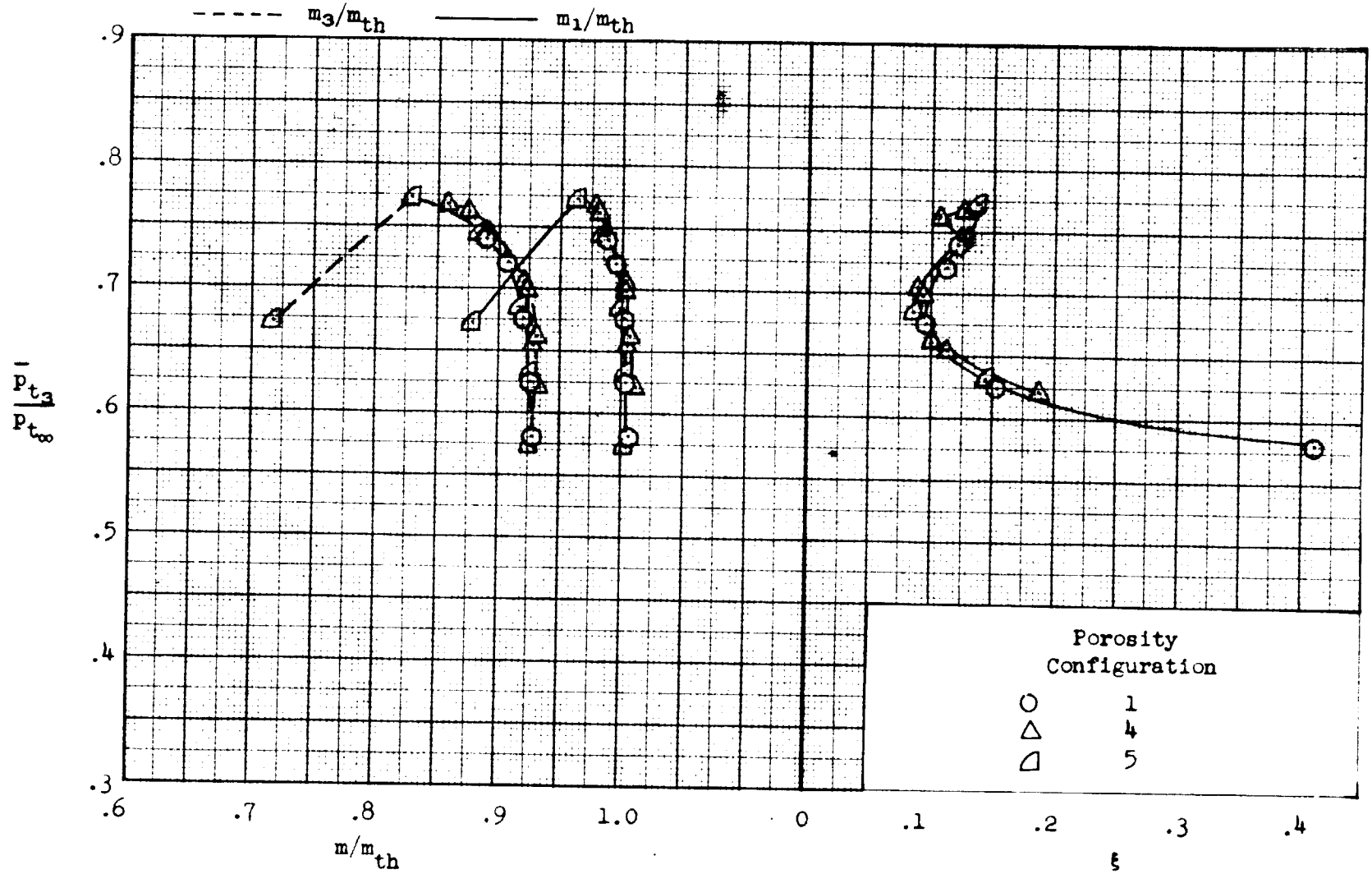

(d) Continued. Inlet performance.

Figure 25.- Continued.

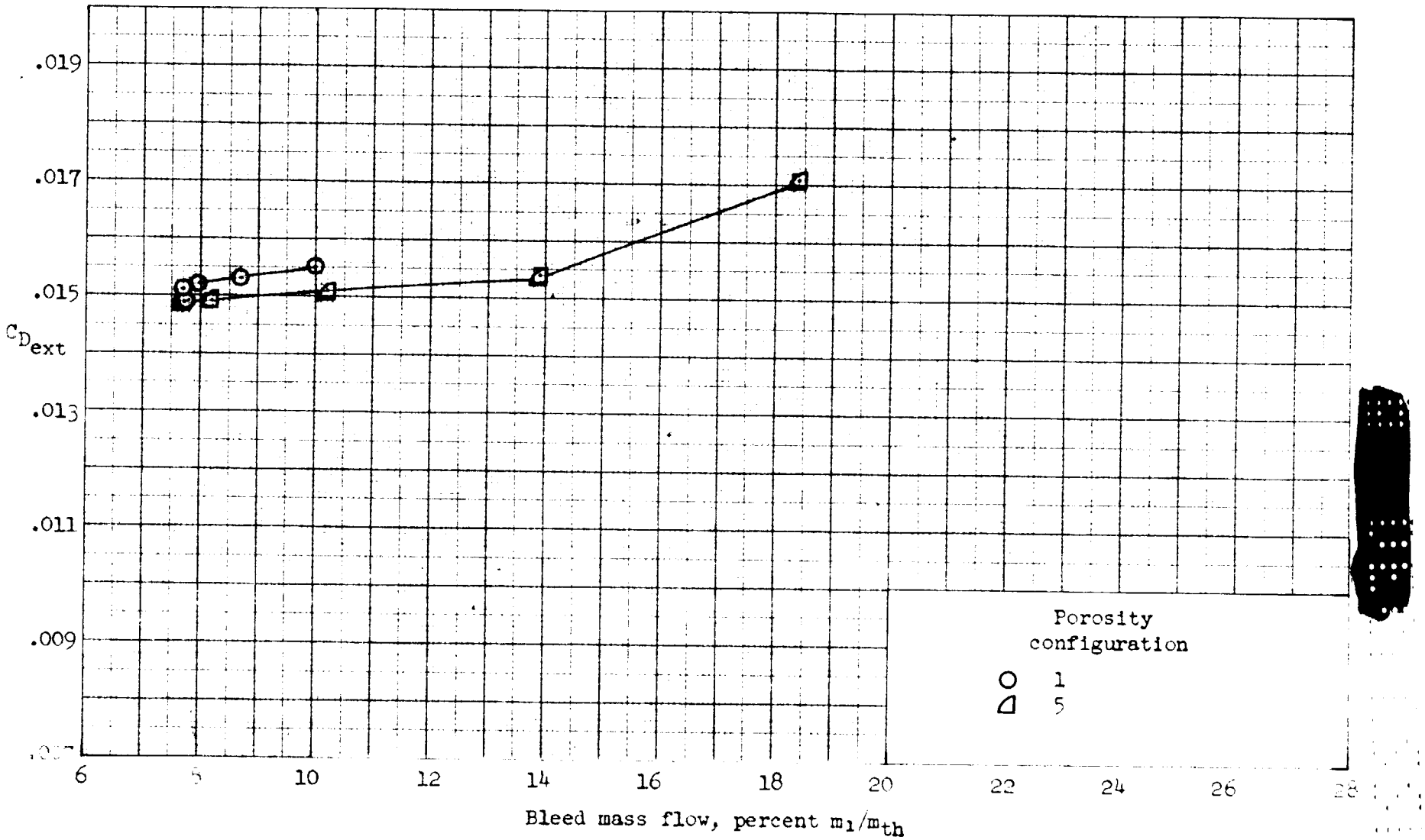

(d) Concluded. External-drag coefficient.

Figure 25.- Continued.

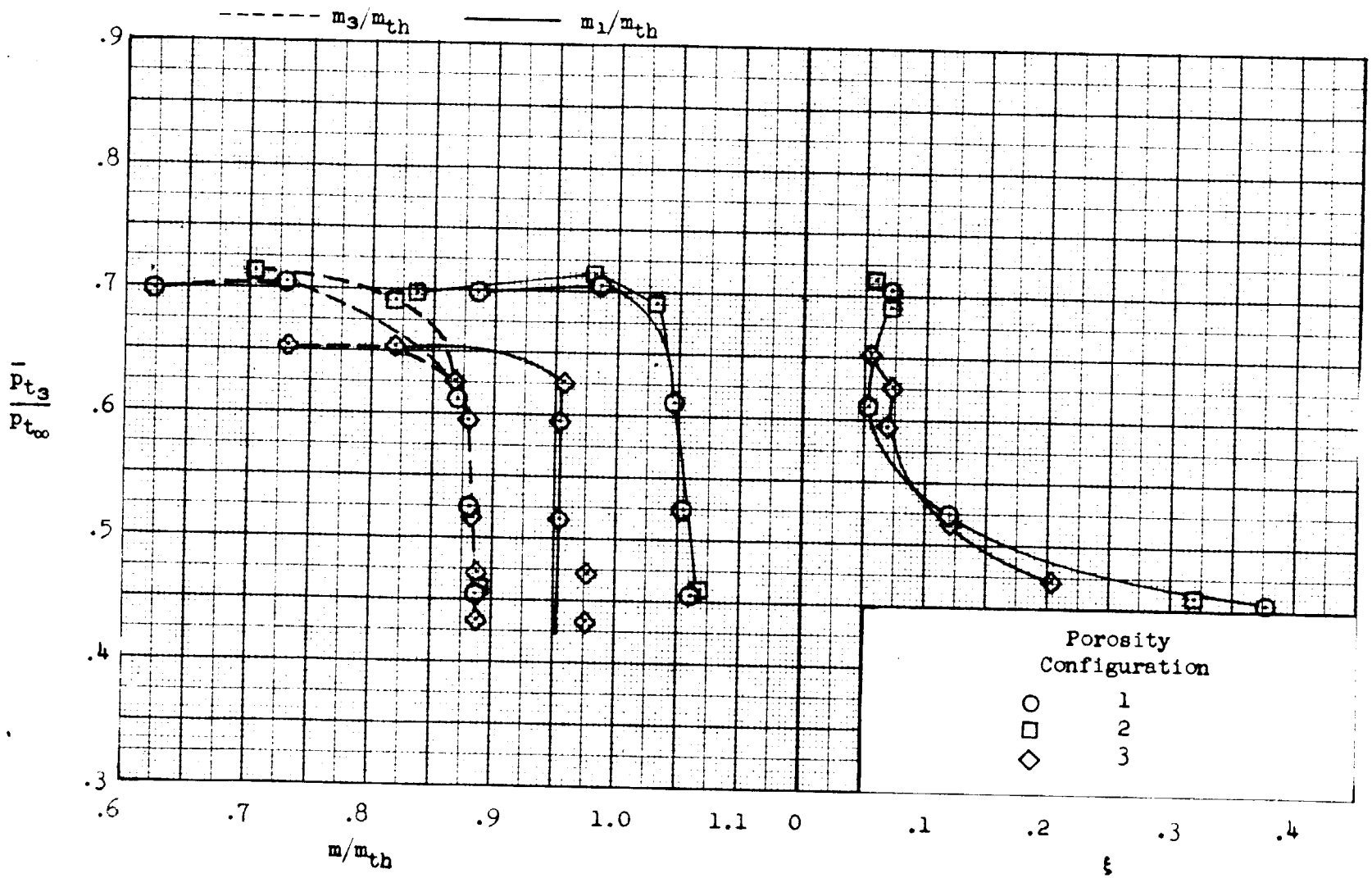

α = 20.0, δ_L = 4.0°, A_{ref}/A_{th} = 0.9792; inlet performance.

Figure 25.- Concluded.

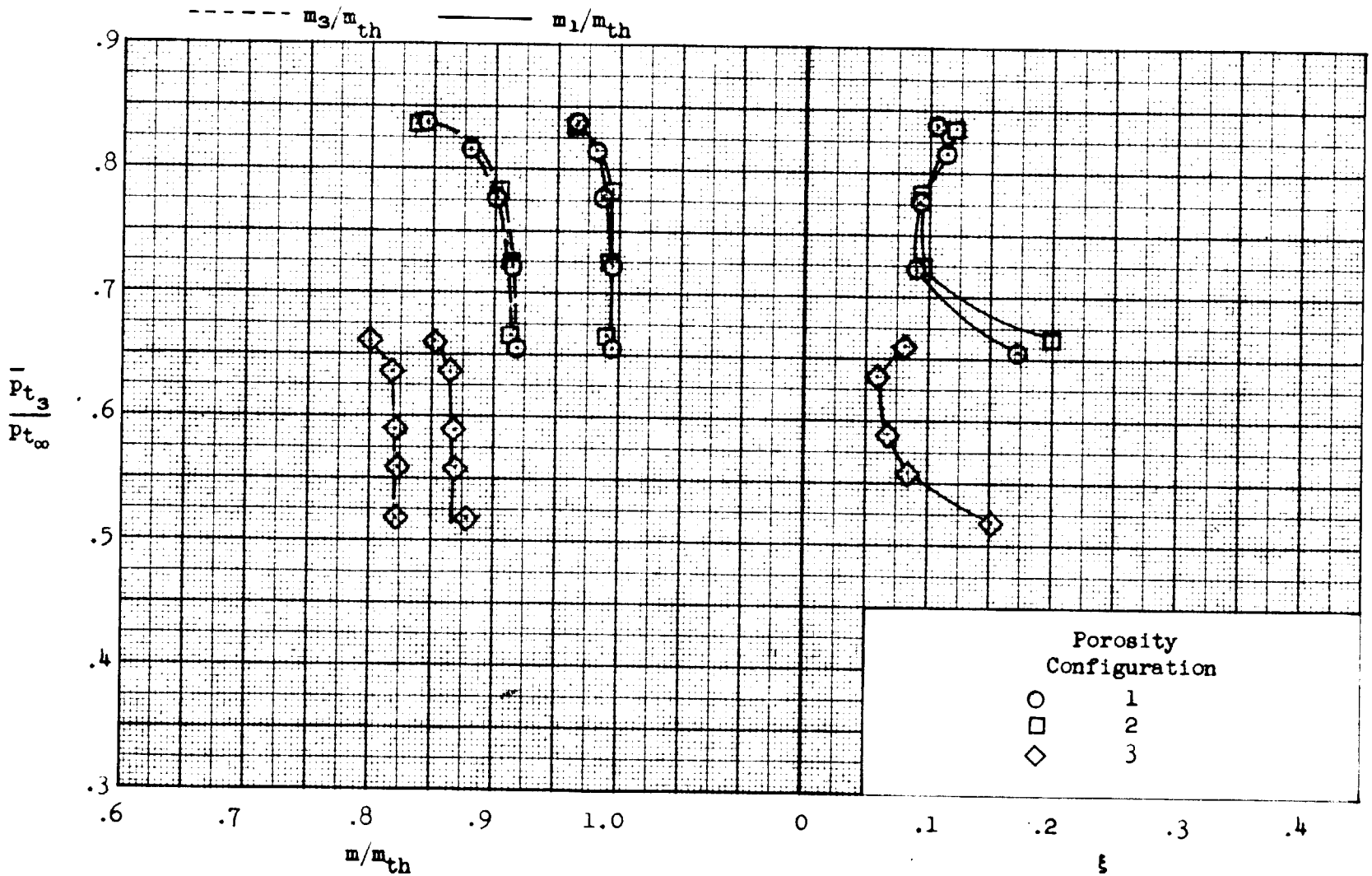

(a) $\alpha = 0°$, $\delta_R = 18.5°$, $\delta_L = 0.5°$, $A_{ref}/A_{th} = 1.0968$; inlet performance.

Figure 26.- Effect of variation of bleed surface porosity on inlet performance and external-drag coefficient; M = 2.76, $\beta = 0°$. Configuration: nose 1, diverter 2, bleed exit 1.

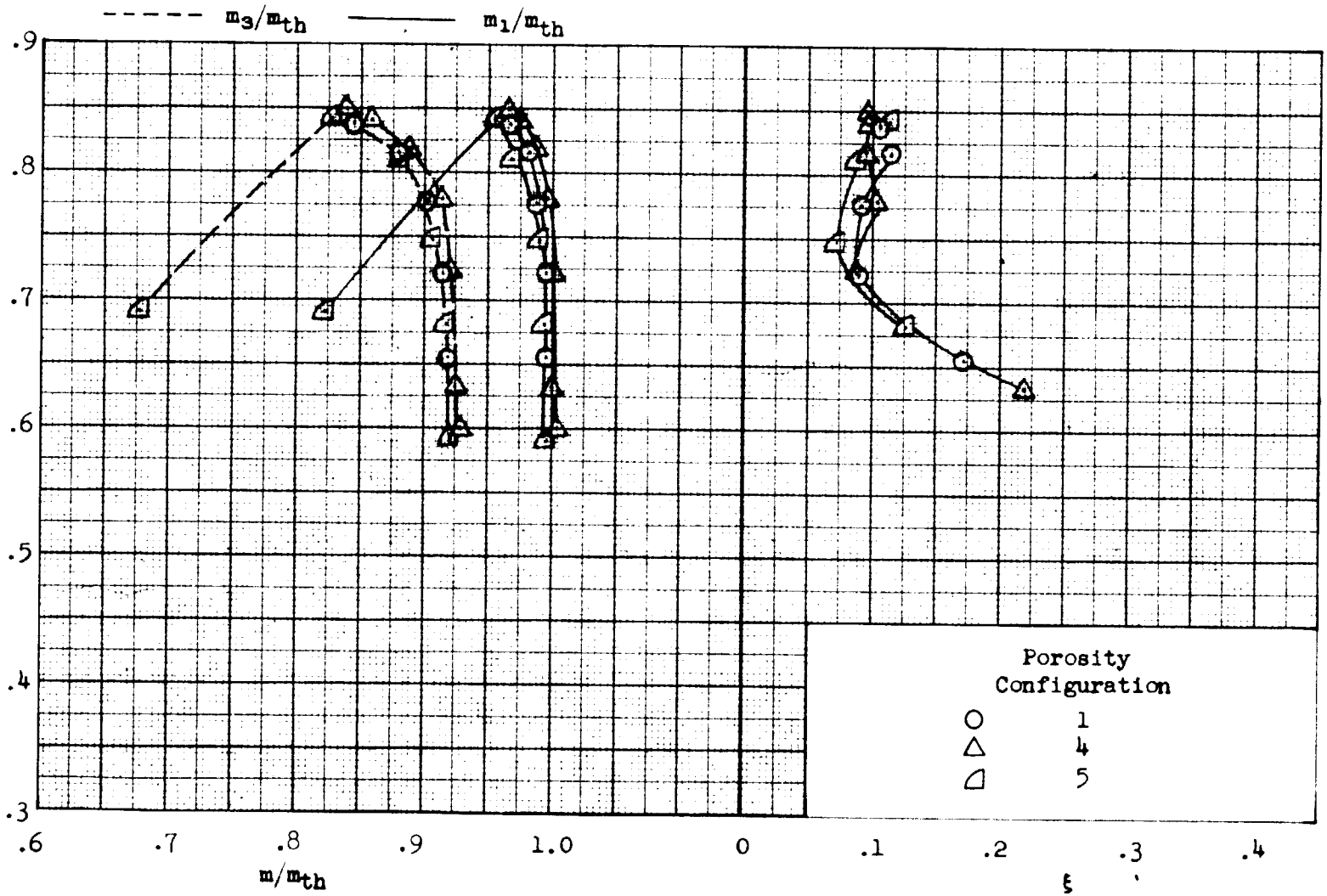

(a) Continued. Inlet performance.

Figure 26.- Continued.

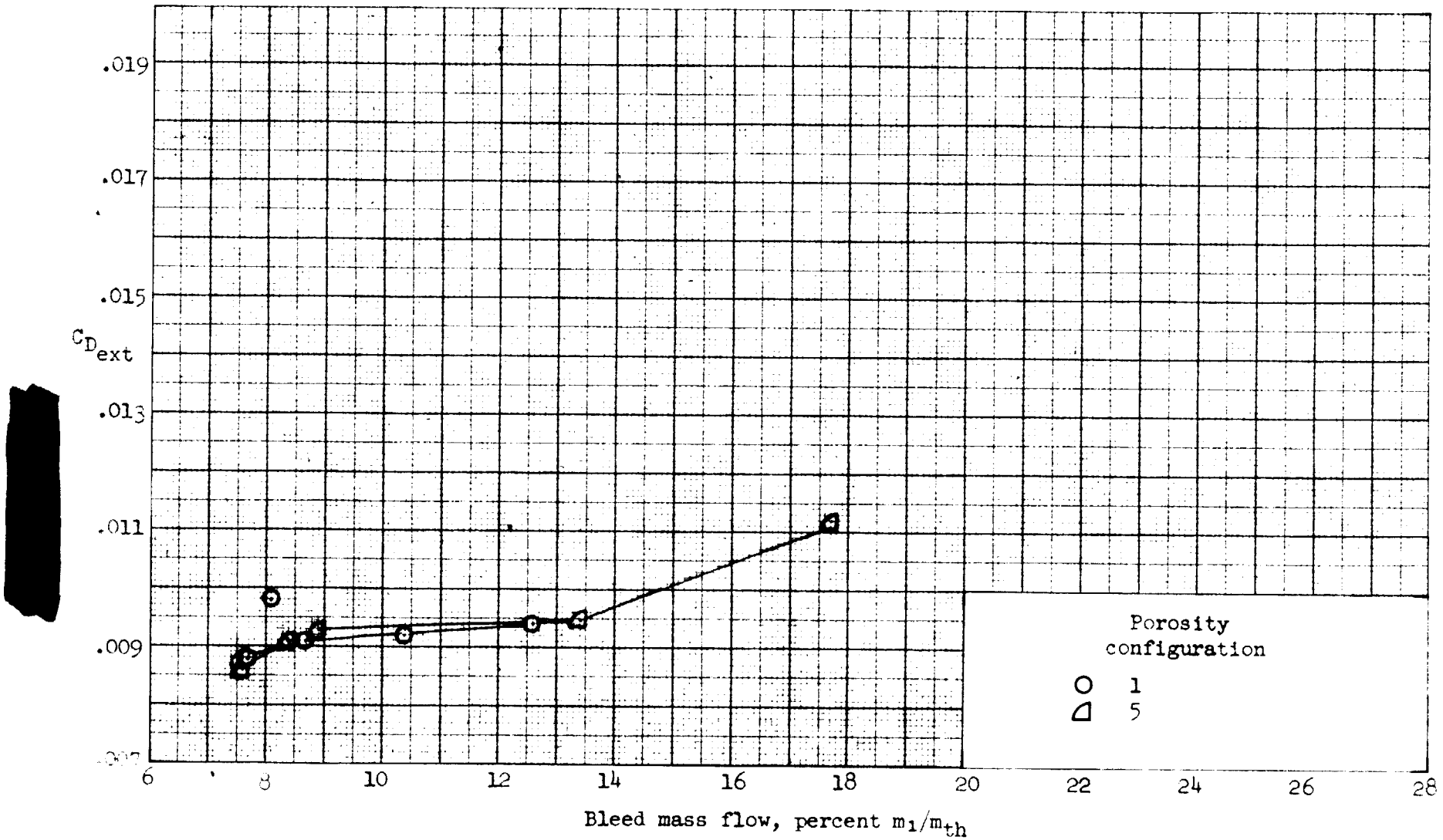

(a) Concluded. External-drag coefficient.

Figure 26.- Continued.

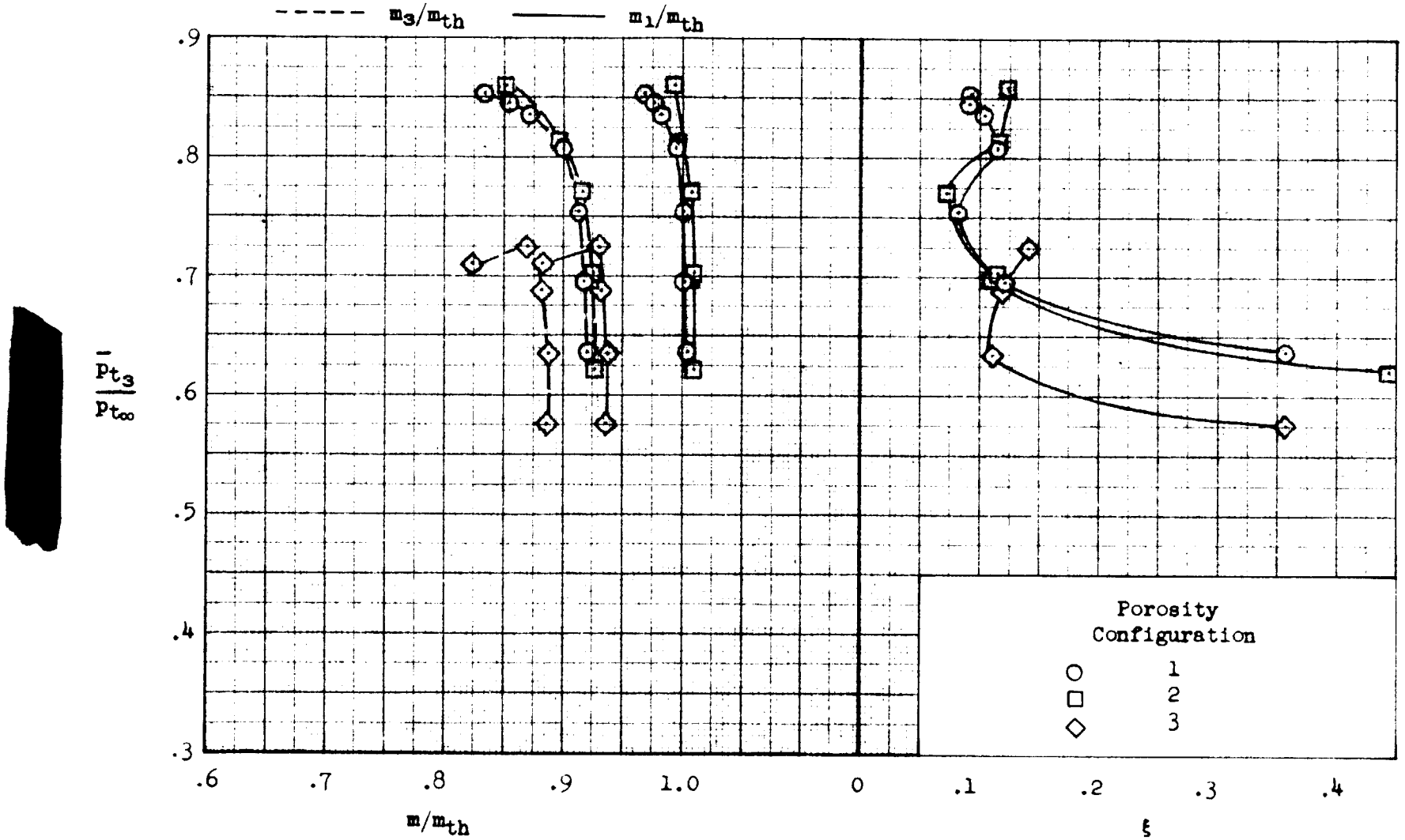

(b) $\alpha = 2°$, $\delta_R = 18.5°$, $\delta_L = 1.5°$, $A_{ref}/A_{th} = 1.0706$; inlet performance.

Figure 26.- Continued.

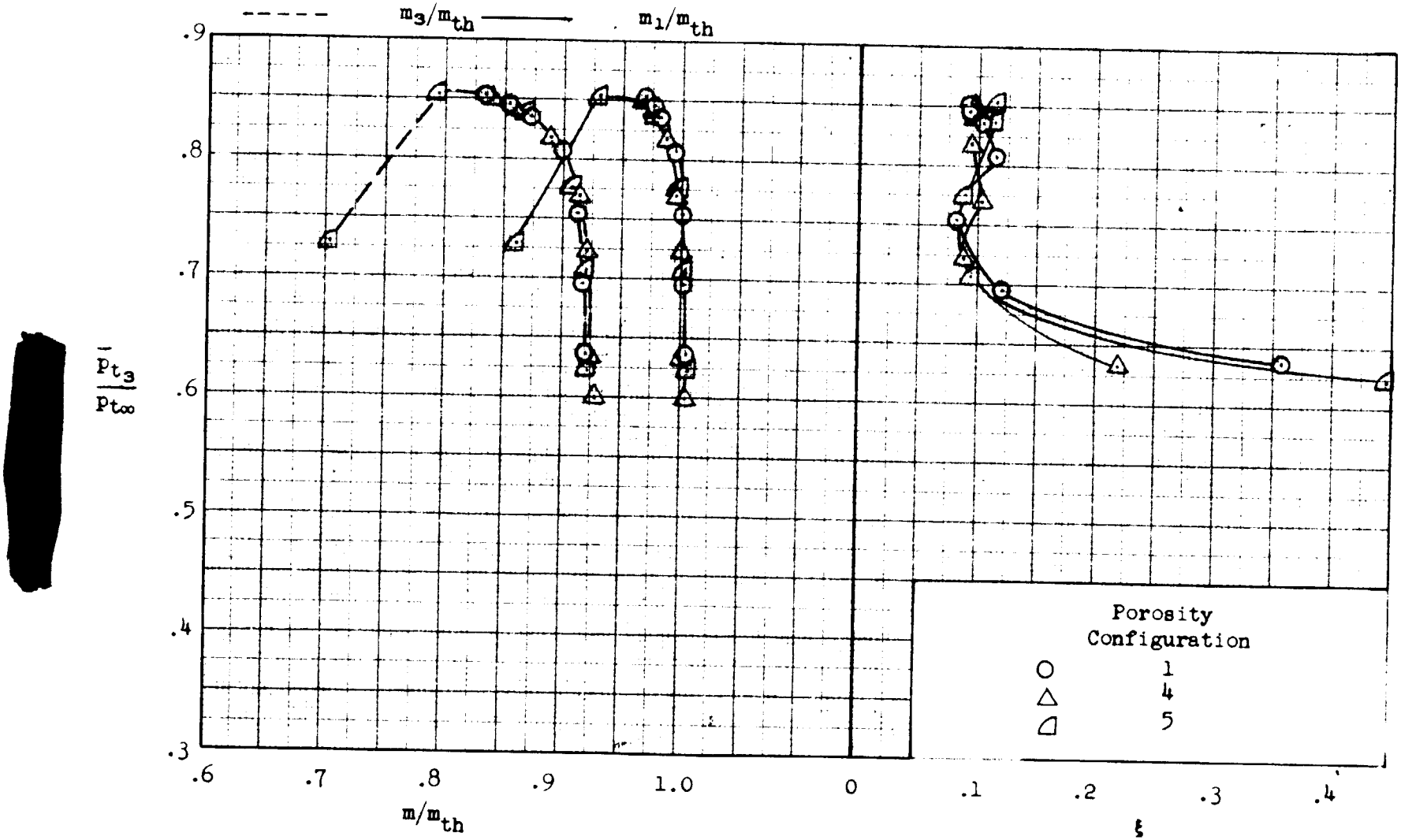

(b) Continued. Inlet performance.

Figure 26.- Continued.

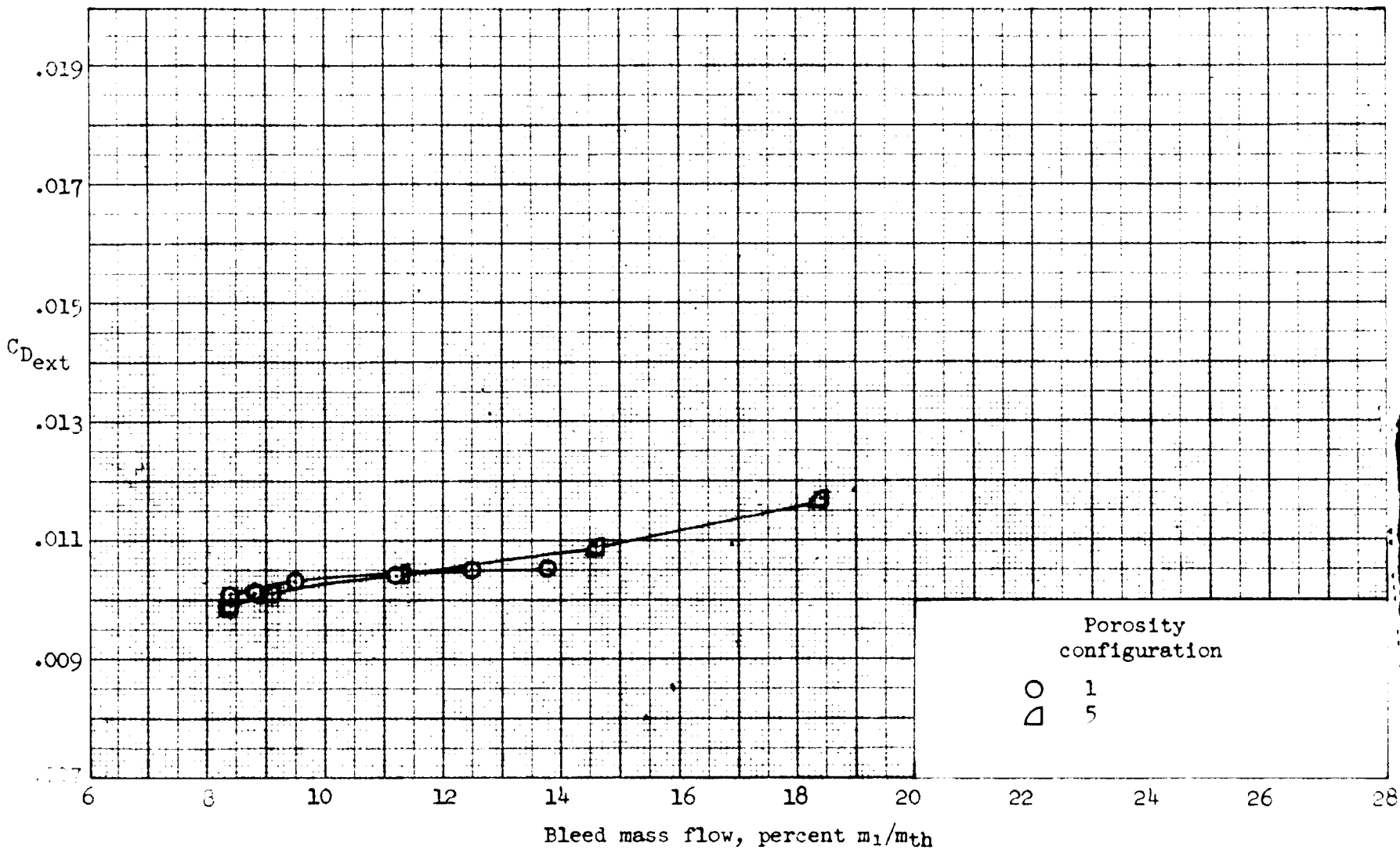

(b) Concluded. External-drag coefficient.

Figure 26.- Continued.

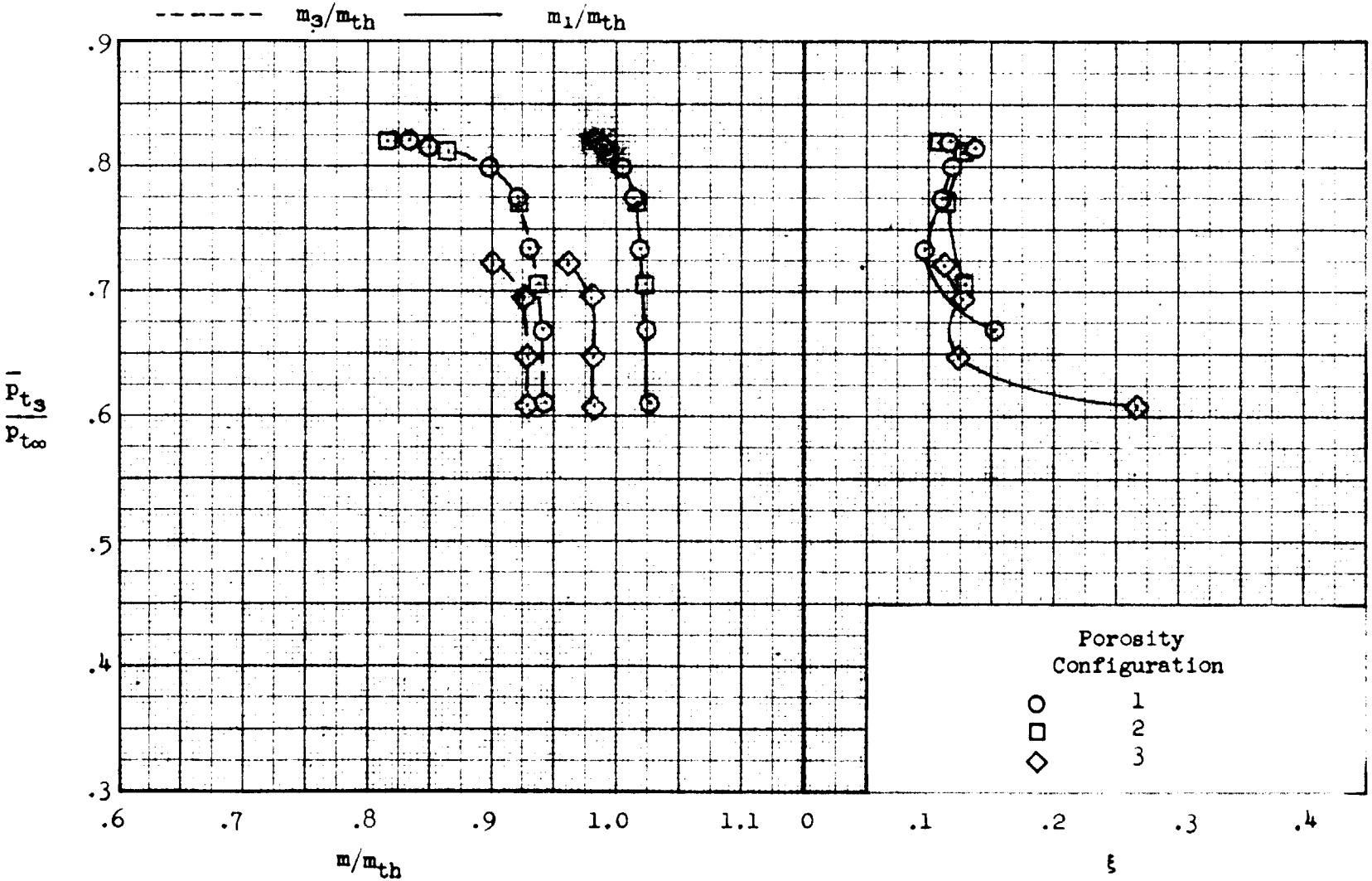

(c) $\alpha = 4°$, $\delta_R = 18.0°$, $\delta_L = 3.5°$, $A_{ref}/A_{th} = 1.0703$; inlet performance.

Figure 26.- Continued.

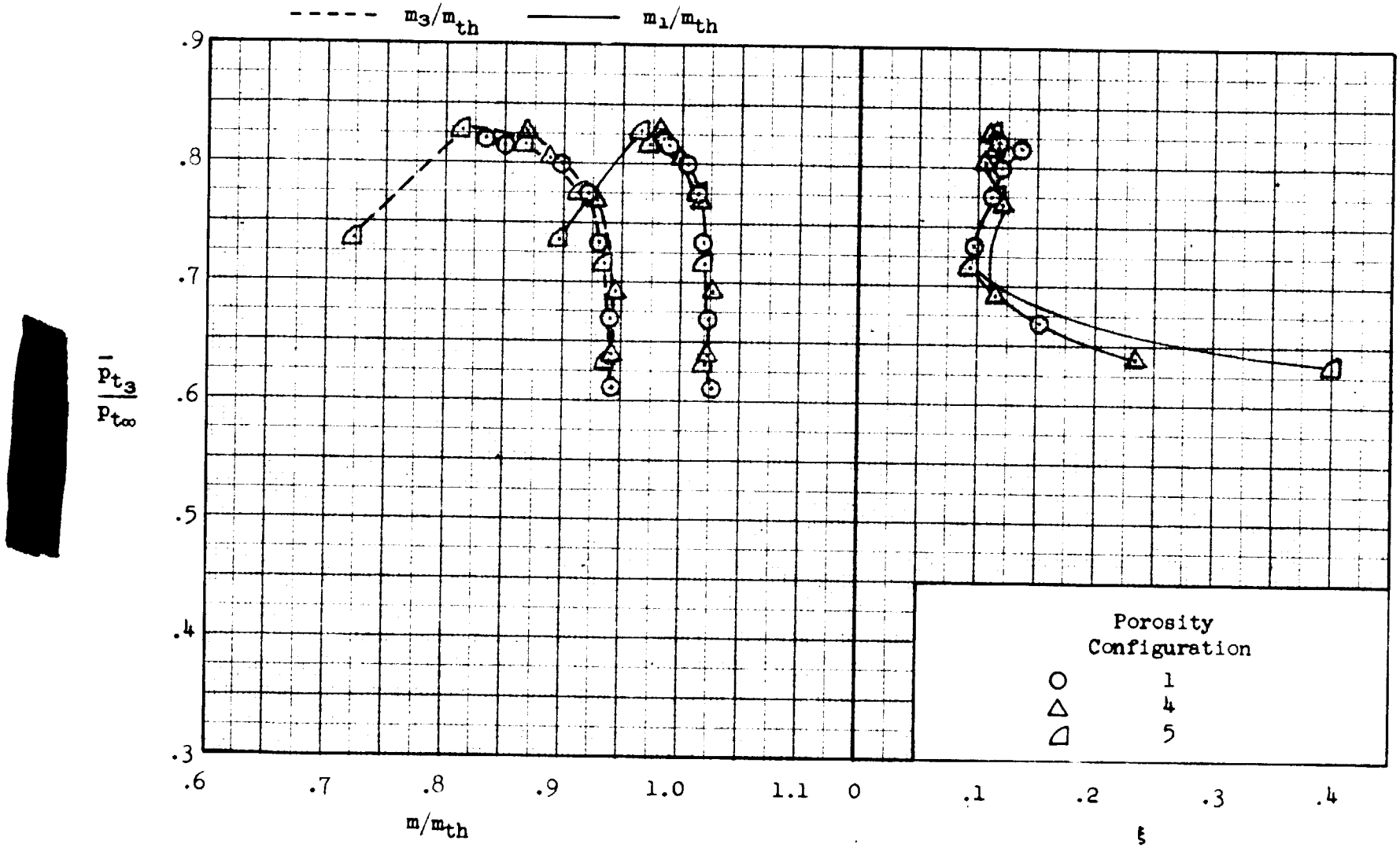

(c) Continued. Inlet performance.

Figure 26.- Continued.

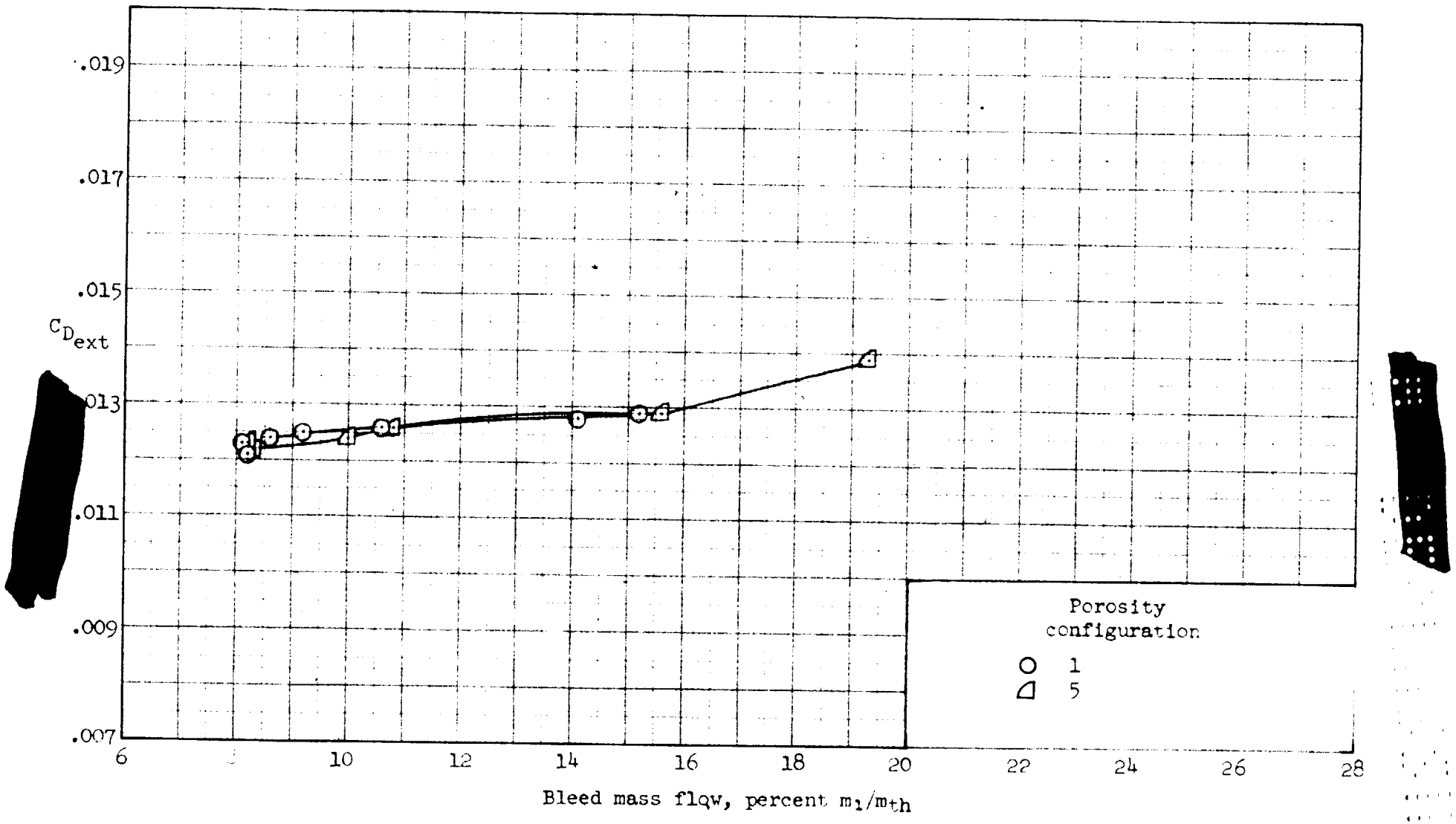

(c) Concluded. External-drag coefficient.

Figure 26.- Continued.

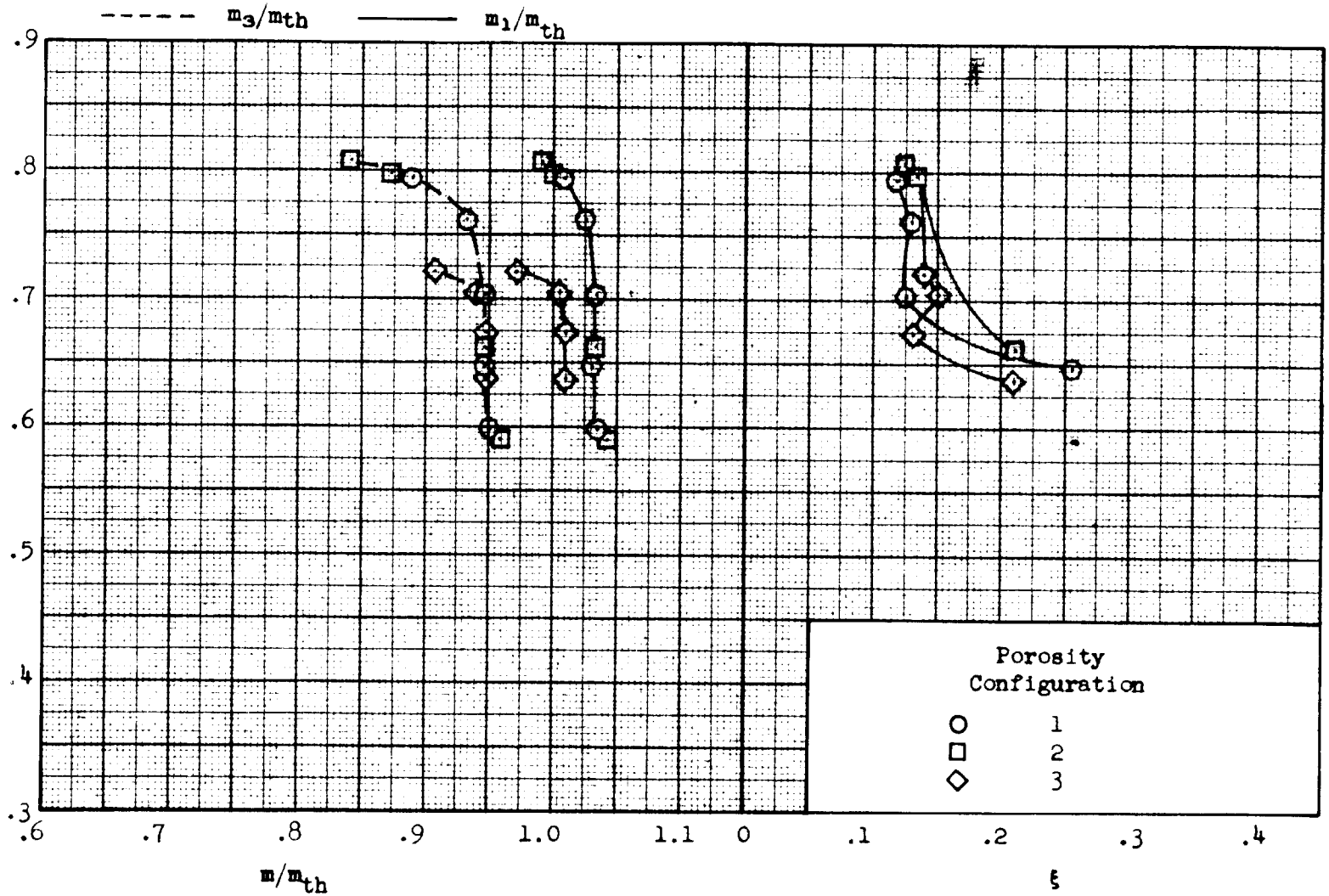

(d) $\alpha = 6°$, $\delta_R = 17.5°$, $\delta_L = 4.0°$, $A_{ref}/A_{th} = 1.0313$; inlet performance.

Figure 26.- Continued.

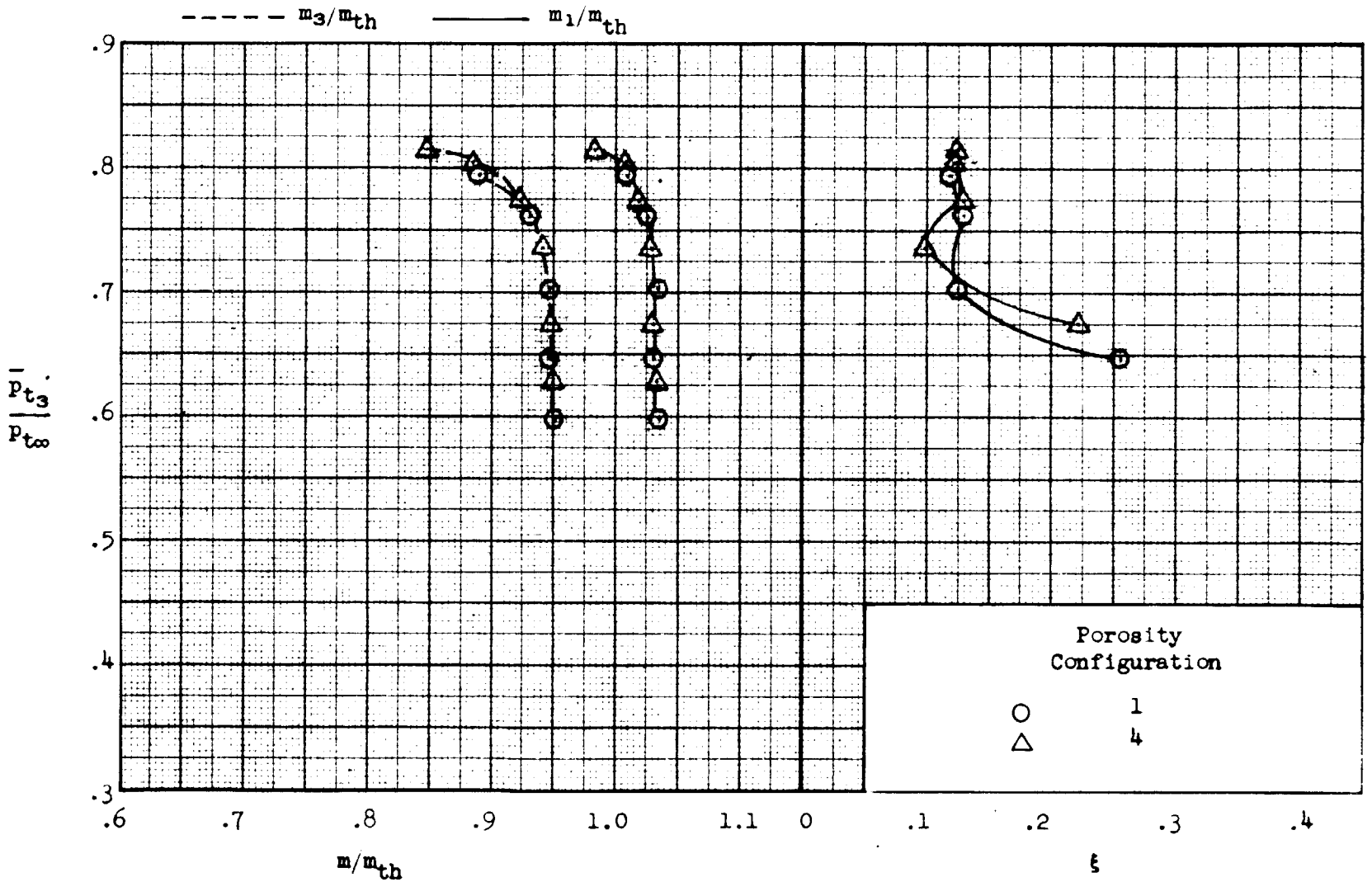

(d) Concluded. Inlet performance.

Figure 26.- Continued.

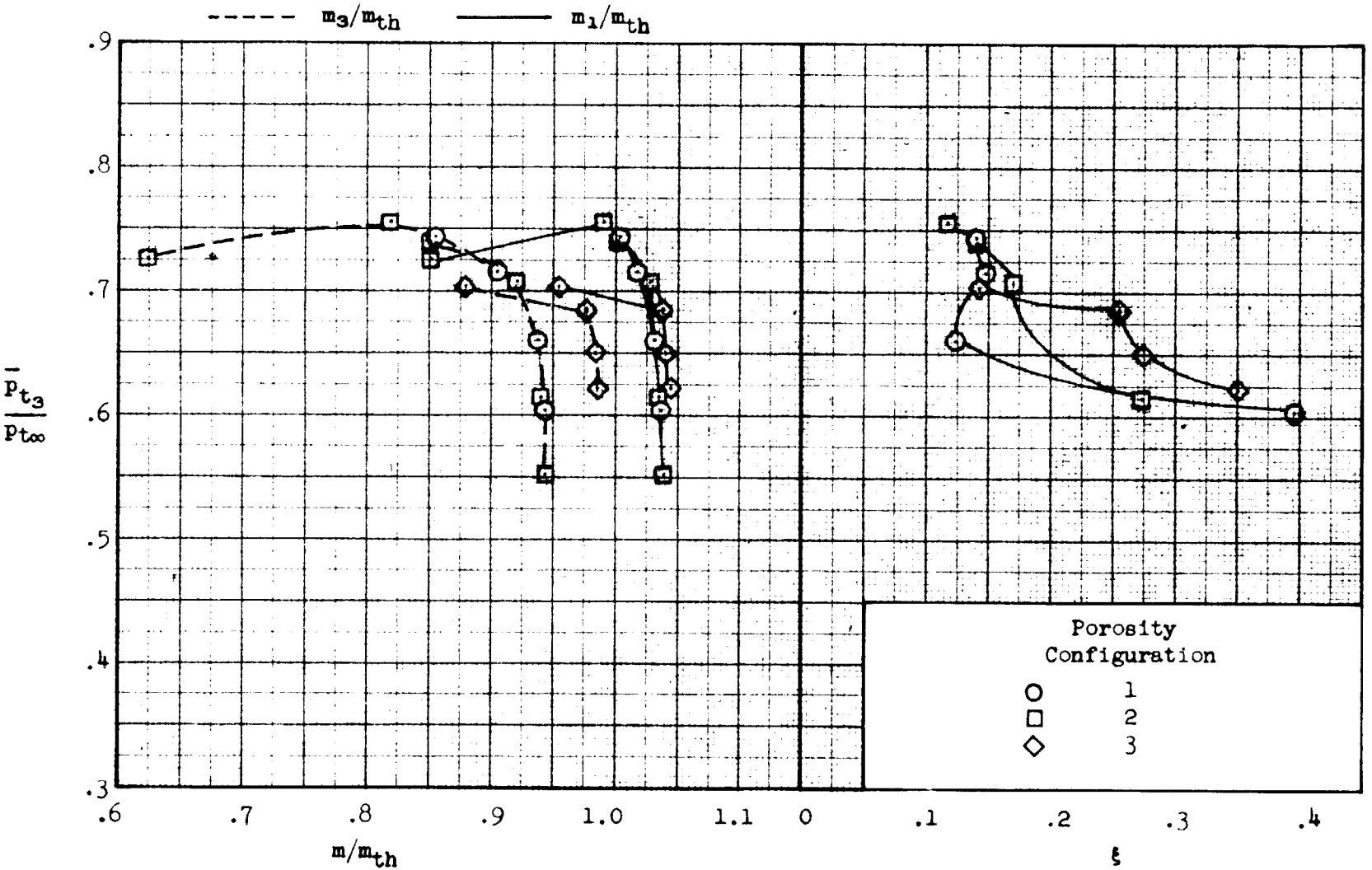

(e) $\alpha = 10°$, $\delta_R = 17.0°$, $\delta_L = 7.5°$, $A_{ref}/A_{th} = 1.0624$; inlet performance.

Figure 26.- Concluded.

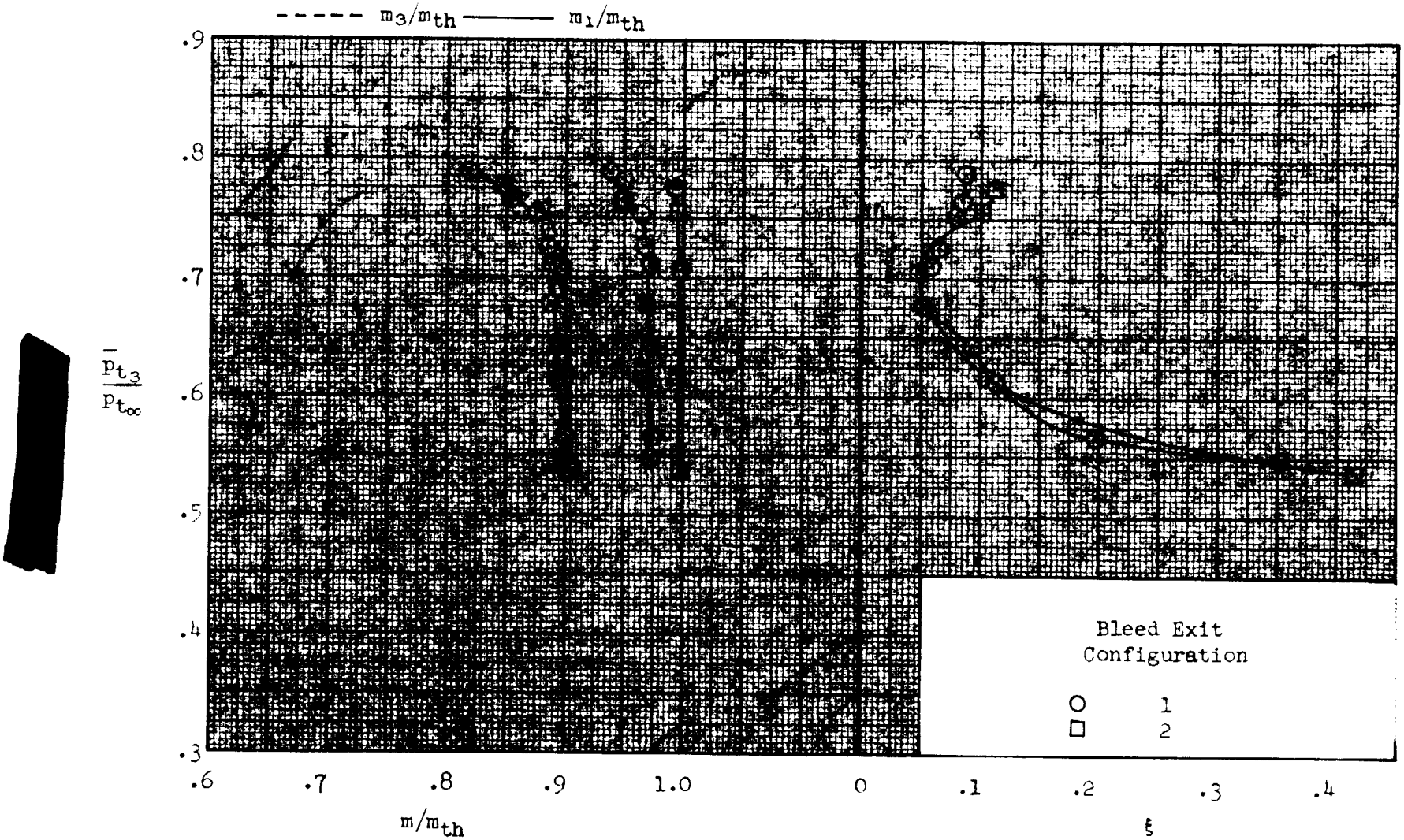

(a) $\alpha = 0°$, $\delta_R = 19.5°$, $\delta_L = 0.5°$, $A_{ref}/A_{th} = 1.0432$.

Figure 27.- Effect of variation of bleed-exit configuration on inlet performance; M = 3.00, β = 0°. Configuration: nose 1, diverter 2, porosity 4.

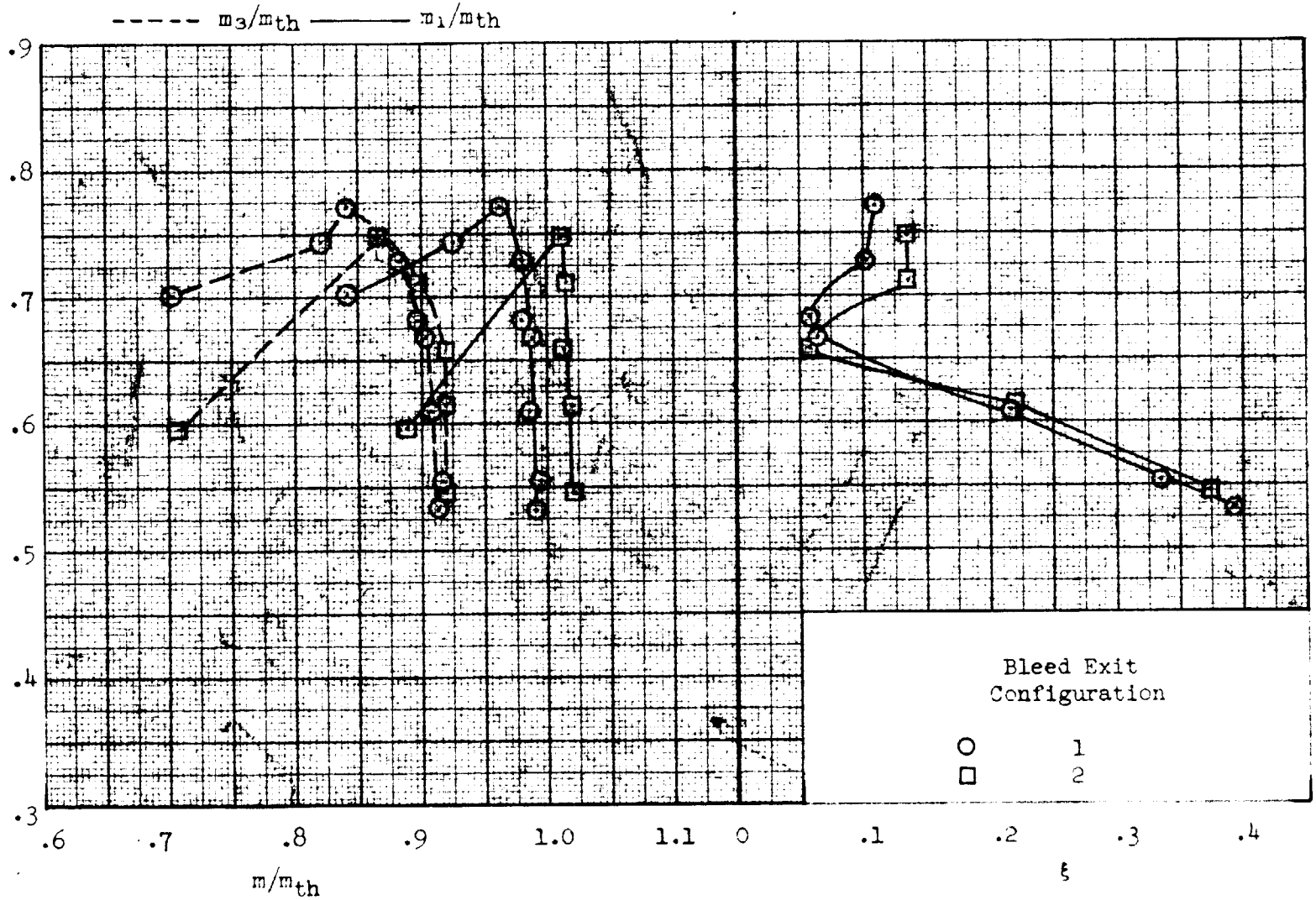

(b) $\alpha = 2°$, $\delta_R = 19.5°$, $\delta_L = 4.0°$, $A_{ref}/A_{th} = 1.0930$.

Figure 27.- Continued.

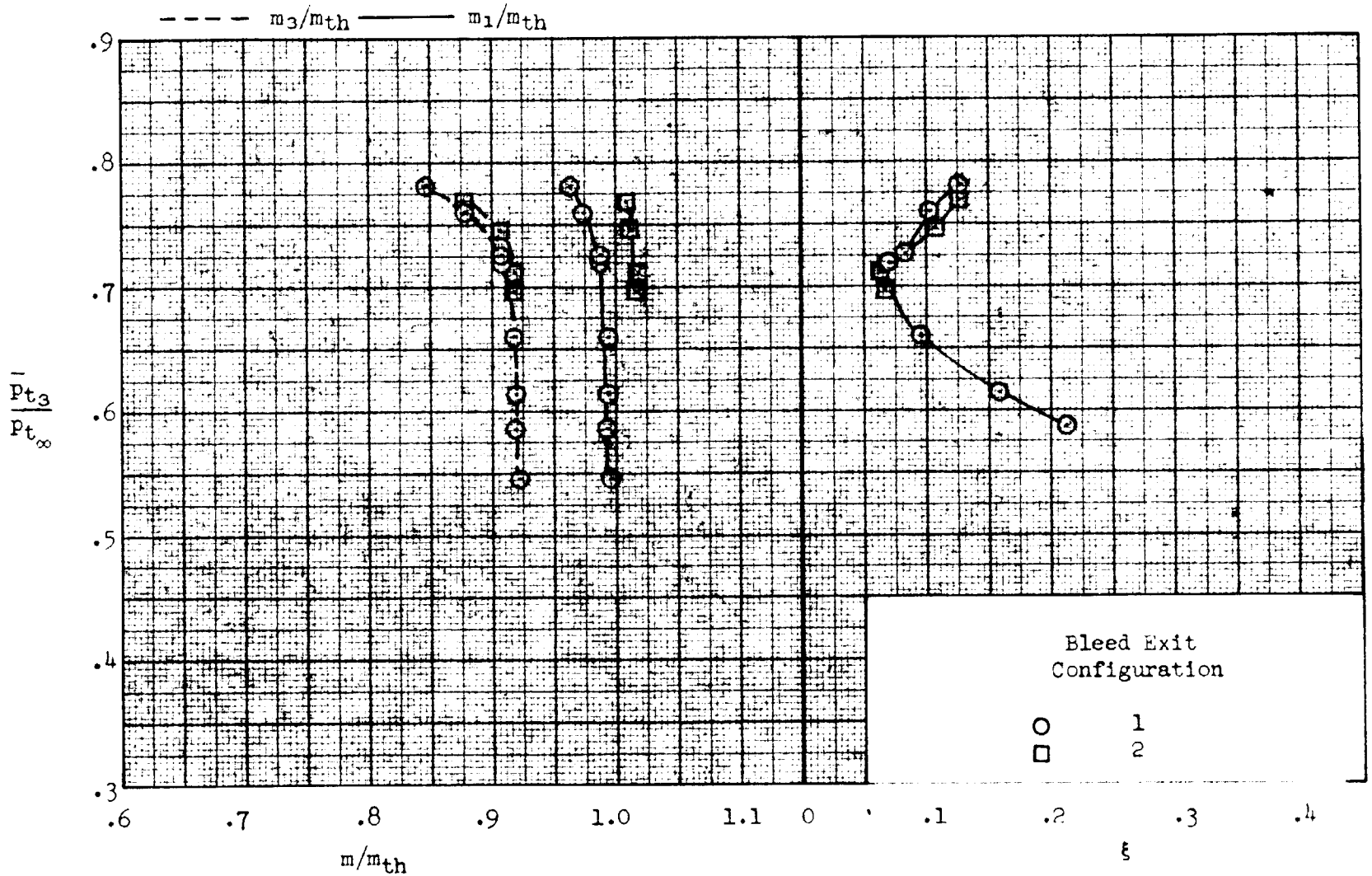

(c) $\alpha = 4°$, $\delta_R = 18.5°$, $\delta_L = 1.0°$, $A_{ref}/A_{th} = 0.9325$.

Figure 27.- Continued.

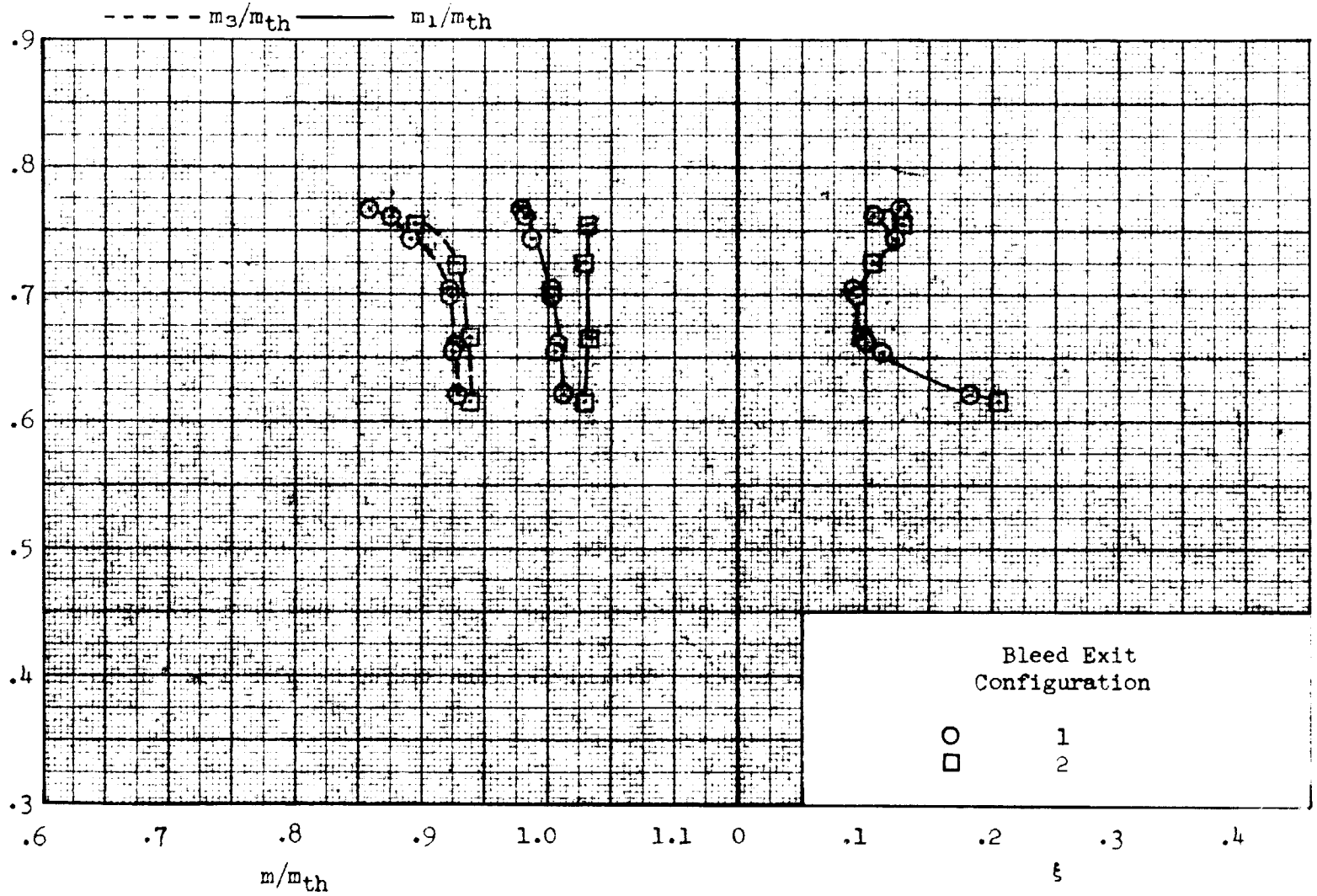

(d) $\alpha = 6°$, $\delta_R = 18.0°$, $\delta_L = 1.5°$, $A_{ref}/A_{th} = 0.8968$.

Figure 27.- Concluded.

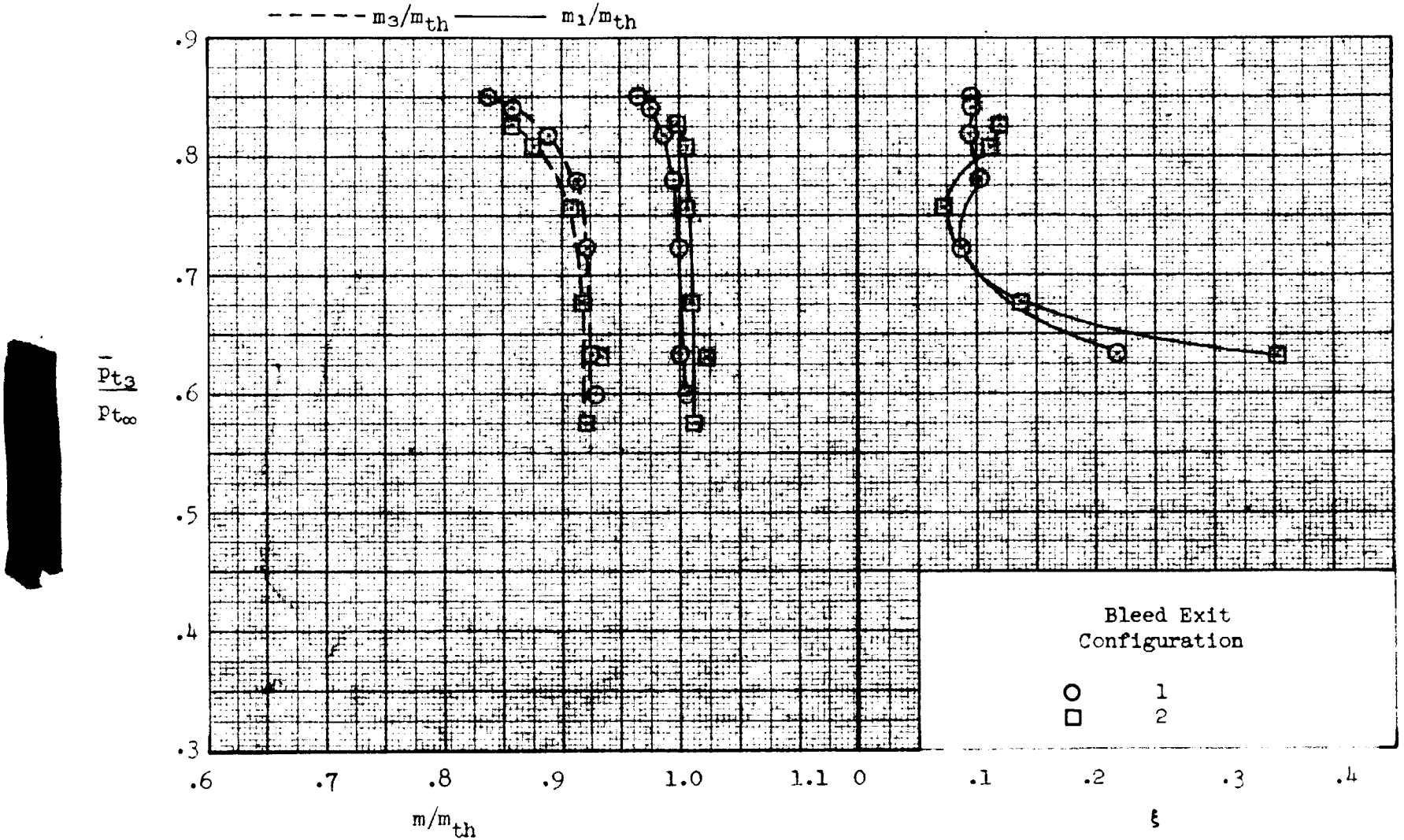

(a) $\alpha = 0°$, $\delta_R = 18.5°$, $\delta_L = 0.5°$, $A_{ref}/A_{th} = 1.0968$.

Figure 28.- Effect of variation of bleed-exit configuration on inlet performance; M = 2.76, $\beta = 0°$. Configuration: nose 1, diverter 2, porosity 4.

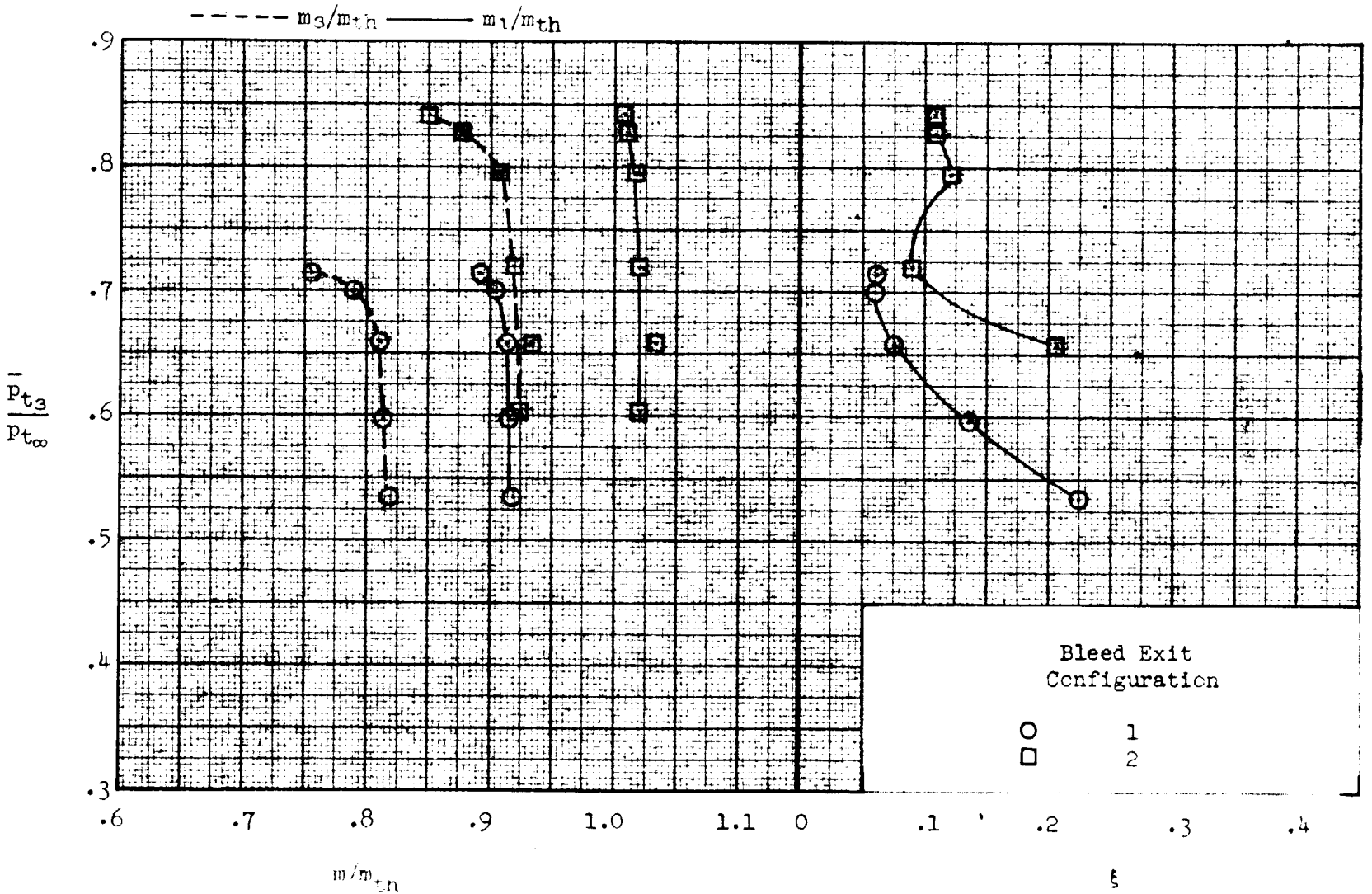

(b) $\alpha = 2°$, $\delta_R = 18.5°$, $\delta_L = 1.5°$, $A_{ref}/A_{th} = 1.0706$.

Figure 28.- Continued.

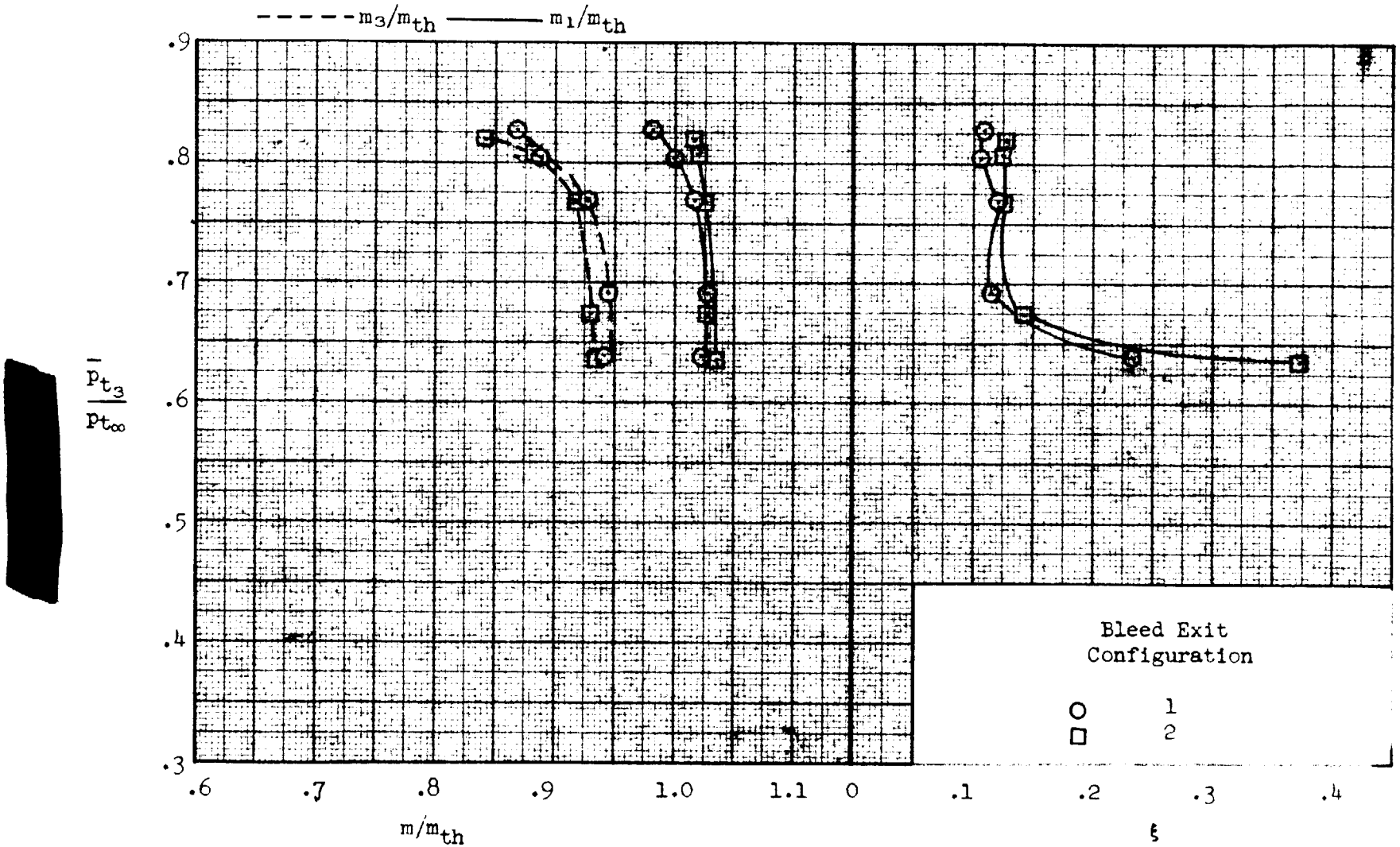

(c) $\alpha = 4°$, $\delta_R = 18.0°$, $\delta_L = 3.5°$, $A_{ref}/A_{th} = 1.0703$.

Figure 28.- Continued.

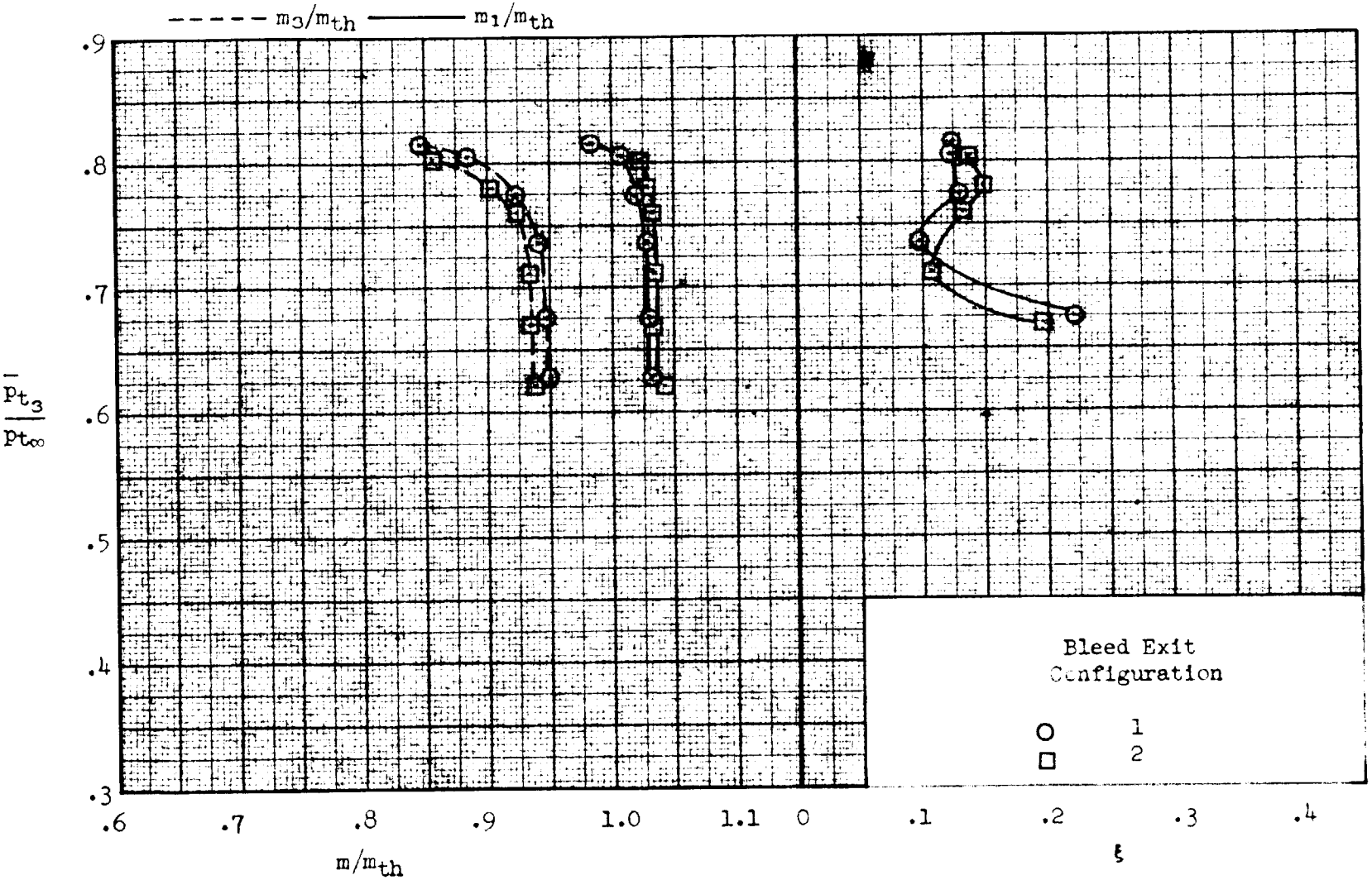

(d) $\alpha = 6°$, $\delta_R = 17.5°$, $\delta_L = 4.0°$, $A_{ref}/A_{th} = 1.0313$.

Figure 28.- Concluded.

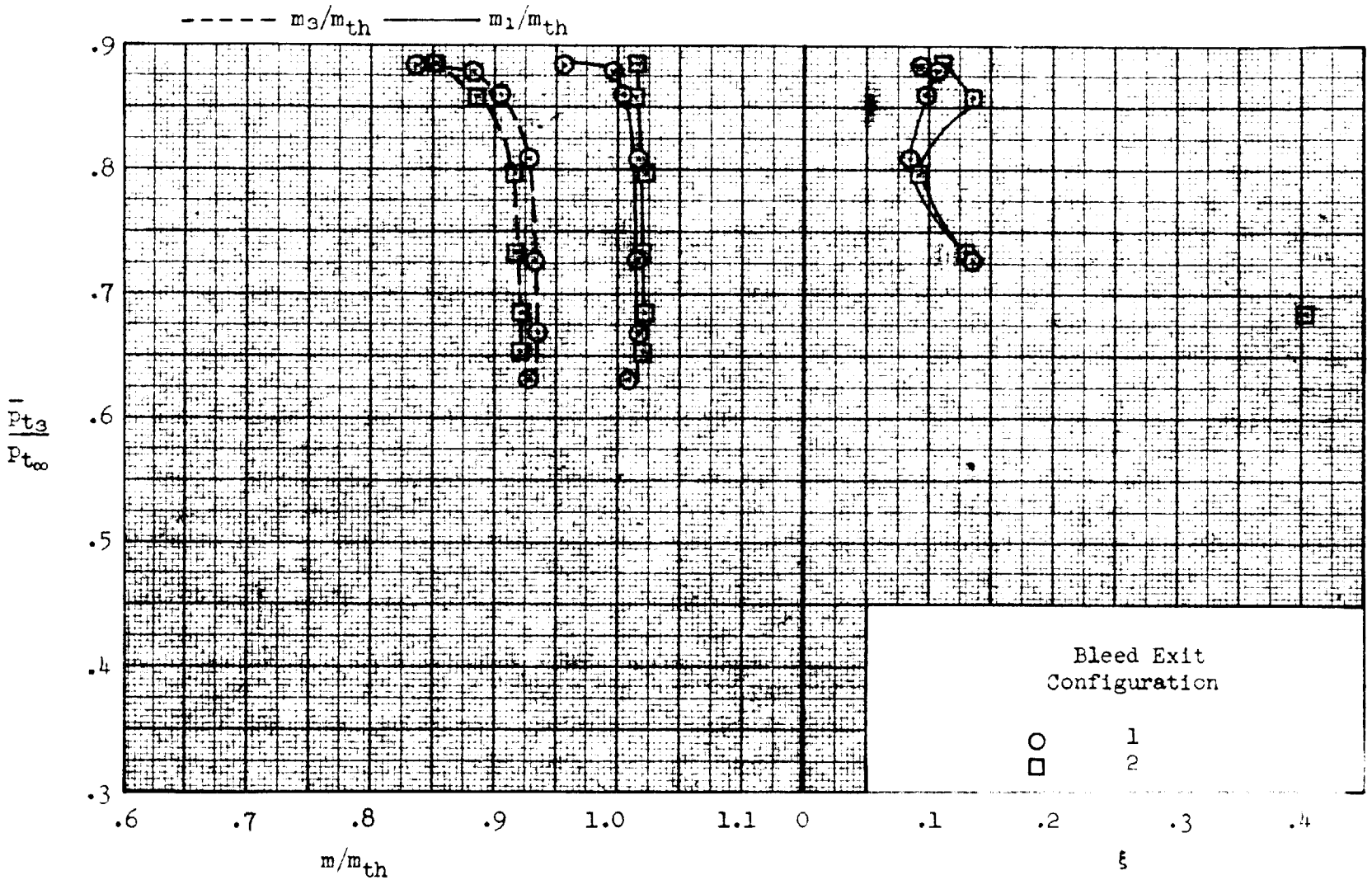

(a) $\alpha = 0°$, $\delta_R = 18.0°$, $\delta_L = 3.0°$, $A_{ref}/A_{th} = 1.2483$.

Figure 29.- Effect of variation of bleed-exit configuration on inlet performance; M = 2.50, $\beta = 0°$. Configuration: nose 1, diverter 2, porosity 4.

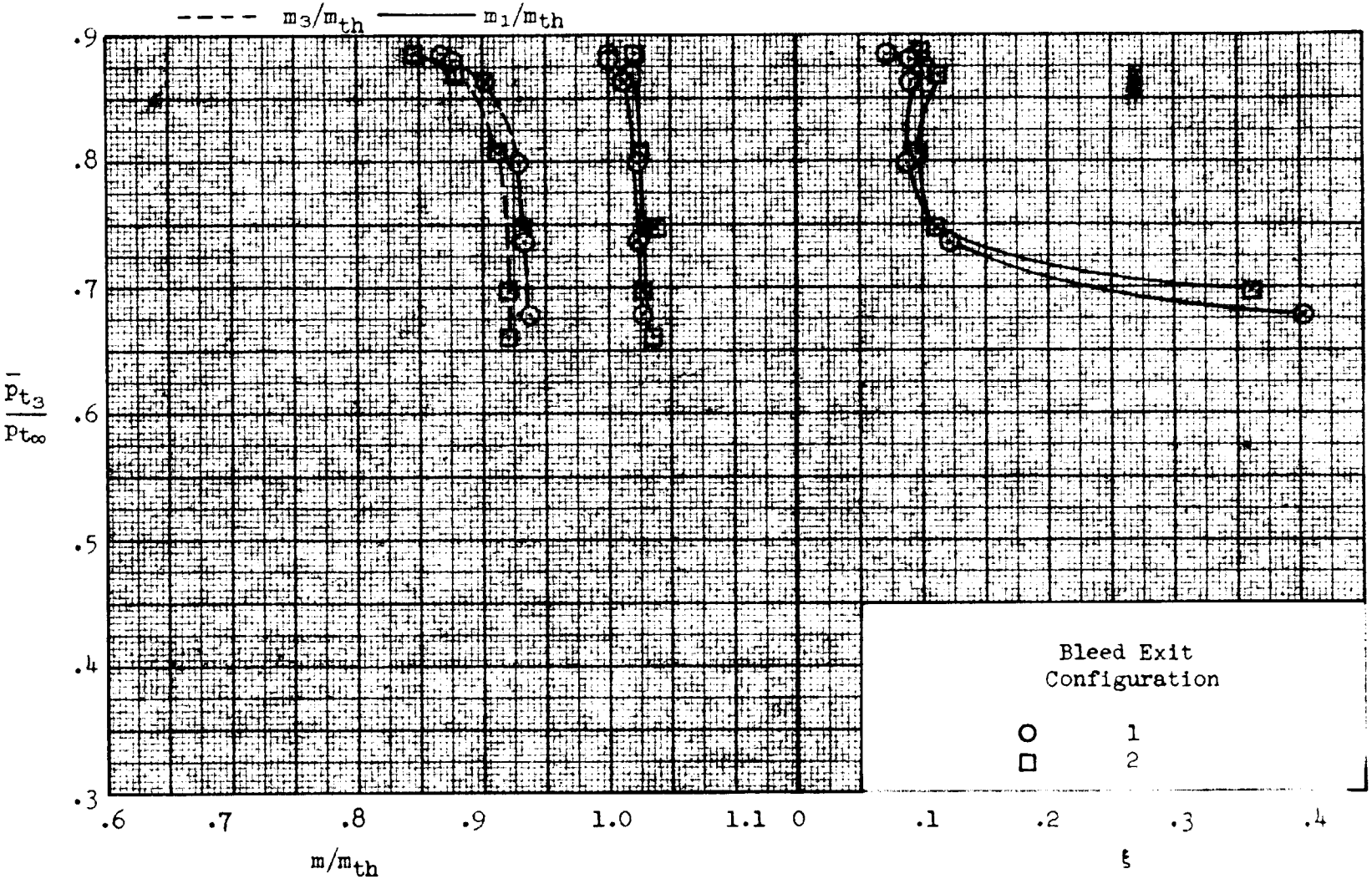

(b) $\alpha = 2°$, $\delta_R = 18.0°$, $\delta_L = 4.5°$, $A_{ref}/A_{th} = 1.2448$.

Figure 29.- Continued.

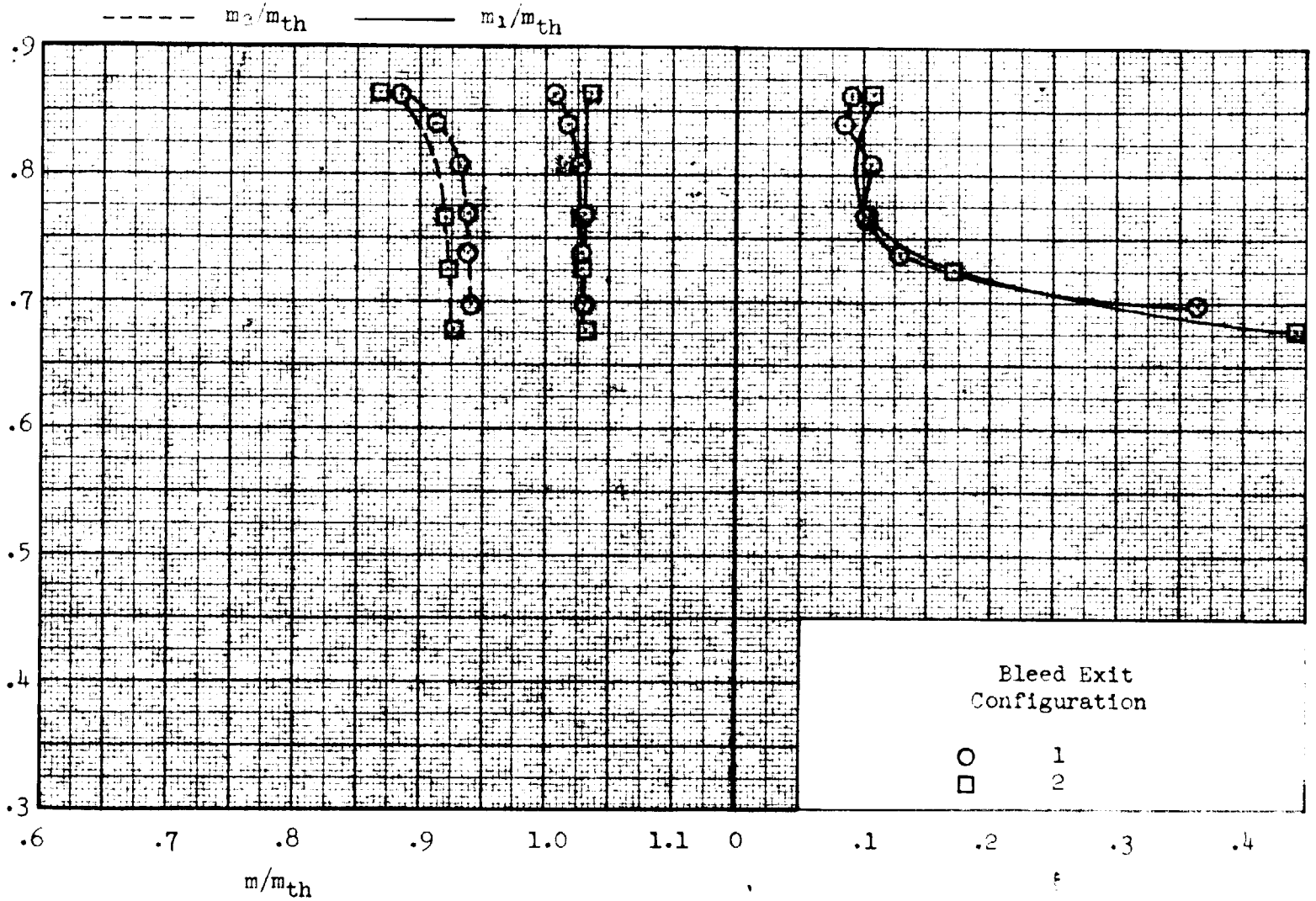

(c) $\alpha = 4°$, $\delta_R = 17.5°$, $\delta_L = 5.0°$, $A_{ref}/A_{th} = 1.1977$.

Figure 29.- Continued.

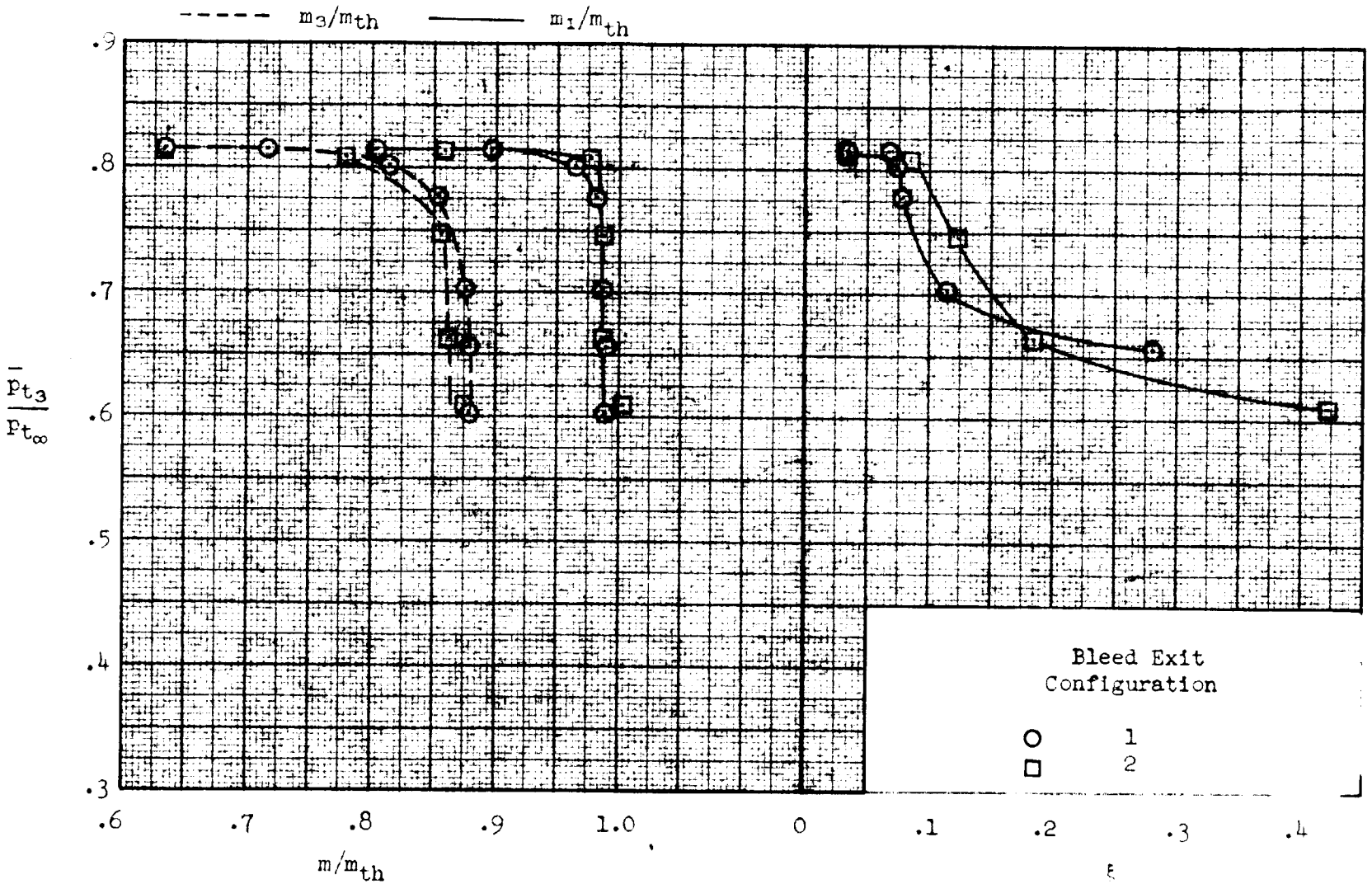

(d) $\alpha = 6°$, $\delta_R = 17.5°$, $\delta_L = 6.0°$, $A_{ref}/A_{th} = 1.1939$.

Figure 29.- Concluded.

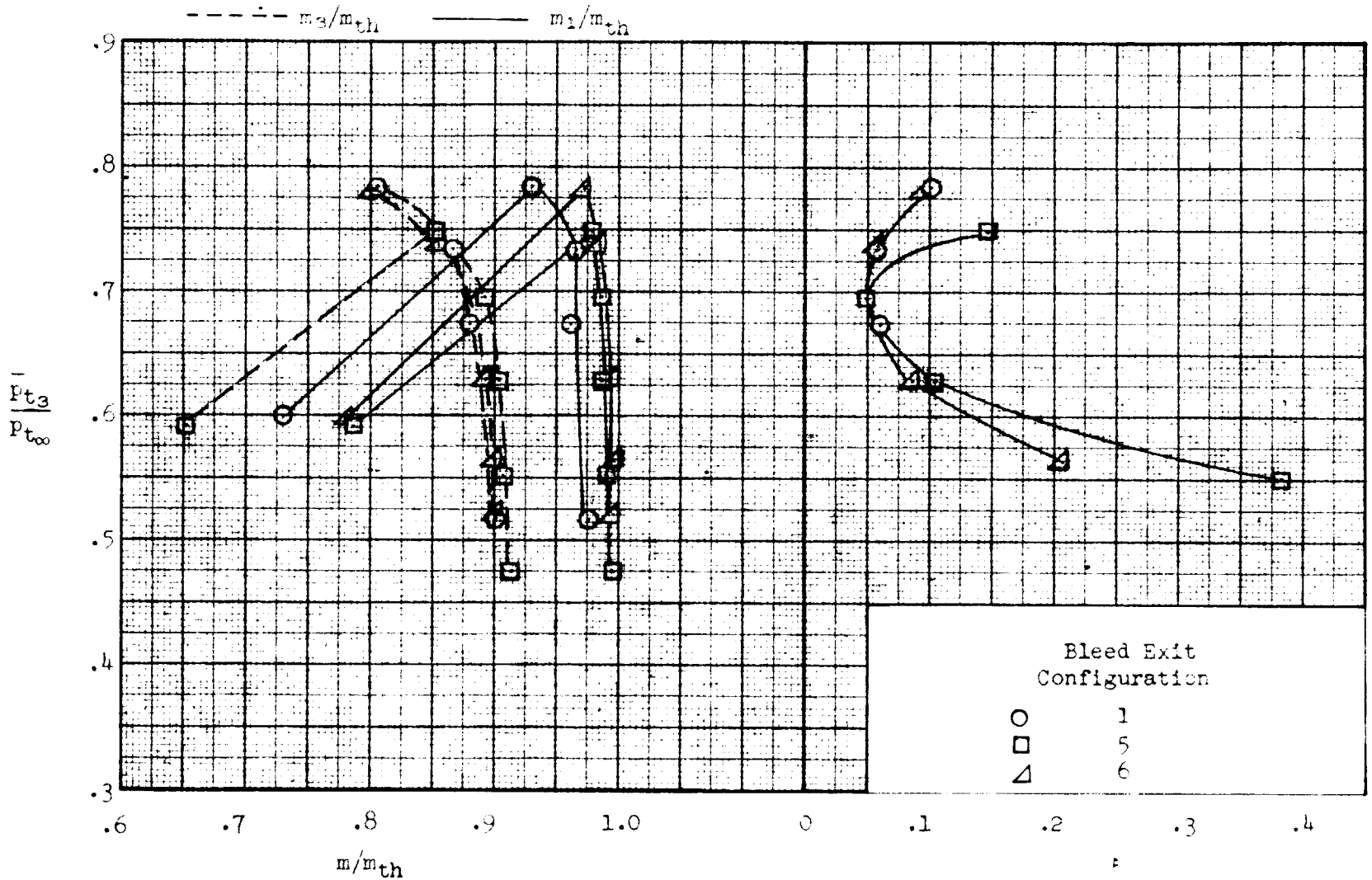

(a) $\alpha = 0°$, [illegible] = 19.[illegible]°, [illegible]$_L$ = [illegible]°, [illegible]$_{ref}$/[illegible]$_{th}$ = [illegible] inlet performance.

Figure 30.- Effect of variation of bleed-exit configuration on inlet performance and exter[illegible] coefficient; M = 3.00, β = 0°. Configuration: nose 1, diverter [illegible], porosity 5.

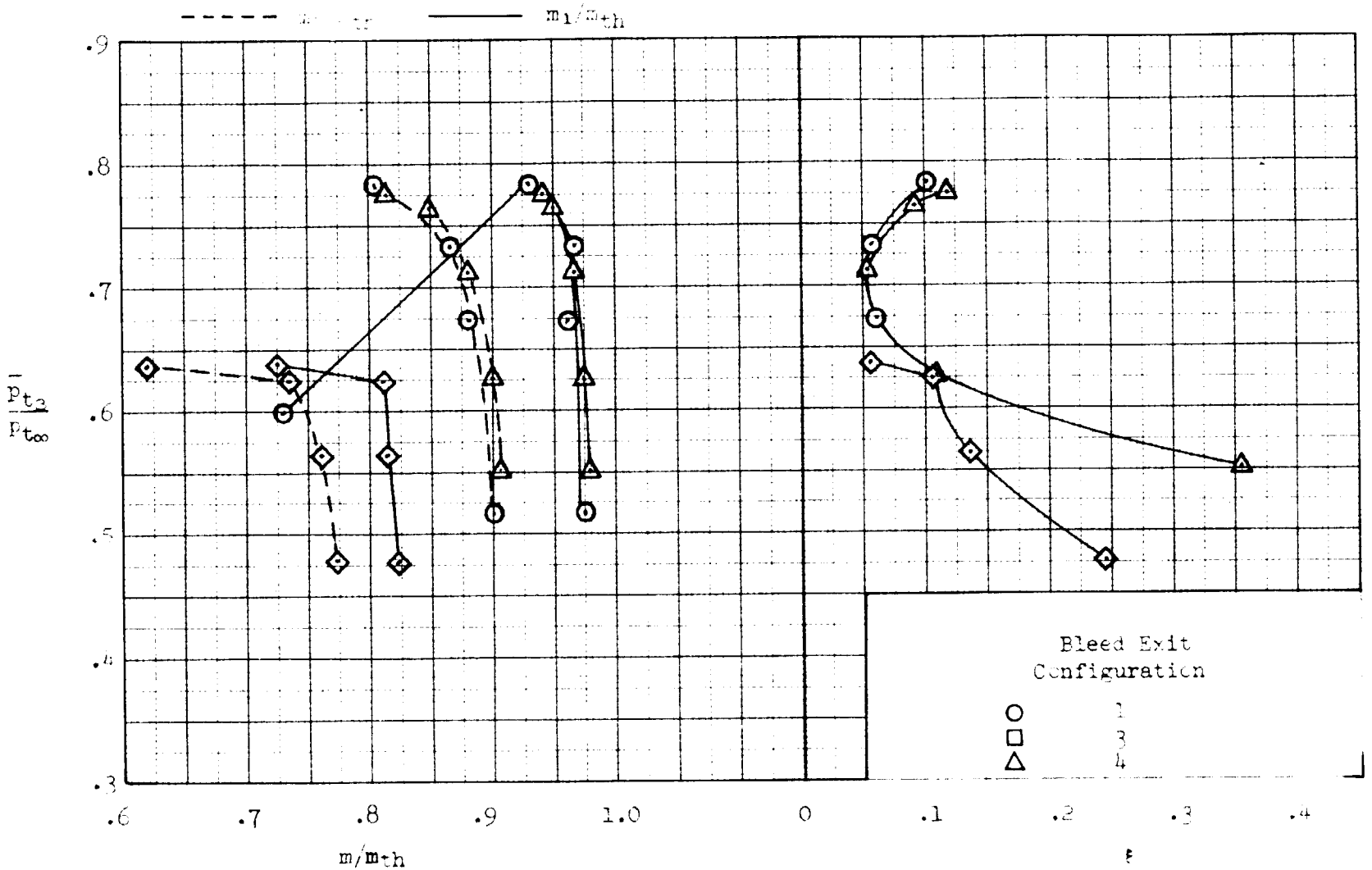

(a) Continued. Inlet performance.

Figure 30.- Continued.

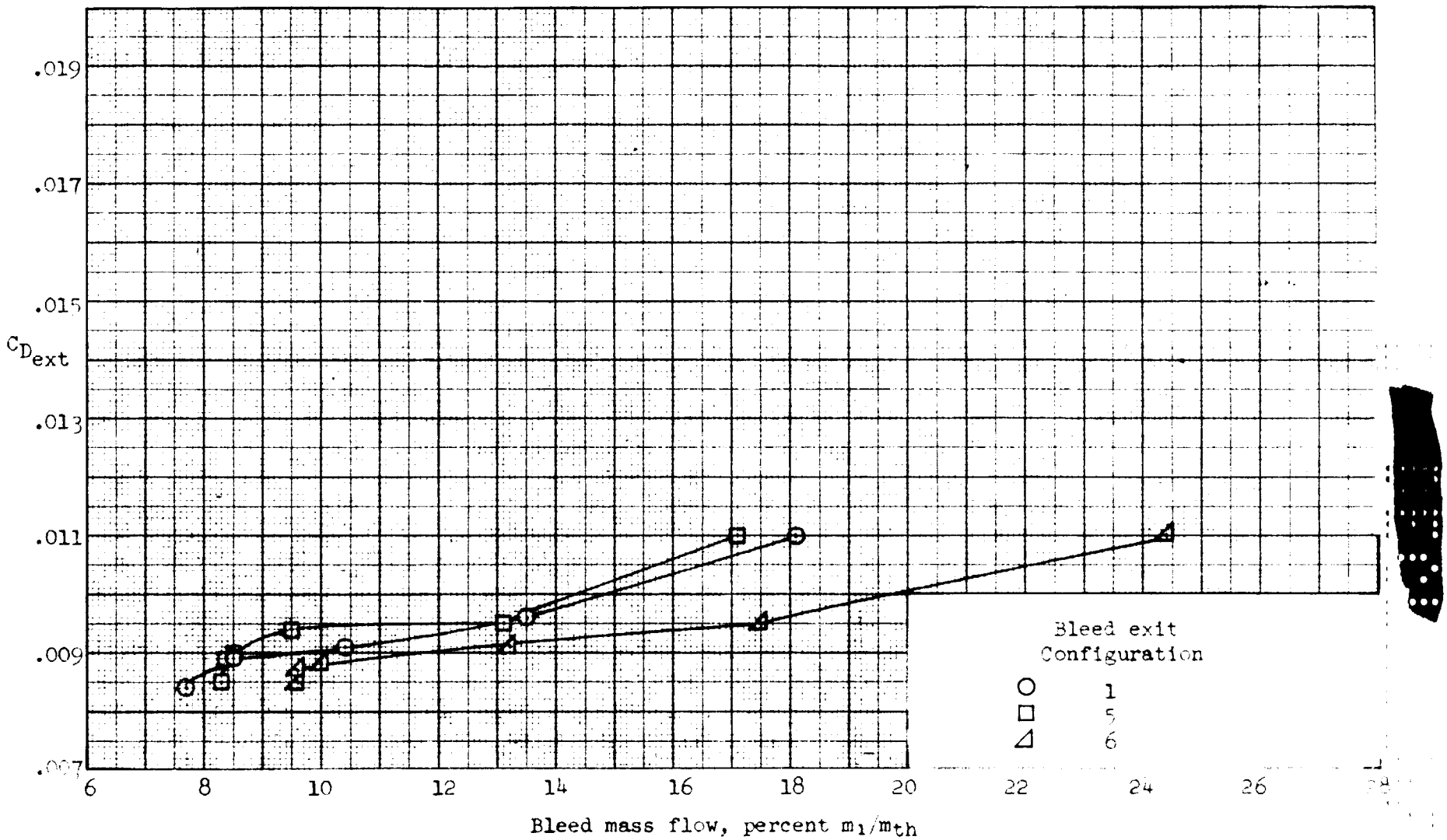

(a) Continued. External-drag coefficient.

Figure 30.- Continued.

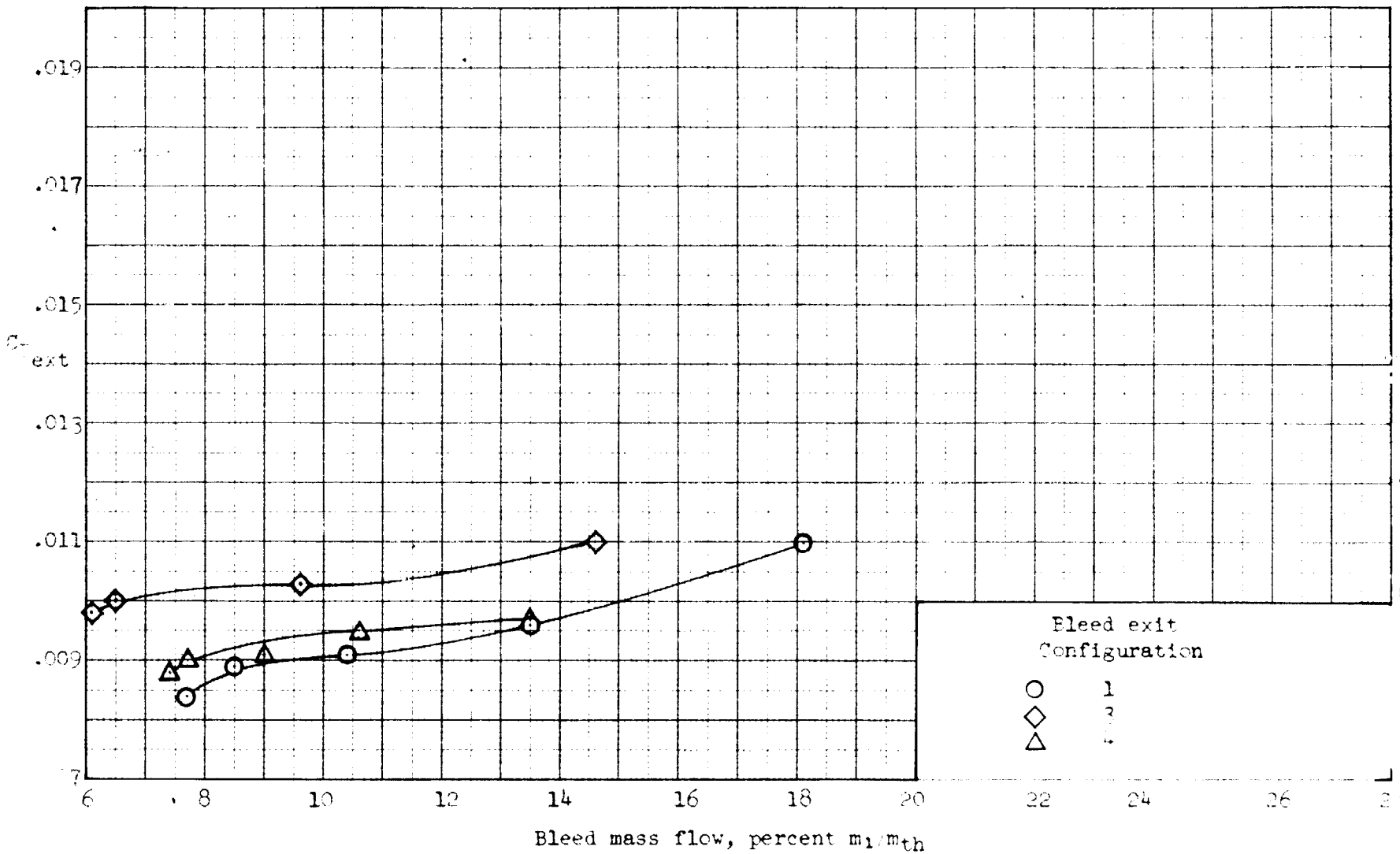

(a) Concluded. External-drag coefficient.

Figure 30.- Continued.

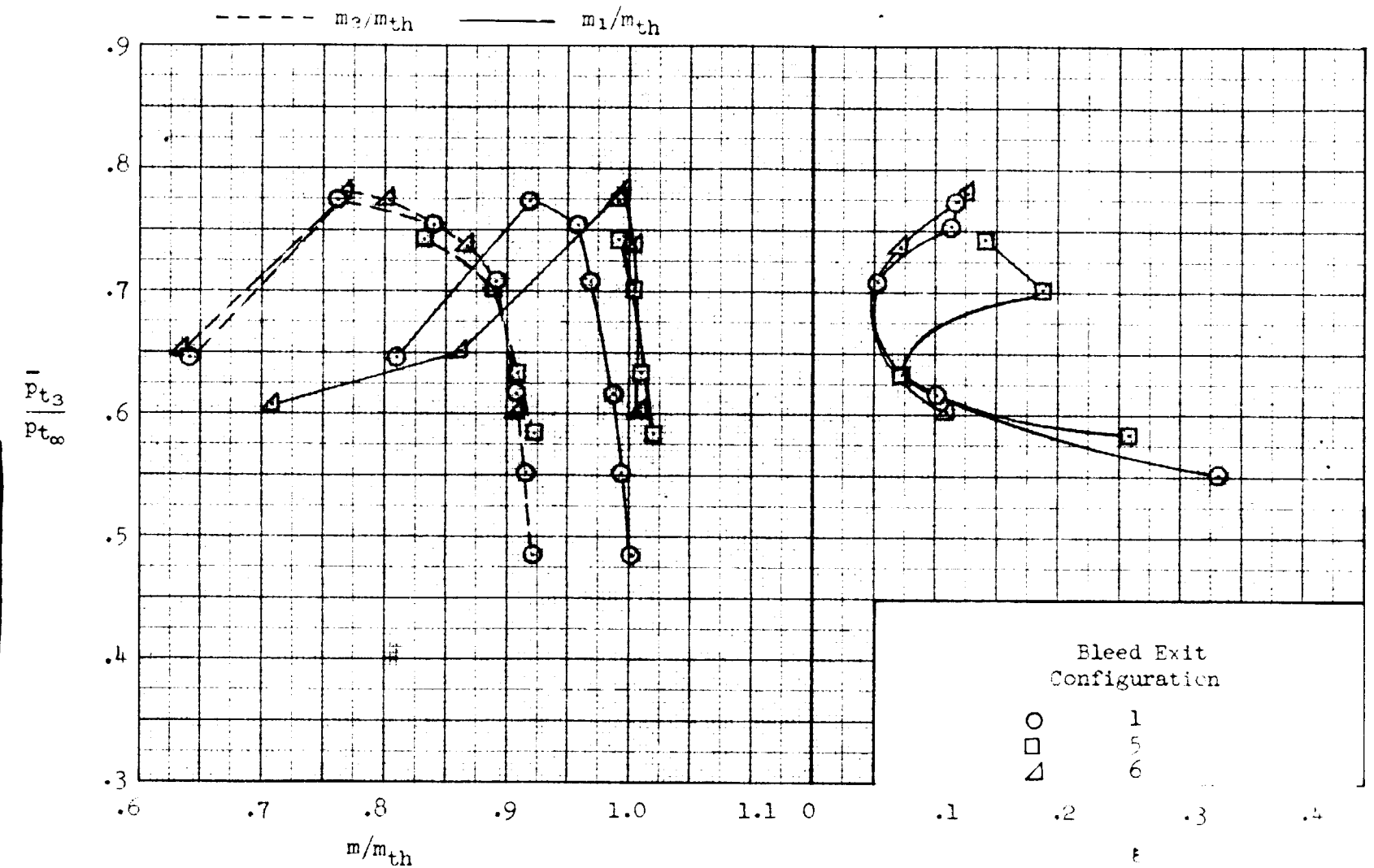

(b) $\alpha = 2°$, $\delta_R = 19.5°$, $\delta_L = 4.0°$, $A_{ref}/A_{th} = 1.0930$; inlet performance.

Figure 30.- Continued.

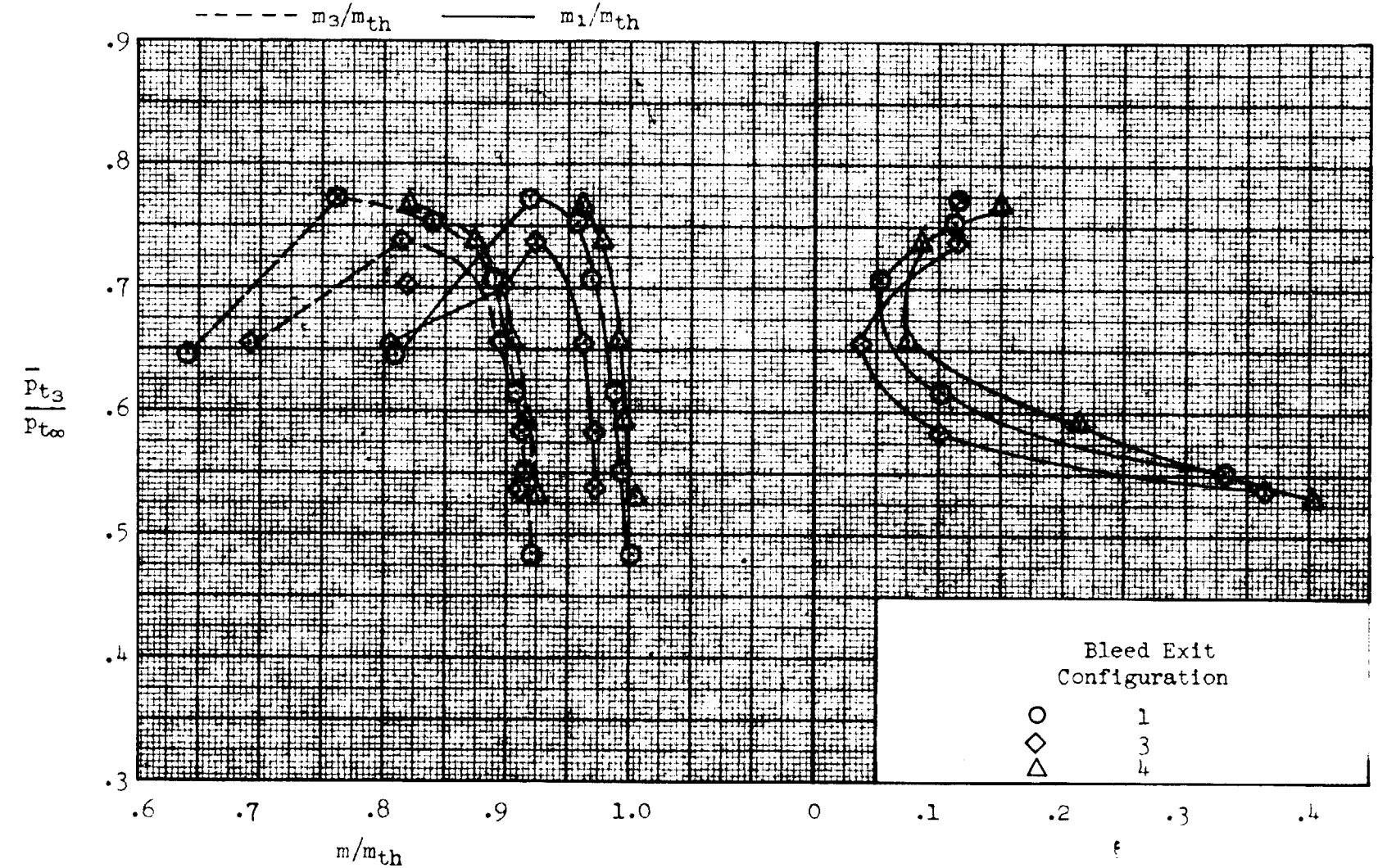

(b) Continued. Inlet performance.

Figure 30.- Continued.

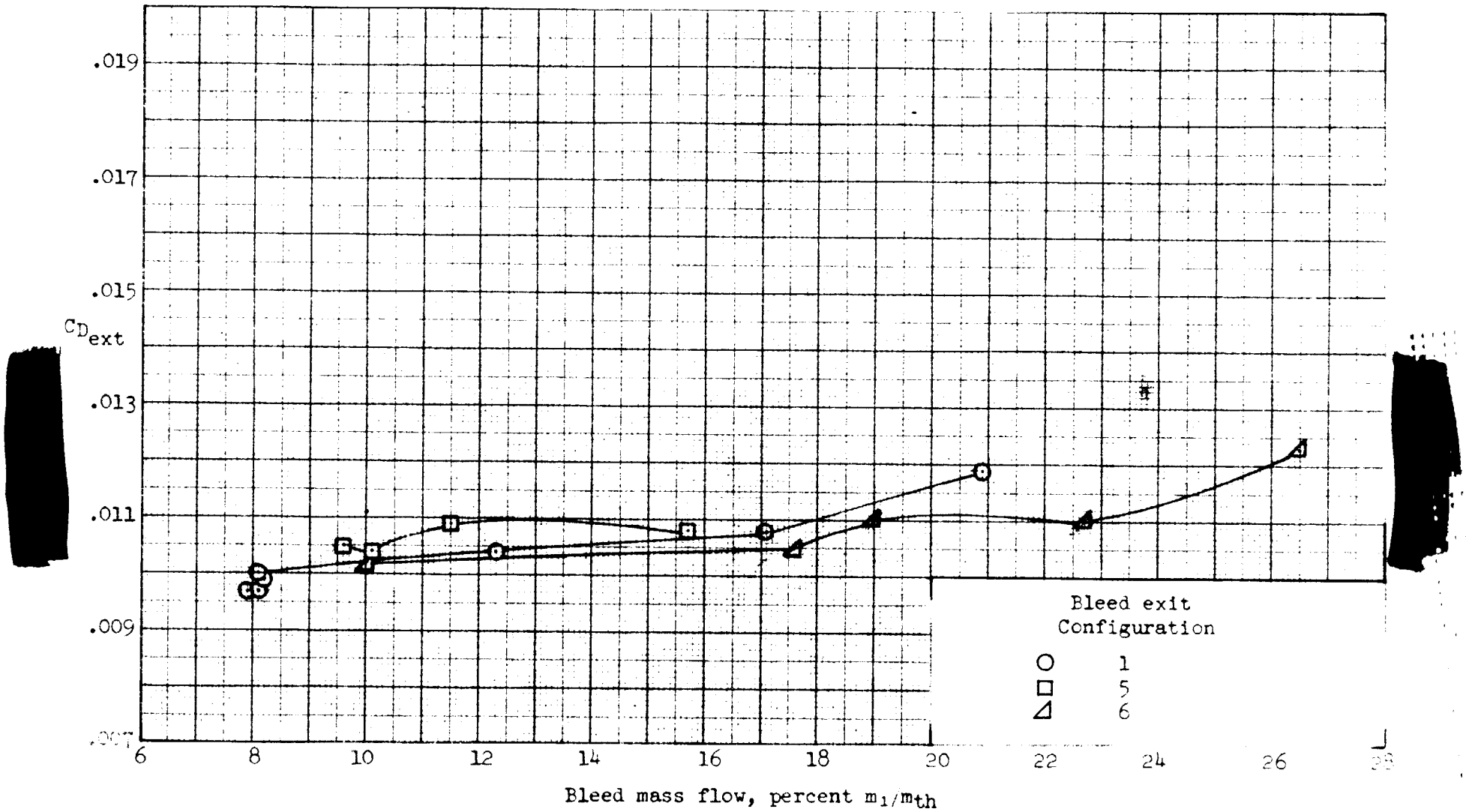

(b) Continued. External-drag coefficient.

Figure 30.- Continued.

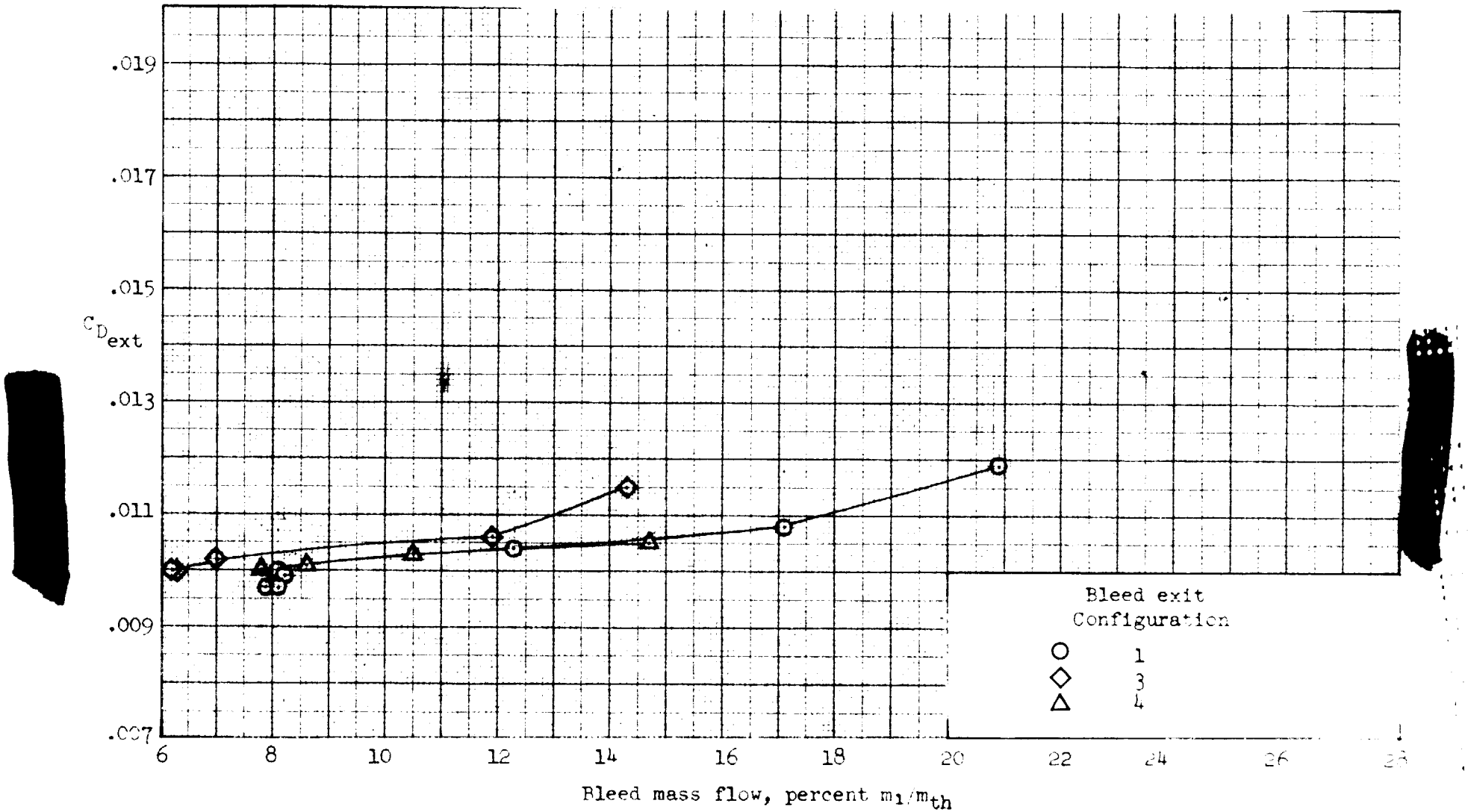

(b) Concluded. External-drag coefficient.

Figure 30.- Continued.

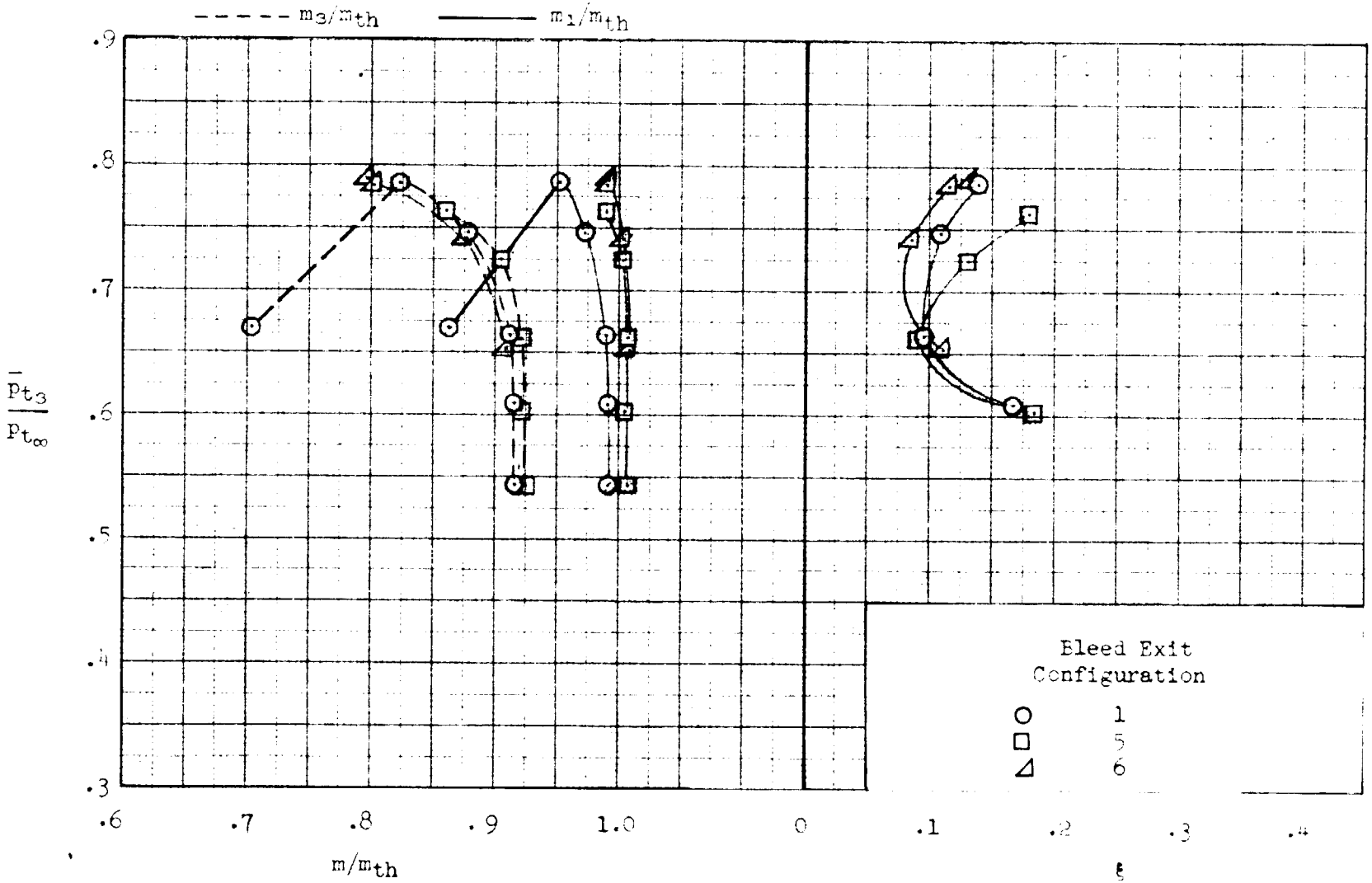

(c) $\alpha = 4°$, $\delta_R = 18.5°$, $\delta_L = 1.0°$, $A_{ref}/A_{th} = 0.9325$; inlet performance.

Figure 30.- Continued.

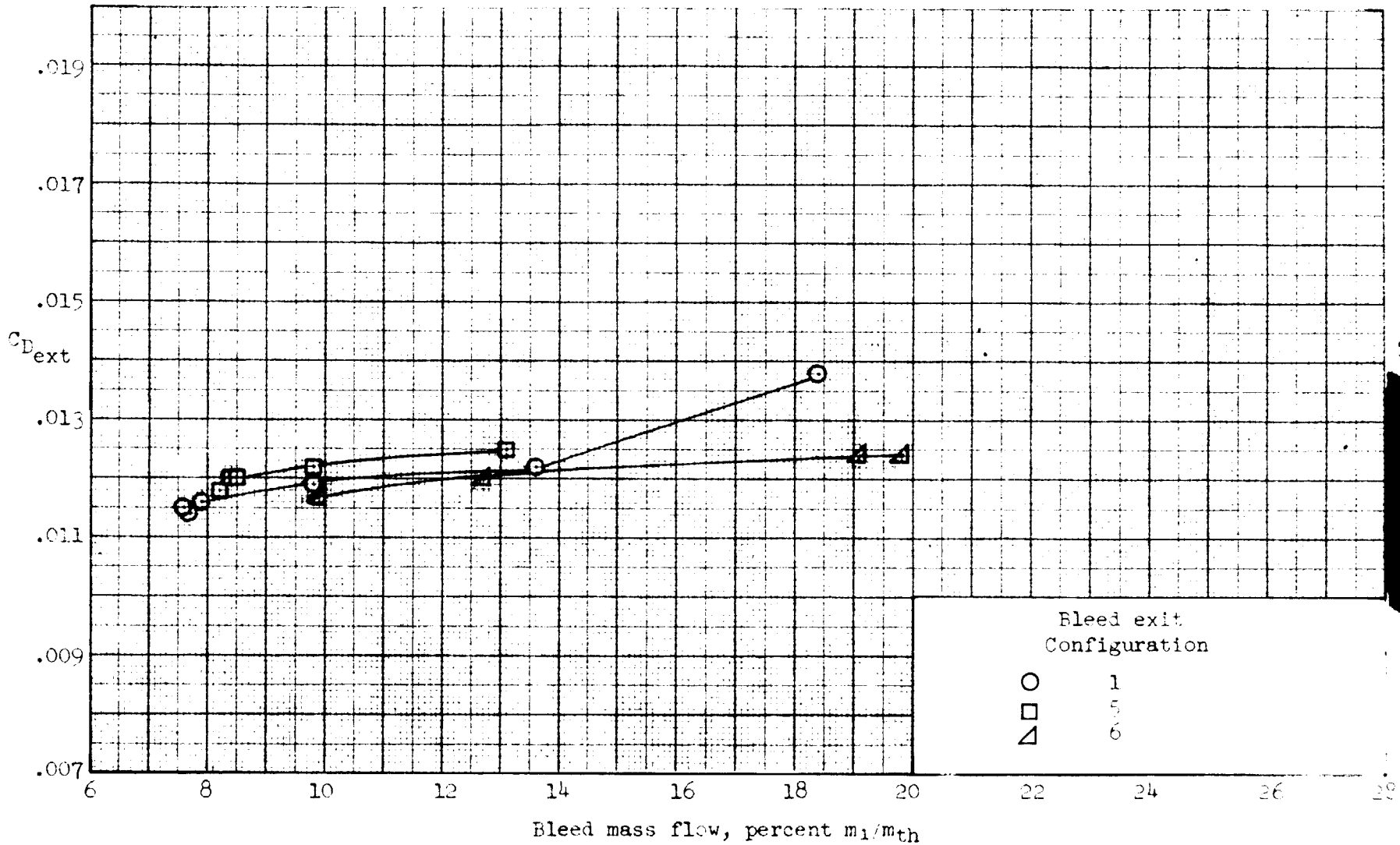

(c) Continued. External-drag coefficient.

Figure 30.- Continued.

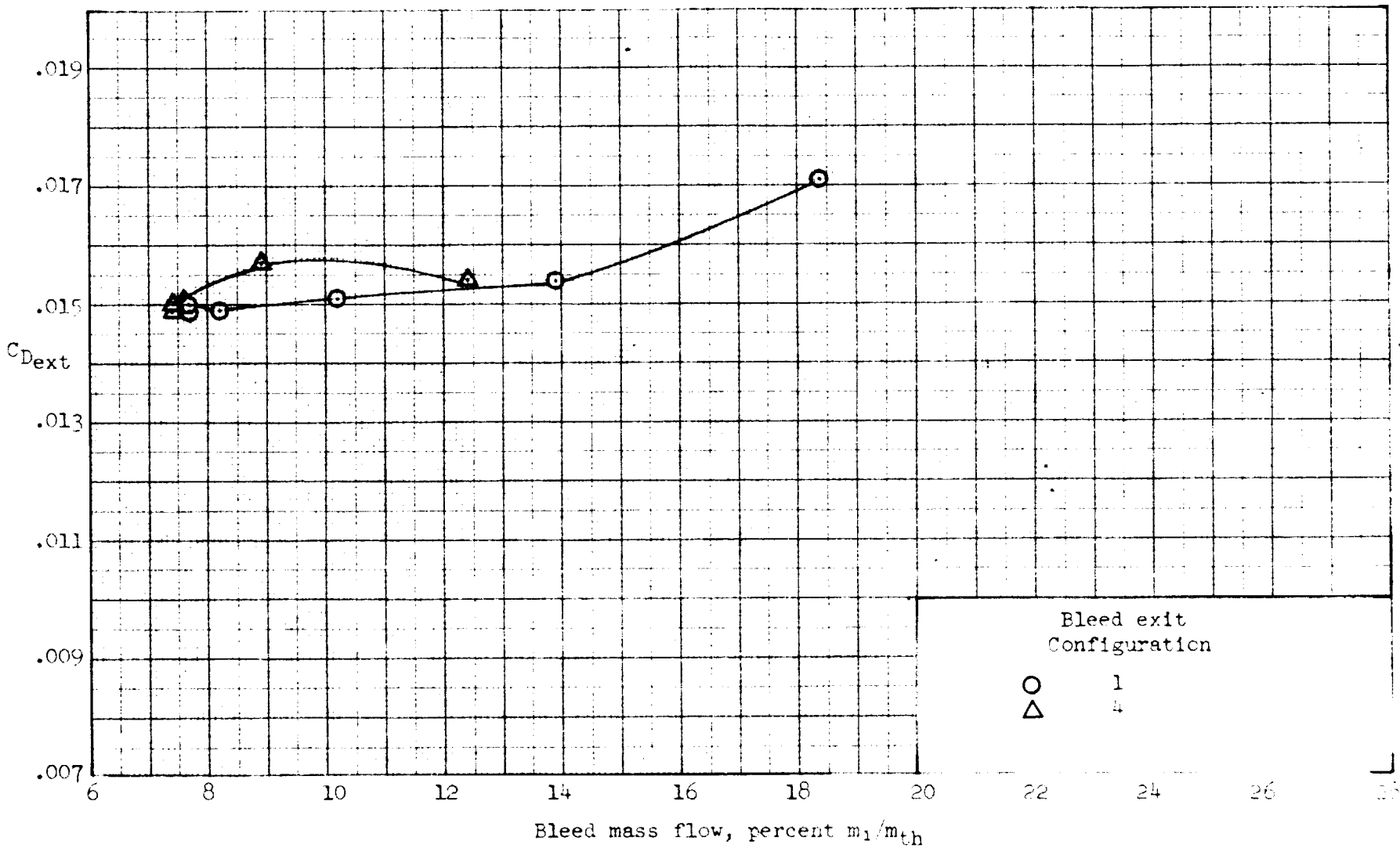

(d) Concluded. External-drag coefficient.

Figure 30.- Concluded.

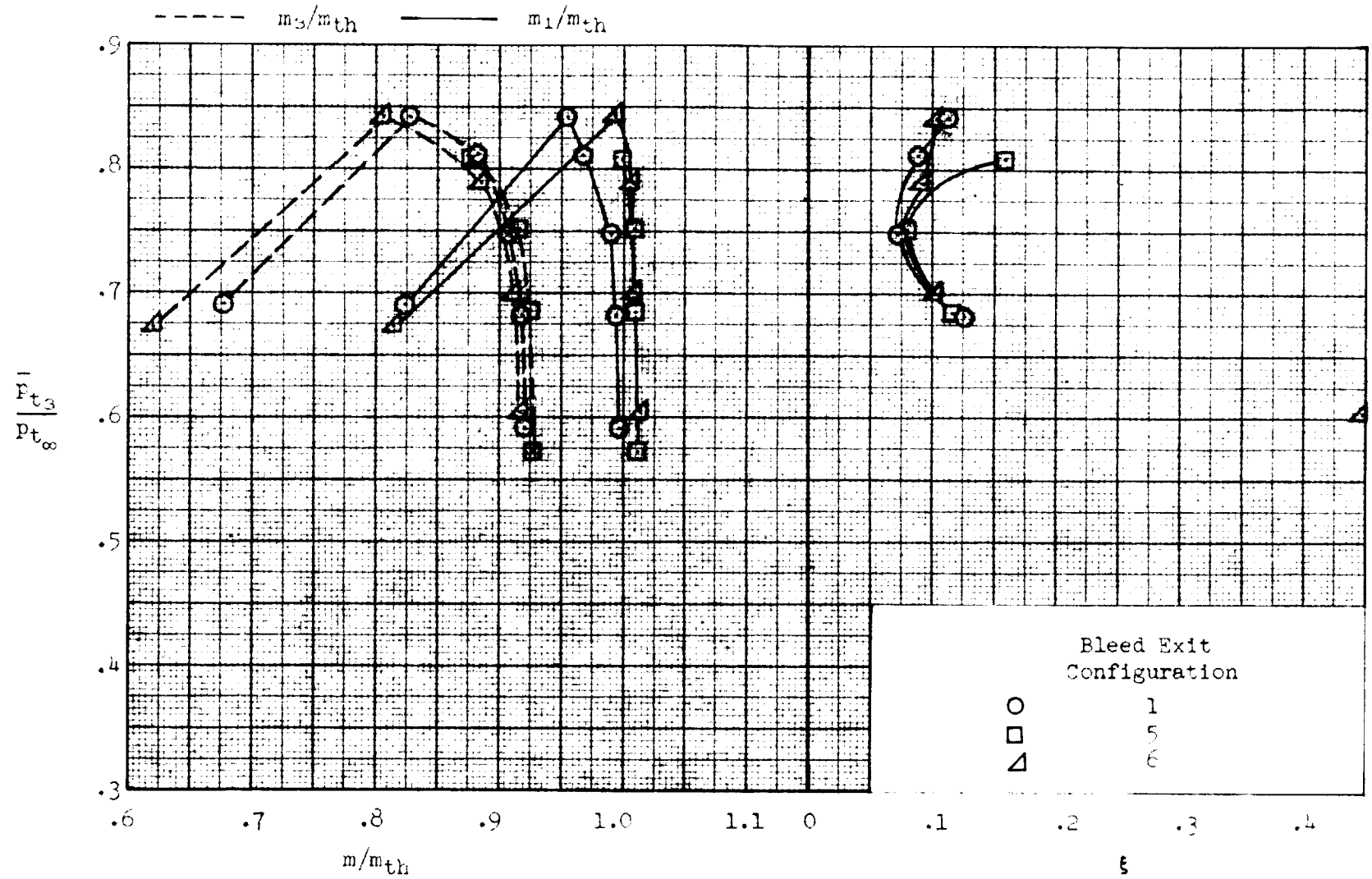

(a) $\alpha = 0°$, $\delta_R = 18.5°$, $\delta_L = 0.5°$, $A_{ref}/A_{th} = 1.0968$; inlet performance.

Figure 31.- Effect of variation of bleed-exit configuration on inlet-performance and external-drag coefficient; M = 2.76, $\beta = 0°$. Configuration: nose 1, diverter 2, porosity [illegible].

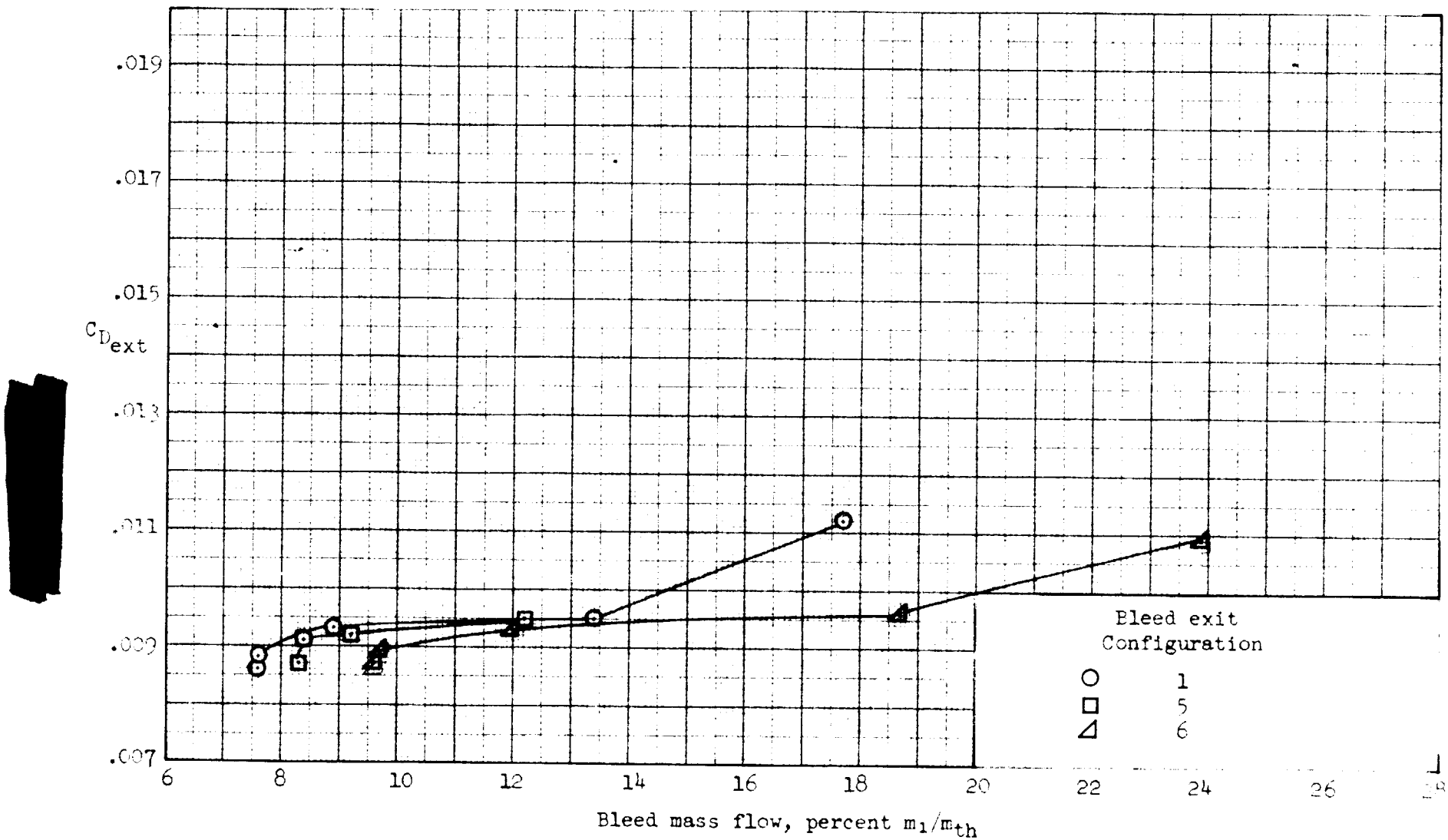

(a) Continued. External-drag coefficient.

Figure 31.- Continued.

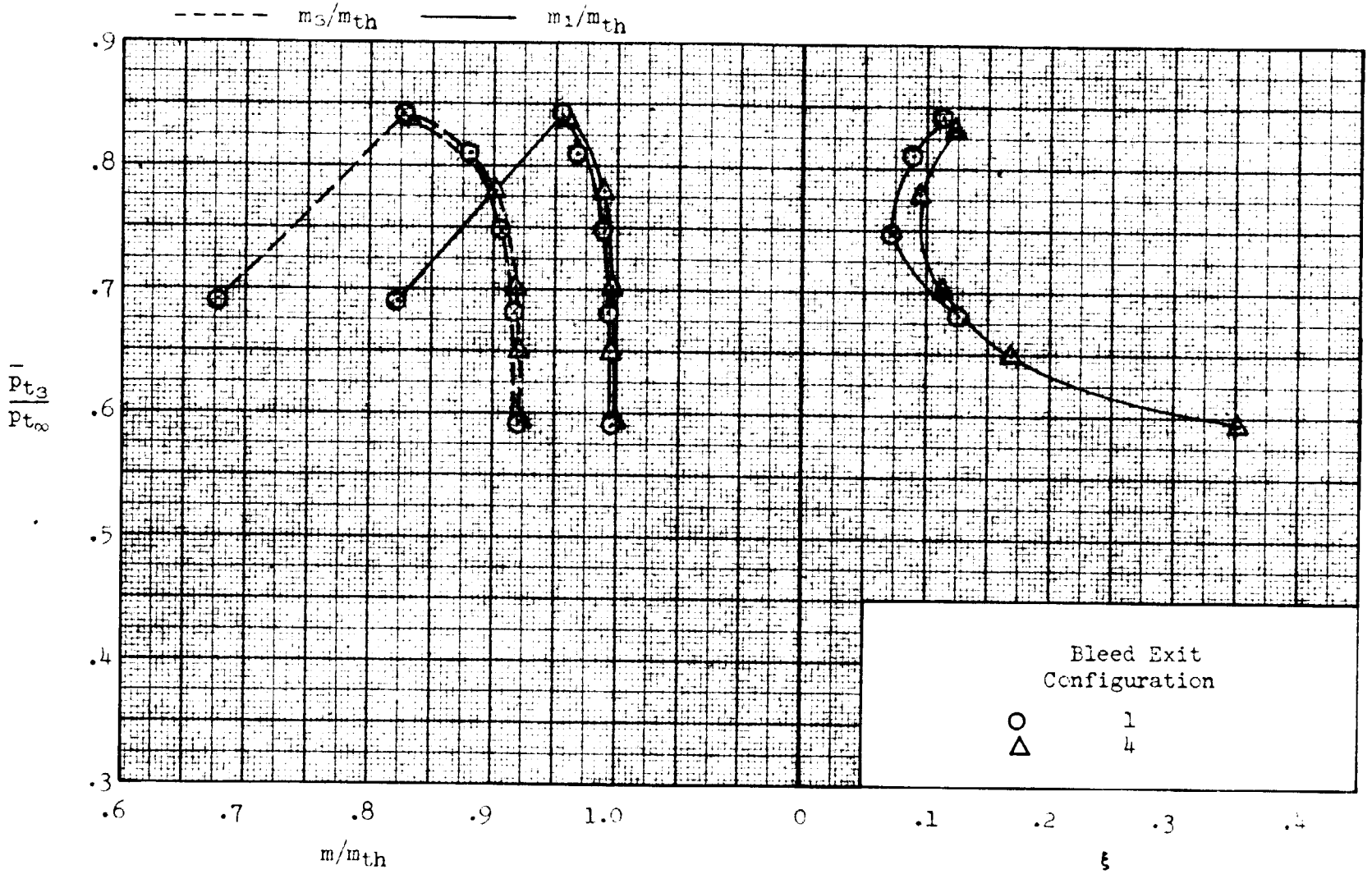

(a) Continued. Inlet performance.

Figure 31.- Continued.

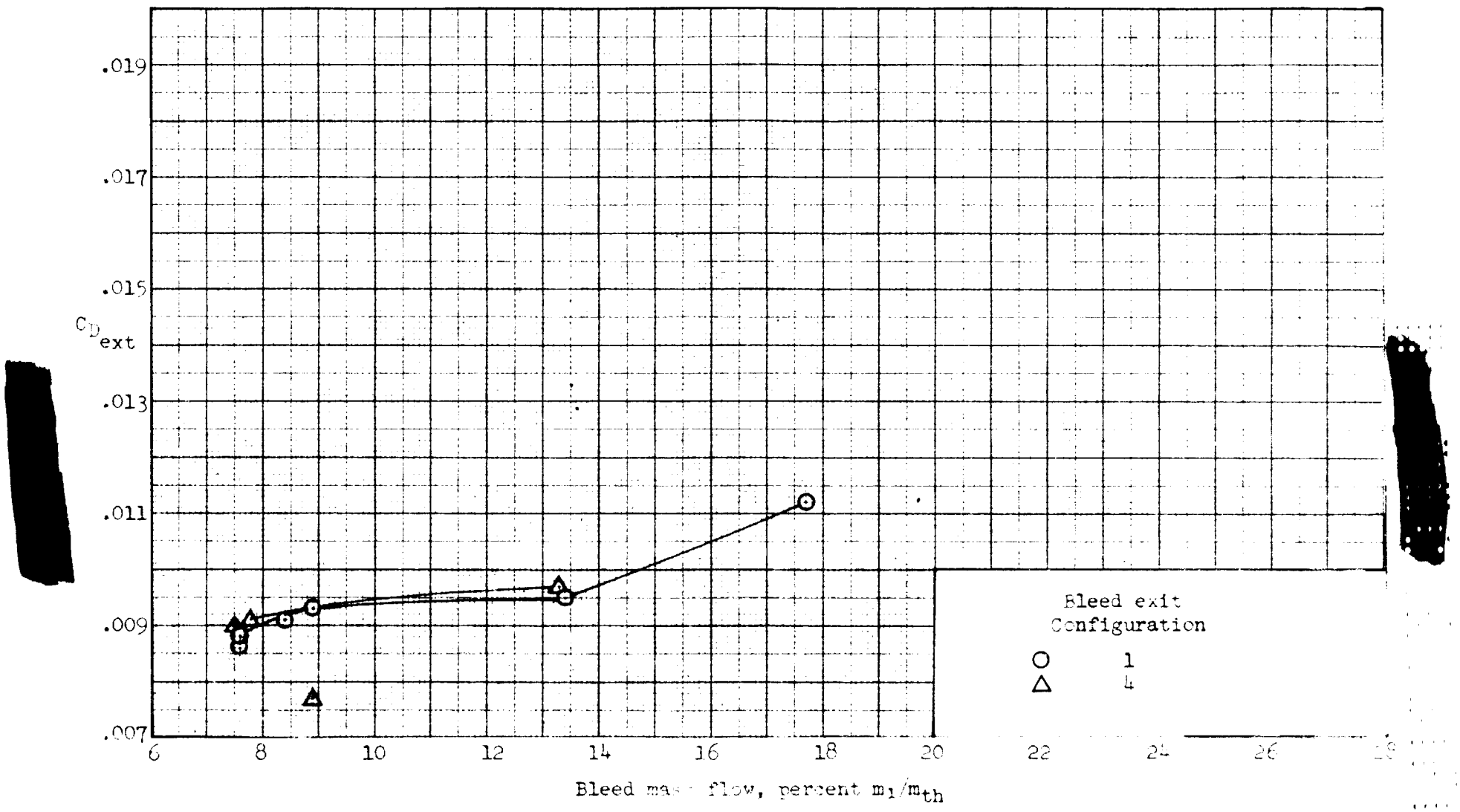

(a) Concluded. External-drag coefficient.

Figure 31.- Continued.

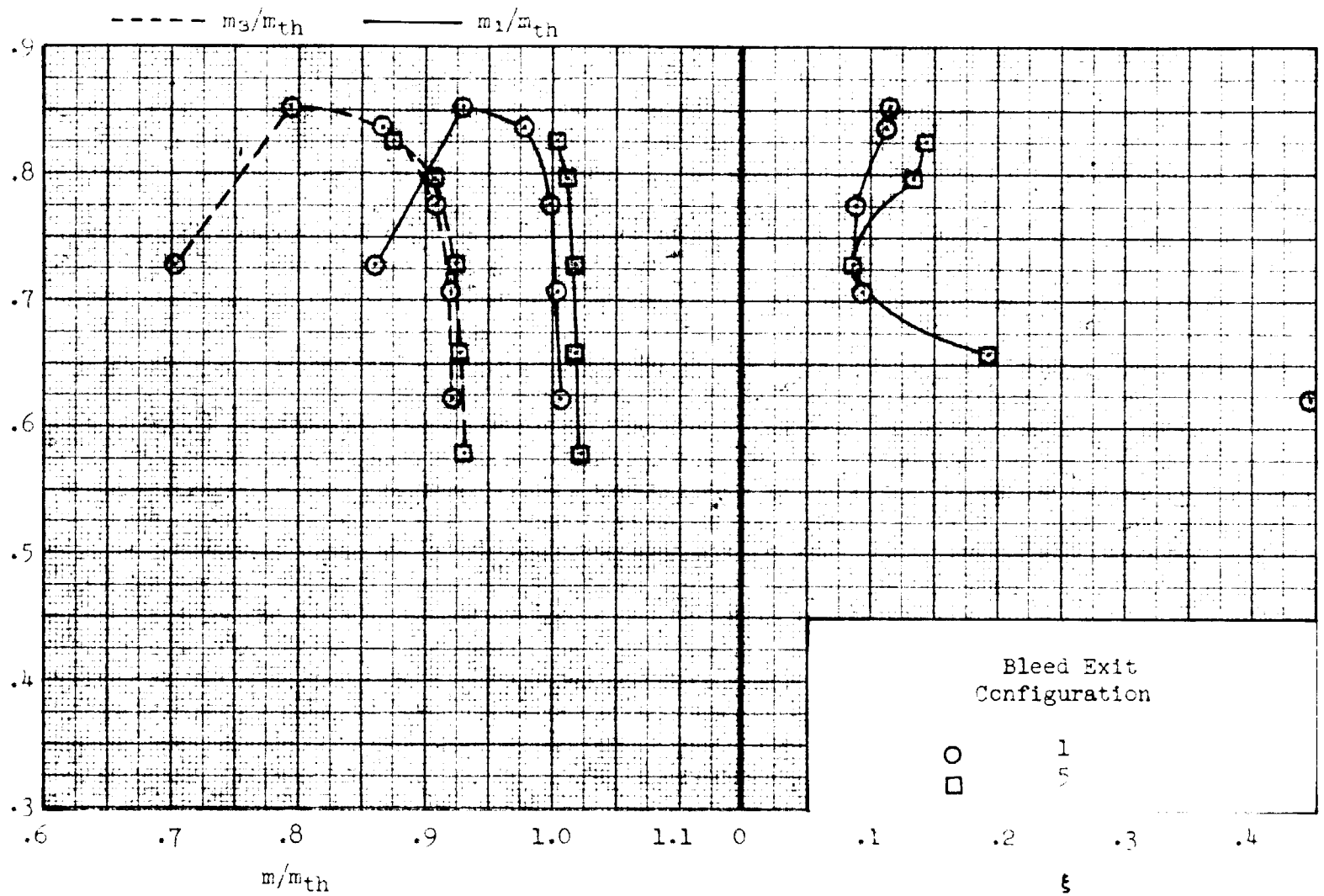

(b) $\alpha = 2°$, $\delta_R = 18.5°$, $\delta_L = 1.5°$, $A_{ref}/A_{th} = 1.0706$; inlet performance.

Figure 31.- Continued.

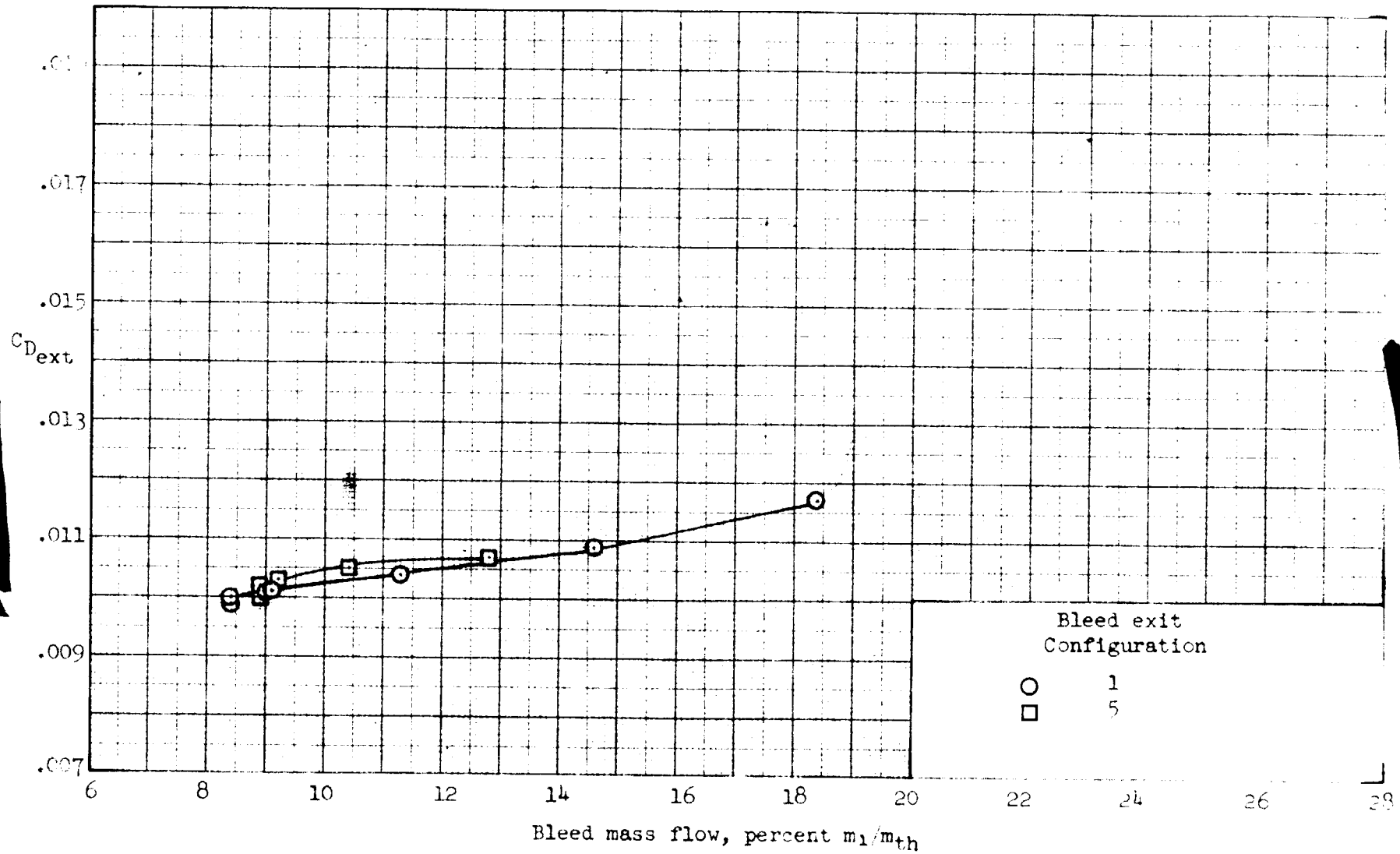

(b) Continued. External-drag coefficient.

Figure 31.- Continued.

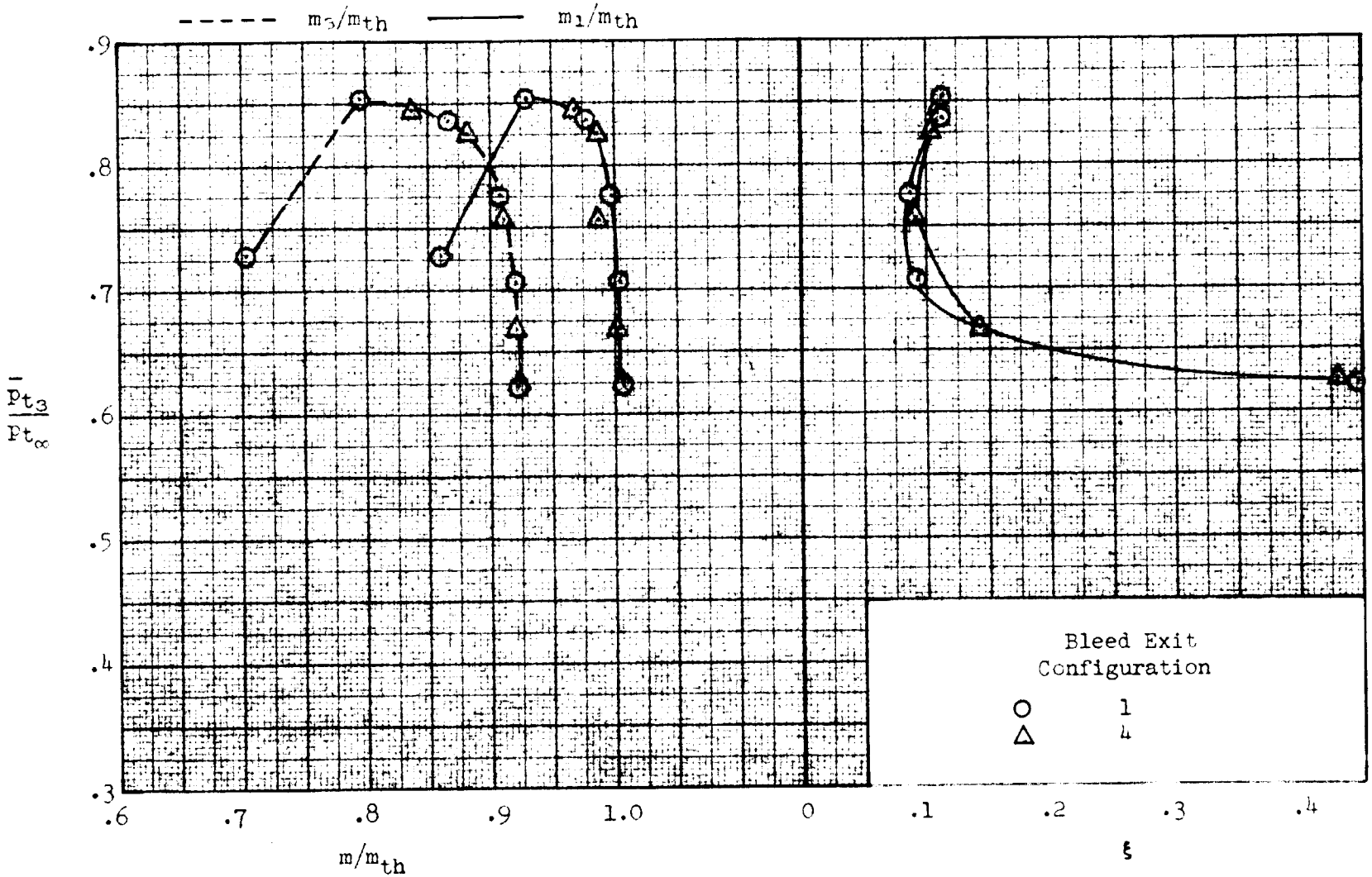

(b) Continued. Inlet performance.

Figure 31.- Continued.

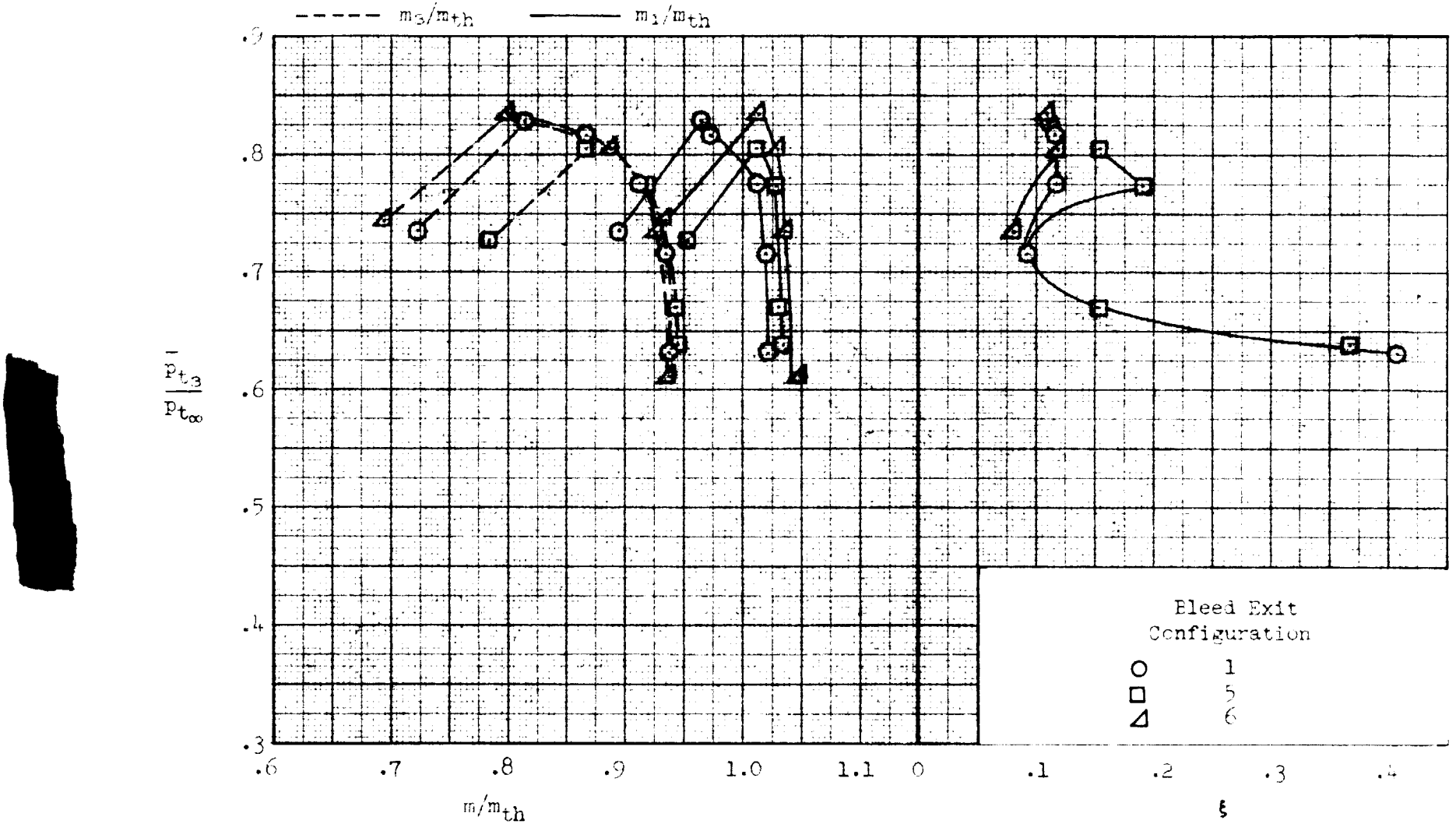

(c) $\alpha = 4°$, $\delta_R = 18.0°$, $\delta_L = 3.5°$, $A_{ref}/A_{th} = 1.0703$; inlet performance.

Figure 31.- Continued.

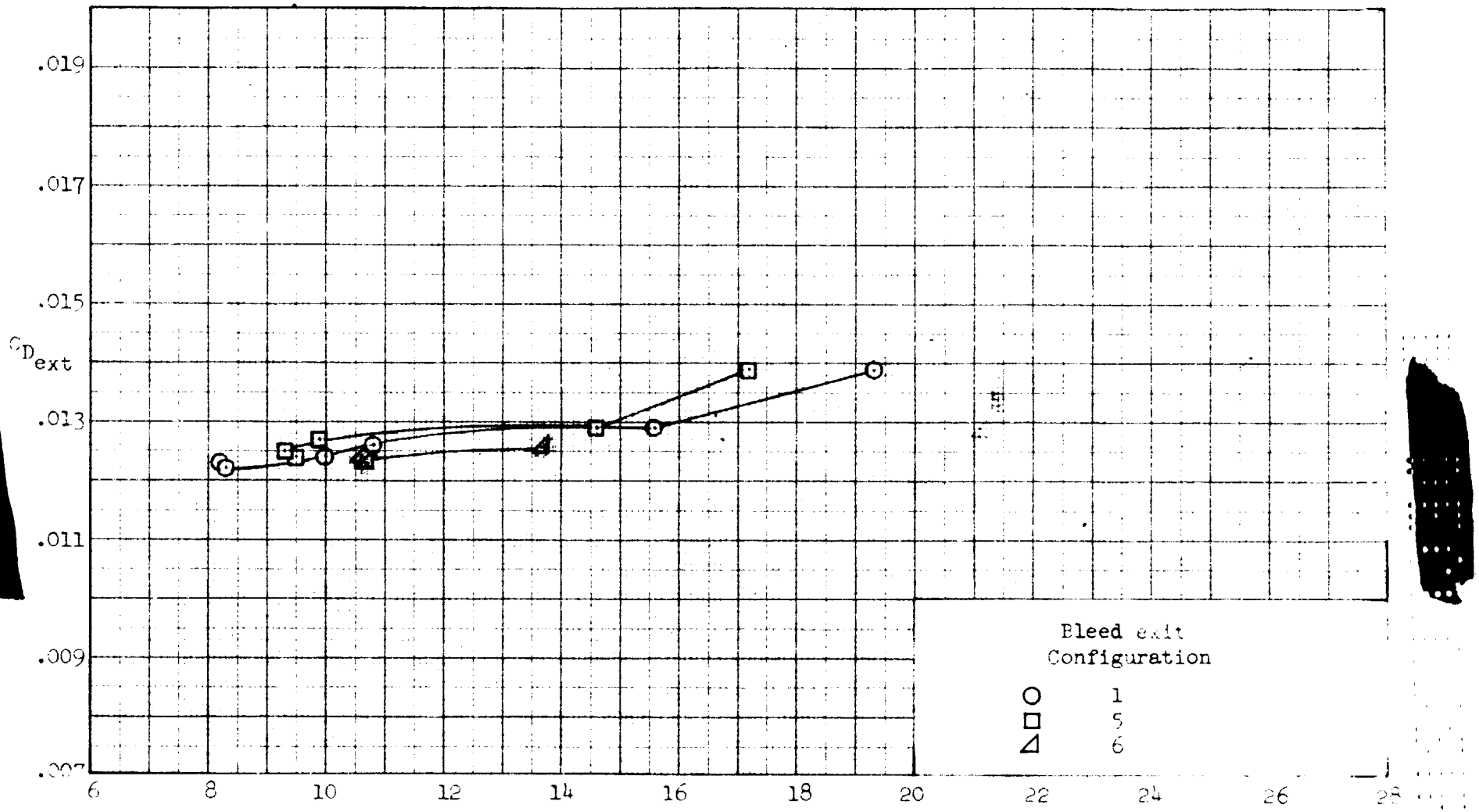

(c) Continued. External-drag coefficient.

Figure 31.- Continued.

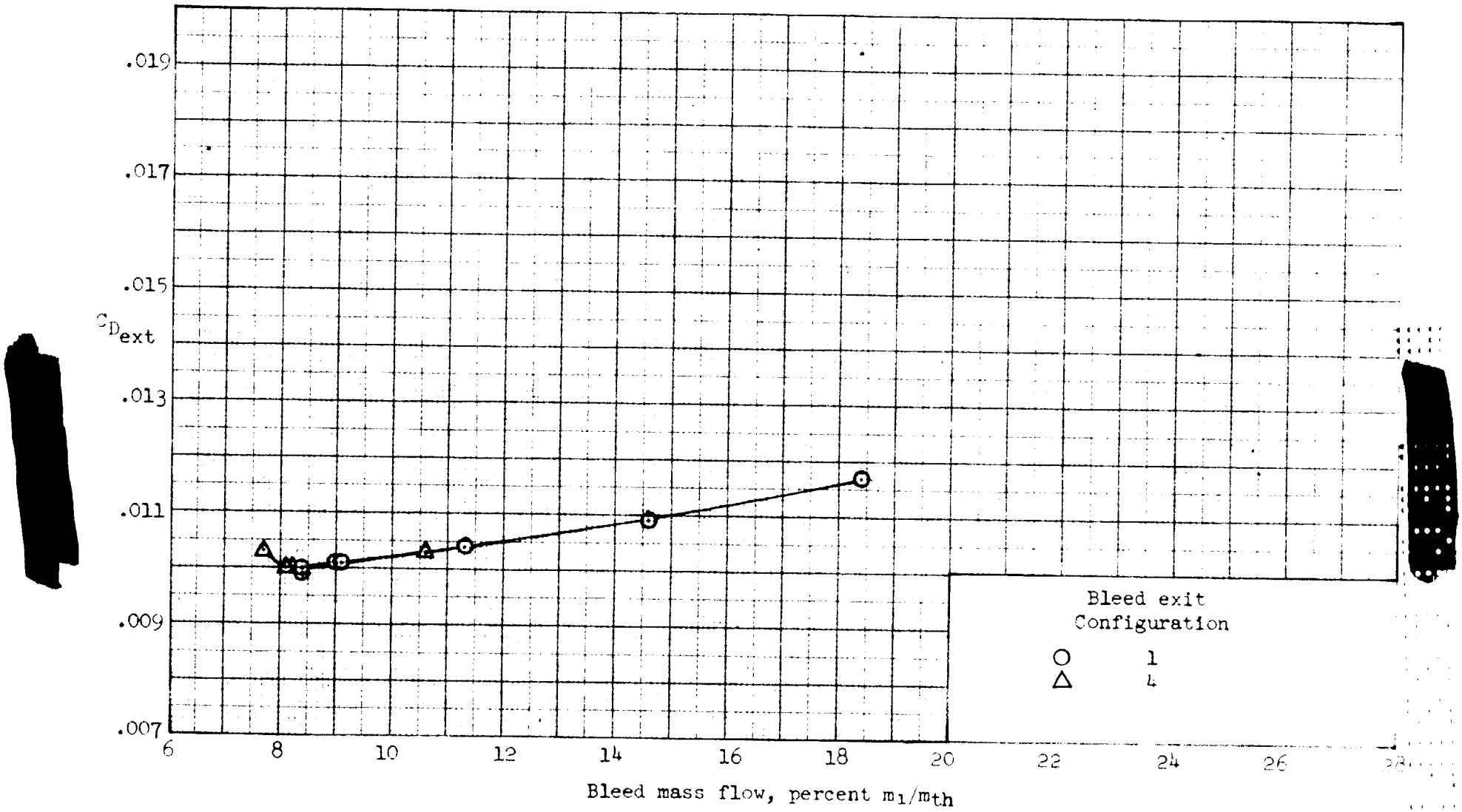

(b) Concluded. External-drag coefficient

Figure 31.- Continued.

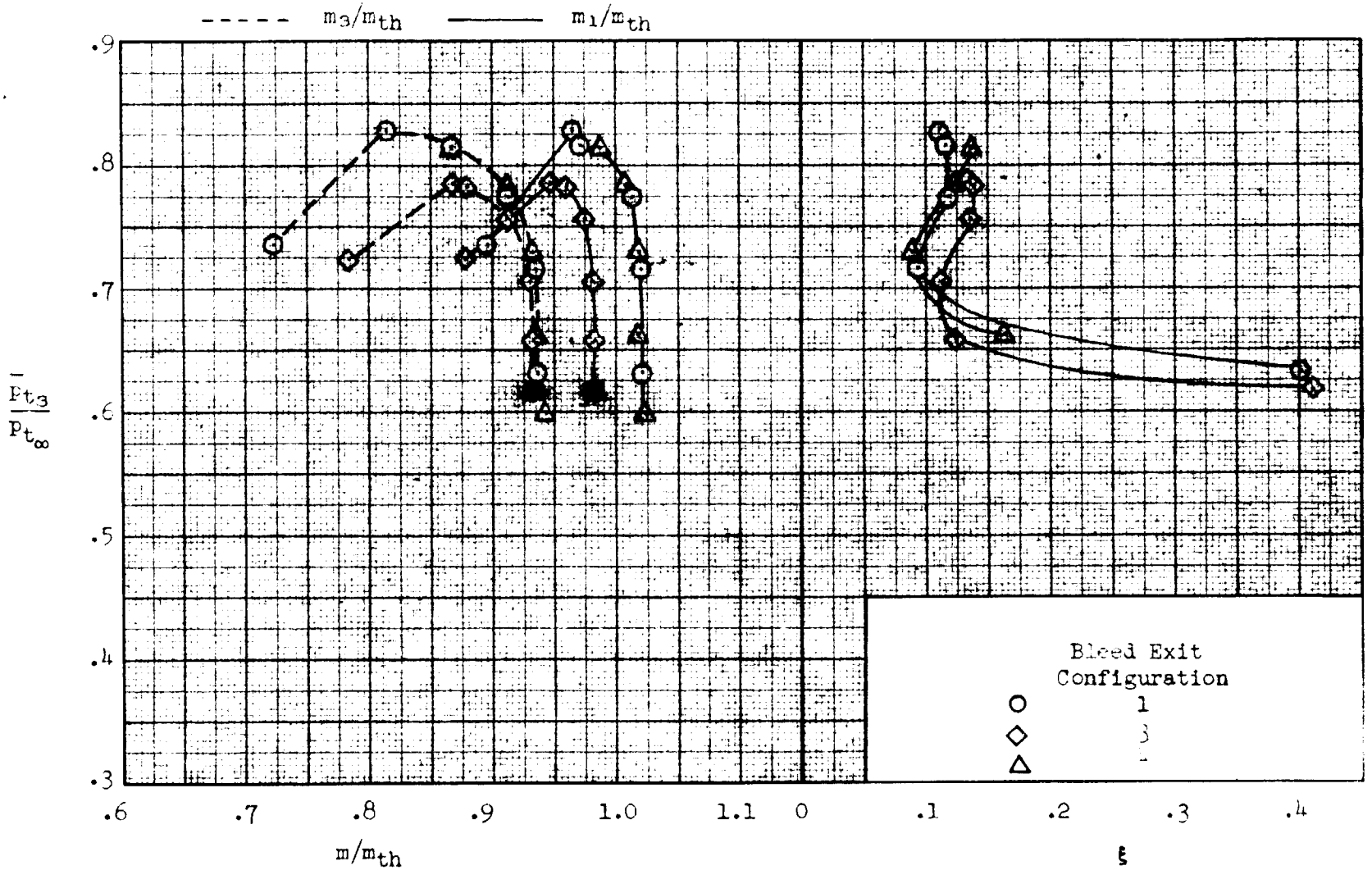

(c) Continued. Inlet performance.

Figure 31.- Continued.

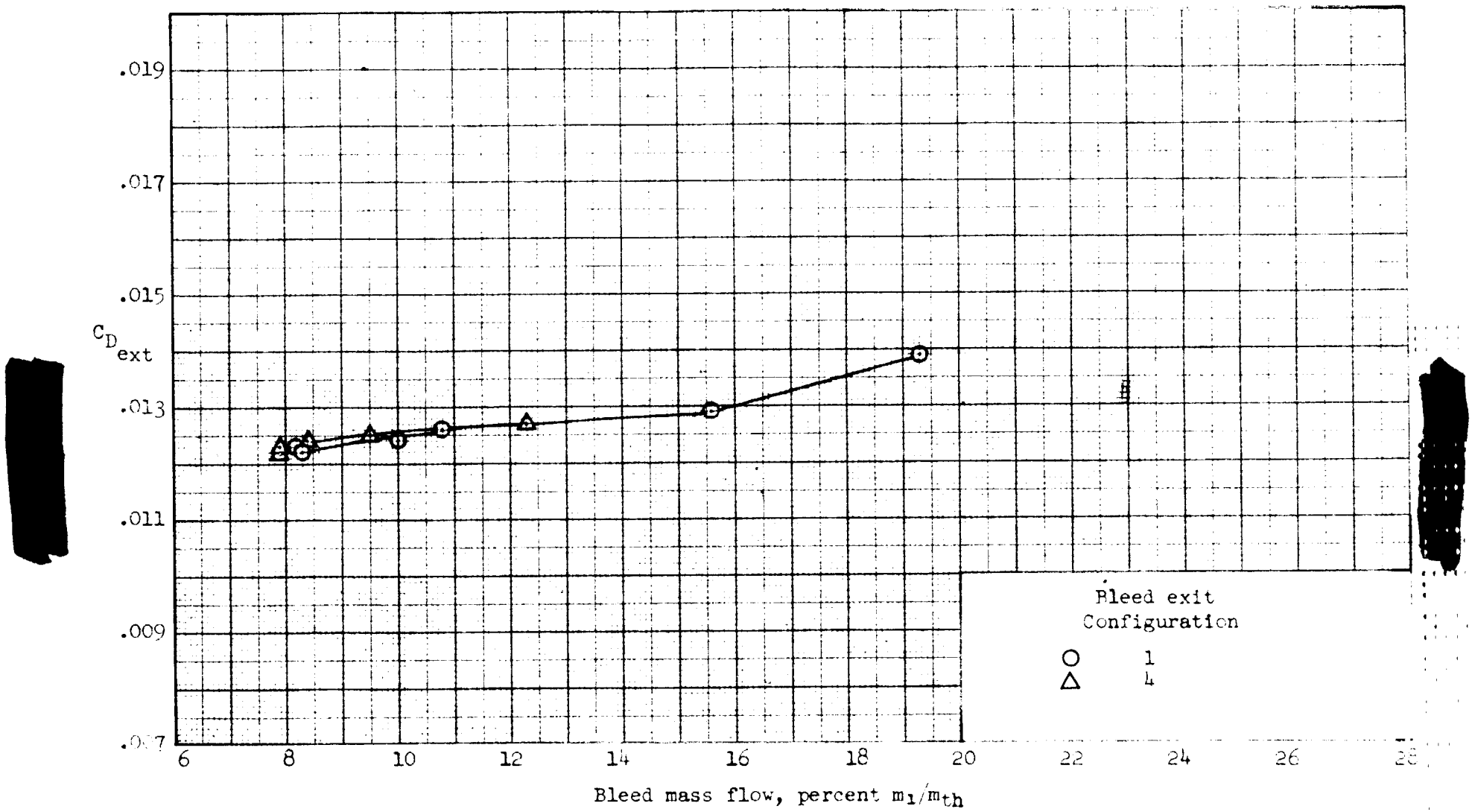

(c) Concluded. External-drag coefficient.

Figure 31.- Concluded.

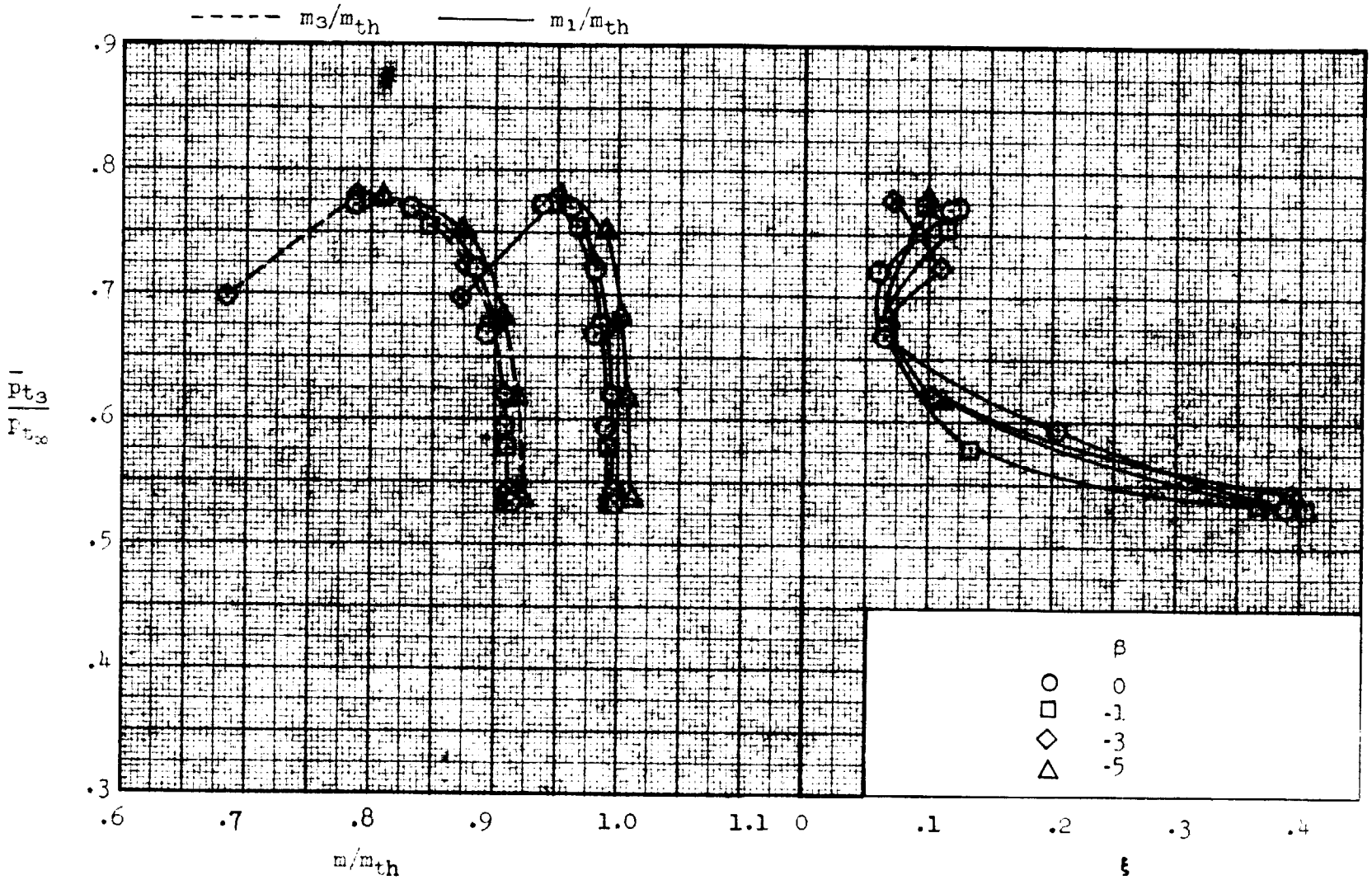

(a) $\alpha = 2°$, $\delta_R = 19.5°$, $\delta_L = 4.0°$, $A_{ref}/A_{th} = 1.0930$.

Figure 32.- Effect of variation of angle of sideslip on inlet performance; M = 3.00. Configuration: nose 1, diverter 2, porosity 1, bleed exit 1.

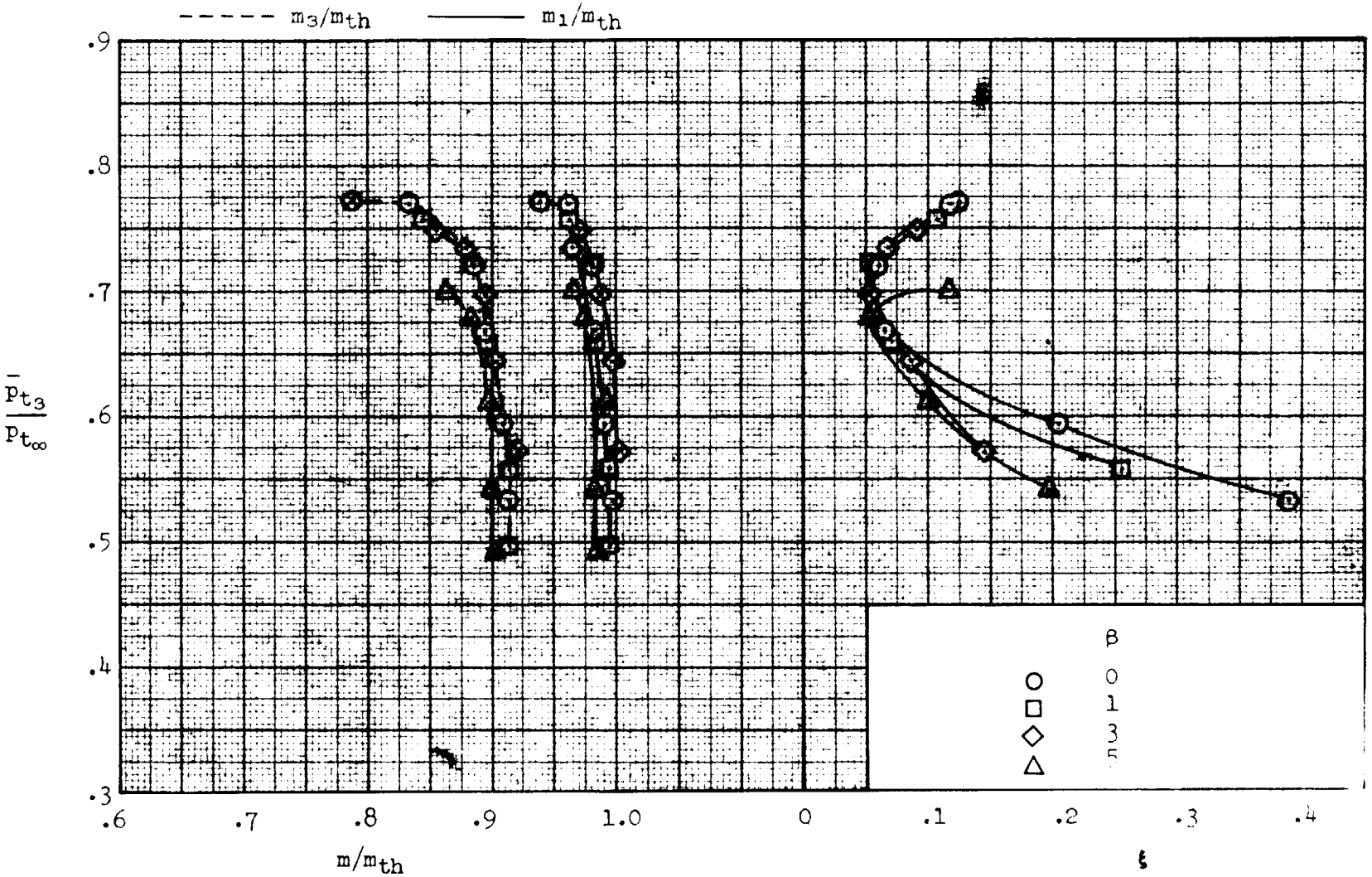

(a) Concluded.

Figure 32.- Continued.

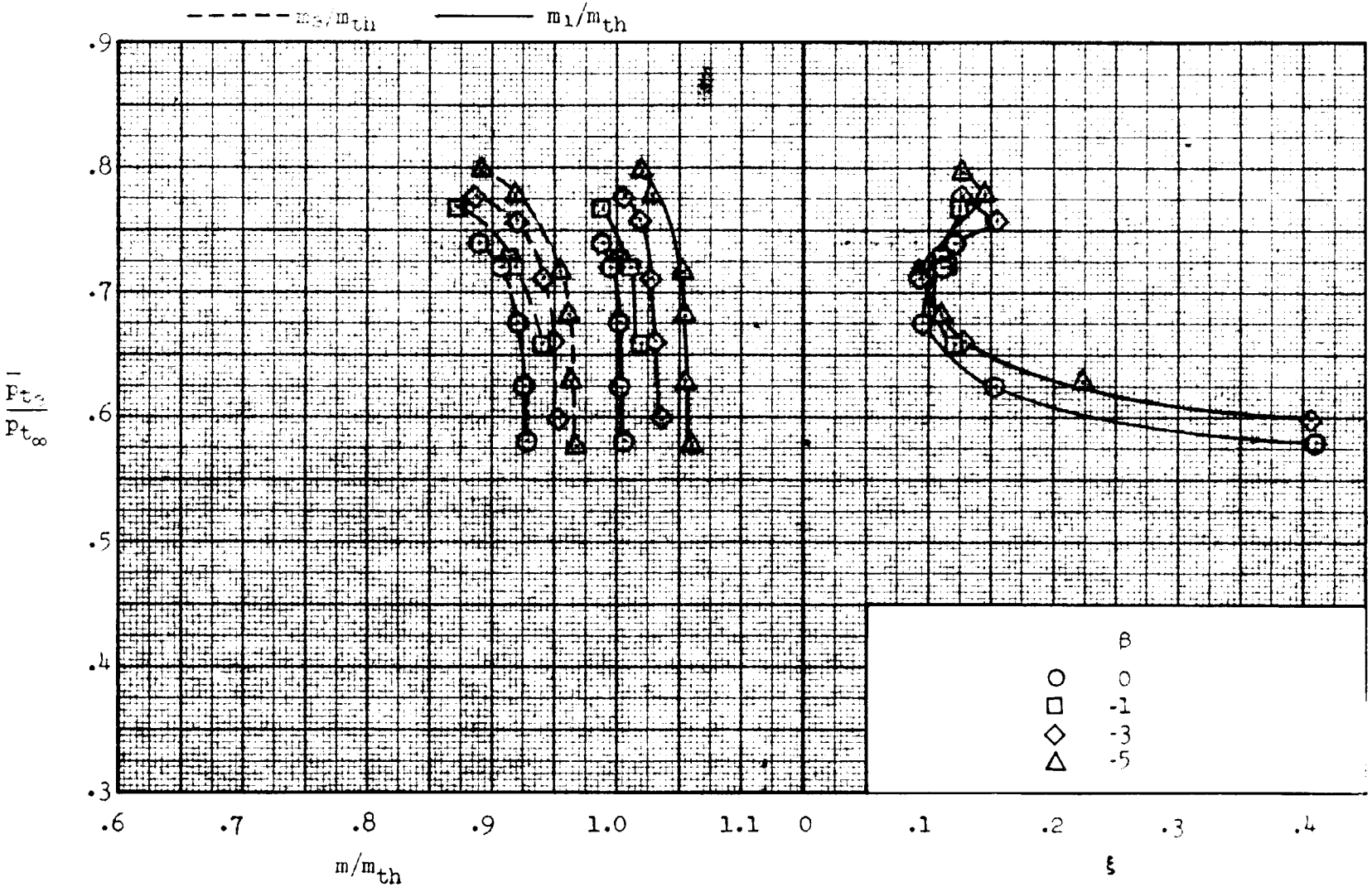

(b) $\alpha = 6°$, $\delta_R = 18.0°$, $\delta_L = 1.5°$, $A_{ref}/A_{th} = 0.8968$.

Figure 32.- Continued.

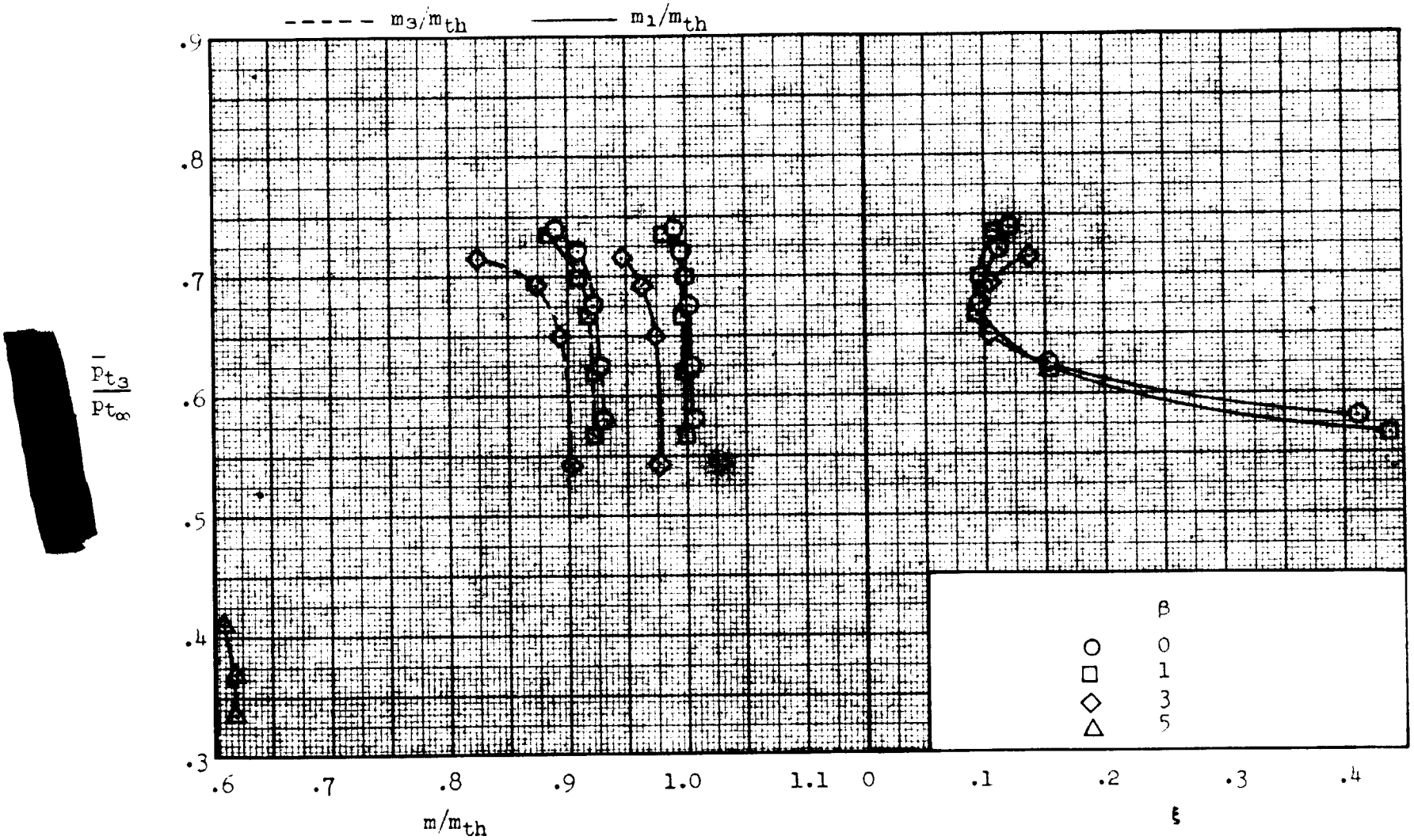

(b) Concluded.

Figure 32.- Continued.

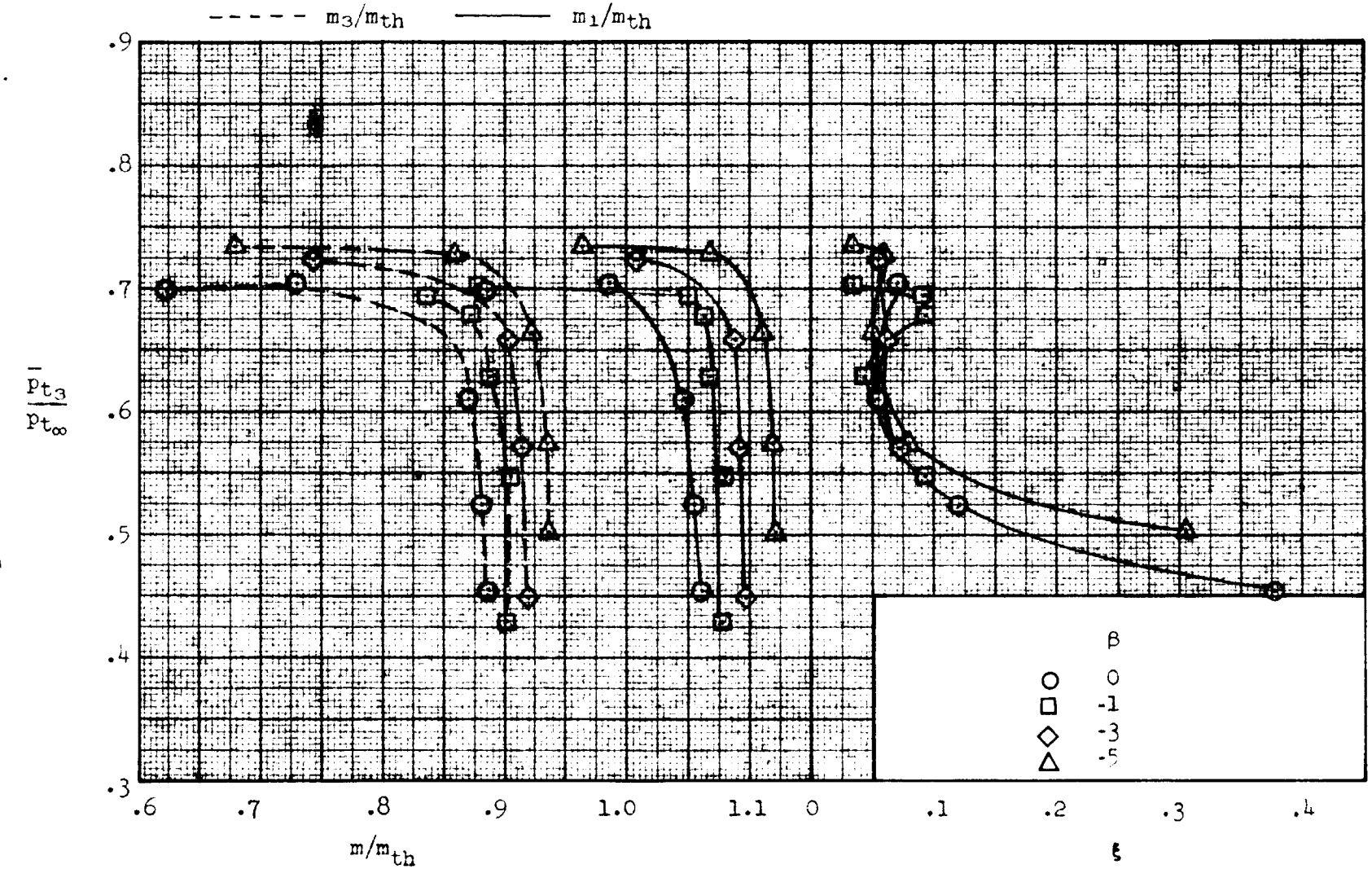

(c) $\alpha = 10°$ $\delta_R = 20.0°$, $\delta_L = 4.0°$, $A_{ref}/A_{th} = 0.9792$.

Figure 3?.- Continued.

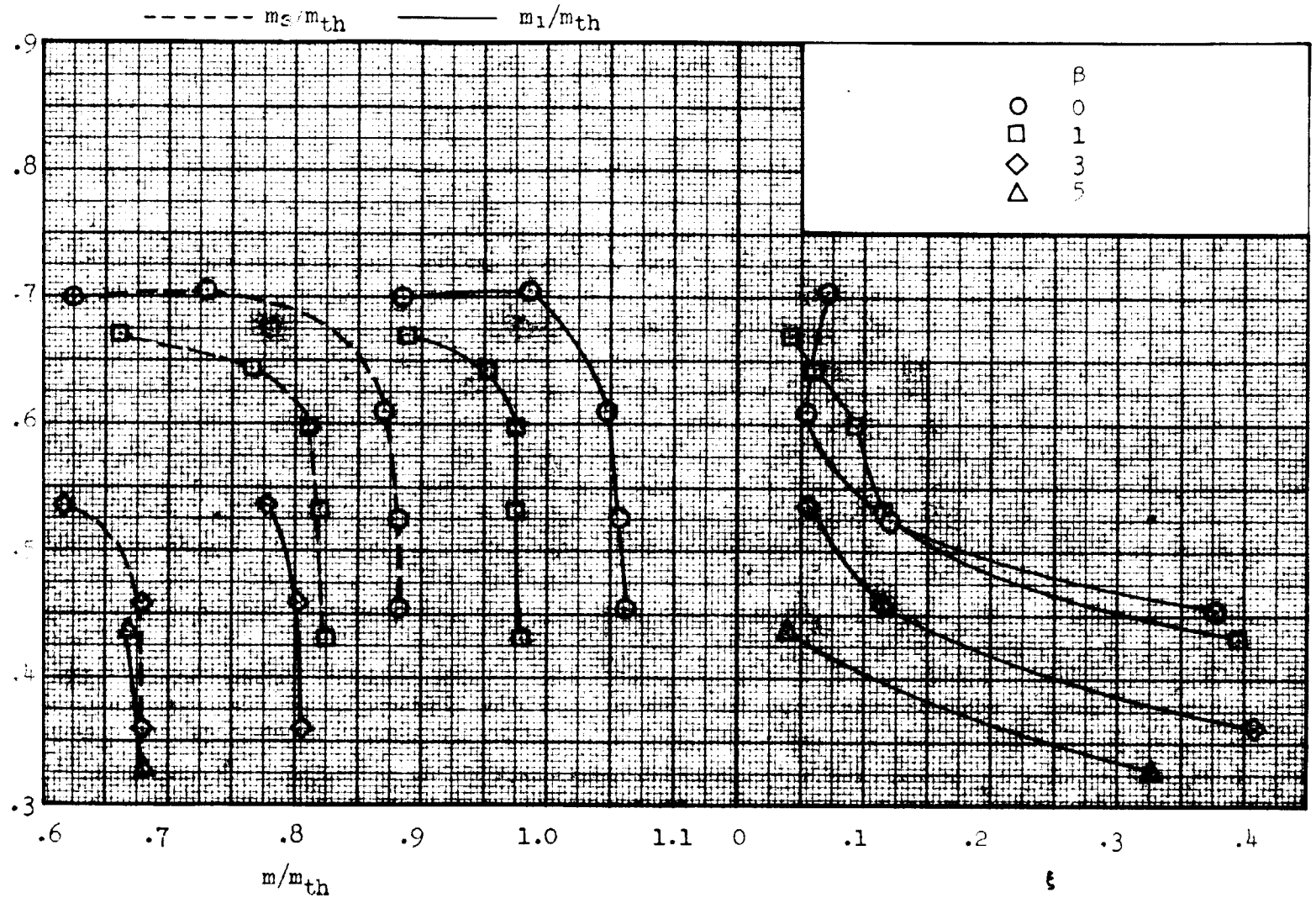

(c) Concluded.

Figure 32.- Concluded.

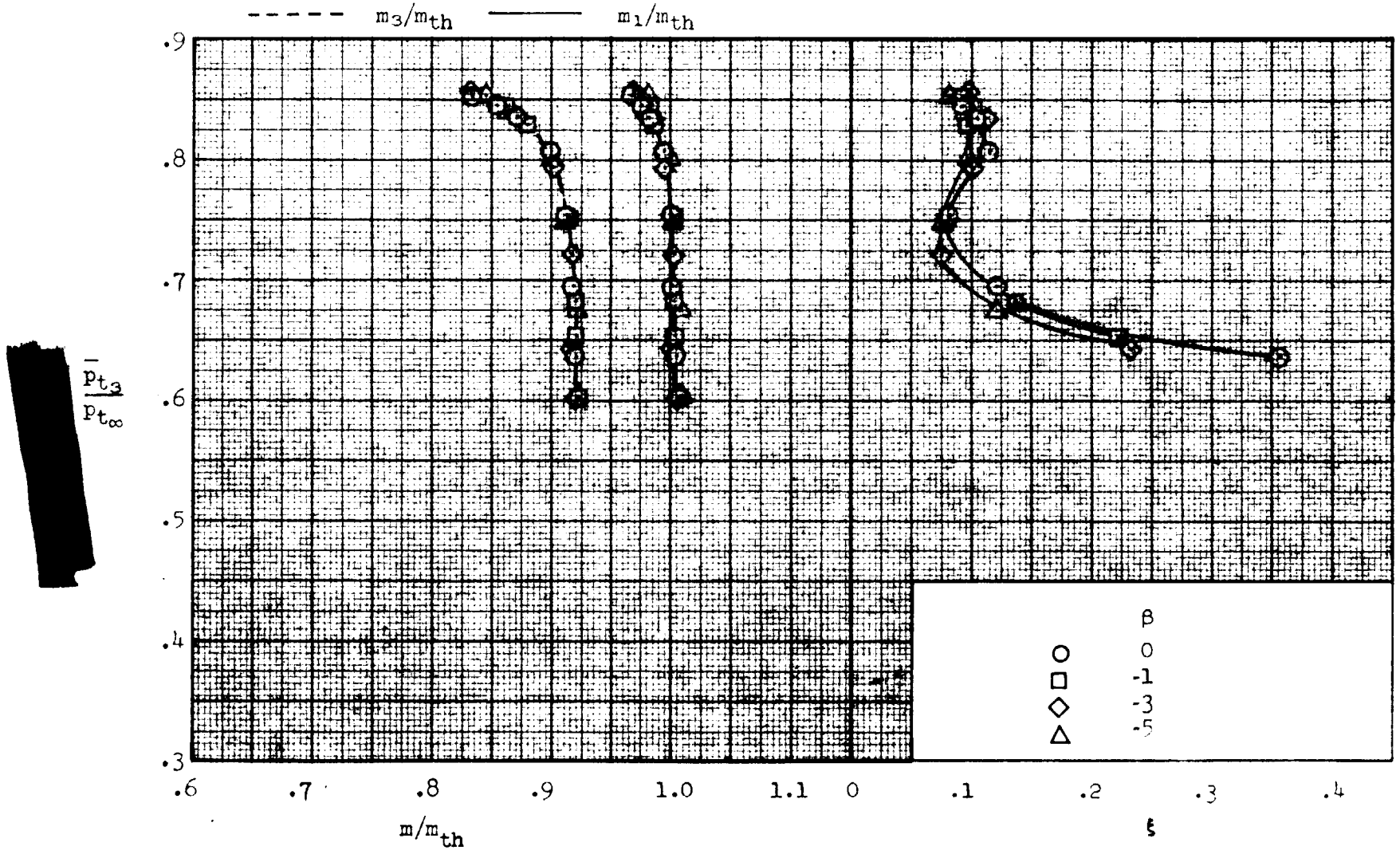

(a) $\alpha = 2°$, $\delta_R = 18.5°$, $\delta_L = 1.5°$, $A_{ref}/A_{th} = 1.0706$.

Figure 33.- Effect of variation of angle of sideslip on inlet performance; M = 2.76. Configuration: nose 1, diverter 2, porosity 1, bleed exit 1.

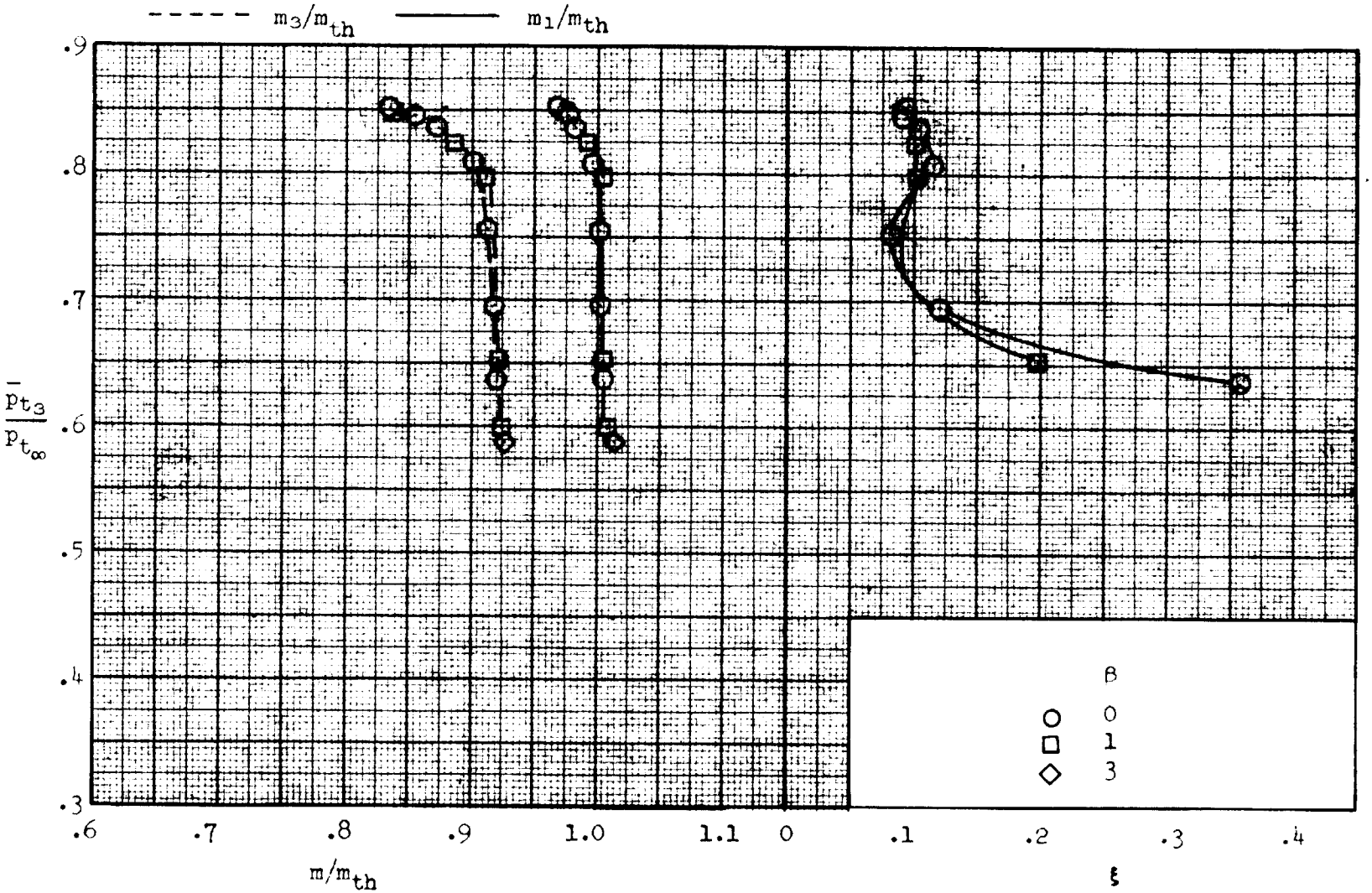

(a) Concluded.

Figure 33.- Continued.

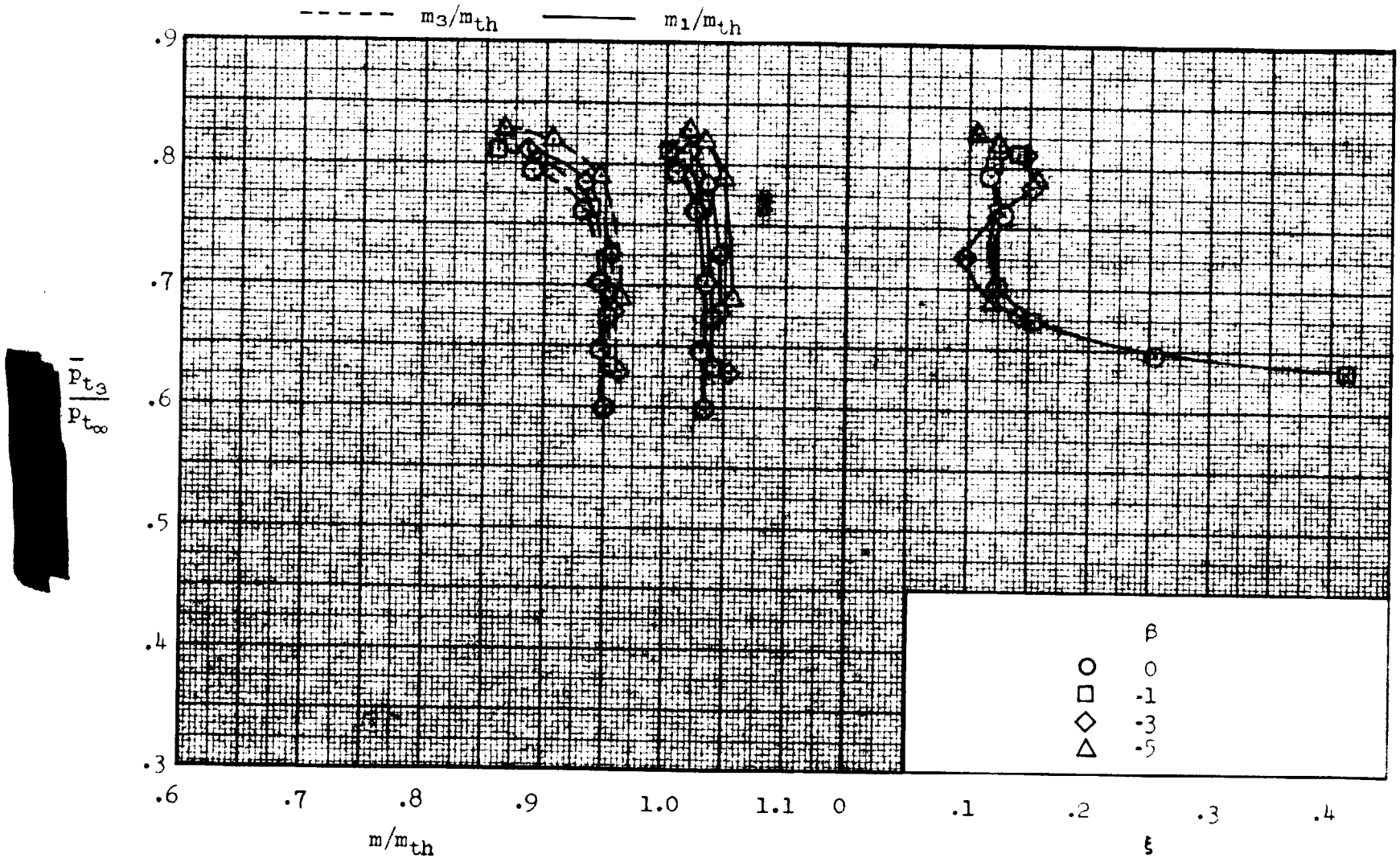

(b) $\alpha = 6°$, $\delta_R = 17.5°$, $\delta_L = 4.0°$, $A_{ref}/A_{th} = 1.0313$.

Figure 33.- Continued.

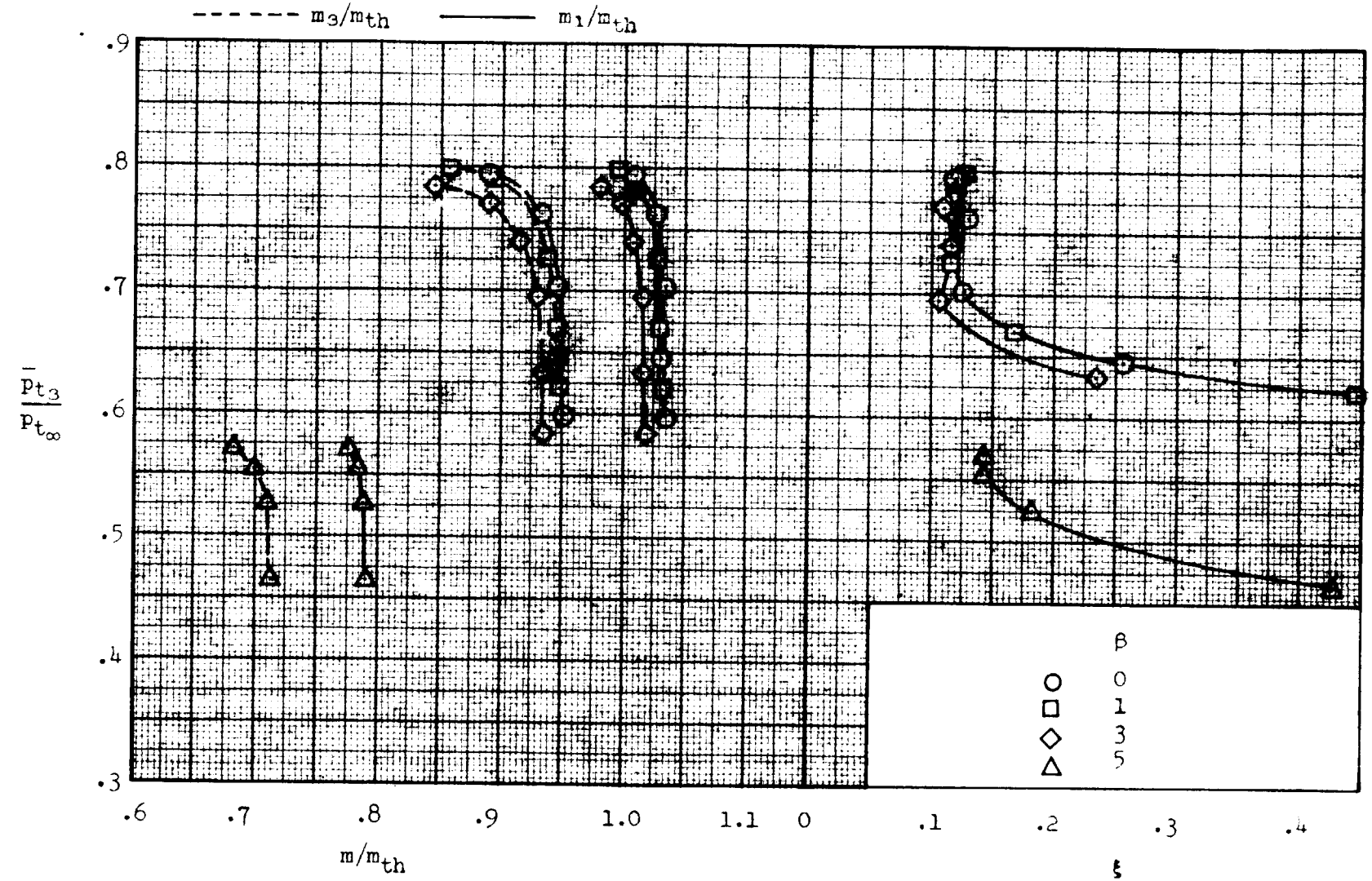

(b) Concluded.

Figure 33.- Continued.

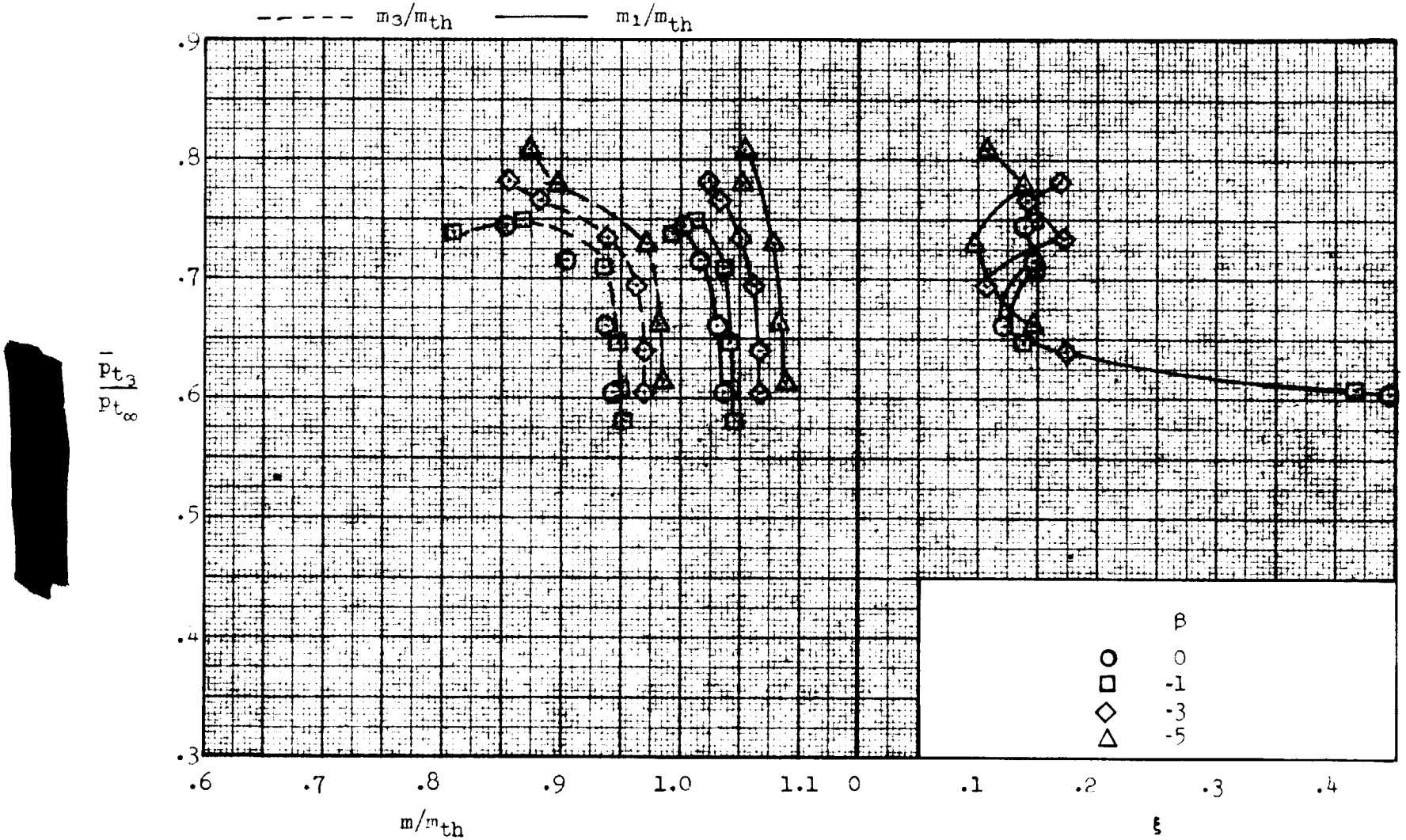

(c) $\alpha = 10°$, $\delta_R = 17.0°$, $\delta_L = 7.5°$, $A_{ref}/A_{th} = 1.0624$.

Figure 33.- Continued.

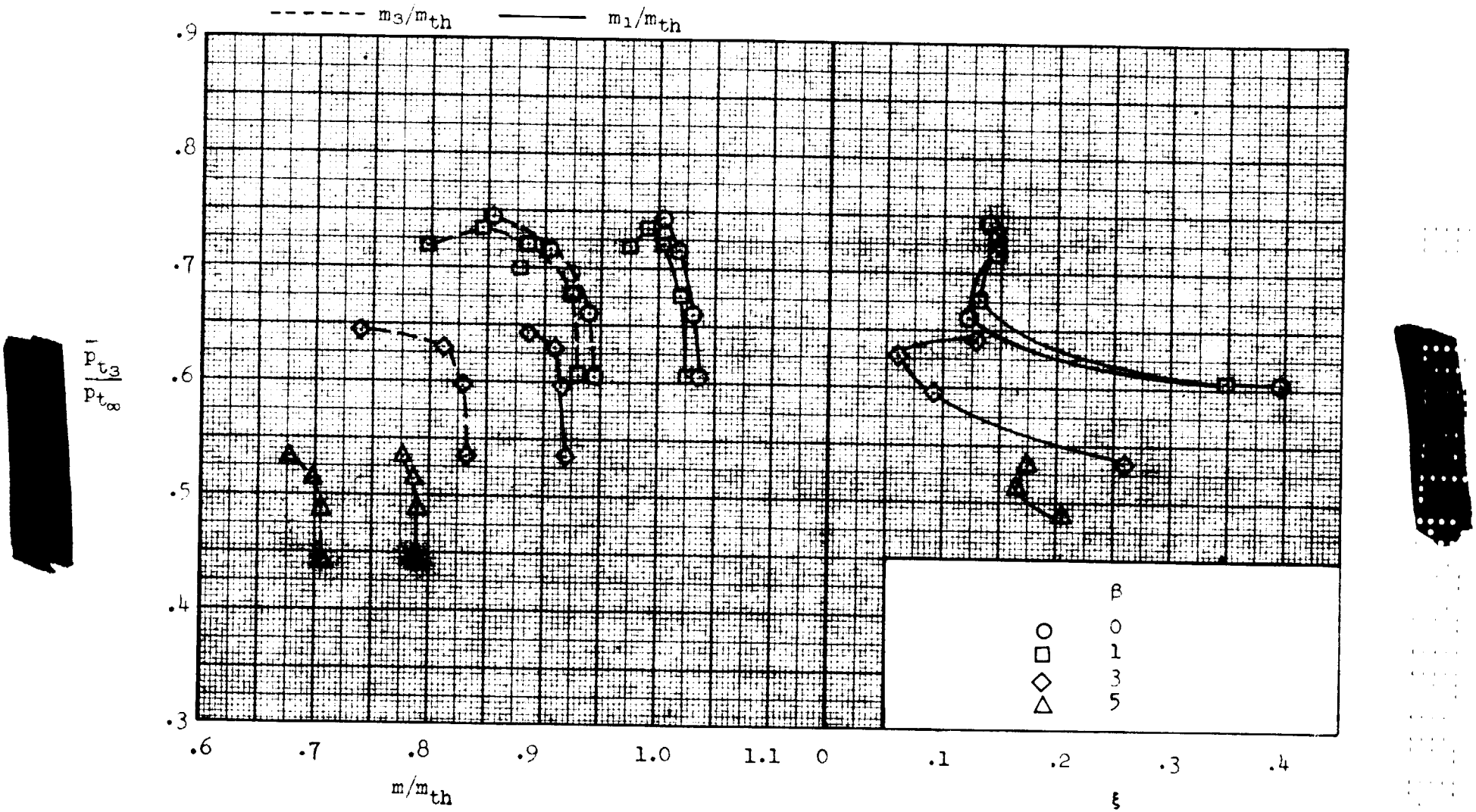

(c) Concluded.

Figure 33.- Concluded.

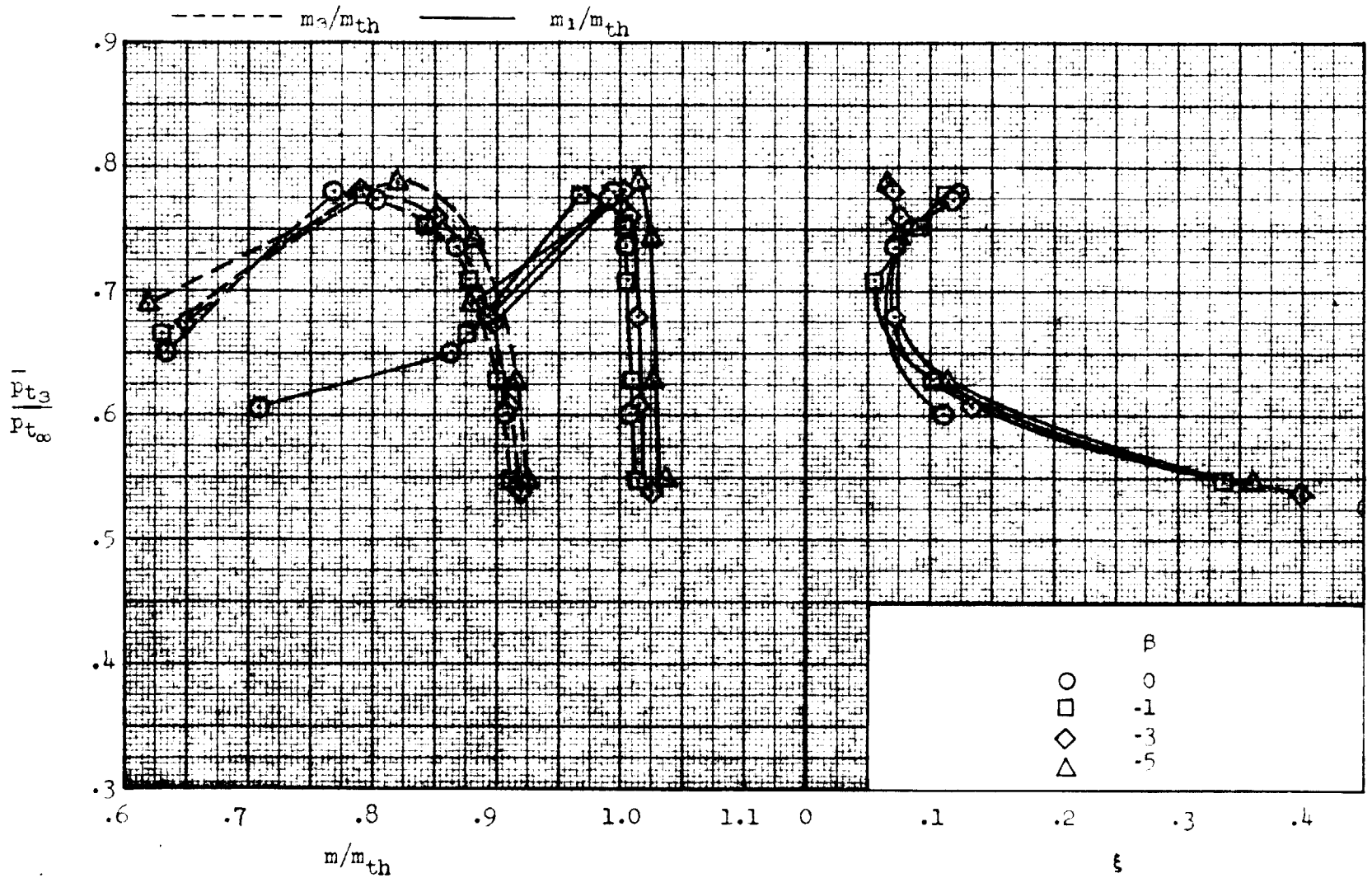

(a) Inlet performance.

Figure 34.- Effect of variation of angle of sideslip on inlet performance and external-drag coefficient; $M = 3.00$, $\alpha = 2°$, $\delta_R = 19.5°$, $\delta_L = 4.0°$, $A_{ref}/A_{th} = 1.0930$. Configuration: nose 2, diverter 2, porosity 5, bleed exit 6.

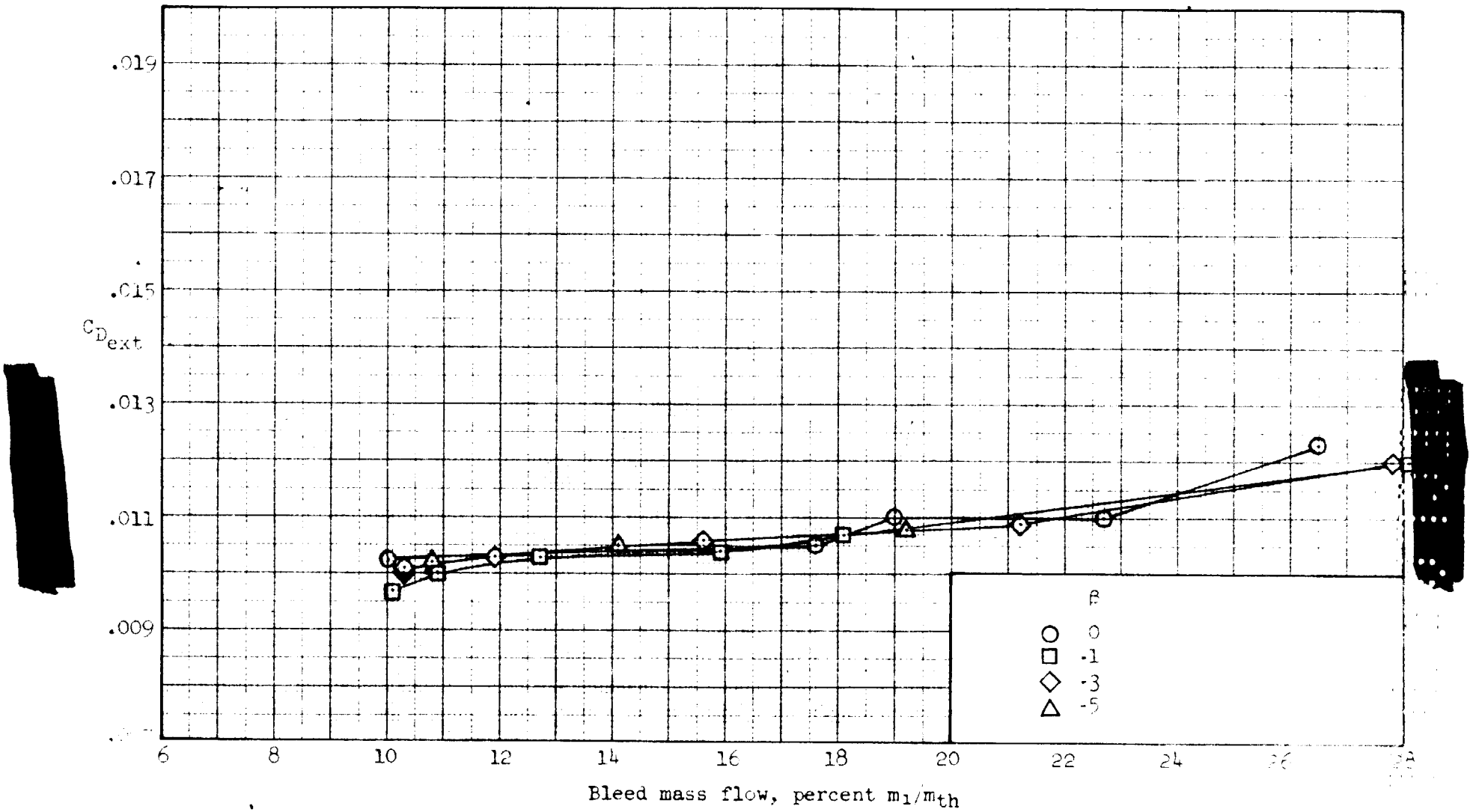

b. External drag coefficient.

Figure 34.- Continued.

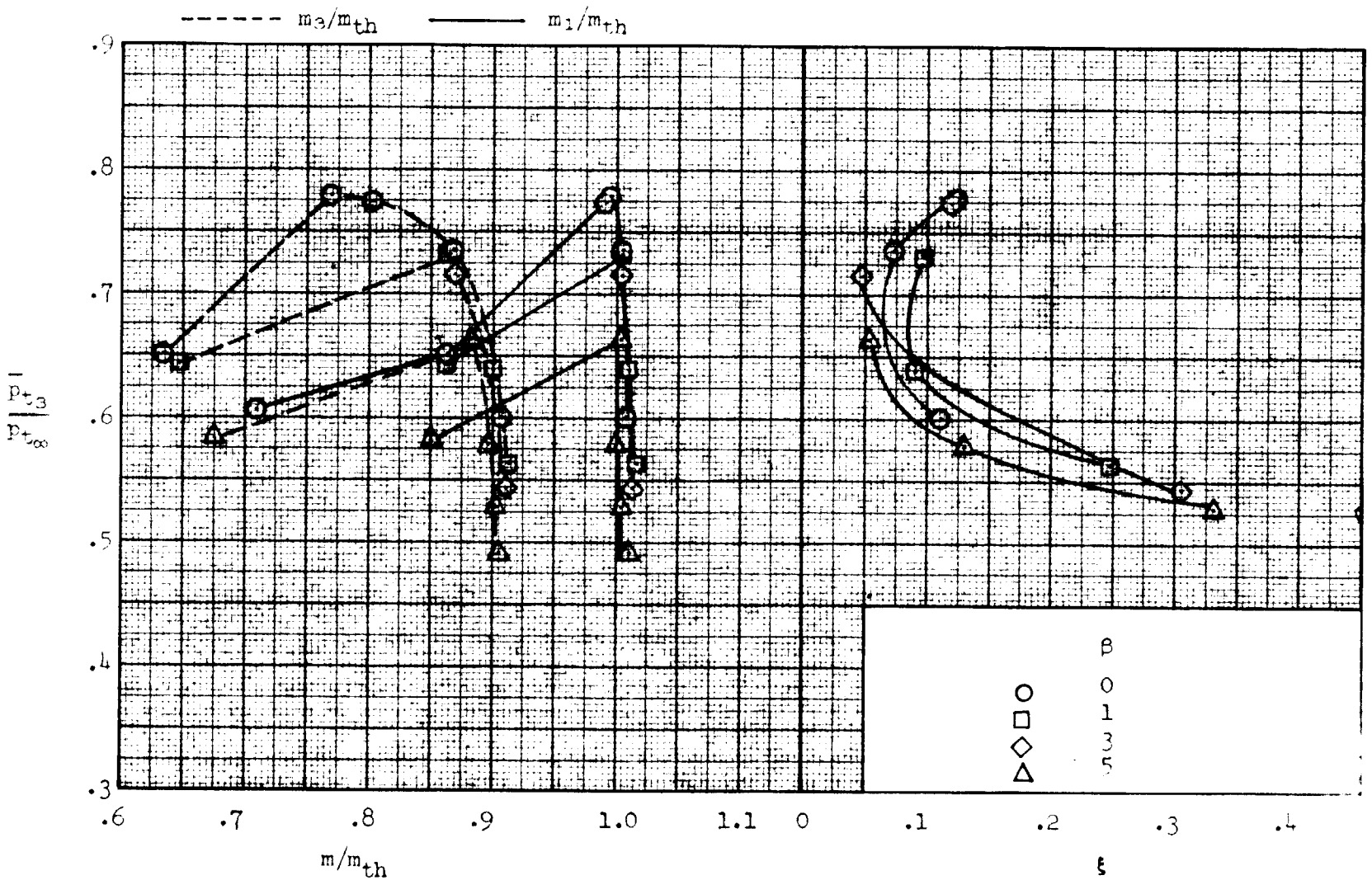

(c) Inlet performance.

Figure 34.- Continued.

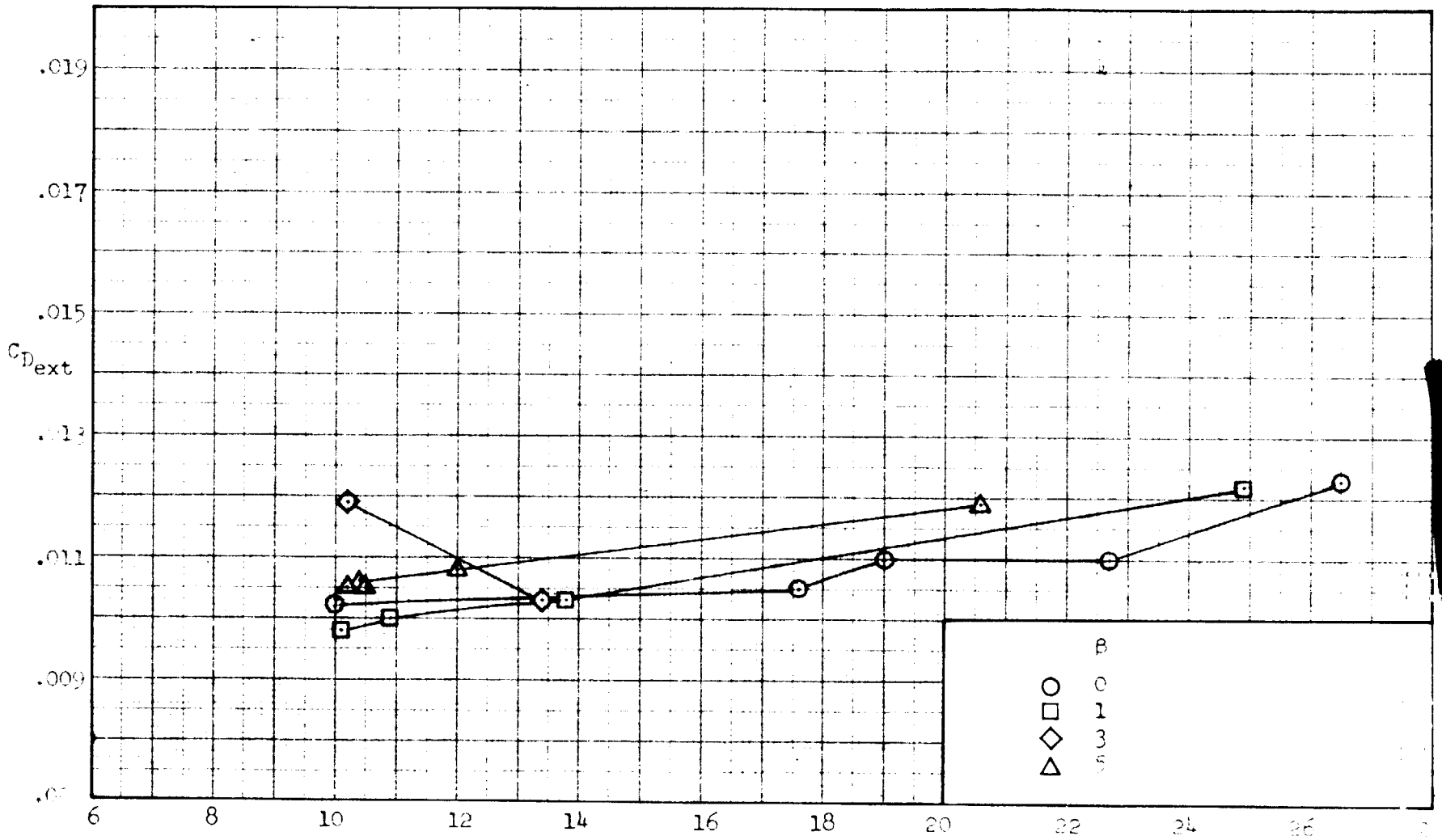

(d) External-drag coefficient.

Figure 34.- Concluded.